Fermilab Library
0 1160 0052531 5

SDC-90-00146

SDC
SOLENOIDAL DETECTOR NOTES

SSC DETECTOR SUBSYSTEM SUMMARY REPORT AND PROPOSAL FOR FY 1991:
Central and Forward Tracking Collaboration

G. Hanson, Contact Person

August 31, 1990

John Kadyk SDC-90-00

SSC DETECTOR SUBSYSTEM SUMMARY REPORT AND PROPOSAL FOR FY 1991

CENTRAL AND FORWARD TRACKING COLLABORATION

B. Brabson, A. Dzierba, R. Foster, G. Hanson, X. Lou, X. Luo, C. Neyman, H. Ogren, D. R. Rust, and D. Zieminska
Indiana University

G. Baranko, J. Carr, H. Cheung, J. P. Cumalat, E. Erdos, W. T. Ford, J. Ginkel, M. Lohner, U. Nauenberg, P. Rankin, G. Schultz, and J. G. Smith
University of Colorado

F. M. Newcomer, R. Van Berg, and H. H. Williams
University of Pennsylvania

Y. Arai
KEK National Laboratory

D. Hess, J. A. Kadyk, A. P. T. Palounek, and J. Wise
Lawerence Berkeley Laboratory and University of California, Berkeley

J. W. Chapman
University of Michigan

J. C. Hart, J. W. Hiddleston, N. A. McCubbin, B. T. Payne, and D. J. White
Rutherford Appleton Laboratory

J. M. Bailey, G. A. Beck, S. F. Biagi, J. B. Dainton, E. Gabathuler, S. J. Maxfield, J. M. Morton, G. D. Patel, and P. Sanders
University of Liverpool

N. Brook, P. J. Bussey, A. Doyle, J. Forbes, and D. H. Saxon
University of Glasgow

D. T. Hackworth and R. L. Swensrud
Westinghouse Science and Technology Center

T. Ryan and D. Vandergriff
Oak Ridge National Laboratory

S. Newfield and C. Sadler
Los Alamos National Laboratory

OUTLINE OF SUMMARY REPORT

I. Introduction

II. Central Tracking R&D

III. Intermediate Angle Tracking R&D

IV. Engineering

V. Front End and Triggering Electronics

VI. Computer Simulation

References

I. INTRODUCTION

The goal of our subsystem R&D project is to carry out a detailed study and design of a complete wire chamber tracking system for the SSC. The system includes central tracking with straw tube chambers and intermediate angle tracking with wires transverse to the beam direction. The system should provide identification of charged particles over $|\eta| \leq 3$ and momentum measurement over $|\eta| \leq 2.5$.

Some of the collaborating institutions already had funds through the SSC detector generic R&D program. We encountered severe difficulties in funding for those institutions that were depending on funding from the subsystem R&D program; in most cases, that funding was not available until August 1, 1990, which was only three weeks ago. In one case, the institution still has not received funding. In at least two cases, slow progress can be attributed to late arrival of funding. We hope that this situation will be alleviated during the coming fiscal year. Fortunately, in a few cases work was carried out with only the hope of payment in the future.

The institutional participation has evolved somewhat since the Memorandum of Understanding. D. Saxon has moved to the University of Glasgow and has a group there. J. Kadyk's group (including LBL, which was already participating, and SLAC) that had been working on generic R&D has joined ours . The U. C. Davis group has dropped out.

We have made substantial progress in the areas of straw tube R&D, design of straw chamber modules (including endplates for connection of gas, high voltage and electronics), engineering studies for support structures, and design of front end and triggering electronics. We have also made progress in simulation and intermediate angle tracking R&D. We describe the work in more detail in the following sections.

II. CENTRAL TRACKING R&D

Institutions: Indiana University, University of Colorado, Los Alamos National Laboratory, Lawrence Berkeley Laboratory, University of California, Berkeley and Princeton University

Indiana University

Central Tracking

We have been carrying out a detailed study of a modular straw drift cell tracking system for the central tracking region of the SDC detector. Fig. II-1 shows the tracking system proposed by the SDC collaboration. The tracking volume is about 9 meters in length and 3.6 meters in diameter. In the wire tracking alone the total segmentation will be about 0.25 Million channels. The cell cathodes are formed from light weight plastic straws. During the past year we have carried out a large number of tests on 4 mm diameter cells and constructed several prototype chambers. Although more work needs to be done, these tests and prototypes all indicated that a viable tracking system for the SDC detector can be built using straw chambers. We have proposed that the basic building block of the wire drift chamber system be the module. It would contain approximately 236 straw drift chamber cells. Our study of the tracking system this year has covered the details of the straw drift cell, design of structural modules, and the support structure for the entire tracking system.

Straw Chambers

The basic drift cell is constructed with a plastic based cylindrical cathode structure and a 25 μm diameter wire along the axis. The cathode is formed from an outer mylar wrap 12 μm thick and an aluminized polycarbonate film inner layer. We have been using straws manufactured by Precision Paper Tubes, Wheeling, Ill. The tubes are 4 mm in diameter with a 37 μm wall thickness. The standard aluminized coating is 1000 Å in thickness. From one end to the other the tubes have a DC resistance of 100 ohms, the 25

Straw Drift Time

The time between crossings at the SSC will be about 16 ns. For the high rate regions of the tracking system occupancy considerations dictate that the drift time for the for the cell be not much more than 16 ns. Most drift chamber gases have drift velocities less than 50 μm/ns, but a few are in the range of 100 μm/ns. With these fast gases the drift cell cannot be more than 2 mm in radius in these high rate regions. Using a small 6 cell chamber with a length of 20 cm, we have measured drift times for a number of drift chamber gases. Several are shown in Fig. II-2. The best gas we have studied is CF4 - isobutane(20%)[1].

Straw Efficiency

The efficiency for cosmic rays has been studied in a small 6 straw chamber for several gases and preamplifier thresholds. The basic efficiency of the straw chamber should be limited by the ionization cluster statistics in the drift chamber gas. The efficiency is, of course, also a function of the preamplifier threshold which is in turn limited by environmental and electronic noise. Our preliminary study[1] did not use the low threshold preamplifiers we intend to use for SDC, but it indicated that the CF4-isobutane mixture was fully efficient for voltages above 1900 V. These efficiency plots are shown in Fig. II-3. With the acquisition of the low threshold preamps and the final printed circuit boards, these must be repeated.

Straw Spatial Resolution

The spatial resolution for the 6 straw system has also been measured with a number of different gases using cosmic rays. The results for CF4-isobutane are very encouraging. Our initial measurements[1] show an intrinsic resolution of about 100 μm.

Straw Gas Gain

We have measured the gain of the drift chamber for 4 mm straws with a 25 μm

Signal Attenuation in Straws

One of the potential problems with a long straw system is the attenuation of the signal while traversing the cylindrical transmission line to the electronics at one end of the straw. This attenuation is due to the cathode and wire resistance. The resistance of the cathode and wire are both about 100 ohms/ meter. We have measured this attenuation by constructing a 3.5 meter six straw drift chamber. The attenuation was measured [3] using an Fe^{55} source position at various distances from the electronics at one end, and directly measuring the pulse height. The reflected pulse from the unterminated end was also observed and measured. We verified that it could be eliminated by terminating with the characteristic impedance of the transmission line, 350 ohms. The attenuation that was measure is characterized by a 4 meter attenuation length. We would like this to be as long as possible in order to reduce the dynamic range of the signal and the possibility of introducing z dependent resolution functions. This attenuation length can be increased by decreasing the cathode resistance and the wire resistance. We have purchased some Kapton film with 2500 Å aluminum coating deposited. This has 1/4 of the resistance of the polycarbonate film. The wire resistance can be reduced by increasing the wire diameter.[4] We intend to pursue this promising straw and wire variation in tests during the coming year.

Straw Stability

The construction of a long straw drift chamber requires that the sense wire be positioned accurately along the axis of the cylindrical cathode. We have investigated the stability requirements for this geometry.[5] The result of this study shows that with a 50 gram tension a 25 μm diameter sense wire should be electrostatically stable in a 4 mm diameter straw at 2500 V if the support points are about 1 meter apart.. This is quite critically dependent on the alignment of the wire in the straw. We will need to keep the straw and wire coaxial to better than 100 μm. We have designed several wire support systems.[6] The support system we will be using in the future construction of straw modules is referred to as the "double v" shown in Fig. II-5. It is assembled by snapping together

Module Construction

We have built several prototype straw drift chambers this year. They have given us valuable experience in designing a straw drift chamber module that could be scaled up easily to 236 straws and 4 meters in length. There are two aspects of the design that are critical. One is the outer shell of the module and the other is the endplate. The outer shell hold the straws rigidly in position close packed, maintains the alignment along the length of the module and takes the compressional load of the wire tension which is about 12 kg force. We have had several short shells made by Composite Horizons, Duncanville, Ca. The dimensions of the shell are shown in Fig. II-6. These were made with 4 layers of 2.5 mil prepreg carbon fiber tape. We have measured the short module and found it to be within the ±50 μm tolerance we specified. Several short 64 straw modules will be built and tested with the 30 cm composite shells. (We are now beginning the tooling for a 1 meter long mandrel for production of several longer shells.)

We have also made progress on the endplate design. Fig. II-7 shows a detail of the end of a module. In the present design the straws and wire supports will be premounted in the shell. The wire supports will be attached inside the straws and at each end of the straw. At either end the wire supports will be coated with a conducting paint that will contact the inner cathode as well as the neighboring supports, carrying the cathode ground connection out to the inner shell.The shell will clamp the straws and wire supports in a closed packed geometry. The endplate will be inserted into the shell but will not touch the wire supports. The sense wires will be tensioned by solder clips in the endplate. The endplate acts as one side of a gas manifold.The drift chamber gas enters each straw through the same hole that holds the solder clip. The other side of the gas manifold is a plate that contains feed through for the signals, These extend through the gas manifold and make contact with the solder clips. The printed circuit board for the electronics is attached to the feed through plate. This construction results in a very short end section on each module and a very low mass connection. Our goal is to keep this material to a few percent of a radiation length.

with its associated amplifier/discriminators borrowed from SLAC. The beam pipe aperture is about seven inches in diameter. It provides six layers above and six below this space, with well-understood resolution. At 90 μm precision per point, the interpolated reference trajectory will be established to about 30 μm.

This setup, with scintillators, high voltage, and gas supply is now working to the extent of producing pulses into a FASTBUS TDC. The FASTBUS station itself is being assembled in our lab from other funding sources. The last of the hardware has just arrived, and we have begun programming the data acquisition and transporting track reconstruction code from the SLAC computer.

Los Alamos National Laboratory

The FY 1990 effort was initially oriented toward the development of alternative straw modules. This effort was to have included investigating such cathode structures as: "cold formed" half hex sheets, which would be stack bonded; precision made expanded core honeycomb; filament wound straw tubes; and film wound straw tubes. Upon investigation it was determined that the cost of manufacture for any of these methods exceeded the cost of the conventionally produced straw tubes, typical of a paper drinking straw.

This existing process uses substantially more prevision and the most advanced materials available. Although this production process may not meet all the initial design expectations, the cost benefit of this approach is significant.

We were then requested to support other programmatic efforts including the design of a resistive capacitor termination end cap, and to provide basic and finite element analysis consultation on plastic and composite components. The progress of this effort is as follows:

Resistive Capacitor Termination End Cap

We have proposed a resistor/capacitor end cap design, and will present the design

Plastic and Composite Component Consultation

We have provided consultation on the design, tooling, and manufacture on such components as the: wire guide design variations; composite structural support; straw tube material selection; composite straw tube cell; and wire termination clip.

Fabrication and Tooling Support

We have consulted with I.U. and Composite Horizons personnel regarding all phases of manufacture for the composite straw tube cell. We have also agreed to fabricate the one meter long straw tube cell mandrel at LANL.

Lawrence Berkeley Laboratory

During the past year, work has proceeded in several areas leading to interesting and significant results:

1. Investigations of radiation-hard properties of CF_4-based gases.

2. Accelerated aging tests using a variety of gases and wires, using straw tubes and conventional (three-eights inch diameter) proportional tubes.

3. Studies of the plasma chemistry of avalanche processes in various gases.

4. Measurements of the effects of Freons, and especially Freon 11, on wire chambers using an argon/ethane or dimethyl ether gases, leading to new and useful results.

5. Measurements of the effect of avalanche-generated heat on the gain in straw tubes was measured. It was found that heat is carried away efficiently (and almost entirely) by radial conduction. This observation

Inhibition of Wire Aging Using CF_4

The gas mixture CF_4/isobutane (80/20) recently has been established as a very radiation-hard gas for wire chamber use (see Appendix). It is also expected to have good spatial resolution and large drift velocity, both desirable properties for use at SSC. Experimental tests of these latter properties are in preparation.

A series of aging tests on CF_4 gas mixtures strongly suggests the validity of the Yasuda model of competitive ablation and polymerization (CAP). In this model there is a steady-state balance between polymer etching and deposition. Support for this model was found in the following tests using the CF_4/isobutane (80/20) gas: (1) the aging rate is very low (<2%/C/cm); (2) an anode wire which has been "aged" (coated with silicon polymer) by operating with argon/ethane gas bubbled through silicone oil is subsequently restored to full gain by operating with the CF_4 mixture (Appendix) which "etches" off the coating; (3) a similar test, but replacing the CF_4 mixture with argon/ethane or dimethyl either did not restore gain by etching off deposits; (4) bubbling the CF_4 mixture through silicon oil resulting in a very low aging rate (3%/C/cm), a procedure which has been used to prepare a "coated" wire using argon/ethane (200%/C/cm). Tests with other gas mixtures containing CF_4 are underway (e.g., CF_4/DME). Since CF_4 is somewhat expensive, it is desirable to find a mixture with a smaller CF_4 component, but still with good aging properties, and yet maintaining the good spatial resolution and high drift velocity. It would also be desirable to find a mixture which is non-flammable and contained no hydrogen (such as in isobutane) so as to avoid noise resulting from collisions with neutrons inside the SSC detector.

Accelerated Aging Tests

A wide variety of gases, including the CF_4/isobutane mixture discussed above and dimethyl ether (DME), has been tested over a period of two to three years and recently the results were published in the IEEE Nuclear Science Symposium Proceedings. Pure DME was found to cause very small aging (<10%/C/cm) with the resistive wires Stablohm and Nicotin, a result in contradiction with published results (more below on aging in DME). The aging effects of various oils and tubing commonly used for plumbing were measured

consists of a gas chromatograph to separate the constituents, and a mass spectrometer to identify them. A cryotrap, which can be set to any temperature between ambient and the liquid nitrogen boiling point, is used to concentrate the sample over some time interval (typically ten minutes). The observed signals are quite strong, with excellent signal/background. A permeation device is used to introduce trace components to the gases under test to understand their effects upon the observed molecular species, and upon the aging rate. Among many interesting results found is a large shift downwards in the average molecular weight of the species that are observed when water vapor or oxygen is present even at low concentrations. We believe this has an important bearing on wire aging, since the heavier species are more likely to deposit on wires (they are less volatile). This effect is similar to the observation in "classical" plasma chemistry (1 Torr pressure, rf discharge) where polymer growth is inhibited by oxygen (or oxygen-containing molecules).

Effects of Freons on Aging.

It has been thought for some time that Freons (i.e., chlorofluorocarbons) are powerful agents for inducing aging, especially Freon 11 ($CFCl_3$) in DME, where 1 ppm was thought to be significant. Our recent tests show that Freon 11 has virtually no effect upon permanent gain loss in either DME or argon/ethane, though there is some loss in pulse-height resolution. It is further shown, by direct measurement and by calculation (which agree), that the decrease in gain when DME is used can be directly attributed to Rayleigh ("fractional") distillation of DME and Freon 11 within the gas supply cylinder.

Gas Avalanche Heating Effects

A concern for use of wire chambers at the SSC has been the effect upon avalanche gain due to the local temperature rise due to the relatively large avalanche heating anticipated at the SSC. Naive calculations, assuming laminar flow and heat transported via the heat capacity of the gas predict a temperature rise of thousands of degrees, and only with thorough heat mixing inside straw tubes and very high gas velocities (several cm/sec) are temperature variations kept within acceptable limits. In a set of measurements using a

measurements of temperature rise. This threefold agreement also was valid over a range of power input, and the temperature rise in the most severe SSC environment is only expected to be 0.1°C per straw tube, which is more than an order of magnitude below a reasonable limit. This observation should avoid the necessity for high flow rates in straw tubes, which will simplify considerably the design of the gas system.

Princeton University

We outline the major items of work at Princeton on R&D for straw tube tracking during the past year. The $135K allocated for this by the DOE SSC Division has not yet been received at Princeton. The work accomplished has been supported by funds from the DOE HEP Division, and by redirection of funds from the DOE SSC Division that were allocated for Generic R&D on Silicon Drift Chambers.

The physics motivation for our work on straw-tube tracking has been described in the Bottom Collider Detector Expression of Interest (EOI0008, May 25, 1990). Preliminary reports of our work have been presented at the Workshop on Major SSC Detectors (Tucson, Feb. 19-23, 1990),[7] at the IISSC Industrial Symposium (Miami, Mar. 14-16, 1990,[8] and at the International Conference on Advanced Technology and Particle Physics (Como, Italy, June 11-15, 1990).[9]

Work accomplished in FY 1990:

1. Purchase of 3000 sets of Ultem feedthroughs, brass taper pins, and aluminum collars for 7-mm-diameter straws, according to designs from an Ohio State U.[10]
2. Winding of 4 sets of straw tubes ($1500 total) by Stone Industrial for prototype tests.
3. Purchase of Makrofol conducting polycarbonate foil, 0.5-mil thick. An attempt to copperize this failed. It can be aluminized to about 1 ohm per square by Sheldahl - this is the standard cathode material in use.
4. Purchase of conducting Kapton foil, 0.85-mil thick. Kapton can be copperized. 0.5-mil thickness is available, but with a $200[illegible]

8. Purchase of a set of 25 mandrels that can be inserted into straws during glueing.
9. Purchase of a N_2-driven glueing apparatus.
10. Assembly of a 21-tube prototype (along with M. Convery and D. Marlow of Princeton University), using the mandrels and glueing apparatus of items 9 and 10.
11. Purchase of LeCroy electronics for this prototype (as the electronics expected to emerge from the Front-End Electronics Subsystem R&D are not yet available in sufficient quantity).
12. Construction of two kinds of wire-tension monitors. Results from these have pointed towards an improvement in the OSU scheme for tensioning the wire in the straws.
13. Pressure tests of straws, showing that the straws can hold 10 atmospheres.
14. Creep tests of straws, showing that a 2-m-long straw subject to a 1-lb weight stretches about 10 mils over a 2-month period. The straws also show expansion and contracting of about 10 mils during temperature shifts of 10°F (as expected from the known thermal expansion coefficient).
15. Demonstration that straws could be pressurized during assembly, as an alternative to the use of mandrel inserts.
16. Design of an assembly fixture for 8-layer superlayers using grooved vacuum pads.
17. Design of a coaxial straw end-plug that incorporates gas and high voltage distribution, signal transmission, and wire tensioning. Custom high-voltage capacitors have been obtained for this.
18. Study of the wire instability in long straws, showing the effect of a wire offset and of deformations in the straw.
19. Construction of several prototype straws for studies of gas gain and drift timing. Some modules can be pressurized.
20. Development of a technique using a 0.3-ns N_2 laser pulse to eject single electrons from the cathode wall of a straw.
21. Characterization of gas gain as a function of temperature, pressure, and applied

atmosphere) is 50 μm resolution in $Ar/CO_2(50/50)$ and CF_4/Isobutane (85/15) mixtures.

23. Comparison of amplifier performance between the LeCroy TR402 amplifier and the U. Penn straw-tube amplifier. The latter is measured to have about 1300 electron equivalent noise (15 times better than LeCroy), while contributing less than 0.5 ns to the timing uncertainty.
24. Development of a model of straw-tube response including characterization of the avalanche, electrical performance of the tube, and of the amplifier (with M. Lundin of Fermilab). This permits extrapolations of measurements with the N_2 laser to wider regimes.
25. Construction of a precision gas-mixing system, with control of both flow and pressure.
26. Initial development of a gas-analysis capability based on gas chromatography.
27. Simulation of overall system performance in the SSC environment (with L. Stutte of Fermilab).

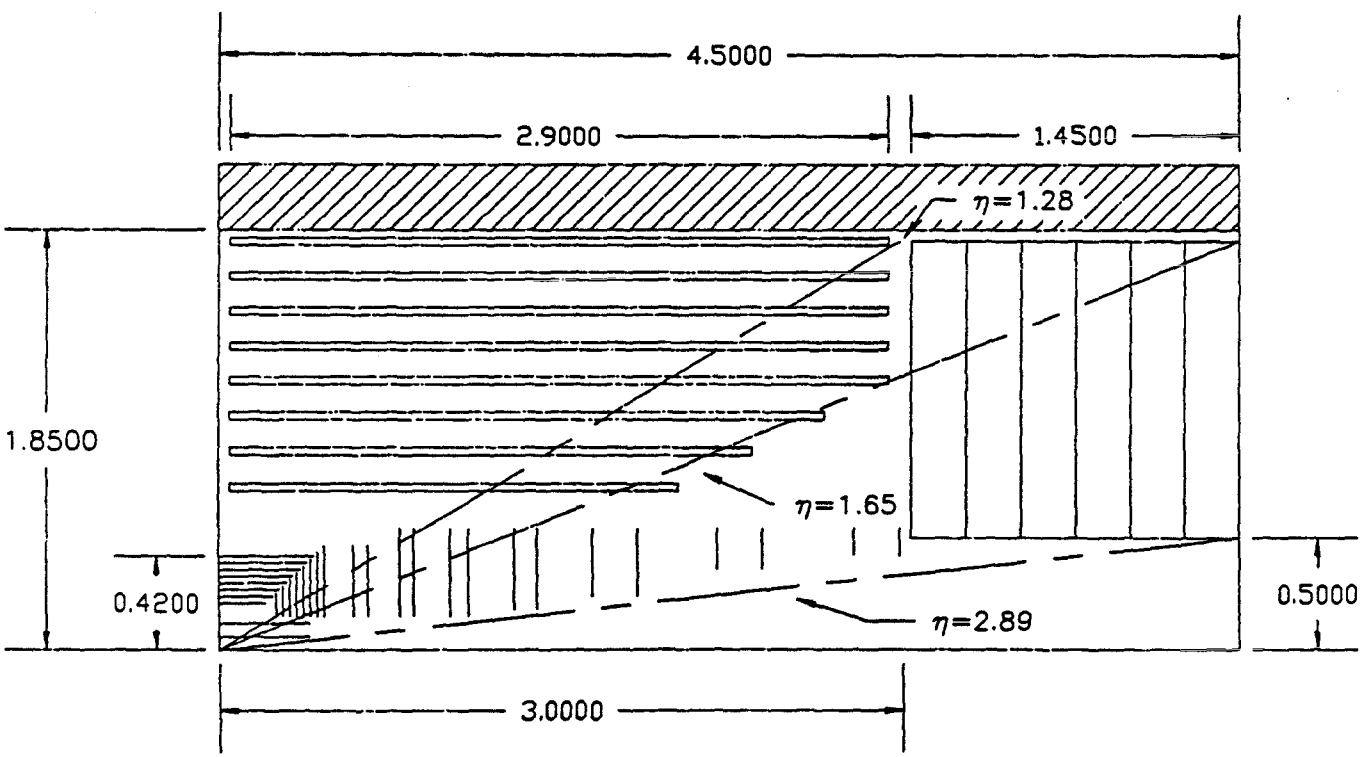

Fig. II-1 The central tracking system for the SDC. This drawing shows the positions of the silicon tracking system near the beam pipe, the straw drift tubes at larger radii, and the intermediate tracking system.

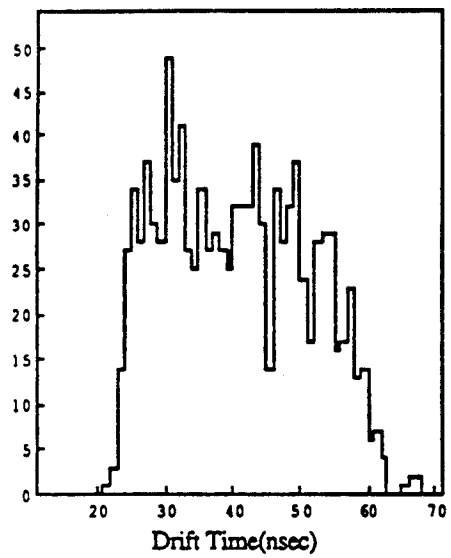

Ar-Ethane(50%)
1700 V Threshold 0.6 mV

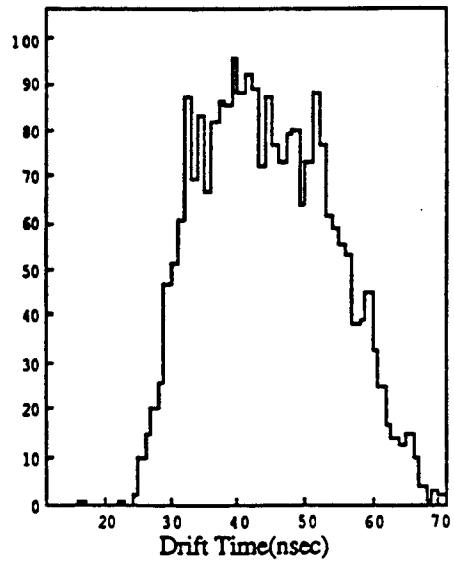

HRS (Ar-CO_2(10%)-CH_4(1%))
1350 V Threshold 0.6mV

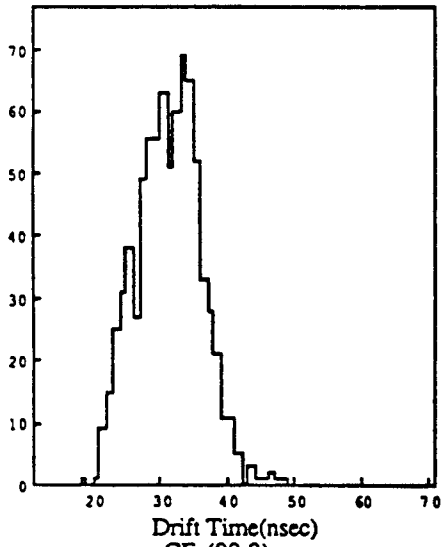

CF_4(99.9)
2300 V Threshold 0.6 mV

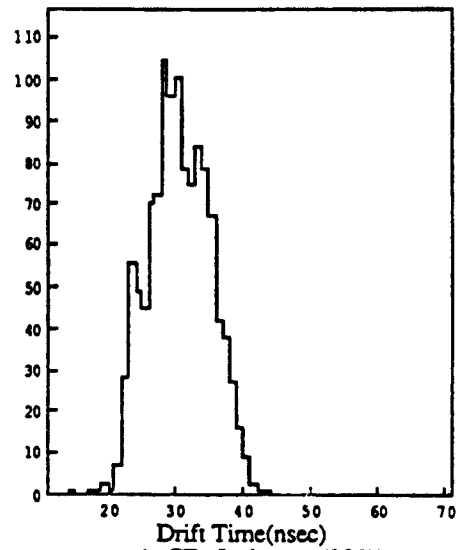

CF_4-Isobutane(20%)
2100 V Threshold 0.6mV

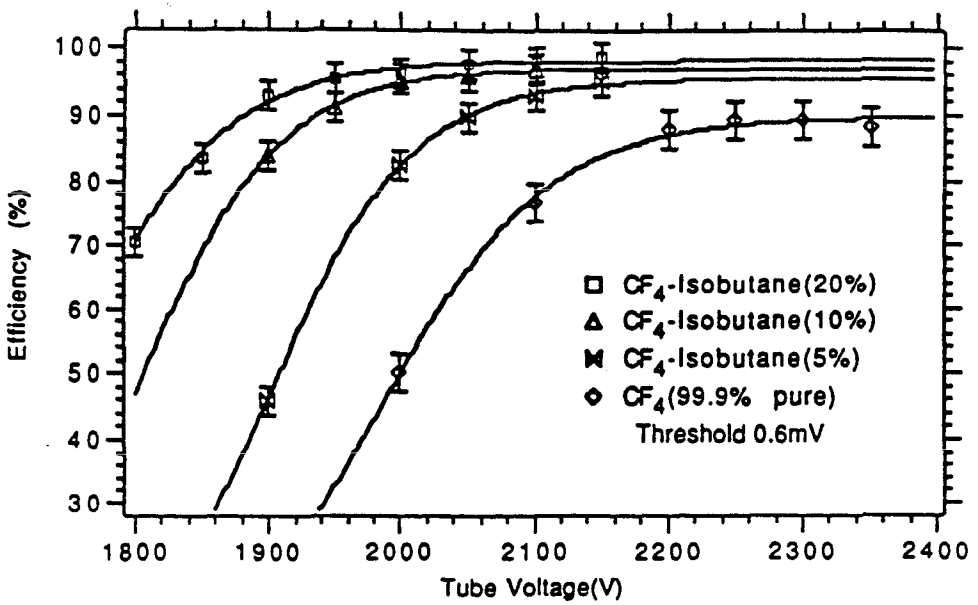

Fig. II-3 The efficiency for cosmic rays traversing a 4 mm straw for several different isobutane fractions in CF_4.

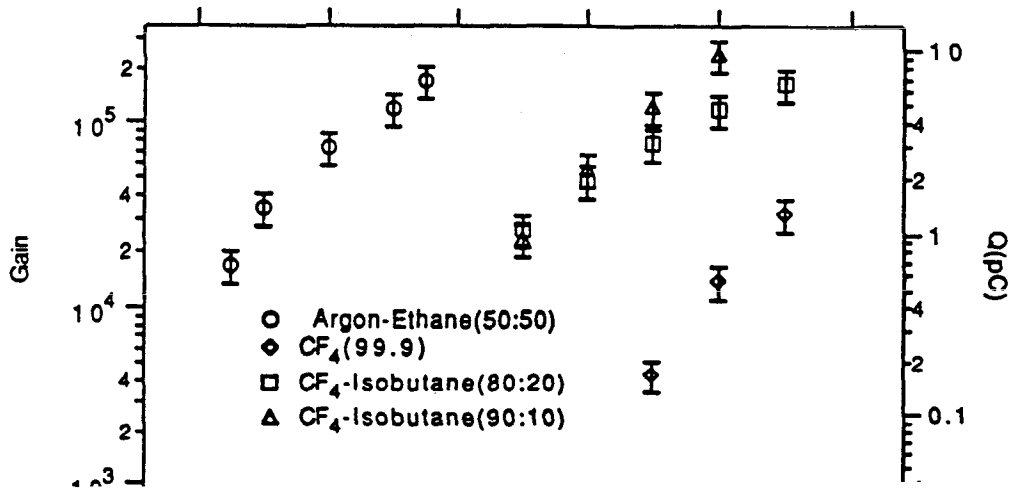

18-APR-90 Sense-wire collar, double "V" design

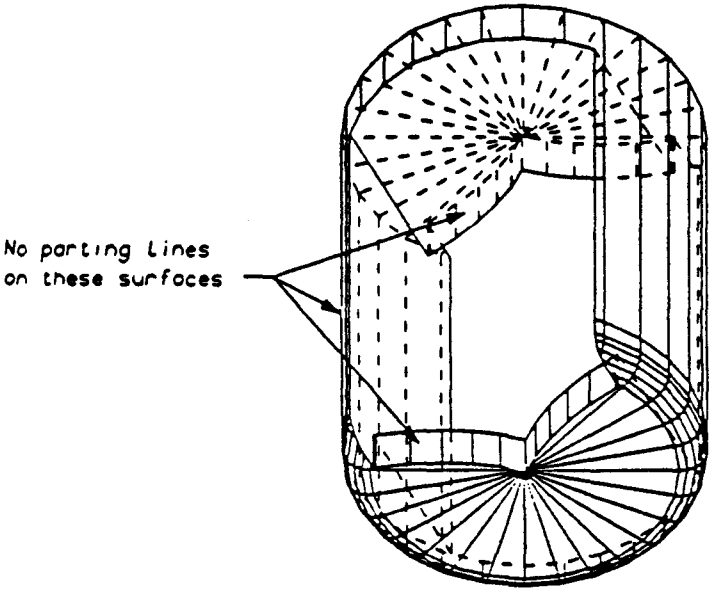

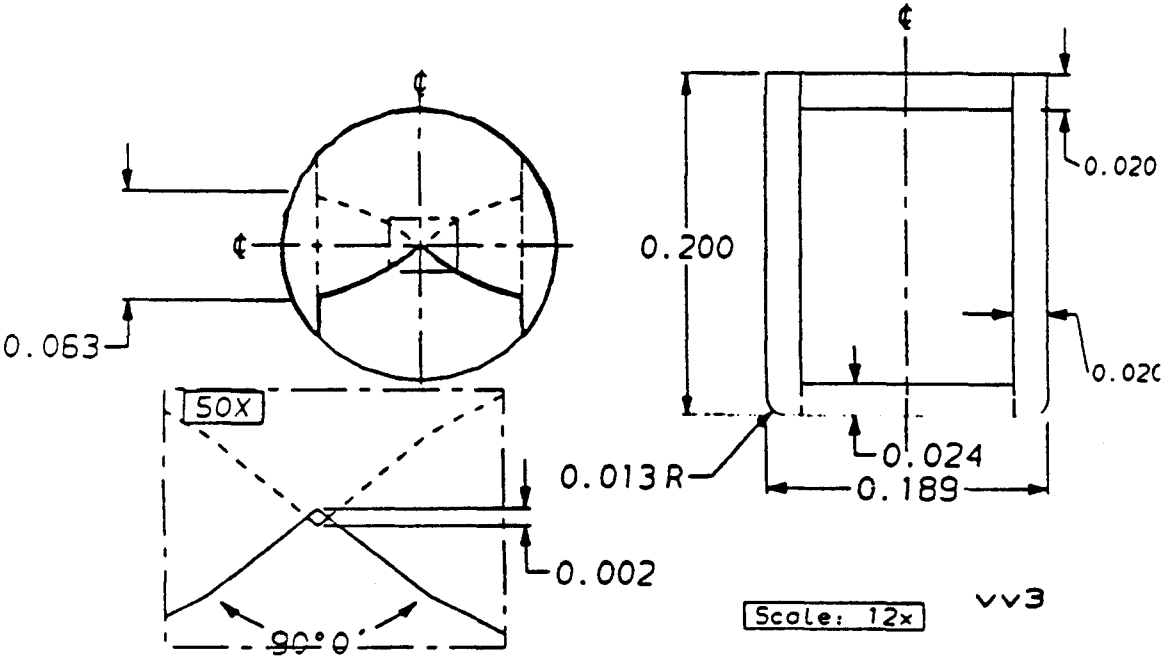

SHELL DIMENSION ANALYSIS AT SUPPORT STATION

Spacer diameter:	.1560
Conductive paint, 2x0.0005:	.0010
2x str.wall:	.0028
Spacer dia. compressed:	-.0002
Packed diameter,D:	.1596
Shell width, (7.062xD):	1.1271
Short diag. (8xD) =	1.2768
Long diag. (13.124xD) =	2.0945

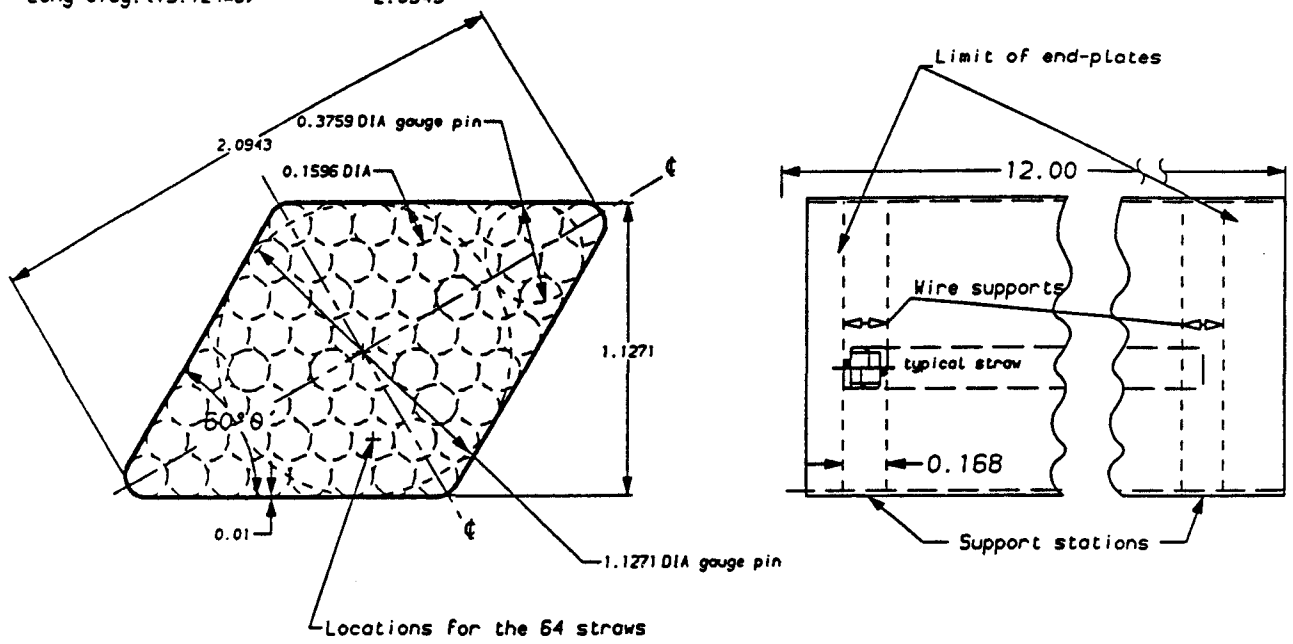

Fig. II-6 Details of a 64 straw module shell showing the position of the straws in the completed shell.

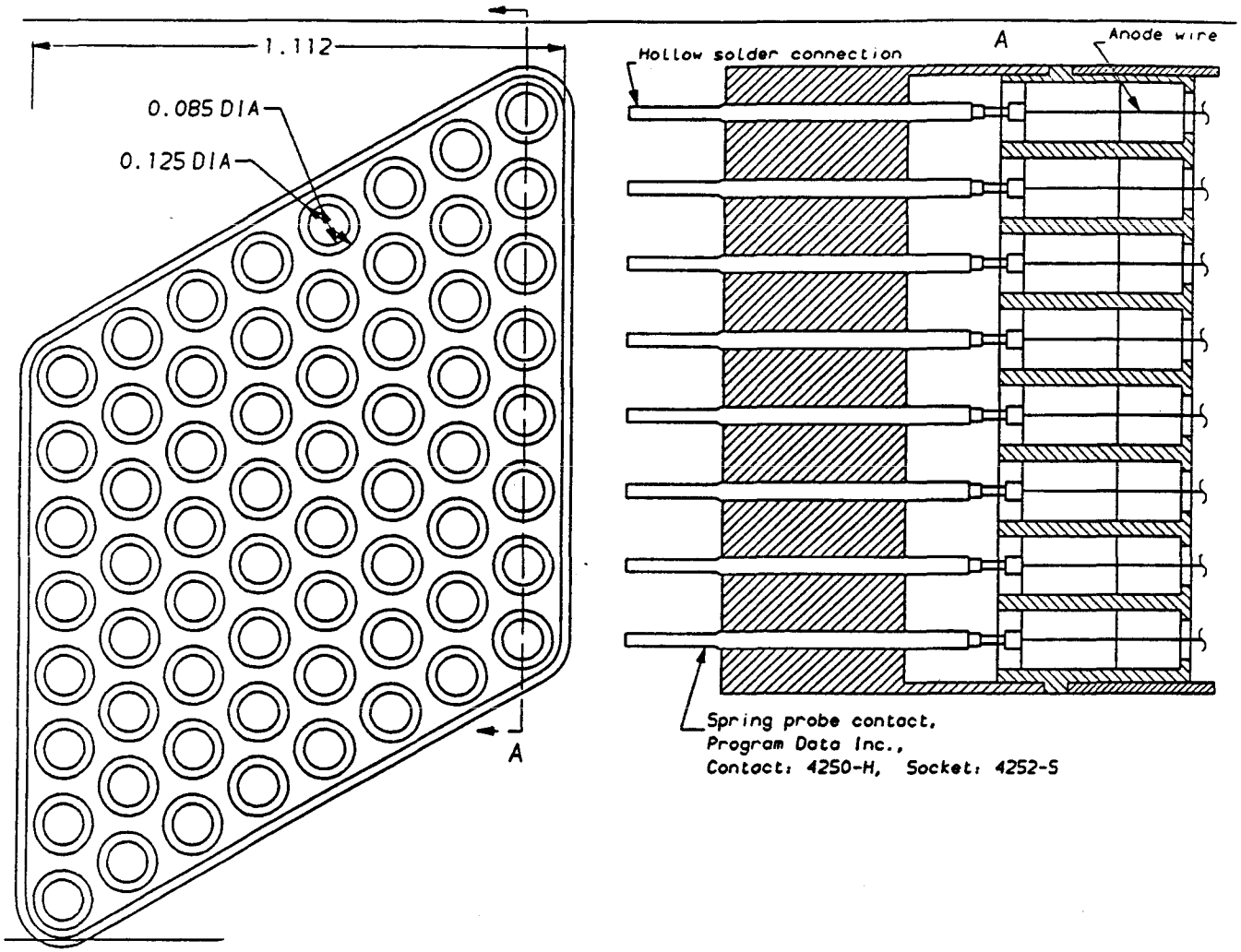

Fig. II-7 Design of the end plate for a 64 straw module. In this two part design the wire tension is held by one section and the electronics attached with a "pogo stick"

III. INTERMEDIATE ANGLE TRACKING R&D

Introduction

Part of our 1990 proposal included justification for development of techniques for a gaseous charged track detector to cover the non-central, intermediate, rapidity range $1.4 < |\eta| < 2.4$ of a hadron supercollider experiment. Coverage of this rapidity range is extremely important for the best possible acceptance for new physics, and it is not easily accessible with sense wires oriented as in a conventional central track detector; i.e, parallel to the beam axis. Called the Intermediate Track Detector (ITD), it would possibly also include enhanced electron identification by means of simultaneous detection of transition radiation (TR) X-rays.

In January 1990 the groups who are more immediately concerned with this part of the our proposal and who have relevant experience, namely from the H1 (University of Liverpool) and Zeus (University of Glasgow, Rutherford Appleton Laboratory - RAL) experiments at HERA, undertook to commence work in preparation for the design of a such a detector using a small part of the funding awarded to the subsystem. In February 1990 requests to the UK SERC by both the Glasgow and the Liverpool groups were approved for funding from October 1990 for detector R&D work concerned with developments specifically for hadron supercollider ITDs. In July 1990 the RAL group requested and were granted support for the project from funds available internally at the laboratory which are earmarked for development.

Since January 1990 three major activities have begun about which progress is reported here. First, using test chambers already constructed for developments in preparation for the Zeus experiment at HERA, a program of measurements of fast drift chamber gases in crossed electric and magnetic fields is underway. Second, using

ITD Layout

Our "prototype" ITD is the H1 FTD at HERA which is now being installed. It operates in a uniform magnetic field[11] with established drift chamber gas mixtures (drift velocity 30 to 50 $\mu m\ ns^{-1}$ and Lorentz angles 25 degrees). The uniformity of the solenoidal field (1.2 T) is fully exploited by employing radial wire drift chambers for optimized track pattern recognition, the best possible momentum resolution, and effective track triggering. The remaining space point ambiguities are resolved with modules of "planar" sense wires following familiar "x-u-v" orientations[12]. The high bunch crossing rate at HERA (96 ns) is monitored using fast multi-wire proportional chambers with pad read-out within a bunch crossing interval. Obviously the experience which is gained with the H1 FTD in the next two years can be expected to have a major influence on the design of the SDC ITD.

The choice of radial wires in such a configuration has a number of advantages which have justified their use in the H1 experiment at HERA. Those of relevance to SDC are listed:

1. The timing measurement from the transverse drift always measures track sagitta, even in the presence of substantial Lorentz angle, so that the most accurate co-ordinate measurement coincides always with track sagitta in the (r-ϕ) bending plane, thereby optimizing momentum resolution;
2. The pairing of sense wires by connecting each with a corresponding partner in a wedge at roughly 90 degrees yields from current division a measure of the radial co-ordinate (r) of clean hits and thus provides track space points without any increase in the number of read-out channels;
3. In a uniform solenoidal magnetic field, track pattern recognition is greatly eased as tracks are straight lines in the ϕ-z plane;
4. Drift cell aperture increases linearly from the inner radius and is thus matched to greater hit multiplicity at smaller radii.

As a result:

3. In a uniform solenoidal magnetic field, the simple relationships between measured space point co-ordinates ($r.\phi$ and r) and track momentum from an event vertex; namely,

$$\phi = eBz/2P_z + \text{constant}$$

and

$$r = 2\,P_T/eB \sin[\,eBz/2P_z\,],$$

makes for a conceptually realizable track trigger.

The above advantages have greater significance at an SSC experiment.

Our presently favoured ITD configuration Fig. III-1, which is still being evaluated, consists of 6 to 8 "supermodules" per ITD, each consisting of (possibly in downstream order):

A "crossing tagger" consisting of three differently oriented planes of fast MWPC capable of giving a strip signal within at best 1 and at worst 3 or 4 bunch crossings and with a wire and strip spacing of about the 2-track resolution of the radial wire drift chamber (3 below), followed by

Adequate length of transition radiator to guarantee (99% confidence) at least one detectable TR X-ray photon per electron (positron) at 300 GeV/c in

An eight sense wire depth (in z) radial drift chamber with coupled sense wires (in different wedges) read out at the outer radius; the wedge dimension (inner maximum drift length 5.2 mm, outer 15.7 mm) is as large as considered operationally feasible in the SSC interaction region environment (see below) and leads to 300 wedge shaped cells per supermodule.

The fast signals from the MWPC planes facilitate the resolution of spatial and temporal ambiguities in the radial wire drift chambers. Strips are read out into updating discriminator latches clocked by bunch crossing number. The strip structure extends in r (approximately) and is coincident with the isochrones in the radial chambers. Thus the straightforward identification of track vector segments in a radial chamber can be

ambiguities involves a tolerable number of read-out channels. Per supermodule there are 2400 drift chamber sense wires with associated ASIC read-out for both time and pulse profile plus 3 planes of 1500 strips of digital (single bit on/off) channels, possibly with a time depth of 5 bunch crossings. With 6 to 8 supermodules for each ($\pm z$) ITD this amounts to < 19200 drift wire channels and < 36000 single bit on/off MWPC latches for up to 5 bunch crossings (total < 180000 bits) per ITD.

Work is in progress to evaluate the performance of such a layout at the SDC experiment. The momentum resolution of of a system traversing the full ITD in a constant axial field of 1.8 T is found to be

$\sigma_p/p^2 = 0.18\%\ \mathrm{GeV}^{-1}$ - no vertex $\qquad$ $\sigma_p/p^2 = 0.025\%\ \mathrm{GeV}^{-1}$ - with vertex.

As expected it is important for full exploitation of the available $\int B.dl$ of a solenoid and for the best possible resolution of track point ambiguity to include track points from an inner track detector (in SDC a silicon detector). The canonical charge determination on a 1 TeV track is then achieved.

Simulation of a conservative system consisting of supermodules with a radial wire chamber and a crossing tagger based on "conventional" MWPC planes with hit ionization clearing time of 3 bunch crossings is under way. At an SSC luminosity of $10^{33}\ \mathrm{cm}^{-1}\ \mathrm{s}^{-1}$ first results are encouraging. The nature of the problem is summarized in Fig. III-2 with the example of the beam's eye view of a Higgs production event in which are shown a) Higgs event charged particle hits in a radial wire plane available to be found after losses due to overlap (they amount to never more than 10%), and b) all radial wire hits read out in the same radial wire plane irrespective of their origin, namely Higgs event or minimum bias background. When the hits read out are checked against the crossing tagger information and only those verified as being consistent with the trigger bunch crossing (to within a conservative timing precision of 3 bunch crossings) are kept, then the elimination of out of time hits is almost complete. Fig. III-2c) shows the result for the sample event already shown. Fig. III-3 summarizes the improvement with the crossing tagger: from 500 fully

the scatter plots of hit bunch crossing against drift time are shown before and after crossing tagger verification. It seems therefore that:

1. The background minimum bias hit multiplicity at the ITD does not eliminate many hits from typical Higgs trigger events
2. A crossing tagger with a hit dead time of 3 bunch crossings is capable of eliminating most out of time hits.

This work is continuing to include a full simulation of the ITD including backgrounds due to photon conversion and charged particle knock-on.

Radial Wire Chambers R&D

At SDC the implementation of such a transverse radial wire array as the basis for an ITD poses many difficult technical problems which have yet to be fully addressed. They derive from the requirement of nearly a factor 10 increase in the number of wedge shaped drift cells so as to ensure that sense wire current draw and hit occupancy is kept at tolerable levels in the high ambient rate of an SSC interaction region. Some considerations are:

1. A low mass wire fixation technique especially at the inner radius of the detector
2. Low mass and low volume cathode planes with correct resistivity for necessary voltage gradients
3. A means of handling Joule heating in cathode planes which must carry substantial current when operating in a high rate SSC environment
4. Sense wire spacing of at most the maximum drift length ($\approx$ 5 mm) for meaningful isochronicity
5. If used with a fast gas, drift cell operation with Lorentz angles which are substantially larger than hitherto
6. Need for additional wire orientation or pad read-out to remove the ambiguity of charge division measurement of the other co-ordinate and to improve its accuracy
7. Use everywhere of radiation resistant materials.

The above difficulties led us initially to consider alternative wire geometries.

construction in which we shall investigate the feasibility of both mechanical construction and operation of small drift cells of suitable dimension. The high density of wires requires a low mass low volume solution for wire fixation. We are using stainless steel wire, which is believed to be less susceptible to ageing problems in a wider variety of gas mixtures than presently used resistive wires such as Stablohm. The wires will be crimped in stainless steel hypodermic needles following D0 and CDF for tensioning and positioning in one coordinate. A comb system is being manufactured for the other co-ordinate. New "High-density D-subminiature" connectors will form the basis of delivering graded HV and bringing out sense signals because they contribute the minimum possible material content other than support plastic and very low mass hollow pins. We are investigating with industry the possibility of manufacturing thin cathode planes with the required resistivity using thin (radiation resistant!) semiconductor films.

TABLE 1

Essential operating characteristics and environment of a radial sense wire in the SDC ITD

Machine luminosity	10^{33} cm^{-2} s^{-1}
Bunch crossing interval	15 ns
<Nr of events> / bunch crossing (σ_{tot} = 130 mb)	1.95
<Charged particle multiplicity / event>	$6/2\pi$ (unit rapidity)$^{-1}$ rad^{-1}
Maximum drift length at inner radius 50 cm	5.2 mm
Maximum drift length at outer radius 150 cm	15.7 mm
Total ion pairs per m.i.p. at normal incidence†	50
Slope of ln(gas gain) v surface field†	0.705 x 10^{-6} m V^{-1}
Positive ion mobility†	1.7 x 10^{-4} m^2 s^{-1} V^{-1}
Sense wire diameter	20 μm
Sense wire surface field	260 kV cm^{-1}
Sense wire position along beam (z)	300 cm
Sense wire pseudo-rapidity (h) bite	$1.44 < /\eta/ < 2.49$
Sense wire gas gain	2 x 10^4
<Current> / sense wire	0.45 μA
<Occupancy> per sense wire (vdrift = 100 μm ns^{-1})	0.26 (c f simulation)
Maximum sense wire hit rate (r = 50 cm)	51 kHz cm^{-1}
Maximum sense wire irradn (r = 50 cm, 10^7 s y^{-1})	0.08 C cm^{-1} y^{-1}

Each radial chamber, and thus the first prototype under construction, will include an X-ray transparent upstream window for efficient TR detection on any of the chamber wires. As in H1 the electrostatic field cage will be closed with low mass low Z materials in a configuration which guarantees the best possible uniformities of timing response for spatial precision, and of gas avalanche gain for pulse integral analysis, together with the best possible ionization collection efficiency for useful X-ray detection. In particular only after successful operation of the H1 FTD in the HERA environment will the rate capability (both signal and background) of the radial chambers and their novel features for simultaneous electron identification by means of TR X-ray detection be finally established.

Calculations of such radial wires in nominal position as per the layout in the SDC EoI[13] are summarized in Table 1. With 300 wedged shaped drift cells of maximum drift length 5.2 mm at the inner radius of 50 cm and 15.7 mm at the outer radius of 150 cm, the current draw remains below 0.5 μA per sense wire for an acceptable gas gain, the chamber lifetime seems acceptable, and calculations of the more obvious effects of space charge do not seem prohibitive. The coupled sense wire occupancy is high but the simulations above already indicate that it may not be prohibitive with the inclusion of a crossing tagger.

The feasibility of such drift cells can only be established after successful operation of the prototype chamber now under construction. If efficient X-ray detection efficiency is to be established with no ionization losses on field (potential) wires, then Fig. III-5 shows that it may be necessary to operate with a somewhat greater drift field than usual (E_{drift} = 1.8 kV cm^{-1}, sense wire surface field $E_{surface}$ = 260 kV cm^{-1}, wire diameter = 20 μm) for adequate gas gain. This may also be desirable if we are to work with a fast gas and manageable Lorentz angle (see section below).

Crossing Taggers

As discussed above the crossing tagger is a set of planes of gaseous proportional detector with cathode strip read-out. Whether we employ wires or knife edge or micron dimension anode strips (lithographically manufactured) for gas avalanching is as yet

ITD supermodule, the MWPCs in the ITD would then also enhance significantly the multi-track reconstruction precision.

Table 2 summarizes the performance of the longest of such "wires", which is tangential to the ITD inner radius of 50 cm, for the conservative lay out of 2 mm pitch used in the simulations discussed above.There seems to be absolutely no reason for concern over operational feasibility of otherwise working proportional planes of such dimension in the SSC environment.

No development work has commenced yet on the development of fast MWPCs for an ITD.

TABLE 2

Essential operating characteristics and environment of the longest MWPC sense wire in the SDC ITD.

Machine luminosity	10^{33} cm-2 s^{-1}
Bunch crossing interval	15 ns
<Nr events> / bunch crossing (σ_{tot} = 130 mb)	1.95
<Charged particle multiplicity / event>	$6/2\pi$ (unit rapidity)$^{-1}$ rad^{-1}
Maximum drift length (parallel to magnetic field)	2 mm
Sense wire pitch	2 mm
Total ion pairs per m.i.p. at normal incidence†	20
Slope of ln(gas gain) v surface field†	0.705×10^{-6} m V^{-1}
Positive ion mobility†	1.7×10^{-4} m^2 s^{-1} V^{-1}
Sense wire diameter	20 μm
Sense wire surface field	260 kV cm^{-1}
Sense wire position along beam (z)	300 cm
Minimum radial distance of sense wire	50 cm
Length of sense wire	100 cm
Sense wire gas gain	2×10^4
<Current> / sense wire	0.015 μA
<Occupancy> / sense wire (v_{drift} = 50 μm ns^{-1})	0.009
Maximum sense wire hit rate (r = 50 cm)	2 kHz cm^{-1}
Maximum sense wire impdn (r = 50 cm, 10^7 s yr^{-1})	0.0014 C cm^{-1} yr^{-1}

Fast Gas Measurements

Given that suitably fast read-out electronics can be developed so that space point precision can be maintained at ~100 μm, it is advantageous (see section above) for gaseous drift chambers in the SDC ITD to have large drift velocity (> ~100 μm ns^{-1}) so that drift cell occupancy is tolerable. Because the drift electric field in the ITD is perpendicular to the (constant) solenoidal field of SDC, ionization drift is at an angle to the former, the so called Lorentz angle, which for a fast gas is likely to be substantial. Therefore for ITD wires strung in planes transverse to the beam axis (and the magnetic field direction), irrespective of their particular orientation, measurements of both the drift velocity and the Lorentz angle are essential if a realistic design of wire layout for an ITD is to be made.

A multi-wire drift cell designed and constructed specifically for this purpose is being used to measure drift velocity and Lorentz angle. The chamber follows closely the design of Atac *et al* .[16] Drift time in a constant electric drift field is measured over perpendicular distances of a 16, 32 or 48 mm from a sense wire, and drift direction is measured using the known position of irradiation by a collimated Sr^{90} source (β end-point energies 0.55 MeV Sr^{90}, 2.23 MeV Y^{90}) and the position of gas avalanche along the sense wire by means of the induced signal on adjacent cathode strips. The chamber itself is operated in the uniform magnetic field of a C-magnet ($B \leq 2T$) with the plane of ionization drift and sense wire perpendicular to the magnetic field direction.

The test chamber has been operated successfully in Ar-CF_4 mixtures with to date no evidence that prohibitively large sense wire surface fields or extreme drift fields are necessary for acceptable operation of the chamber. Therefore acceptable ranges of gas avalanche gains and suitable drift velocities are possible in a substantial crossed magnetic field with gas mixtures which include large proportions of electronegative CF_4 quencher. The effects of CF_4 on materials used in chamber construction are also emerging; for example we have observed significant shrinkage of epoxy-glass support columns after a couple of months of test operation.

after further study. In finite applied magnetic fields where our measurements are unique, there is however a substantial systematic discrepancy between the measured Lorentz angle and the calculated prediction. These calculations involving CF_4 are new so the discrepancy in Lorentz angle should not yet be regarded as established.

It is already clear however that the use of CF_4 as a major component of drift chamber gas for the purpose of increasing ionization drift velocity to at least 100 $\mu m\ ns^{-1}$ is confirmed and for the first time demonstrated in substantial crossed magnetic field. Nevertheless its use in a magnetic field of ~1.8 T (likely in SDC) with a suitable drift electric field may involve Lorentz angles substantially greater than 45° unless the chamber can be operated with a high drift field $\geq 1.8\ kV\ cm^{-1}$. As mentioned above this may anyway be necessary if adequate sense wire surface field for acceptable gas gain is to be obtained.

A major problem associated with the use of CF_4 is the chemical effect it has on materials familiar to us in the construction of low mass drift chambers, e g epoxy based composites. As mentioned above we have already observed prohibitive shrinkage of epoxy-glass based material. We are therefore now carrying out measurements of mixtures with N_2O, which on paper looks also to be suitable for drift velocities of 100 $\mu m\ ns^{-1}$, as quencher while we prepare a new prototype using CF_4 resistant materials. To date it is not yet clear that we can achieve adequate avalanche gas gain in the externally applied magnetic field.

Electronics

To date all our work has involved the use of read-out electronics used in our HERA experiments, namely preamplifiers and 100 MHz FADCs. Developments of future read-out electronics and associated data reduction systems will commence as we gain understanding of the nature of the signals from our smaller SSC size drift cells.

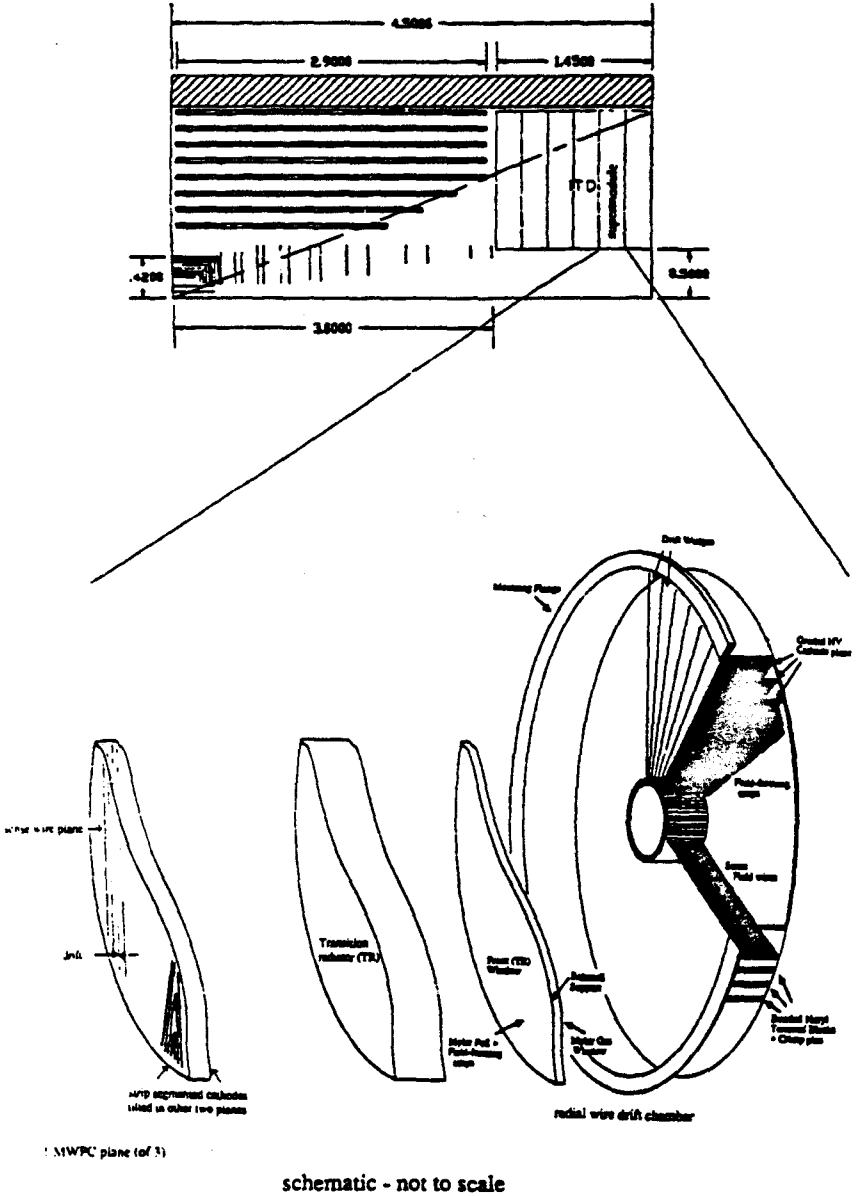

schematic - not to scale

Fig. III-1. A proposed ITD layout in SDC; the space for the ITD is taken from the SDC EoI[13]. the ITD consists of a number (perhaps 6) supermodules each consisting

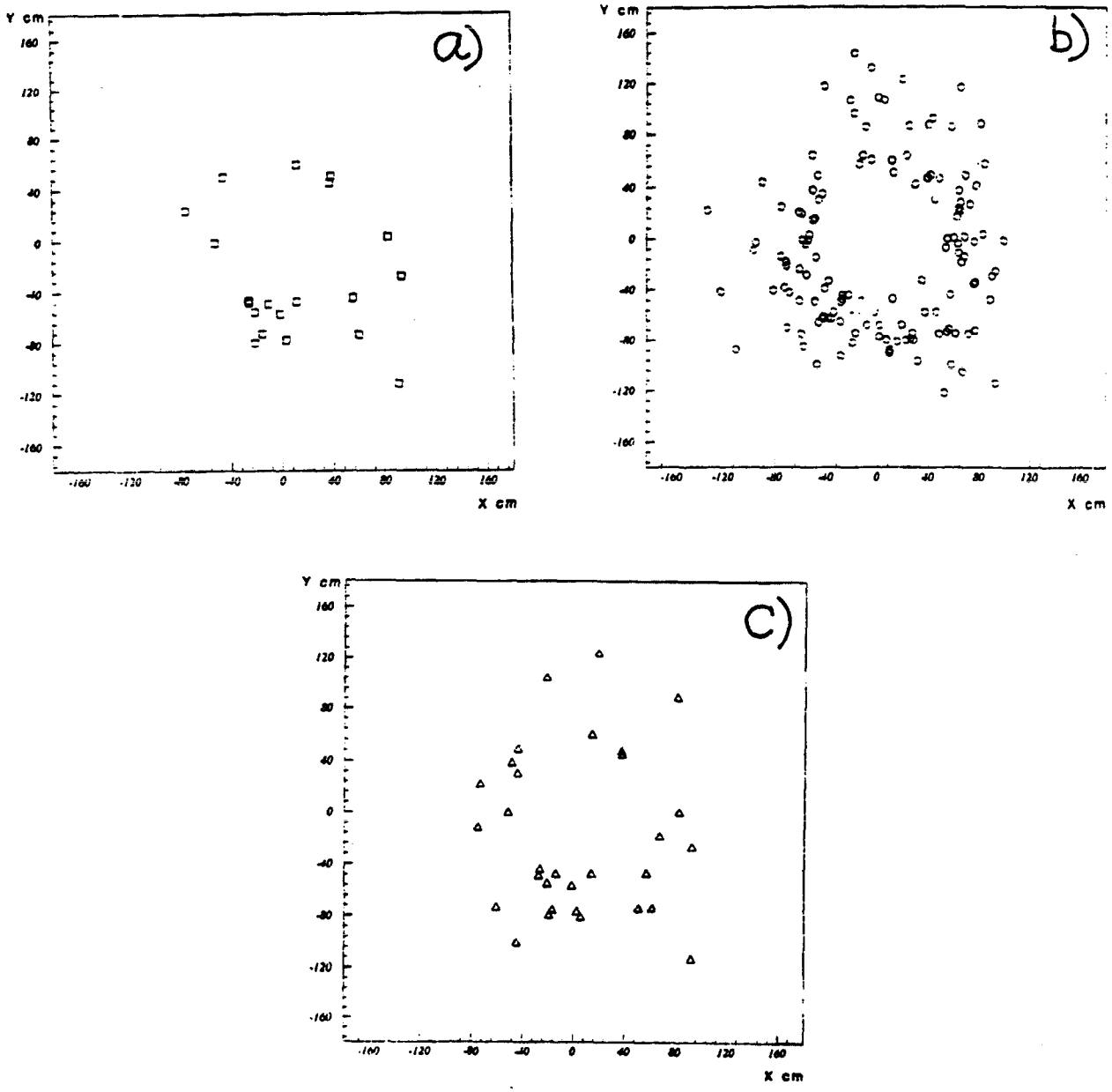

Fig. III-2. a) Impact positions on an ITD drift chamber plane (x,y) viewed along the beam axis (z) due to all secondary charged particles from a Higgs production event where a good radial wire drift chamber hit is not lost due to the proximity of any

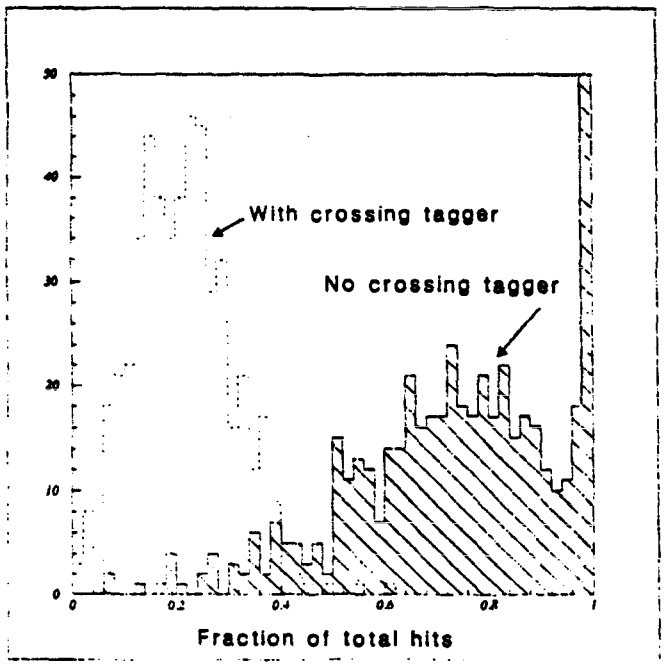

Figure 3 a)

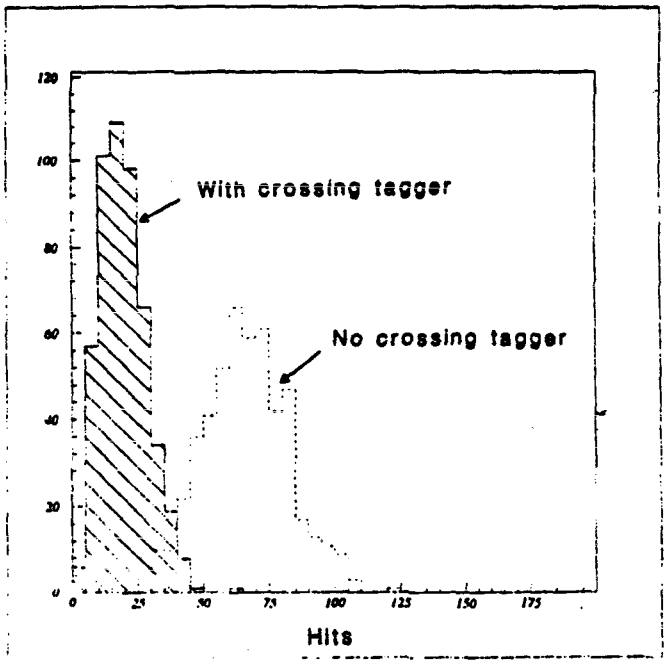

Figure 3 b)

Fig. III-3. a) Histogram of the fraction of reconstructable hits in a radial wire plane for 500 triggers attributable to Higgs production before and after verification of each hit

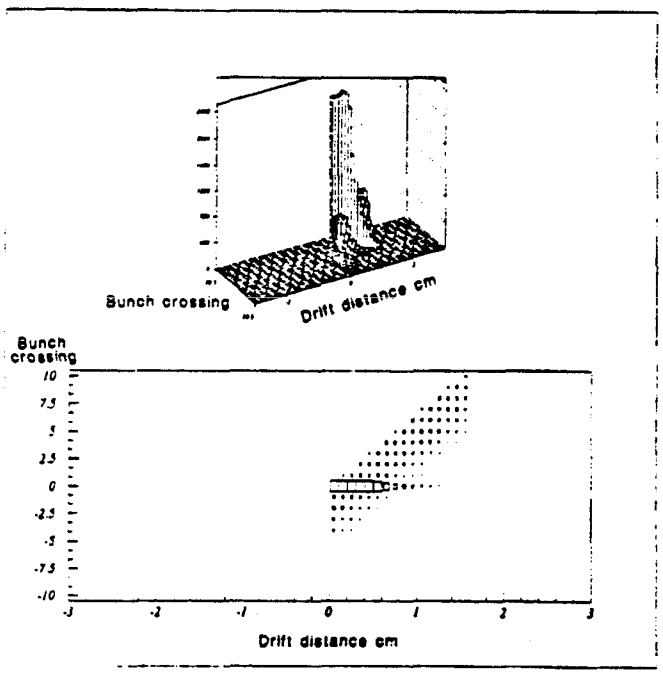

Figure 4 a)

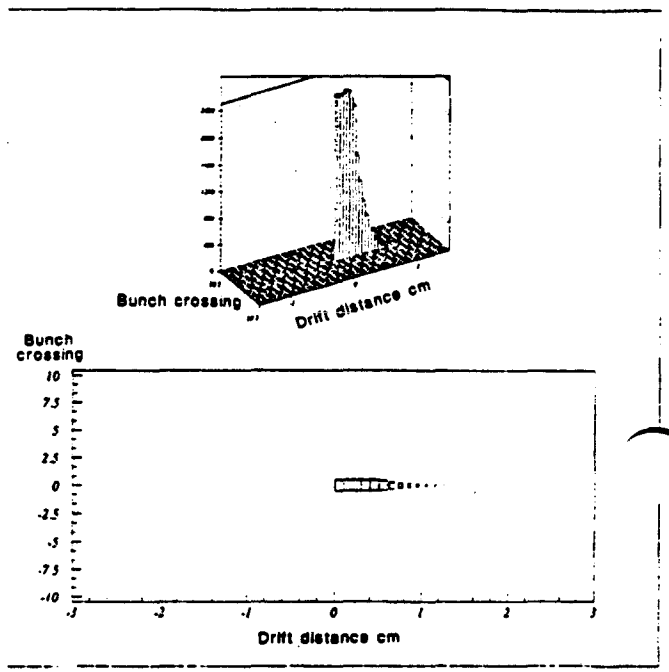

Figure 4 b)

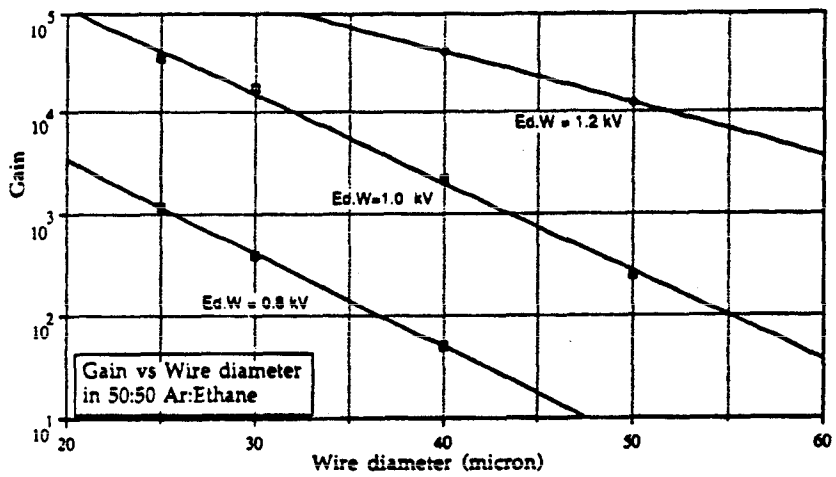

Figure 5

Fig. III-5. Small cell operating conditions summarized as contours of gas gain against wire diameter for an Ar:C2H6 50:50 gas mixture; each contour corresponds to a different product Ed.w of drift field Ed and cell width w in kV. It is clear for small width cells it is necessary to work with substantial Ed and the smallest diameter sense wire (20 5m).

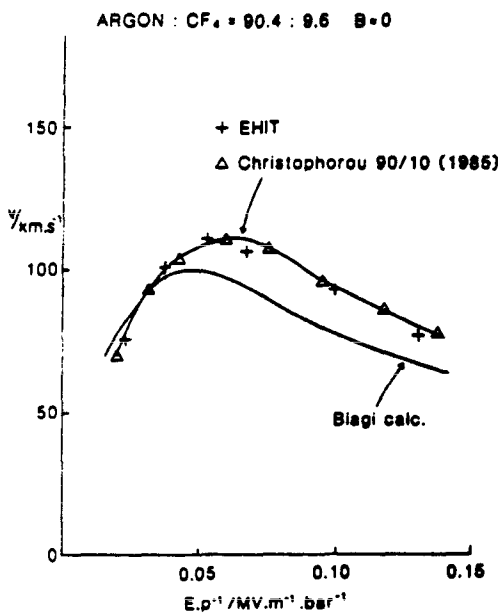

Figure 6 a)

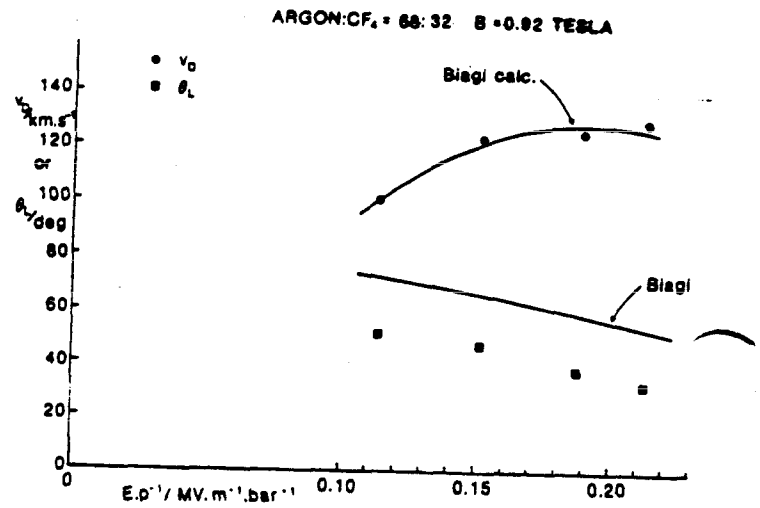

Figure 6 b)

Fig. III-6. a) Drift velocity measurements as a function of surface field for Ar:CF4 90:10 gas mixture in zero crossed magnetic field; also shown are the 1979 measurements of Christophorou et al.[19] and the results of a theoretical

IV. ENGINEERING

Institutions: Westinghouse Science and Technology Center and Oak Ridge National Laboratory

Westinghouse Science and Technology Center

Summary

Westinghouse is in the process of completing the first phase of a preliminary conceptual design, evaluation, and analysis of the feasibility of building a modular type straw tube central tracker for use in the Superconducting Super Collider at the SSC Laboratory. The following list summarizes the status, results, and conclusions of that work:

1. A specification describing and documenting the system has been written.

2. Concept layouts of the following have been developed:

   a) Several conceptual versions of the tracker
   b) Several module cross sectional geometries
   c) Fabrication and assemblies for modules and support structures
   d) Proposed alignment equipment and methods for obtaining required alignments
   e) Module design and fabrication for needed automation

3. Module sizing and spacing geometrical calculations have been done.

4. Conceptual evaluation indicated that for several reasons, including potential for automation fabrication and assembly, ability to accommodate maintenance and repair, and potential for good alignment, the design is very attractive.

A module based central tracker using straw tube technology would have advantages such as simplicity, stability and repairability. With respect to mechanical engineering design issues, conceptual feasibility has been demonstrated, but many conceptual and

ultimately be a subsystem of an overall detector for use in the Superconducting Super Collider at the SSC Laboratory near Dallas, Texas.

Figures and supporting documents referred to in this report are but a few of the many generated during the course of the study. These attached documents are intended to be representative. To prevent this report from becoming burdensome the majority of the balance of the material in the form of an approximately 100 page hard copy viewgraph presentation is attached but is only a reference document with respect to this report.

Functional Design Requirements Specification

A specification describing and documenting the system was drafted and revised twice. This document is a "living document" that requires periodic revisions as the conceptual design process evolves. The specification contains a general description, guiding physics principles and other design considerations. Firm numbers and requirements are defined in the component constant and design limit sections of the specification.

Materials

Material requirements for inactive or structural components in detectors from the engineering sense are very restrictive. The support structure materials must be of minimum material (infinitely thin) but of maximum stiffness (infinitely stiff). These are conflicting requirements, of course, and a compromise is required. Additional material requirements require stability (minimum creep) and resistance to radiation (radiation hard). Beryllium is the best known material to satisfy the above requirements, but because it is costly and difficult to work with, graphite fiber composites have been selected.

Concept

The concept for this tracker has a basic building block called a module. A module consists of eight layers of 4 mm diameter straws, approximately 32 straws wide surrounded by a rectangular shaped shell of graphite composite of 10 mil thick wall. These nominal 130 by 28 millimeter modules of roughly 3 meters long are arranged in eight

Conceptual evaluation indicates that for several reasons including potential for automatic fabrication and assembly, ability to accommodate maintenance and repair, and potential for good alignment, the design is very attractive.

Assembly

The assembly sequence developed here describes the support structure methodology. This methodology dictates that to get good quality micron type long term alignment requires: 1) structural stability by using an absolute minimum number of mechanical joints and thus forming a monolithic support structure with glue joints between graphite composite components, and 2) elimination of tolerance buildup between components by a one step final alignment on the fully assembled support structure in its fully simulated in-service gravity loaded support environment. This strategy is not only needed, it reduces costs by requiring precise registration of components only at the module-structure interface referenced to the overall support points.

Module and structural component fabrication (which can be done in parallel), the assembly sequence, and required conceptual tooling is described chronologically in the following paragraphs. The first parallel operation is to fabricate the module shells, followed by assembly of the straws, wires, and electronics into the shells. The shells would have previously been fitted with three key type attachments along the length where it interfaces with the support structure. The keys are precisely located to the inside surface of the module via precision and thus repeatable tooling.

In parallel to the module fabrication and assembly, the support structure cones and disks shown in Figure IV-2 are fabricated on tooling while the inner and outer torsion cylinders are fabricated on mandrels. None of these components, their assembly shown in Figure IV-3, or the assembly of the two halves shown in Figure IV-4 are required to be manufactured to tolerances for precise registration.

The support alignment shown in Figure IV-5 establishes the precision. The support structure equipped with equivalent module temporary weights is mounted in a fixture that

Analysis

The analysis performed as part of this study has been limited to geometry studies aimed at establishing a concept. Module shape issues such as rectangle versus trapezoids versus parallelograms, chord versus arc inside and outside surfaces, stacked versus nested straws, and equal versus unequal radial spacing are not addressed. Five candidate module shapes have been studied. The nested trapezoid shown in Figure IV-7 is the most viable candidate, because it is the most compatible with a good trigger while producing the most stable shape.

Several computer programs were written to study compatibility between superlayer and missed hits. It is felt that at least a 3 millimeter gap between modules would be required for the support structure. An interesting innovation of unequal radial spacing between modules reduces the required spacing between modules for support structure can be maintained while reducing the number of missed hits to zero.

The geometry study for stereo layers is in its infant stages. The unequal radial spacing appears to render the design of the stereo layers less complicated.

More geometry analysis remains to be done which mainly includes a three dimensional solid model. A finite element deflection analysis of the entire structure must also be performed.

Oak Ridge National Laboratory

Indiana University 64 Straw Array Analyses

The structural response of a prototypical 64 straw array module was analyzed, the results of which are summarized herein and documented in MMES Report DM-017040-001. It was assumed that pressure can be exerted on the straws and wire supports by either of the following: (a) by first warping the parallelogram shell, thereby increasing its volume,

adding a .004-in. (.1 mm) shim all around the shell (between the shell and electrical supports called M&M's).[6]

The same finite element model was used both for the analysis of deformation of the M&M's as well as for the deformation of the straws in a plane remote from the plane of electrical supports (M&M's). This was accomplished by using different properties for the M&M's than for the straws.

It was found that the M&M's remain round and the deflections range from about 1/3 of a mil (.001-in/3) in the center to .004-in. at the outside edges. No problem in stresses were encountered.

The resulting deflections in the straws due to the equivalent .004-in shim all around between straws and shells, caused the interior straws to become hexagonal as desired, but the straws become pentagonal along edges and distort badly at the corners. It was determined that there was little difference (.0005-in. maximum) in the deflection of the straw sections centered by the M&M's and the straw sections remote from the M&M's.

It was found, however, that the membrane hoop stress, induced in the straws (-154 psi compression), far exceeded the buckling stress of -12.8 psi; thus, the straws would buckle (become unstable). Because of tolerances and variable clearances, only a few of the straws would buckle, resulting in only a few straws to distort, squirm, and to destroy the symmetry.

Another FEA model was developed to examine a 1-G load response and the effect of a 50 gram compression load induced by the sensor wire tensioning. The cross section of the previous model was extruded 12-inches and appropriate end conditions were applied. The results of the analysis show maximum deflections of 8.34×10^{-5} inches for gravity loading and 2.26×10^{-4} inches for the 50 gram compression loads.

Conclusions drawn from these analyses are tentative, but since the deflections should vary approximately to the fourth power of the length, it appears that the shell will

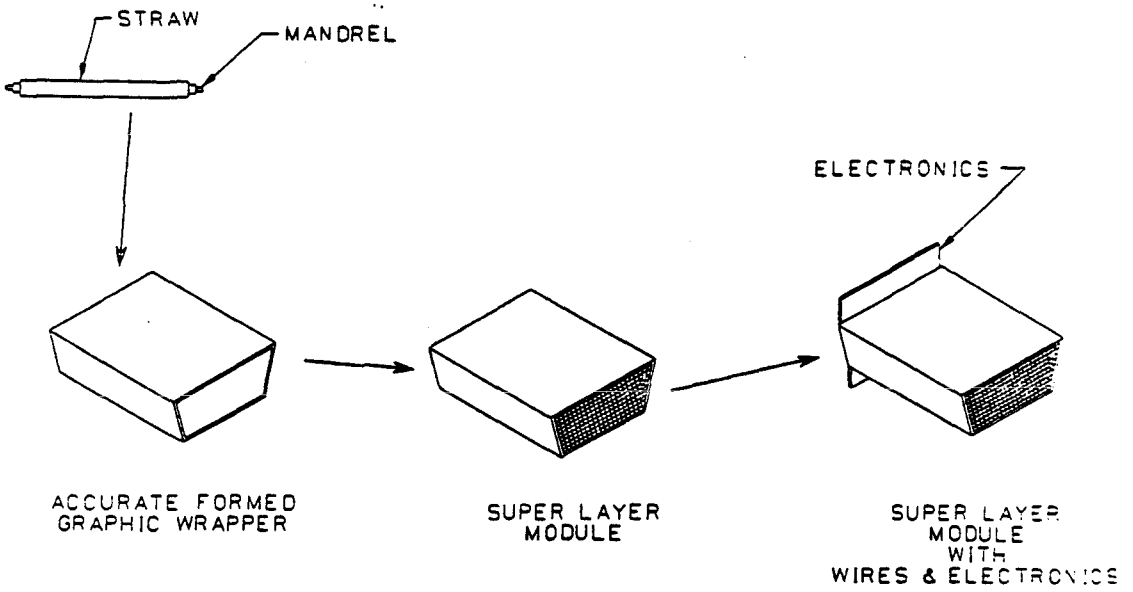

Fig. IV-1 A module manufacturing and assembly scheme.

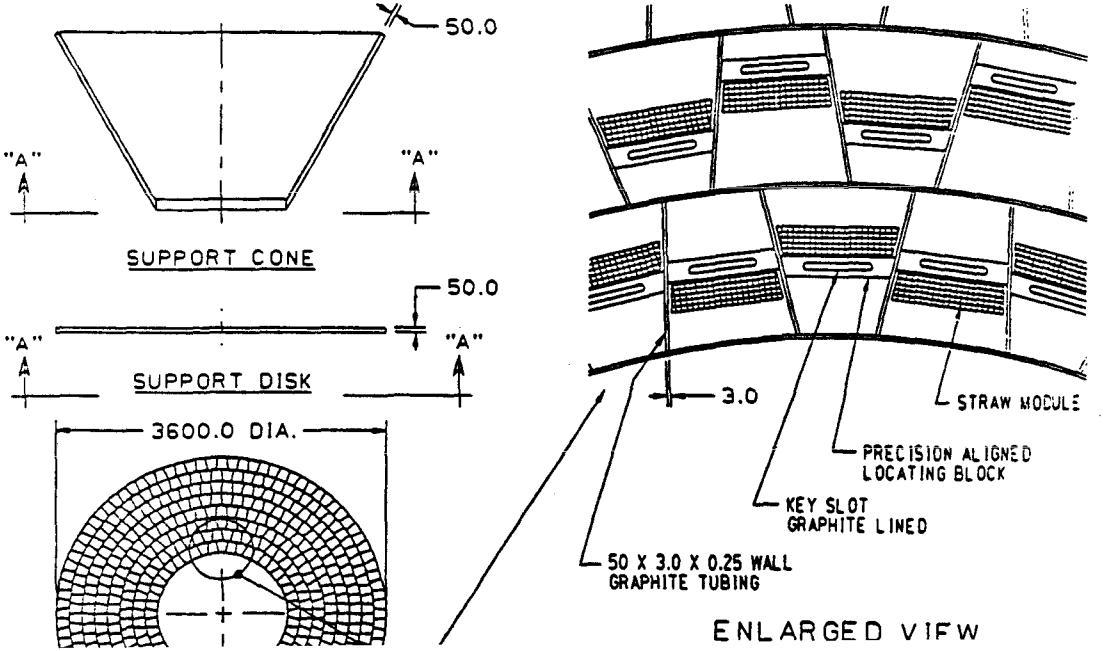

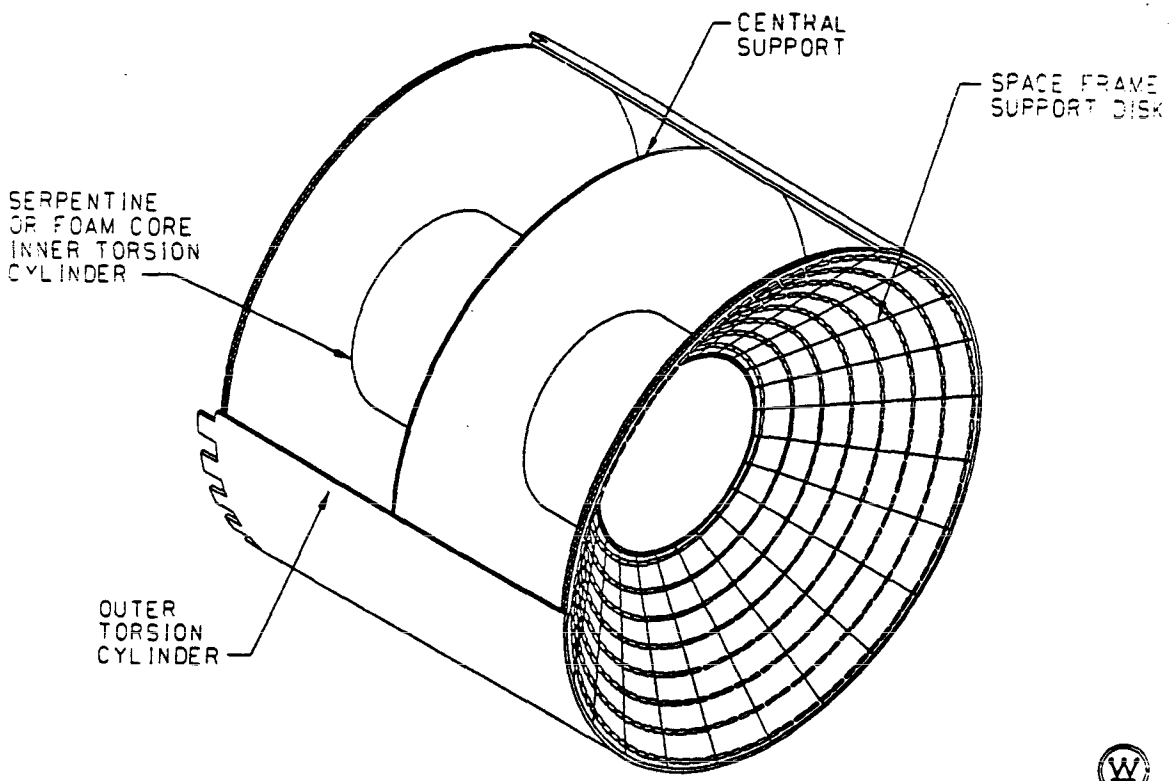

D.389.4136A13.6

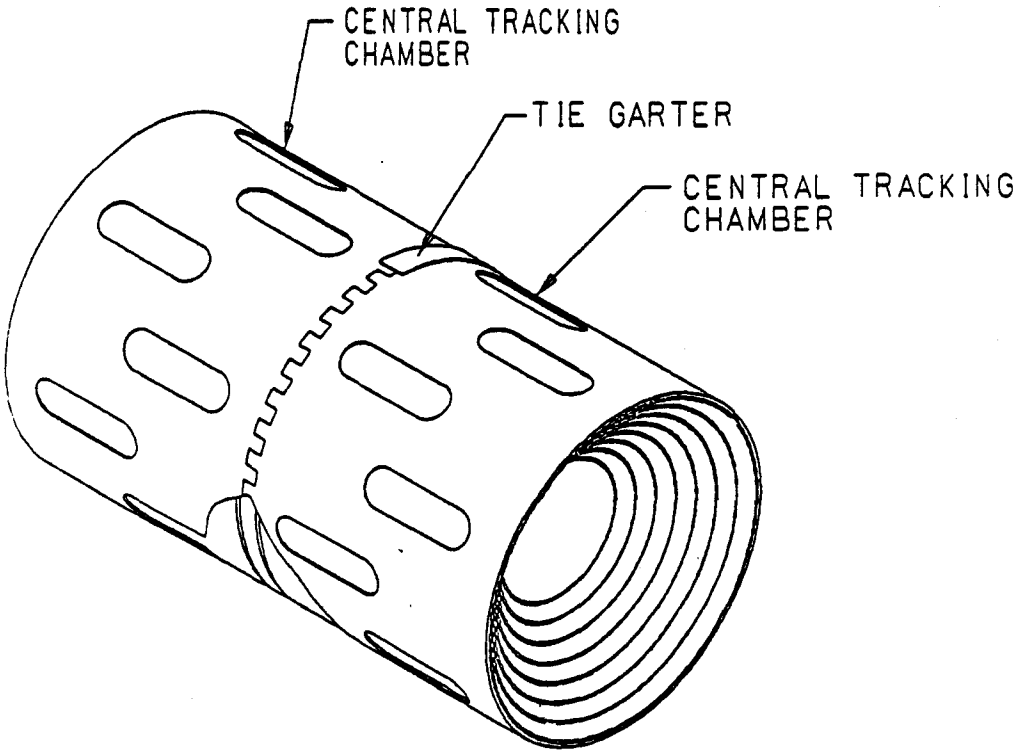

Fig. IV-4 The completed modular tracking support system

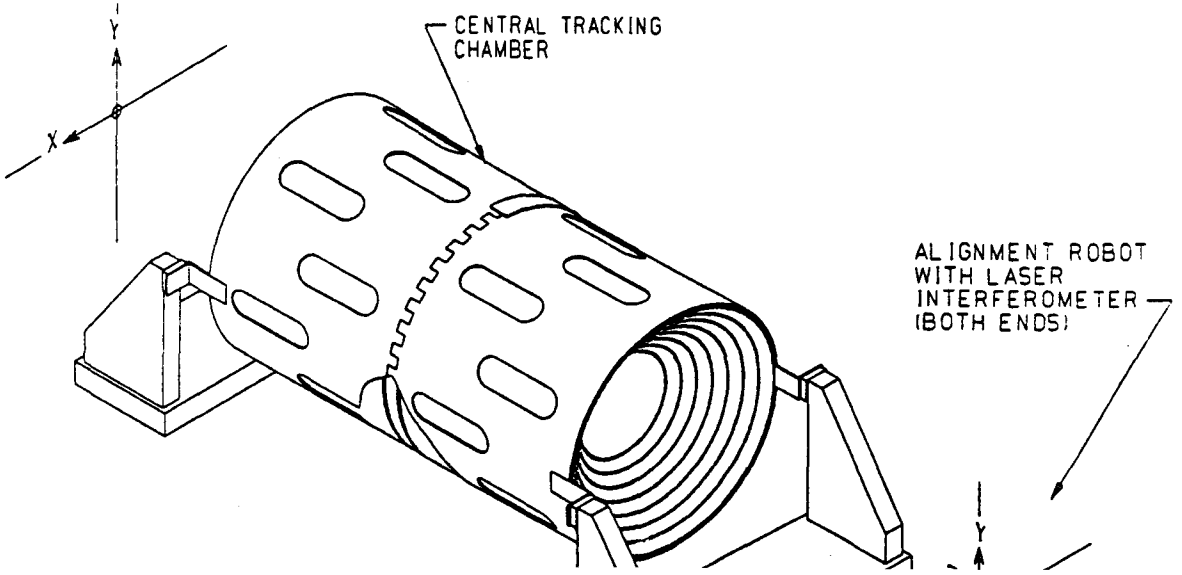

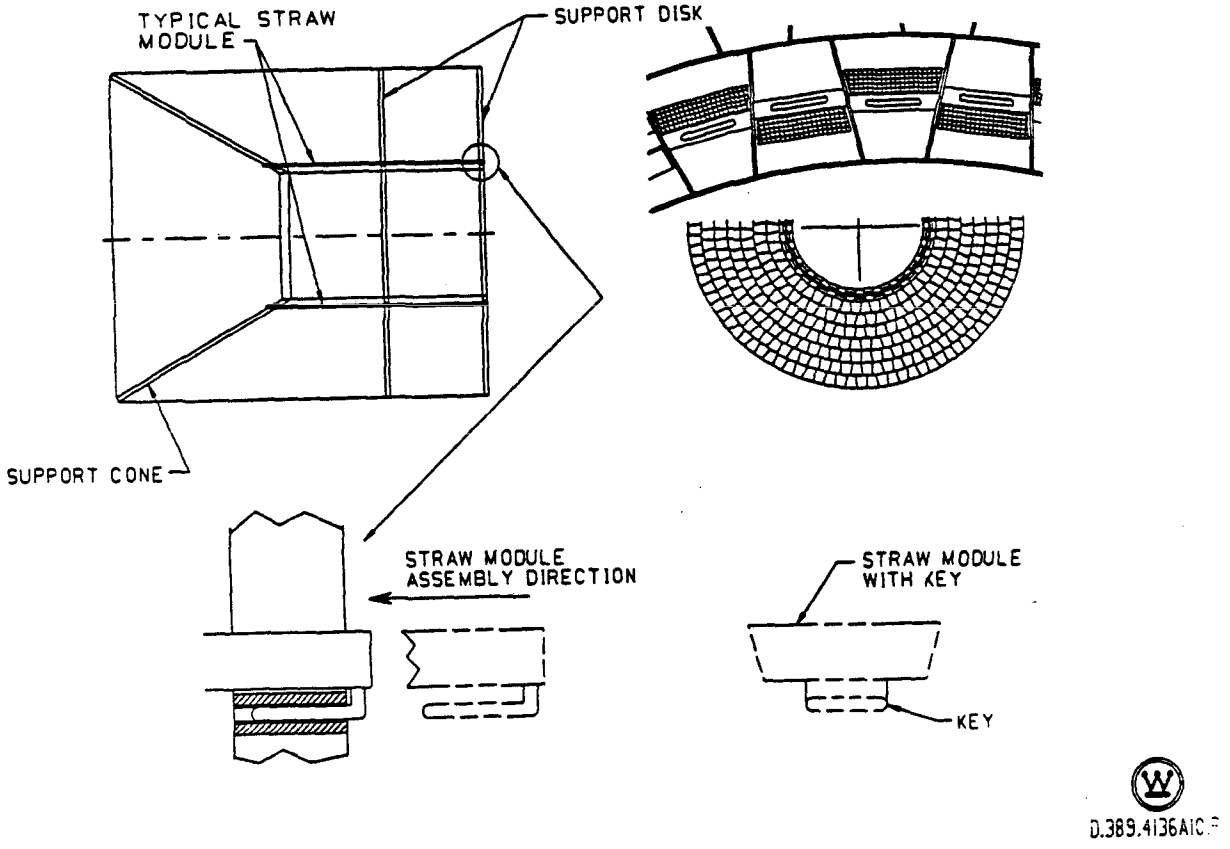

Fig. IV-6 Details of the module pinning structure.

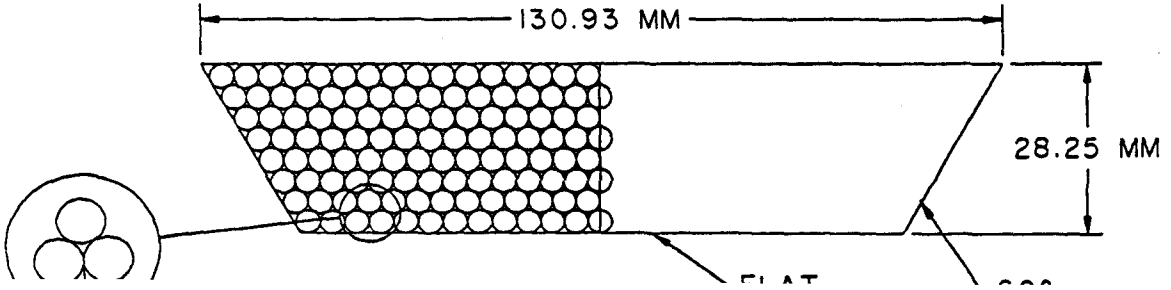

V. FRONT END AND TRIGGERING ELECTRONICS

Institutions: University of Pennsylvania, KEK, University of Michigan, University of Colorado

Introduction

During the past year the electronics effort has concentrated on developing a greater understanding of the signal environment presented by a straw detector and translating that understanding into optimized front end signal processing elements. In addition, we (Penn and Colorado) have developed a conceptual model of a final SSC compatible mechanical mounting and connecting scheme and have used the straw detector case as the model for a comprehensive SSC front-end, DAQ and triggering architectural design. This section refers to work specifically directed at the straw tracking detector subsystem; for further detail on the overall electronics effort, the reader is referred to the report of the Front End Electronics Subsystem (H.H. Williams spokesperson).

Electrical Modeling

A detailed lumped sum model of a straw has been developed[20] and compared with the measured properties of a series of idealized mechanical models and with the behavior of actual straws measured at Indiana as described in Section II. The model seems to reliably predict actual detector behavior, and this model has been incorporated into SPICE simulations of various preamplifier configurations in order to sharpen our picture of the entire system. As a result of this activity we have a much better idea of the importance of far and near end termination and attenuation length in the straw environment.

exacts a compensating price in terms of additional attention required for board layout and grounding and shielding (pointing out one of the potentially critical problems for a full system design).

Detector Tail Effects

The very long signal tail associated with the slow movement of positive ions away from the straw anode would be a severe limit on the use of straw (or any other gas ionization detectors) detectors in a high rate environment unless some tail compensation could be included in the detector design. In conventional designs this detector tail is cancelled with a simple R-C combination used as a pole-zero, and external passive compensation used on the AT&T single channel preamp has demonstrated excellent response - good enough to allow a double pulse resolution approaching 15 ns. In an integrated design, however, it is difficult to control the time constant of the pole-zero accurately enough as the inherent accuracy of integrated Rs and Cs is only about 30%. Normally a circuit can be designed using ratios of Rs or ratios of Cs and thus achieve reasonable accuracies. In this case, though, we must provide some means of trimming either R or C to achieve the desired accuracy.

While there are a variety of possibilities that have been investigated including laser trimmable resistors, fusible capacitors or resistors, and programmable current sources, the most likely solution to this problem seems to be the use of varactor diodes as programmable capacitances. By changing the standing current through a given diode it is possible to change the effective capacitance by more than the required ±30% and suitable diodes are compatible with most of the relevant bipolar integrated circuit processes. Further work on this problem will be needed through the next year, but a low cost, low power solution seems possible.

of a variety of potential bipolar integrated circuit fabricators. While optimal designs vary in detail, depending upon the particular process, all of the processes which have been examined to date seem capable of producing a workable or even superb circuit.

The primary remaining difficulty in discriminator design is the selection of a method of coupling the preamp-shaper signal into the discriminator. All preamp-shaper designs exhibit significant D.C. offsets at their output due to process, ageing, and radiation effects. A number of techniques are potentially able to compensate for the D.C. offsets:

1. Initial trim to zero - may drift with radiation or ageing.
2. Programmable injection current - easy to implement but involves an additional overhead at the system level (connections, etc.).
3. DC feedback - complex to implement but perhaps most attractive, to be examined more in the coming year.

TVC/AMU

The last block in the straw readout system is the Time to Voltage Converter / Analog Memory Unit. A one channel prototype containing most of the architectural features needed in the final design has been fabricated in a 1.6 mμ MOSIS CMOS process. Tests of the prototype revealed a number of design errors which are now being corrected; a revised prototype should be available in the Fall.

Packaging

A successful readout system must not only include optimized silicon, but must connect the active electronic elements to the detector(s) and to the readout system in a high circuit density, low mass (and low Z), high reliability fashion. A conceptual design has been made (below) that meets the density requirements of the detector and seems to have

TMC

Time Memory Cell (TMC) has been designed[22] at KEK and the wafer process was finished in July 1990. The chip has 4 channels of circuits and records input signals in 1 ns resolution for 1 microsecond period. Data are read out through encoding logic and does not cause any deadtime. The process used was 0.8 μm Bi-CMOS process and has about 100k transistors. The estimated power consumption for the 100 kHz trigger rate is only 7 mW/channel. The wafer is being tested and packaged chip will be available soon. Perhaps this chip is the first chip which can be used under the SSC experiment condition.

Triggering Electronics

First Prototype Synchronizers

The synchronizers are being developed at Michigan. The first prototype synchronizer ASICs were delivered in May of 1990. They were tested for basic functionality and found to match the CAD simulations very well. More elaborate tests were developed and are continuing to date. The first units contain a single version of the synchronizer circuit with externally provided currents that provide the time scale. The units contain all auto-reset features and include a programmable momentum restriction.

The test results are exhibited in the single most important feature of the circuit, its timing accuracy. Since the circuit is to provide a pulse that appears a fixed time after the particle passage independent of the location of the track within the drift cell, the timing variation of the pulse is of critical importance. Our simulations, for example, assume 5 ns coincidence for combinations of synchronizer circuits. It is important, therefore, that the circuit deliver its pulse with jitter significantly less than the 5 ns coincidence. Figure V-1. displays the timing variation for simulated tracks distributed within the tubes. The jitter is less than 1 ns.

counter and a 100 ns cycle. For straw tubes a single cycle would be used. For large tubes some multiple up to 1.5 μs total time is possible.

Compound Trigger Simulations

Several schemes of compound triggers were studied in simulation. These compound triggers included multiple synchronizers and various majority logic patterns. The goal of such studies is the determination of which pattern provides for the greatest efficiency in stiff track sensing while rejecting random coincidences of soft track backgrounds. The most promising pattern found to date combines the 21 tubes of a 9 depth superlayer shown in Figure V-2a. This scheme is anchored on a single central tube and includes all tubes hit by tracks that pass through the anchor tube with angles to the normal of the layer less than ±10°. The pattern makes use of 10 synchronizer circuits and a 32 pairwise AND-OR circuit. Since the synchronizer is relatively small in silicon area and the AND-OR structure is exceptionally compact, one might expect to construct the full unit on a single chip.

The simulation program attempts to answer the three basic questions, 1) What is the efficiency of the resulting OR output as a function of the individual tube efficiencies, 2) What is the false triggering rate for the system when subjected to a bath of hits from the numerous soft tracks of the event and minimum bias events overlaid on the event, and 3) What is the degradation of the overall efficiency for finding a stiff track due to the flood of extraneous hits from soft tracks.

For the simulation work a 5 ns coincidence was used. Since most tracks pass through 3 synchronizers and only 2 are required to satisfy the AND portion of the compound trigger, we expect that the overall efficiency will exceed the individual tube efficiency for high tube efficiencies. This is observed to be true in the plot of Figure V-2b. The combination of soft track hits into a synchronizer output at the time appropriate for a fast track output is relatively unlikely. The coincidence of two such events is further

same as in the previous plot. Again the cutoff for a good trigger is above the 25% mark. Though a better compound trigger may be found, we have a good candidate in hand.

Interface Between Electronics and Straw Module

The Colorado group has completed an exercise to demonstrate in detail how the front-end and digitizing electronics may be packed into the available space with interconnections to the sense wires and to the data acquisition system. Fig. V-3 shows a layout to match a 228 tube trapezoidal straw module. Two multilayer boards, one bearing the high voltage distribution, the other carrying the readout electronics, are bridged by blocking capacitors. The readout circuitry comprises bipolar chips centered over the straw groups of four that they serve, with TVC and data collection (DCC) chips on the panel extension to the side. This work is closely coordinated with the chip design efforts at Penn.

The circuit boards in this scheme are removable with the connections to the wires maintained by compressible conducting rubber contacts. We have worked out also a design for securing the wires, supplying gas and mechanically connecting the circuit boards. Ideas in this area are shared back and forth with the Indiana group and others.

One of the issues that we have recognized in the course of this design work is the importance of minimizing the material contained in the chamber end structures and electronics. Substantial changes in our system design concept have been motivated by this concern, and it has been helpful to have at this stage a reasonably detailed picture of this part of the detector.

For more immediate application we have designed and are nearly ready to produce connection boards to interface 64-cell Indiana prototype straw modules with commercial preamplifier-discriminators (or any other non-integrated readout packages). These will

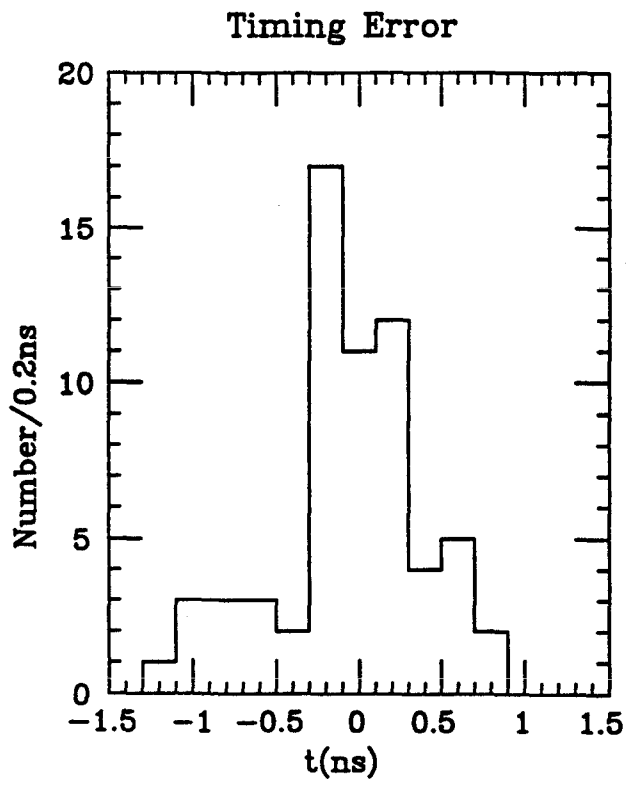
Timing Error
Number/0.2ns
20
15
10
5
0
−1.5
−1
−0.5
0
0.5
1
1.5
t(ns)

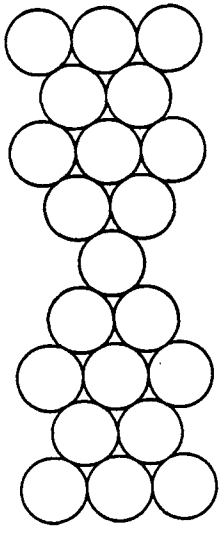

(a)

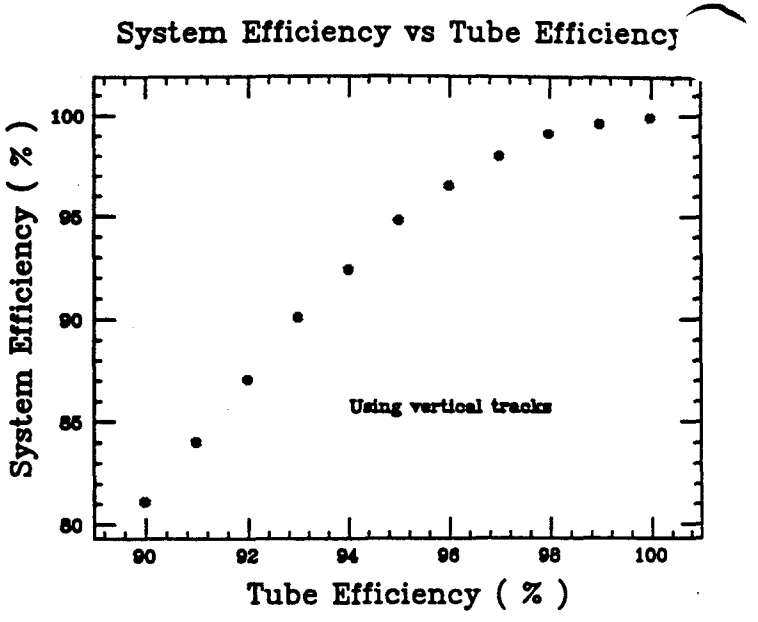
System Efficiency vs Tube Efficiency
System Efficiency (%)
Tube Efficiency (%)
Using vertical tracks
100
95
90
85
80
90
92
94
96
98
100

(b)

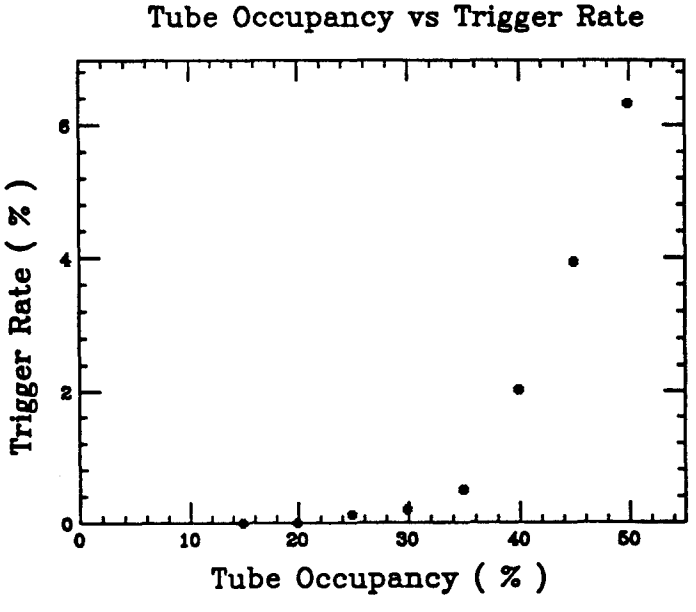
Tube Occupancy vs Trigger Rate
Trigger Rate (%)
Tube Occupancy (%)
6
4
2
0
0
10
20
30
40
50

(c)

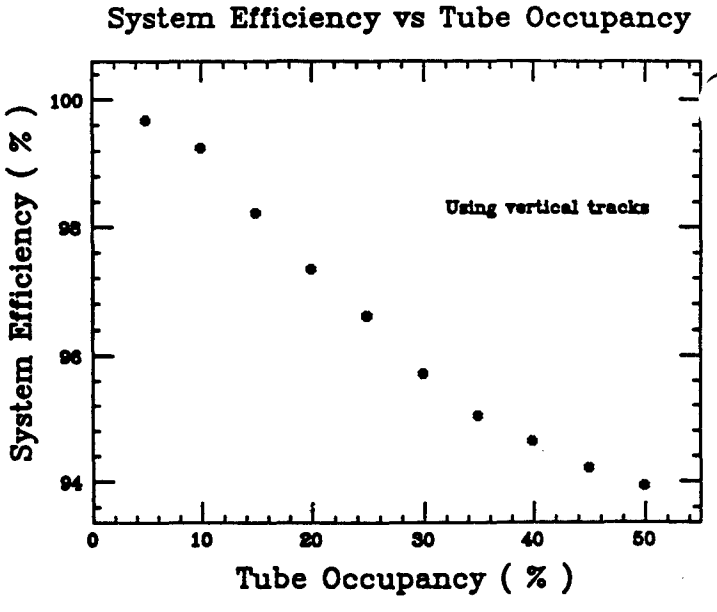
System Efficiency vs Tube Occupancy
System Efficiency (%)
Tube Occupancy (%)
Using vertical tracks
100
98
96
94
0
10
20
30
40
50

(d)

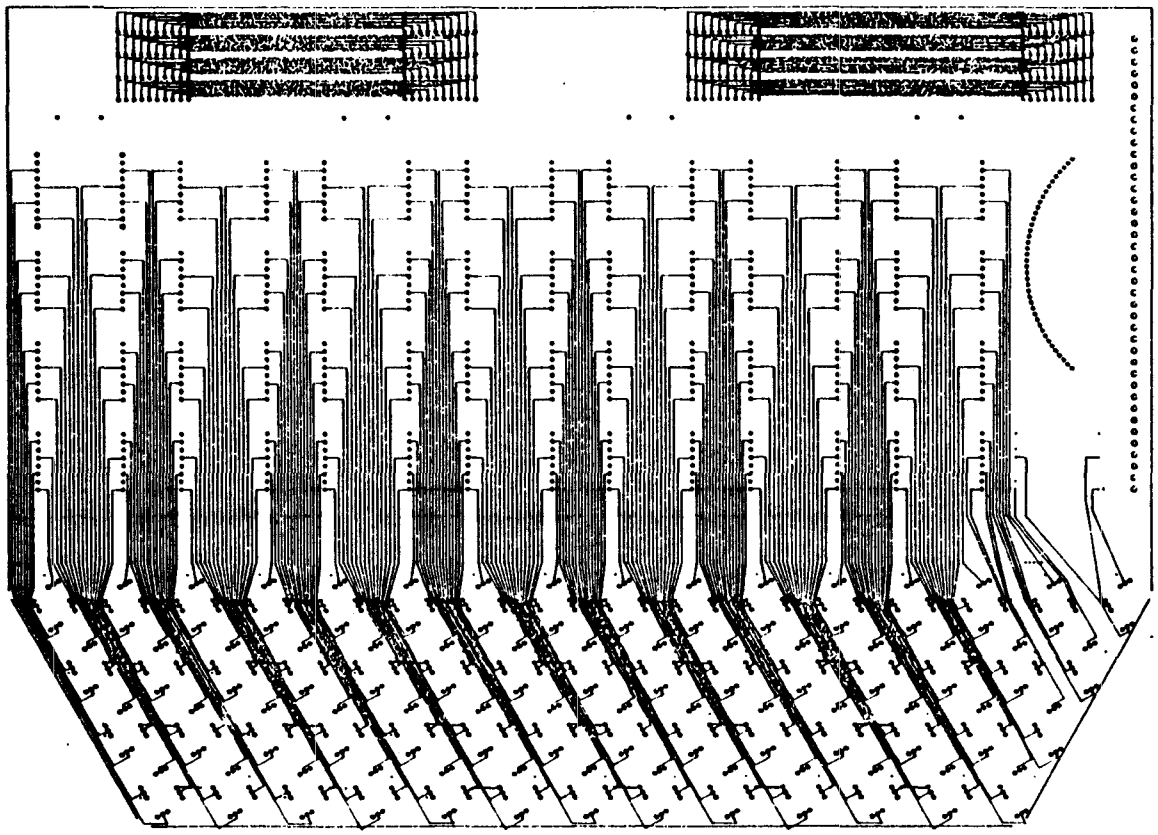

VI. COMPUTER SIMULATION

Institutions: Indiana University, University of Colorado, Lawrence Berkeley Laboratory

Introduction

Computer simulation work was centered on the areas of simulation of the detectors themselves, evaluating the performance of the detectors, and pattern recognition and track fitting studies. We use ISAJET to generate events and GEANT to simulate the detector. Although members of this collaboration have had considerable experience simulating SSC tracking, there have still been inefficiencies due to reorganization and startup of new efforts. Most of this work was funded with DOE generic detector R&D or institutional money.

Simulation at University of Colorado

Some considerable startup effort was required to learn how to build the CERN program libraries from source code, chase bugs in unfamiliar code, etc. We now have the ISAJET and GEANT packages working on both the VAX 8800 and on the DECstation cluster (currently two DS3100's shared between this and the CLEO effort). We have started with a drift chamber model developed by Hanson, Palounek, *et al.*

To get an accurate picture of the background for tracking we have set up to superimpose minimum-bias events from nearby bunch crossings, and to convolute the bunch structure, time of flight, propagation and drift time delays to see just what background hits underlie the signal. We show a preliminary result in Fig. VI-1. Plotted there are the hit arrival times for ±7 bunch crossings around a Higgs event occurring in the

peak comes from a fluctuation in which five minimum-bias events occur in a crossing preceding the one of interest.

We have begun work on segment finding algorithms and have code to measure their reliability and efficiency. We are also looking at the azimuth *vs.* curvature clustering of segments that belong together on tracks against the background of nearby real or fake segments.

Simulation at Indiana University

The simulation work at Indiana University was hampered because the generic R&D money for Hanson was sent to SLAC instead of Indiana in October, 1989, and did not arrive at Indiana until May, 1990. That money was to have been used for a full-time person to work on simulation. We are now searching for such a person and expect to have someone starting this Fall. Most of the work was done by a part-time computer science graduate student funded by the University.

The simulation at Indiana is carried out on a VAX 6340 computer. Hanson previously had the code running on the IBM 3081 at SLAC, and some changes had to be made in transporting it, particularly in the command files. We also moved from GEANT 3.11 to GEANT 3.13. Various bugs were found and fixed in the process. We also had to buy GKS for the displays. The packages are now working.

The accomplishments at Indiana were:

1. An automatic procedure was developed to generate the hits from both the minimum-bias background events and the event of interest at the same time in GEANT. First a file of generated minimum-bias events is created. Then from within a driver ISAJET is called to generate the event of interest and the file is

procedure will make comparison of different detector geometries, for example, much easier.

2. A new pattern recognition procedure was developed, including matching track segments in curvature and azimuth.

3. More realistic tracking geometries were incorporated into the simulation, including larger tracking radius, fewer superlayers, and intermediate angle tracking.

4. At this time we are beginning to incorporate stereo superlayers.

Simulation at LBL

The simulation work at LBL was primarily concerned with more general detector simulation issues, such as integration of tracking simulation into complete detector simulation, defining data structures, providing parametric tracking simulation, etc. A GEANT shape for stereo layers was defined and implemented. This new shape, HYPE, has been included in the most recent release of the program, GEANT 3.14. It describes the hyperboloid formed by the surface of straws or wires whose ends are displaced by some angle in order to facilitate a z measurement, and is described by the volume's inner and outer radii, half length, and the stereo angle.

Most of the studies of the several possible tracking system configurations require a comparison of their track pattern recognition, momentum resolution, and track triggering capabilities. A fair comparison has proved very difficult, so we have been writing a tracking simulation shell which can easily accommodate any proposed configuration and apply any analysis. This shell uses only easily available facilities and standard FORTRAN to facilitate its use by many users with many computer systems. The analysis section

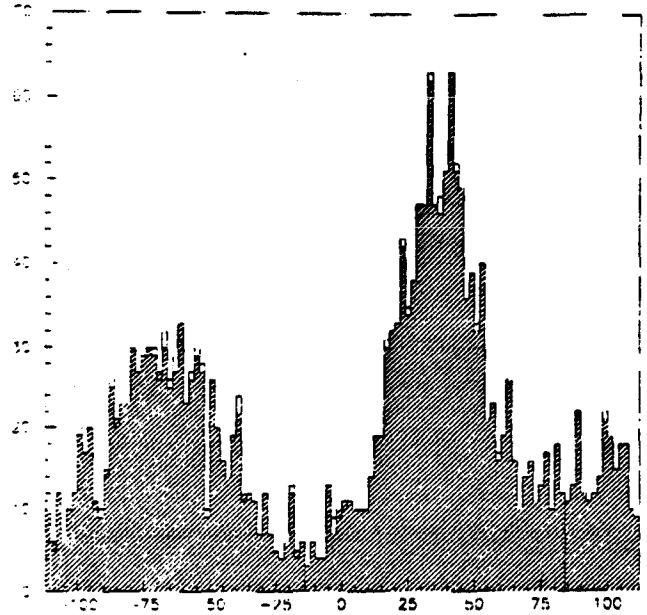

FIG 7 MF OF 21 BUNCHCROSSINGS WITH 1 HIGGS BEFORE DOUBLE HIT REMOVAL (−7ewin

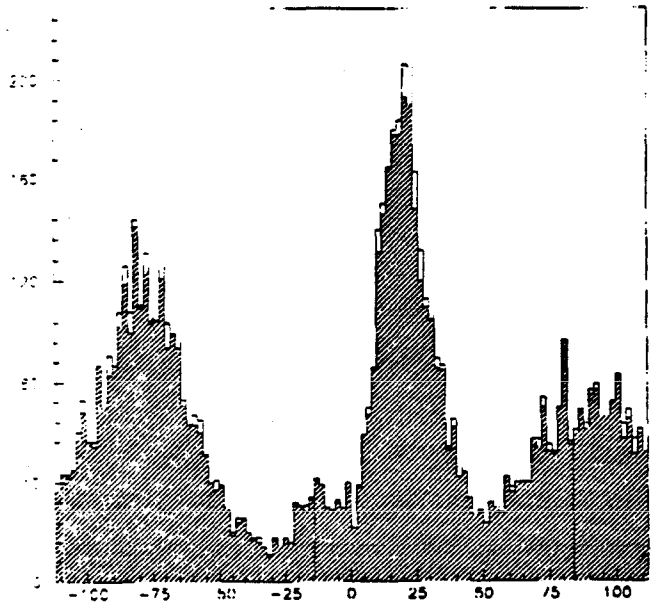

FIG 8 MF OF 21 BUNCHCROSSINGS WITH 1 HIGGS BEFORE DOUBLE HIT REMOVAL (−7ewin

REFERENCES

1. C. Neyman *et al.*, "Gas studies of 4 mm Diameter Straw Drift Chambers," Indiana University IUHEE-90-1.

2. C. Neyman *et al.*, "Gain of a 3.65 m Straw Drift Tube," Indiana University IUHEE-90-12.

3. C. Neyman, "Attenuation Studies of 3.5 m Straw Tubes," Indiana University IUHEE-90-7.

4. D.R. Rust, "Some Facts Concerning the Electrical Resistance of Straw Chambers," Indiana University, IUHEE-90-11.

5. H. Ogren *et al.*, "Wire Stability Tests on 4 mm Straw Chambers," Indiana University, IUHEE-90-2.

6. R. Foster *et al.*, "A Wire Support Design for Straw Drift Chambers," Indiana University, IUHEE-90-3.

7. C. Lu, "Prototype Study of the Straw Tube Proportional Chamber," Princeton University preprint DOE/ER/3072-56 (Feb. 15,1990).

8. C. Lu and K. T. McDonald, "A Straw-Tube Tracking System for the SSC," to appear in the Proceedings of the IISSC (Miami, Mar. 14-16, 1990).

9. C. Lu and K.T. McDonald, "Drift-Chamber Timing Studies with a N_2 LASER," Princeton University preprint DOE/ER/3072-60 (June 10, 1990).

10. M. Frautschi, "The AMY Inner Tracking Chamber," Ohio State University preprint (Oct. 1989), submitted to Nucl. Inst. and Meth.

11. D. Newton, private communication and H1 note in press; throughout the H1 FTD tracking volume the B field major component (about 1.2 T) is constant to within 3% and minor components never exceed 3% of the major component.

12. H1 Technical Proposal, DESY, 1986; J.B. Dainton, in *Proceedings of the Workshop on Tracking Systems for the SSC, edited by W. Frisken, TRIUMF Vancouver Canada, 1989.*

13. SDC Expression of Interest, SSC Laboratory, May 1990.

14. P. M. McIntyre *et al.*, private communication, May, 1990.

19. L.G. Christophorou *et al.*, Nucl. Inst. and Meth. **163** (1979) 141; J. Appl. Phys. **58** (1985) 3001.

20. T. Ekenberg and F. M. Newcomer, "Modeling Small Diameter Straw Tubes in Terms of their High Frequency Electrical Characteristics," to appear in IEEE Trans. Nucl. Sci.

21. F. M. Newcomer *et al.*, "A Fast Monolithic Preamp and Shaper for High Rate Gas Tracking Detectors," to appear in IEEE Trans. Nucl. Sci.

22 .Y. Arai, "Development of TMC Chip and On-Chip Processing," *Proceedings of the International Workshop on Solenoidal Detectors for the SSC, edited by F. Abe and K. Hasegawa, KEK, 1990*, p. 453.

OUTLINE OF PROPOSAL FOR FY 1991

I. Summary of Proposal

II. Central Tracking R&D

III. Intermediate Angle Tracking R&D

IV. Engineering

V. Front End and Triggering Electronics

VI. Computer Simulation

VII. Project Organization

VIII. Milestones

IX. Budget

Appendices

I. SUMMARY OF PROPOSAL

We are proposing to carry out detailed design studies of a wire chamber tracking system for the SSC. The system will include a complete design for both the central tracking system and the intermediate angle tracking system, with momentum measurement over $|\eta| \leq 2.5$ in a solenoidal magnetic field. The design includes the drift cell designs: straw tubes for the central tracking region and wires transverse to the beam direction for the intermediate angle region. In the central region straw tubes will be grouped together to form superlayers in order to provide local track segments. Such concepts will also play a role in the intermediate angle region. We are designing endplates for the straw tube modules to allow the connection of high voltage, gas, and electronics. We are investigating a support structure and developing techniques for precise mechanical alignment of the entire tracking system. Mechanical design studies also include evaluation of materials, thermal studies, and engineering studies of fabrication processes.

We are also developing front end electronics specifically for this tracking system. We are building on the R&D that is being carried out for more general front end systems. Triggering electronics is also being developed for this system, although we are not requesting funding for the triggering electronics as part of this proposal.

We propose to fabricate full-scale prototypes of sections of chambers for both the central and intermediate angle tracking systems for beam tests in 1993 (test beams will then be available at Fermilab). These prototypes will test all of the designs for the full tracking system - chamber design and construction, mechanical support and alignment, and electronics. To this end we will be building prototypes to study various elements of the designs. We will test prototypes of front end and triggering electronics on prototype wire chambers. We will investigate the layout and interfacing of the electronics on the chamber, including any on-chamber signal processing.

We propose to continue our computer simulation studies of the tracking system. As

for the SSC will probably be less than optimal, even though it is already known that the environment will be harsh. It will be imperative to evaluate the performance characteristics of a minimal tracking system for an SSC detector.

We have already made substantial progress on the R&D for an SSC tracking system and are beginning to determine detailed designs, as described in our Summary Report. However, a great deal remains to be done. Some of the institutions in our collaboration were funded primarily by SSC detector generic R&D money in the past, and since the generic program has been stopped, this funding should now be picked up by the subsystem R&D program. This is particularly important since some of these institutions now have rather well established SSC programs with people whose salaries are paid through this source. A large fraction of the progress that was made on subsystem work in the past eight months was actually funded by the generic R&D program since subsystem R&D money was very late in arriving.

II. CENTRAL TRACKING R&D

Institutions: Indiana University, University of Colorado, Los Alamos National Laboratory, Lawrence Berkeley Laboratory, University of California, Berkeley and Princeton University

Introduction

The heart of the tracking chamber is the drift cell. We will concentrate in this proposal on a continuous cathode design in modular packages. There are many practical advantageous to a tubular design. The tubes are physically and electrically isolated from one another. This isolation is especially important for 200,000 cells, where in an open design one broken wire could put the entire chamber out of service. Coupled with the self supporting cathode, this means that each module can support its own tension, and the superlayer support requirements are reduced.

The optimum size of a drift cell at the SSC has been discussed in the Snowmass meetings and at the Vancouver Tracking Workshop. For wires to survive at distances of 0.5 meters from the SSC beam pipe the cells must be no larger than 4 mm. On the other hand cells much smaller than 4 mm will suffer from poor efficiency due to limited track ionization length and from electrostatic stability problems. This proposal will cover the R&D on straw drift tubes and the assembly of the straws into modules.

The engineering for design and construction of a tracking support system for the SDC will be done by Westinghouse Science and Technology Center and Oak Ridge National Laboratory. They will be assisted by Indiana University. This work is also described in this proposal in the Engineering section. Our philosophy is to carefully work through tests on chambers of increasing size and complexity and confront the problems that arise from increase in scale. We have completed 3 six-straw modules with lengths from 25 cm to 3.5 meters. We are now testing a 16-straw module 25 cm long to understand the endplate design. We will then proceed to a 64-straw chamber in a composite shell to understand production techniques and finally to a full-length 236 straw module.

will test the first module to determine cross talk, chamber efficiency, and track resolution. We will carry out these tests in Bloomington. Most of the data acquisition and support equipment have been purchased for this test and are already in place. When they are complete and the design is finalized we will begin construction of the remaining chambers. Much of the work on the design and assembly of these modules will be done by the research support scientist and the programmer designer who are presently working on this project. and a university supported technician. Some of the engineering work on the endplate design will be done by Oak Ridge. This work is described in the Engineering Section. The interface boards for these chambers will be designed at Colorado. This work is described in the Electronics Section.The 64-straw module design is well under way. In Fig. II-7 of the Summary Report we show the composite shell, the straws and the endplate present design. A prototype test of the general design is now underway with a 16-straw module.

2. We will also assemble a full scale drift module, concentrating on fabrication techniques that will be required for automatic assembly of a complete system. This full scale drift module will be 4 meters long and contain 236 tubes. It will be used to develop and test alignment and support systems. and to directly determine the resolution of a module as a function of its length. The full length module will be the first of several full scale modules that will be used for the 1993 SDC beam tests. The engineering for the composite shell is already underway at ORNL and will be continued this contract year. It is detailed in the Engineering Section. The circuit boards and electronics will be designed by Colorado and Pennsylvania and is discussed in the Electronics Section. These components will assembled in Bloomington and the original tests carried out there. The resolution of this module and others will also be mapped at Colorado.

3. We will also carry out an investigation of gas properties in a 2 T magnetic field. This will give us a direct measurement of the Lorentz angle for the final gas mixture selected for use in the central tracker. The drift in a high magnetic field is slower than in when a magnetic field is absent.The Lorentz angle, however, depends on the gas, as well as the electric and magnetic fields, so there might be an optimum gas mixture that would minimize the drift time. The requirements of SSC detectors are consequently sufficiently

A test drift cell with uniform electric field is being constructed. It will be placed in a uniform magnetic field using a research magnet in operation at Indiana University. The research magnet has been tested at fields up to 2.3 T . It appears that the field uniformity will be adequate for this test. The source of ionization will be an UV laser. This is very convenient because the timing of the light pulse is easily detected and the ionization path is well collimated. The laser has been ordered and the necessary test setups are being designed.

University of Colorado

The goals for the coming year include:

Straw tube engineering and development

Experiment with alternative designs of the straw feedthroughs, end bulkhead, wire connections etc. to aid choice of the most workable schemes.

Prototype resolution tests.

1. Continue and complete data acquisition programming and transporting of track reconstruction code for the reference tracker.
2. Conduct resolution measurements on phase 1 prototypes.
3. Begin design of a mechanical alignment bench for testing resolution over larger distance scales.
4. Alternative cathode structure development. Provide physics coordination and testing support for the work at Los Alamos. The Dubna group have also indicated an interest in collaborating on tests of their structure.

Los Alamos National Laboratory

for precision machined mandrels and molds. This level of support is further outlined as follows:

Development Of A Termination End Plate

The straw termination end plate will provide two function. The first will be to provide tension support for the straw tube charged wires. The second will be to incorporate resistor/capacitor features which will decouple the electrical pulses from wire to wire.

This end plate design is ongoing and will attempt to attain several goals. The first is the successful decoupling of electrical pulses. The second is providing a lower mass construction than conventional resistor/capacitor electronics. The third is producibility. Approximately 780 end plates will be requires for the 200,000 straw tubes, (calculated at an 8 x 32 straw cell unit).

The preliminary design approach is to have an injection molded non-conductive base plate. Wire termination "clips" will be injection molded out of conductive thermoplastic, providing a 270 ohm resistive path for each wire. A thin aluminum conductive plate will carry the series resistor 2,000 volt potential to the edge of the end plate. A two-sided aluminized "Kapton" film will be attached to the aluminum plate on one side, and to the straw tube "ground" on the other side, providing capacitance. The film dimensions will be designed to achieve a 12.8 nf (50 pf x 256 straws) performance.

Material & Design Consultation

We will provide consultation for plastic molded and composite fabricated components based upon our industry expertise. This consultation will be extended toward any plastic or composite component that we can contribute on, including Indiana and Westinghouse requesters. The level of support may vary according to instructions by Indiana personnel.

Tooling Support

We will provide tooling support for two main components, the termination end

Tool design and fabrication consultation will also be extended toward any other plastic or composite component, according to instructions from Indiana University personnel.

Lawrence Berkeley Laboratory and University of California, Berkeley

We expect to continue some "generic" research and development, since it is important to the operation of straw tubes as well as other types of wire chambers, but we expect to shift emphasis toward studies specifically directed toward understanding and planning for operating straw tubes and the SSC. This implies, in particular, the determination of the operating gases, gains, gas flow rates, etc.

Plans for further studies:

1. Search for better gases (for SSC) (non-flammable, non-hydrogenic, inexpensive, etc.
2. Better understanding of aging reactions, to gain insight into suppressing them (especially effects of oxygen and oxygen-containing compounds).
3. Qualitative and Quantitative understanding of mechanism of breakdown suppression by water vapor.
4. Continuing studies of straw tubes: resolution, drift velocities of candidate gases, optimal operating conditions, design and fabrication
5. These studies are of immediate importance, since they may impact future designs, etc. (Example: clarification of gas heating just described.)

Princeton University

We present a brief summary of work accomplished at Princeton University in FY 1990 towards a straw-tube tracking subsystem with precision spatial resolution at the SSC. A budget of $195k is proposed for FY 1991 to continue this work. We seek an additional

CAMAC TDCs for 784 channels from PREP, but amplifier/shaper/discriminators for only 48 channels unless more become available via the SSC Front-End Electronics Subsystem effort.)

Mechanical assembly procedures will be studied in more detail, requiring fixtures, and clean work space on a larger scale. We should set up a second straw-tube test station in the assembly building, which requires a second gas system, computer, CAMAC crate, and various electronic test equipment. We wish to continue our efforts towards an online gas analysis system, both for proportioning of the gas mixtures, and detection of trace contaminants. This will require a substantial investment in stainless-steel plumbing and in research-grade gas chromatography, as well a specialized modules of trace analysis of oxygen and water. In the pursuit of high resolution we must deal with shorter time intervals. It will be very beneficial to purchase a high-bandwidth, high-sampling-rate digital oscilloscope.

Central Tracking R&D Issues

We have summarized the major R&D issues for the straw tracking system. The particular areas of research are indicated, and the activities of our group are summarized

Drift cell

Issue: Attenuation length
The present attenuation length is 4 meters. For long straw applications less attenuation will allow lower gas gain operation.

Area of R&D: Thicker cathode materials, new straw films, larger signal wires.

Action: Kapton and lower resistance materials now being used for straw production. New cells constructed at Indiana University in Fall, 1990.

Issue: Fast non-flammable gas

Issue: High rate effects

The drift cell recovery time and the tail cancellation electronics must be optimized for minimum dead time. Presently a 15 ns recovery time is assumed in occupancy calculations and it seems realistic.

Area of R&D: Investigate possible high current effects. Establish maximum current draw limit with radioactive source and beam tests. Must look at prototype electronics.

Action: Use 64 straw modules which will be ready in the Fall of 1990. Electronics needed from Penn. Must schedule beam (Indiana University Cyclotron?) Must also examine this for 3-4 meter straws as soon as possible with Penn. electronics in early 1991.

Straw Module

Issue: Module structural study

We are presently looking at a trapezoidal geometry for the straw modules, but we need to examine alternatives that will have a uniform trigger efficiency and a low (or zero) hit loss at the boundaries for stiff tracks. This needs to be done with the constraint of maintaining the 10 mil wall thickness.

Area of R&D: Use finite element analysis to determine strength and defections or full length modules. Develop a 3D model of system.

Action: ORNL study under way for 64 straw module with comparison of first production shell in Fall of 1990. Followed by full length study and construction at ORNL 91. Westinghouse will begin a 3D model of system in Fall 90.

Issue: Straw alignment

The shells of the modules must be thin, but at the same time must hold the straws straight. Holding straws on mandrels and bonding during construction should insure straightness. Small prototype measurements indicate straws will self align to about 2 mils. This is an important issue for modular concept with direct impact on momentum resolution.

Area of R&D: Finite element study of compression of straws and supports in the module shell. Direct measurements of

Issue: Optimum module size
Present modular size has been optimized for eight superlayers. It needs to be looked at for "descoped" version. A possible layout exists, but it is not elegant, especially for stereo.

Area of R&D: Study module construction techniques. Examine impact on electronics modualization. Study effects of possible track loss at boundaries and in stereo layers. Look at possible module size change with superlayer. Re-examine the requirements for 8 straws/layer (more/less).

Action: ORNL study underway for module structure strength, sag. ORNL design for construction of module in 91. WTSC study of module layout and stereo position with 3D model is underway. Simulation will be required to optimize the super layer thickness (Colorado, Indiana)

End plate

Issue: Minimum material end plates
Several designs now have acceptable material in end plates, but much hinges on capacitors. Prototype construction is valuable. This has impact on superlayer geometry and interface to forward region.

Area of R&D: Determine if termination capacitor can be built into wire support. Simplify the end plate design and find nonmetallic components. Design the $z=0$ end for minimum dead space.

Action: ORNL study of end plates underway. 3D model will be produced. Los Alamos is working on a design of termination low mass Indiana prototype of end plates underway. Colorado design of printed circuit electronics is underway.

Issue: "Utilities" optimization
Material budget not complete until this is worked out. Cooling and electronics power requirements will have important impact on integration design.

Area of R&D: Look at gas flow requirements. Determine electronics cooling methods. Establish HV requirements. Specify electronics power requirements. Work out signal outputs and structure.

III. INTERMEDIATE ANGLE TRACKING R&D

Institutions: University of Liverpool, University of Glasgow, Rutherford Appleton Laboratory

Layout of the Intermediate Angle Tracking Detector

Simulation work will continue in parallel and in a symbiotic manner with all development work outlined below. In this way we hope to be able to optimize the somewhat conflicting requirements of multi-track reconstruction and X-ray detection for an SSC environment. Such a procedure proved very effective in the early stages of the design of the H1 FTD. The simulation will be developed to include:

1. charged particle knock-on and photon pair conversion in all upstream material, in particular in the beam pipe, in the central track detectors (straws or fibres in SDC), and in the inner track detector (silicon in SDC)

2. the details of any inhomogeneity in the solenoid magnetic field and their effect on both drift chamber operation and track reconstruction

3. a more realistic set-up for a crossing tagger with the hope of evaluating the minimal requirements for a fast signal from such a device

4. a more realistic set-up for the radial chambers for the purposes of trigger simulation in an SSC experiment and for a more realistic evaluation of reconstruction efficiency and precision. We will then be able to study in detail the feasibility of particular Intermediate Tracking Detector (ITD) layouts and to evaluate and compare their efficacies as a charged track detector with electron identification when operating as part of the overall inner tracking of an SSC detector.

Chamber R & D

Radial Wire Chambers

The R&D work outlined above has only just commenced. Most important of all is

program of fast gas measurements. The latter will of course include components (Kr and Xe) with superior X-ray sensitivity in preparation for possible TR detection, as well as charged track dE/dx measurement, in the ITD.

The problems associated with the design of radial chamber modules for the SDC experiment will be pursued in a design program which we foresee lasting for some years yet. This is because of the difficult problems outlined above which will involve a systematic program of mechanical and electrical R&D using materials compatible with the corrosive or other properties of our favoured gas mixtures. Considerable interaction with industry will be absolutely essential. This work can only commence in earnest when the principle of operation of radial wire chamber wedges at SSC is established with our prototype.

In FY 1991 we expect to have unique data from our radial wire chambers in the H1 Forward Tracking Detector (FTD) at HERA to establish that our earlier test beam work, and thus original design criteria, were valid in a real experimental environment. Analysis of these data will therefore play a vital role in our design of SSC compatible radial wire chambers.

Crossing Tagger

The emergence of the need for a fast proportional chamber like component in the ITD requires a considerable program of R and D. None of the UK groups in the FY 1990 proposal have experience in the more exotic techniques, such as knife edge or MISGAC chambers, proposed above. Nevertheless it is intended that investigations exploiting the expertise of the RAL Electron Beam Lithography (EBL) facility should begin as soon as possible into the feasibility of laying down the necessary electrode structures over the dimensions necessary in the ITD. A construction and test program would then follow.

Fast Gas Measurements

Our program of fast gas measurements will continue throughout FY 1991. Apart from establishing the drift properties of each mixture in substantial magnetic fields as close

Electronics

We have commenced discussions with the RAL electronics group concerning the use of the RL114 analogue pipeline chip as a basis for ITD chamber read-out. It would be used in a hybrid which includes a quality analogue shaping circuit and discriminator plus a digital TDC for good spatial precision, and it would latch charge into an analogue pipeline (50 ns bucket). This chip is a prototype for LHC/SSC read-out. Our test prototype chambers will of course be used in the development of this hybrid.

IV. ENGINEERING

Institutions: Westinghouse Science and Technology Center, Oak Ridge National Laboratory and Indiana University

Westinghouse Science and Technology Center

Westinghouse is in the process of completing a preliminary conceptual evaluation/analysis of the feasibility of a modular type straw tube central tracker for use in the SSC. The following list attempts to summarize the results and conclusions of that work:

1. A specification describing and documenting the system analyzed has been written.

2. Concept layouts of the following have been developed:

   a) Several conceptual versions of the tracker
   b) Several module cross sectional geometries
   c) Fabrication and assemblies for modules and support structures
   d) Proposed alignment equipment and methods for obtaining required alignments
   e) Module design and fabrication for needed automation

3. Module sizing and spacing geometrical calculations have been done.

4. Conceptual evaluation indicated that for several reasons, including potential for automation fabrication and assembly, ability to accommodate maintenance and repair, and potential for good alignment, the design is very attractive to build when compared to rival technologies.

A module-based central tracker using straw tube technology would have advantages such as simplicity, maintainability and repairability when compared to other technologies.With respect to mechanical engineering design issues, conceptual feasibility has been demonstrated, but many conceptual and preliminary design and analysis tasks remain to be addressed.To assist in addressing these issues, a design and analysis program

Task 3	Develop the preliminary composite support design material properties in sufficient detail including manufacturing fabrication feasibility in order to develop valid required finite element material properties. This work is a prerequisite to Task 4.
Task 4	Analyze deflections of module layout with stereo using 3D finite element computer analysis.
Task 5	Investigate an alignment measurement tool design.
Task 6	Investigate manufacturing and auto assembly.
Task 7	Develop a 3D model for integration study.
Task 8	Assist the subsystem collaboration in developing costing.

The deliverable would consist of:

1. Conceptual design layouts that result for the design and analysis efforts.
2. Requirements, specification, and procedures developed as part of the effort.
3. Conceptual and preliminary engineer analysis, summaries, and conclusions that result from finite element and classical analyses.
4. Input to a final report.

Since this program is in its early stages and many unknowns still remain, this Statement of Work and its associated deliverables and estimated costs must be considered on a level of effort basis. It is believed, based on an engineering appraisement, that the deliverables can be achieved within the projected costs.

Oak Ridge National Laboratory

Mechanical Design and Fabrication Proposal for FY 1991

fabrication. It is essential that both areas receive adequate attention to ensure the success of the project.

Numerous tasks have been identified for further study in FY 1991. These include the design and fabrication of a 236 straw carbon fiber module; design and fabrication support for a prototype end plate including gas and cooling fluid studies and development of assembly concepts for the modules. Study of these items will determine the requirements for individual modules. Additional evaluation will be required at the system level. This will be coordinated with the Westinghouse group. The final area identified for engineering support is cost estimating. This is essential for accurate costing of the Wire Chamber Subsystem.

Module Design and Fabrication

A trapezoidal module has been identified as the primary element in the Wire Chamber Subsystem design. This module will be fabricated from carbon fiber material. The length of the proposed module equals three meters. The overall alignment of the Wire Chamber Subsystem relies upon the module being extremely accurate. The module must also withstand compression loads generated by the sense wires and have sufficient rigidity to minimize the number of intermediate supports. To verify the ability of the module to perform under these conditions, a series of finite element analyses are proposed. It is also proposed that a full size prototype module be fabricated. This will provide a means of determining fabrication procedures that retain the structural integrity and accuracy of the modules. This module will be designed to accept end plates for assembly into an operating prototype.

End Plate Design and Prototype Fabrication

The termination point for all straw tubes is the end plate. The end plates will provide the registering for the straw tubes as well as supply them with all electrical and mechanical services. Additionally, the end plates will play a significant structural role in the Wire Chamber Subsystem design. These components will provide the structural load

To support the Detector Proposal in September, 1991, a complete bottoms-up cost estimate for the Central Tracking System will be made based on the conceptual design established during FY 1991. This cost estimate will be complete by September 30, 1991.

The bottoms-up cost estimate will break-out by WBS Engineering, assembly labor and materials, tooling and procurement. Confidence levels and methods of arriving at cost numbers will also be provided. The data will be provided in both electronic (spread sheet) and paper formats.

Indiana University

The engineering work for the central tracker is being done by Westinghouse and ORNL. The scientific liaison for the tracker is H. Ogren. The detailed design work on the tracker components at ORNL and the tracking support system at the Westinghouse Science and Technology will build on the prototype designs we are completing at Indiana. In particular the chamber endplate designs, and the first composite shell designs now being used at Indiana will establish the parameters for both engineering studies. During this coming contract year we will require continual meetings at both ORNL and Westinghouse to coordinate activities. This is reflected in the increased travel costs.

R&D Issues in Engineering

Support Structure R&D

Issue: Optimize layout of modules
Present system design is not as elegant as we would desire. The alignment and support of each module has not yet been finalized and will strongly affect the design.

Area of R&D: Study the support requirements for the modules. Look at the optimum layout of superlayers. Look at issues of repair, replacement, and assembly. Work out designs that do not require each module support to be aligned, but used predrilled tooling.

Action: WSTC has initial study complete. 3D model will be completed Fall 90 to assist us in overall design. An assembly study will be

Area of R&D: Look at alignment requirements. Study stability of structure and module supports. Set temperature variation requirements. Investigate alignment and assembly.

Action: WSTC will develop 3D model for study Fall 90. Finite element analysis will begin Fall 90. ORNL will set requirements for the module alignment and Westinghouse will work out the assembly and alignment techniques in 1991.

Issue: z=0 support structure
Difficult feature of modular design is the z=0 region. We must try to reduce material and keep dead space very small.

Area of R&D: Attempt a design with no "utilities" at z=0.Specify the mass and size of z=0 support.

Action: ORNL design of module to begin Fall 90. WSTC 3D model in Fall 90 and more design work on this area. Simulation of material and dead space at z=0 must be done. Los Alamos will design low mass terminations.

V. FRONT END AND TRIGGERING ELECTRONICS

Institutions: University of Pennsylvania, KEK, University of Michigan, University of Colorado

Front End Electronics

The University of Pennsylvania has been involved, first through its generic electronics R&D effort and now through the Front End Electronics subsystem R&D, in the development of custom integrated circuits for gas ionization chamber readout. Through this separate subsystem effort we intend to develop a prototype of a fully functional radiation hard set of circuits.

As members of this proposal it is our intention to facilitate the use of intermediate versions (for instance single channel and non radiation hard) of the readout chips on prototype and test chambers and to help develop a useable end version packaging scheme compatible with all of the mechanical, electrical, cooling, radiation, and other problems of the full SSC environment. In addition, we will include appropriate detector specific (e.g. trigger) enhancements to the basic circuitry as needed and will help arrange for the manufacture of production quantities of the final integrated circuits.

The TMC development will continue at KEK. We are not asking for funds for the KEK work in this proposal.

Triggering Electronics

The Michigan group will continue to test the first group of synchronizer chips. In particular we will test the sample-to-sample variation, the auto-calibration capabilities, and momentum restriction accuracy and variation with time and sample. Schemes for

the goal of compressing the circuit to minimal size so that many copies can be constructed on a single chip. In 1991 we will investigate fabrication of the circuit on radiation hard processes and continue discussions with the tracker and front-end electronics groups regarding the physical interconnections of synchronizers with the tubes. The triggering electronics development will be funded through a separate subsystem R&D project.

Interface Between Electronics and Straw Module

The Colorado group will continue the development of the interface boards to connect the sense wires to the electronics, working in close collaboration with the groups at Pennsylvania and Indiana. The goals for the coming year include:

1. Fabricate the interface boards for stage 1 prototypes. Prototype modules will be distributed among the collaboration for testing and development of associated components.

2. Design electronics board for phase 2 prototype incorporating Penn front end circuits, with connections to commercial TDCs.

3. Extend the fully integrated readout board layout design to include trigger circuitry.

VI. COMPUTER SIMULATION

Institutions: Indiana University, University of Colorado and Lawrence Berkeley Laboratory

The goal of the tracking simulation program for FY 1991 will be to evaluate a complete integrated tracking system design for a solenoidal detector for the SSC. So far, we have not put much emphasis on measurement of the coordinate along the wire, the intermediate angle tracking, or integration with a silicon detector at smaller radius, so these will be major goals for FY 1991. Also, we need to evaluate the performance characteristics of a non-optimal, "descoped" tracking system. In more detail, the work for FY 1991 will include:

1. Consolidation of the work at Indiana, Colorado, and LBL into a single simulation program.

2. Finish incorporating stereo layers into the central tracking and evaluate the linking of stereo and axial track segments to form complete tracks with momentum and z information. Study track segment finding including the time when the track crosses the superlayer be a parameter in the fit.

3. Include intermediate angle tracking and silicon detectors. Study pattern recognition and determination of the coordinate along the wires in the intermediate angle region. Study pattern recognition using the complete system. Study possibilities for using scintillating fibers, such as cylinders of scintillating fibers for determining the z -coordinate. Work with silicon and wire/scifi hybrid groups on integrated simulation.

4. Study occupancy and performance as functions of cell size, layer radius, and

6. Simulate performance of trigger.

7. Develop some short-cut methods to improve our understanding of how reliable the pattern recognition will be.

8. Integrate tracking simulation into overall detector simulation.

9. Provide parametric simulation based on our studies so that those studying other parts of the detector or doing quick simulations of physics processes based on four-vectors can obtain the effects of track measurement without going through the full simulation, pattern recognition, and track fitting steps.

VII. PROJECT ORGANIZATION

Contact Person: G. Hanson

The project can be broken down into the following tasks. For each task we list the participating institutions and contact persons.

Central Tracking R&D

Indiana University - H. Ogren
University of Colorado - W. T. Ford
Los Alamos National Laboratory - C. Sadler
Lawrence Berkeley Laboratory and University of California, Berkeley - J. A. Kadyk
Stanford Linear Accelerator Center - J. Va'vra
Princeton University - K. McDonald

Intermediate Angle Tracking R&D

University of Liverpool - J. B. Dainton
University of Glasgow - D. H. Saxon
Rutherford Appleton Laboratory - N. A. McCubbin

Engineering

Westinghouse Science and Technology Center - R. L. Swensrud
Oak Ridge National Laboratory - T. Ryan

Front End and Triggering Electronics

Computer Simulation

Indiana University - G. Hanson
University of Colorado - W. T. Ford
Lawrence Berkeley Laboratory - A. P. T. Palounek

VIII. MILESTONES

Central Tracking R&D

R&D for straw feedthroughs, end connectors	11/90
End plate electronics for 64 straw module	11/90
Assembly of 64 straw modules	10/90
Complete evaluation of efficiency, resolution	3/91
High rate beam tests of 64 modules	591
Endplate electronics layout for full scale	4/91
Assembly of full scale module	6/91
Complete evaluation of efficiency, resolution and attenuation of full length module	8/91
Module testing facility complete for Full scale module	4/91
Resolution tests *vs. z* for full length module	10/91
Complete construction of second full length module	11/91

Los Alamos National Laboratory

Finish 1 meter mandrel	11/90
Low mass termination	11/91

Intermediate tracking R&D

Computer simulation of cell	1/91
R&D on materials, gases for ITD	3/91
Detail cell design	4/91
Complete test module prototype of sector	6/91
R&D for fast proportional chambers	6/91
Design of fast proportional chambers	9/91
Electronic design for chambers	6/91
Prototype fast chamber	11/91

Engineering

Westinghouse Science and Technology Center

Complete conceptual layout module geometry	10/90
3D Euclid model of support system, modules	11/90
Finite element analysis of structure	1/91
Alignment measurement tooling design	4/91
Develop costing for central tracker	4/91

Oak Ridge National Laboratory

Full scale module engineering design	11/90
Analysis of prototype	11/90
Endplate design complete	1/91
Utilities layout	6/91
Electronic cooling design	6/91
Assembly of full scale shell	5/91
Complete analysis of full module	11/91

Front end and Triggering Electronics

Single Channel Preamp/shaper in package	10/90
Two channel P/S in package	12/90
4 channel P/S in package	2/91
4 channel Discriminator in package	2/91
4 channel P/S/Disc in discrete package	4/91
4 channel P/S/D for multichip module tests	7/91
Single channel proto-TVC/AMU in package	12/90
Single or dual TVC/AMU, full logic in package	4/91
Rad hard 4 channel P/S/D	4/91
Rad hard 4-8 channel TVC/AMU, full logic	10/92
Full Multi chip Module Assembly- near final	10/92

Computer Simulation

Consolidate work at Colorado, Indiana, and LBL	10/90
Include stereo wires and segments	10/90
Include intermediate angle tracking	10/90
Include silicon tracking	10/90
Develop short-cut methods to evaluate pattern recognition performance	4/91
Integrate tracking simulation into overall detector simulation	4/91
Provide parametric simulation	4/91
Simulate trigger performance	10/91
Study pattern recognition and track segment finding algorithms in complete system	10/91
Study track fitting for entire system	10/91
Study occupancy and performance as a function of cell sizes, radii, and number of layers	10/91

IX. BUDGET

FY91 SUBSYSTEM BUDGET LISTED BY INSTITUTION

(funding for FY90 shown for comparison)

INSTITUTION	FY90	FY91
Indiana University (see note 1)	$325,000	$399,406
Westinghouse S.T.C. (subcontract to Indiana University)	62,000	461,000
University of Liverpool (subcontract to Indiana University)	50,000	78,774
Subtotal for Indiana University	437,000	939,180
University of Colorado	73,000	360,750
Oak Ridge National laboratory	60,000	369,000
Lawrence Berkeley Laboratory (see note 2)	55,000	65,000
Los Alamos National Laboratory	40,000	65,000
University of Pennsylvania	50,000	155,000
Princeton University	135,000	160,000
Total Budget	**$850,000**	**$2,113,930**

1. FY90 funding for I U includes $310K generic + $15K subsystem
2. FY90 funding for LBL includes $50K generic + $5K subsystem

FY91 SUBSYTEM BUDGET LISTED BY TASK

Central tracking	
Indiana University	332,839
University of Colorado	162,338
Los Alamos National Laboratory	65,000
Lawrence Berkeley Laboratory	60,000
Princeton University	160,000
	780,176
Intermediate Tracking	
University of Liverpool	78,774
Engineering Research and Development	
Westinghouse Science and Technology Center	461,000
Oak Ridge National Laboratory	369,000
	830,000
Electronics	
University of Pennsylvania	155,000
University of Colorado	162,338
	317,338
Simulation	
University of Colorado	36,075
Lawrence Berkeley Laboratory	5,000
Indiana University	66,568
	107,643
Total Budget	**$2,113,930**

INDIANA UNIVERSITY

1. Salaries	
a. Research support scientist (to be named)	$25,000
b. Program designer (R. Foster)	31,930
c. Simulation programmer (to be named)	35,000
d. Hourly help	10,000
e. Graduate students (3 for 2 mos. ea @ $1100/mo.)	6,600
Total Salaries	108,530
2. Fringe benefits	23,656
3. Supplies	
a. Composite modules	40,000
b. Straws and wire supports	15,000
c. Gas supplies	10,000
d. Assembly supplies	10,000
Total Supplies	75,000
4. Equipment	
a. CAD software	12,000
b. CAD workstation	20,000
c. 2 MACII terminals	14,000
Total Equipment	46,000
5. Travel	
30 trips to meetings @ $1000/trip	30,000
6. Indirect Costs	
49% of salaries, supplies, travel and fringe benefits	116,221
Total Budget	**$399,406**

WESTINGHOUSE SCIENCE AND TECHNOLOGY CENTER

1.	Senior level mechanical engineer 8/12 year (1280 hr.)	$131,000
2.	Senior level composites engineer 2/12 year (320 hr)	32,000
3.	Senior level designer 6/12 year (900 hr)	102,000
4.	Draftsman/designer 6/12 year (900 hr)	64,000
5.	Materials technician 4/12 year (640 hr)	45,000
6.	Materials	63,000
7.	Travel	24,000
	Total Budget	**$461,000**

UNIVERSITY OF LIVERPOOL

1. Engineering Physics Support	
a. Physicist-engineer for design, construction and testing of ITD drift chambers	
-full-time salary for 12 mos.	$30,704
-fringe benefits	8,042
b. Trainee physicist-engineer (part-time)	
-salary including fringe benefits	5,400
Total Engineering Physics Support	44,146
2. Equipment	
-for chamber prototype tests (includes consumable items)	26,000
3. Travel	
3 physicists each to make 2 trips to U.S.	
-air travel @ $738 ea.	4,428
-7 nights subsistence @ $100/day	4,200
Total Travel	8,628
Total Budget	**$78,774**

UNIVERSITY OF COLORADO

1. Salaries and Wages	
a. Research associate (to be named) (50% time, 12 mos.)	$15,500
b. Design engineer (G. Schultz) (50% time, 12 mos.)	24,600
c. Graduate research assistants (1 @ 50% time for 9 mos, 100% time for 2.5 mos.)	16,000
d. Undergraduate student assistants (2 FTE, hourly basis)	28,000
Total Salaries and Wages	84,100
2. Fringe Benefits	6,400
3. Supplies and Materials	
a. Equipment repair and maintenance	3,000
b. CAD software upgrades	2,000
c. Laboratory supplies	1,000
d. Materials for fixtures, etc.	1,500
e. Electronic components, connectors, wire, cables, etc.	3,500
Total Supplies and Materials	11,000
4. Equipment	
a. For electronics interface	55,000
b. For prototype fabrication	97,900
c. For drift chamber readout	15,000
Total Equipment	167,900
5. Travel	
Domestic; to coordinate collaborative R&D effort	30,000
6. Other Direct Costs	
a. Machine shop time	4,000
b. Publications	500
Total Other	4,500
7. Indirect Costs	
41.8% of MTDC	56,850

OAK RIDGE NATIONAL LABORATORY

1. Design	
a. Prototype	$52,000
b. End plate	45,000
c. Module assembly concepts	23,000
d. Electronics	38,000
e. Cost estimating/planning	23,000
Total Design	181,000
2. Fabrication	
a. Prototype	150,000
b. End plate	38,000
Total Fabrication	188,000
Total Budget	**$369,000**

LAWRENCE BERKELEY LABORATORY

1.	Wire Aging Tests	$15,000
2.	Plasma Studies	15,000
3.	Straw Tube Tests and Measurements	30,000
4.	Travel for computer simulation	5,000
	Total Budget	**$65,000**

LOS ALAMOS NATIONAL LABORATORY

1. Staffing	
a. scientific (.05 staff years)	$10,000
b. other (.05 staff years)	5,000
2. Materials and Services	5,000
3. Subcontracts, Major Procurement (T.E.P. Injection Mold, W.C. Injection Mold)	45,000
Total Budget	**$65,000**

UNIVERSITY OF PENNSYLVANIA

1.	Engineering (1.0 FTE)	$100,000
2.	Technical support (.25 FTE)	15,000
3.	Test equipment	20,000
4.	Supplies	10,000
5.	Travel	10,000
	Total Budget	**$155,000**

PRINCETON UNIVERSITY

1.	Metallization of cathode foils, winding of straw tubes	$10,000
2.	Components for straw-tube end plugs	10,000
3.	Fixtures for straw-tube assembly	10,000
4.	4' x 8' granite surface plate	5,000
5.	Supports and alignment tools for straw-tube modules	10,000
6.	Flow and pressure control for 3-component gas mixtures	10,000
7.	Stainless-steel gas regulators, fittings, tubing, filters,etc.	10,000
8.	High- and low-voltage power supplies and related test equipment	5,000
9.	PC-clone computer, CAMAC crate and interface	10,000
10.	Test equipment for front-end electronics: amplifiers, ADC, TDC, etc.	5,000
11.	PRA LN103 nitrogen laser and spare parts	10,000
12.	1-GHz, 2-Gsamples/sec digital osciloscope	35,000
13.	Research-grade gas chromatograph, columns, multiport valve	15,000
14.	Trace oxygen and water analyzers	10,000
15.	High-purity chamber gases	5,000
	Total Budget	**$160,000**

APPENDICES

February 5,1990
IUHEE 90-1

Gas studies of 4 mm Diameter Straw Drift Chambers

C. Neyman, R. Foster, G. Hanson, B. Martin, H. Ogren, D. Rust

SSC R&D Group

Indiana University

1) Introduction

We are investigating the the feasibility of continuous cathode drift chambers using aluminized mylar walls (straw chambers) at the SSC. Several drift chamber designs using small diameter (4 mm) straws of several meters in length have been proposed for SSC detectors. While a number of chambers have been built and run successfully at PEP and CESR, SSC will impose many new demands. The high crossing frequency of the SSC will a require using the very fastest gasses in these chambers. These gasses must be studied and understood. High instantaneous rates and high radiation backgrounds also will impose design requirements.

We have carried out a series of measurements on a six tube straw detector. We measured the efficiency, drift time, gain, and resolution of a number of gases in 4 mm diameter straws.

2) Description of detector

The drift chamber constructed for this series of tests was a six tube array with a length of 40 cm as shown in Fig. 1. The straws were fabricated by Precision Paper Tube Company., Rockville, Ill. Each straw consists of a layer of 0.5 mil polycarbonate film aluminized on the inside surface, covered by an 0.5 mil mylar film. The two films are wound with overlapping pitch and bonded by an application of glue between them. The resulting tube is gas tight, and robust enough to handle easily. The inside diameter is 0.157 in or 4.0 mm.

The anode is a gold plated tungsten wire 25 μm in diameter. It is tensioned and held centered by two Delrin pins inserted in each end of the straw. The Delrin pins are inserted into an aluminum gas manifold, which positions the wires and provides a robust mechanical support. The triangular gas manifolds sit in a precision V groove that is machined in a long aluminum bar. The V groove aligns both manifold ends and holds the straws in position. Mechanical tolerances for the construction were about ± 50 μm.

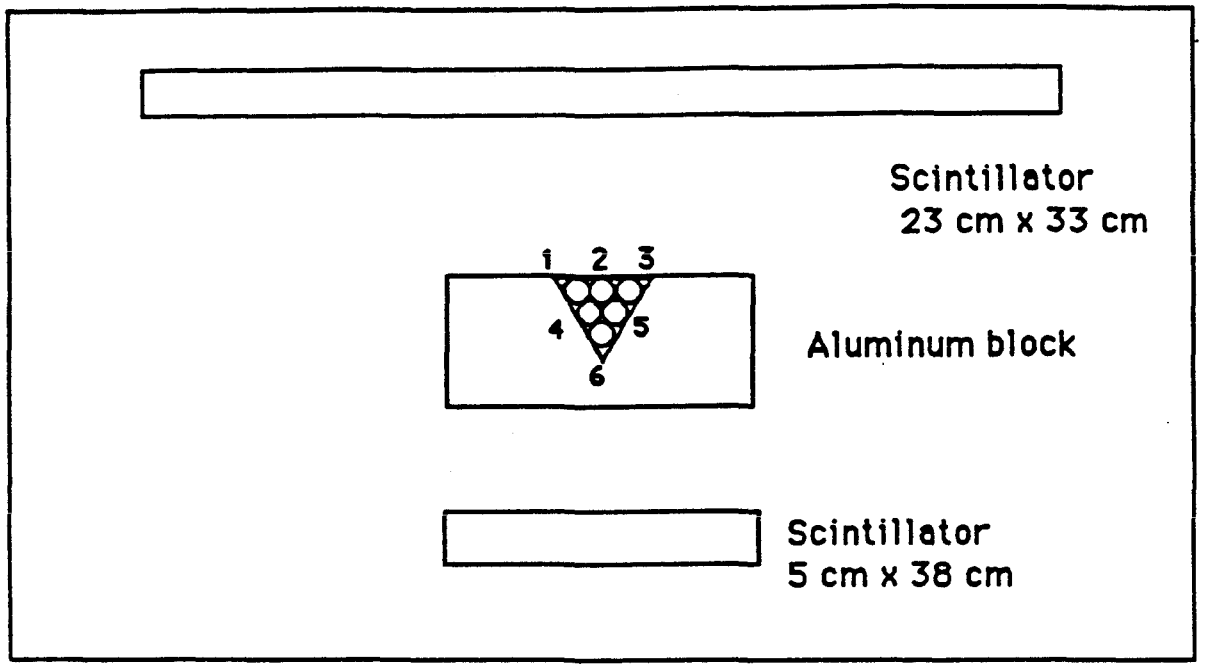

Fig 1 Test array of six straws with cosmic ray trigger

3) Electronics

A negative high voltage supply was used to establish the voltage difference between the cathode surface and anode wire. The anode wire signals were then taken out directly without capacitive coupling. A combination preamplifier-discriminator with typically a 600 μV threshold into 500 Ω. was used to form discriminated signals for the TDC. The coincidence between the two scintillators was used to start a LeCroy TDC (200ps/div) and the discriminated anode signals were used for a stop. The data were collected locally on an LSI-11 and transfered to a VAX system for later analysis.

4). Efficiencies of 4 mm Straw Tubes

We anticipate that with typical ionization constants that there will be about 40 electron-ion pairs produced by a minimum ionizing particle in a 4 mm straw. Electron attachment and lower intrinsic ionization may lower this number for many gasses. One of the first measurements made was a plateau curve for a number of candidate gasses . The following gas mixtures were used in cosmic ray tests: Argon-Ethane(50%), HRS gas {Ar-CO_2(10%)-CH_4(1%)}, CF_4(99.9), and CF_4-Isobutane(20%, 10%, and 5%). These were measured at 600μV into the 500Ω input resistance of the preamp, which was the lowest

The data for Ar-Ethane (50%) and for HRS gas are show in Fig 2. HRS gas did not plateau before the tubes began drawing current above 1350 V. Ar-Ethane(50%) reached 95% efficiency and appeared to plateau before 1700 V where it began drawing excessive current

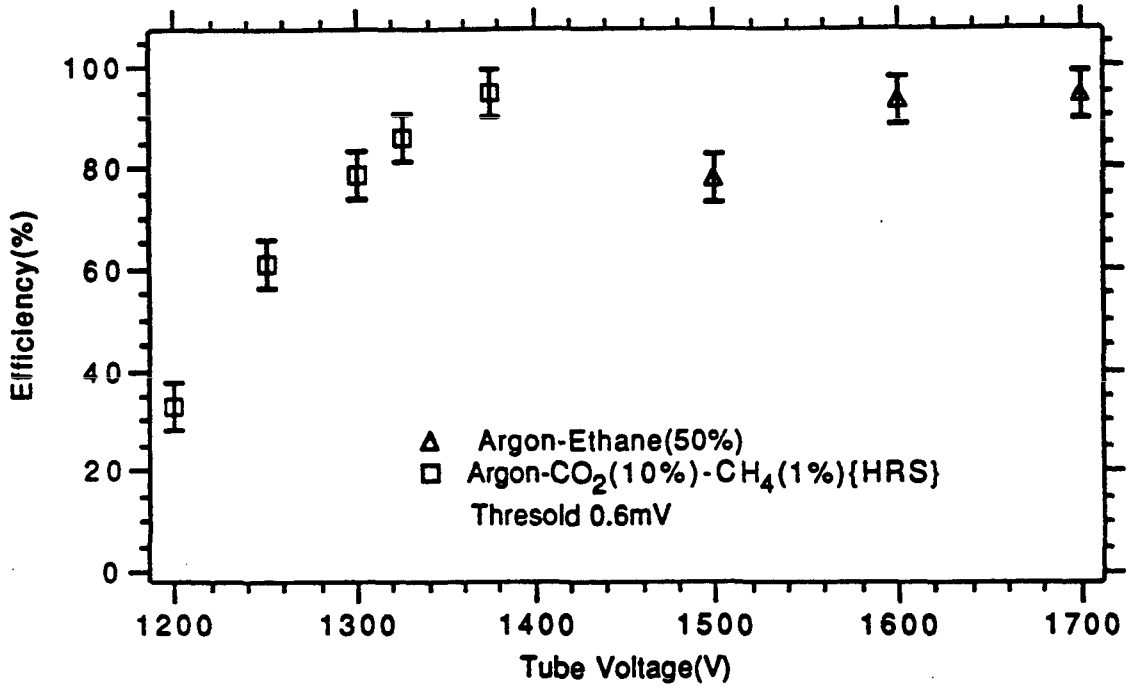

Fig. 2 Plateau curves

The efficiency measurements for the various CF_4 mixtures is shown in Fig.3. The pure CF_4 mixture does not reach full efficiency by 2400 volts.. It is likely that this is due to electron attachment. As has been reported in previous studies [1] the cross section for electron attachment is a resonant reaction. Small fractions of a quenching gas such as Isobutane cools the electrons below the threshold for attachment. Of the mixtures tested 20% Isobutane performed the best, reaching an efficiency of 98%. We expect about 1% inefficiency is due to the 40 microns of wall thickness. The remaining 1% can be ascribed to a 40 micron region near the wall where the path length is less than 300 microns and the cluster statistics are poor.

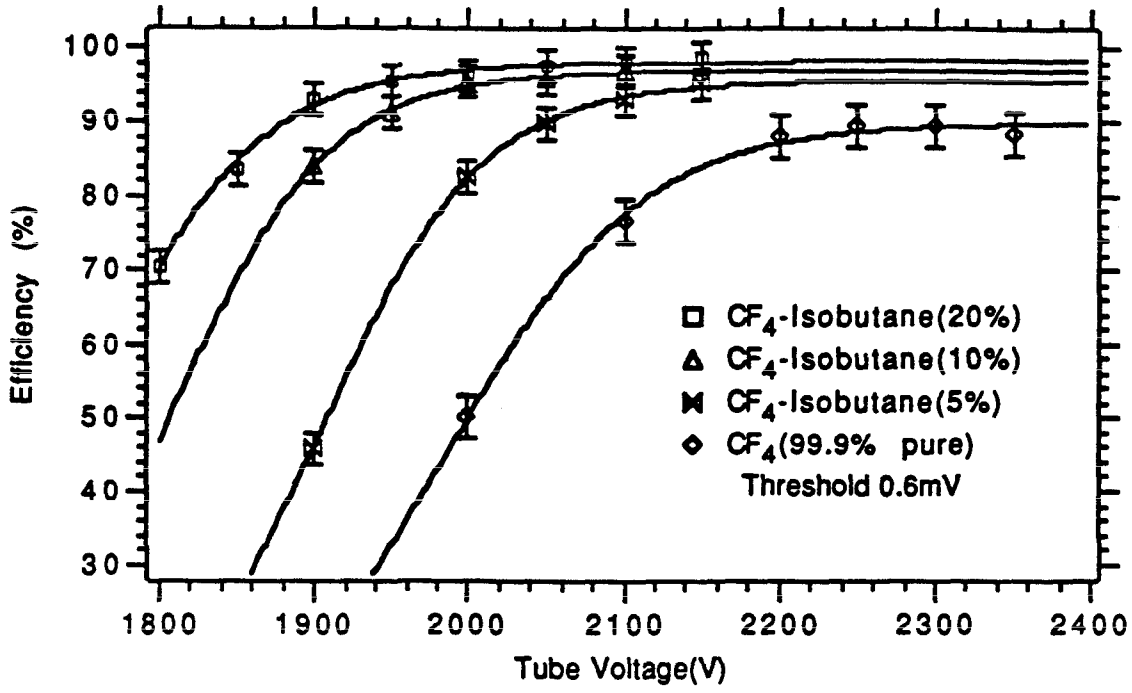

Fig. 3

The efficiencies for CF_4 and CF_4-Isobutane were fit to the function :

$$\varepsilon(v)=\frac{\varepsilon_0}{1+e^{\frac{-(v-a)}{b}}}$$

The values for ε_0, the asymptotic value of the efficiency, are:

CF_4 (99.9%)	89.8%
CF_4-Isobutane(20%)	98.2%
CF_4-Isobutane(10%)	97.1%
CF_4-Isobutane(5%)	95.5%

We also have made a number of more incomplete (quick) measurements on several nonflammable gas mixtures. These are shown in Fig. 4. HRS gas mixed with 50% CO_2 shows an efficiency of 95% and a plateau point near 2000 Volts. Argon-CF_4 (50%) mixture reaches only 87% before drawing current, and CF_4-CO_2(15%) has an efficiency of 85% at 2250 Volts.

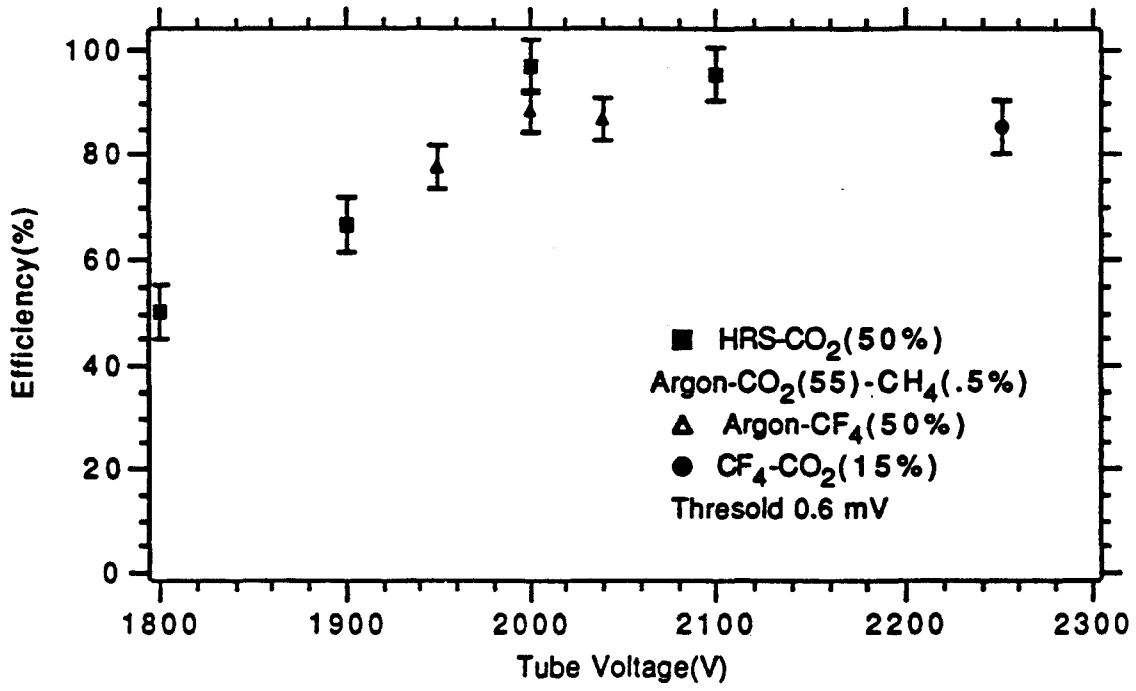

Fig. 4 Efficiency measurements

5) Gain of 4 mm Straw Tubes

The gain of the straw chambers was measured for four different gas mixtures: Ar-Ethane(50%), CF_4(99.9) and CF_4-Isobutane(20% and 10%). A Fe^{55} source was used to produce at constant pulse height signal. The Fe^{55} x-ray has an energy of 5.9 keV. Assuming an average energy to produce an ion-electron pair of 24.5 eV [2], the primary ionization of the xray from Fe^{55} gives 240 electrons in Ar-Ethane. The total charge from each x-ray interaction was measured with a charge sensitive amplifier with an integration time of about 10 μsec, followed by a Ortec model 575 amplifier and then displayed on an Ortec 7100 multichannel analyzer. A calibration of the charge was obtain with a pulser and oscilloscope. The gain for CF_4 and CF_4-Isobutane mixtures was calculated assuming the same primary ionization as Ar-Ethane(50%).[3] The charge and gain are shown in Fig. 5. Notice, in particular, that the gain of the CF_4-isobutane (20%) mixture is about 5×10^4 at 2000 V (at the beginning of the efficiency plateau).

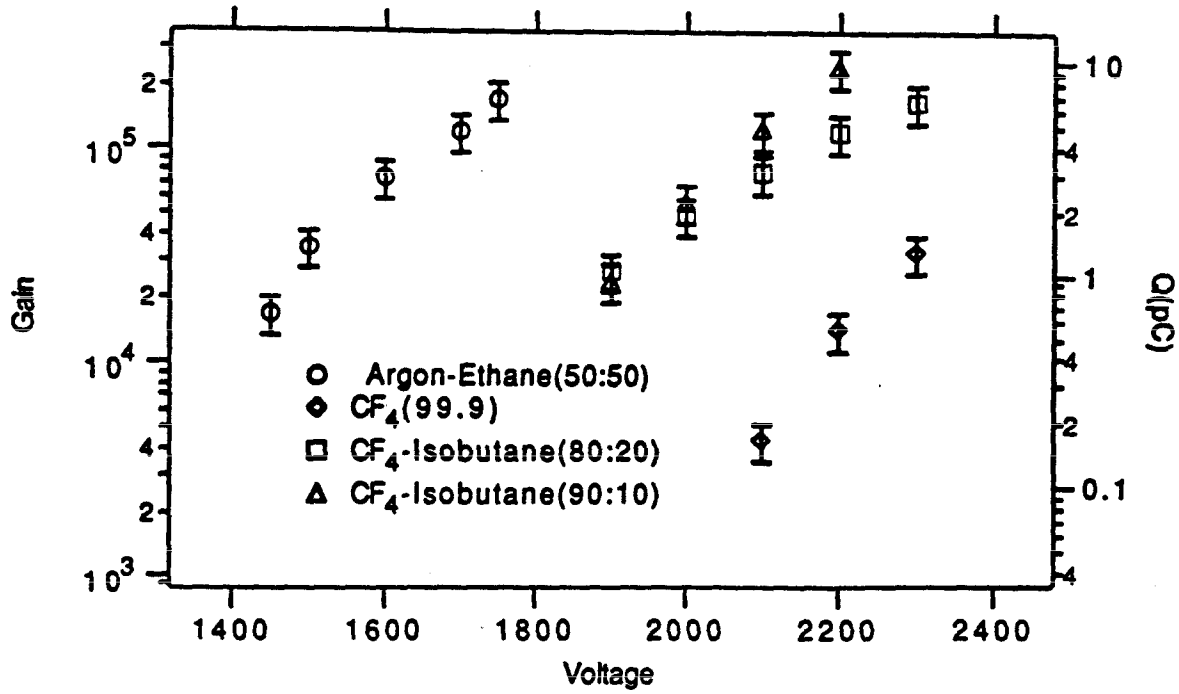

Fig. 5 Gain in 4mm straw with 25 μ sense wire

6) Resolution

The resolution of the middle layer of straws was measured with cosmic rays using the same 6 straw setup described previously. A track was fitted through straws 2 and 6.(see Fig. 1) The distribution of the residual between the track fitted and the actual drift distance in the central two straws (4 and 5) was calculated, displayed, and fitted with a gaussian.The standard deviation of this distribution is directly related to the intrinsic resolution of each straw. The resolution was measured for all the gasses discussed in Sec. 2.

The resolutions for Ar-Ethane(50%) and HRS gas are shown in Fig. 6. Both gasses showed improvement in resolution as the voltage was increased, but the rather poor values (150-200 μ) probably are due the effects of poor cluster statistics which is reflected in the efficiency. Improvements in our drift time model for the gasses might also improve some of the resolution effects.

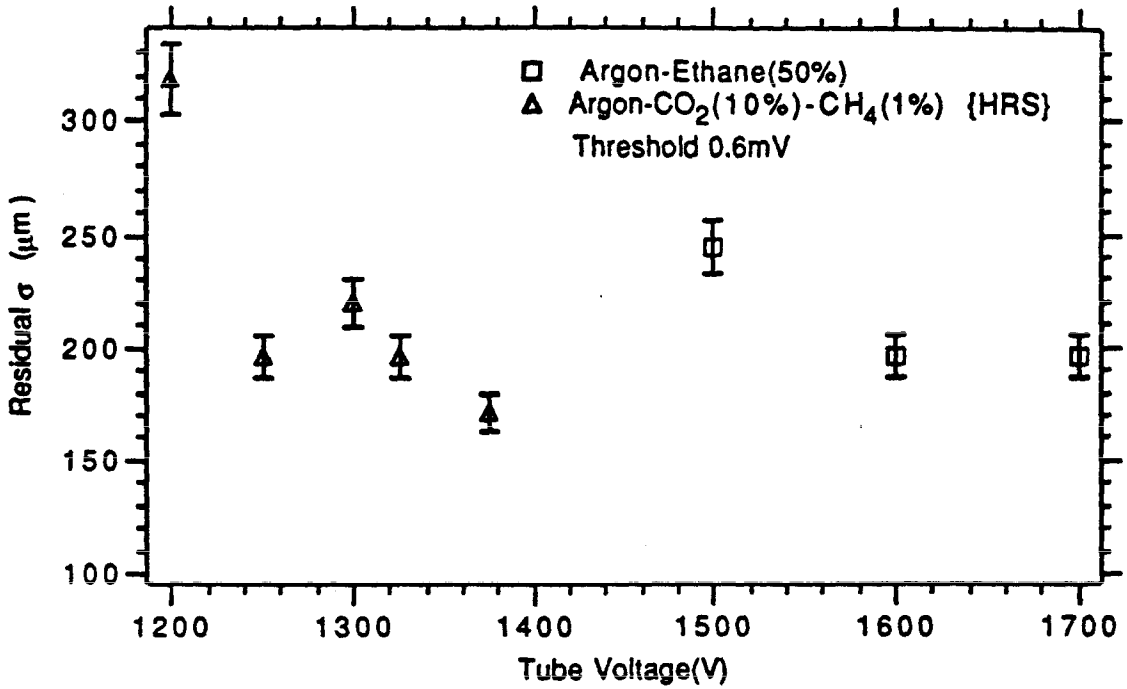

Fig. 6. Resolution measurements for Ar-Ethane(50%) and HRS gas

The resolutions for CF_4 and CF_4-Isobutane(20%-10%-5%) are shown in Fig. 7, 8, and 9, respectively. Due to the known problems with electron attachment in pure CF_4 the resolution is expected to be poor. The plotted data of pure CF_4 represent the average of two points with the horizontal error bar representing the width of the average.The resolution of CF_4-Isobutane (20%), measured to be about 100 μm on the plateau, was the smallest of the CF_4 mixes . We believe that part of the relative performance of the CF_4 to the other gasses is the quality of the drift velocity model we used for CF_4.

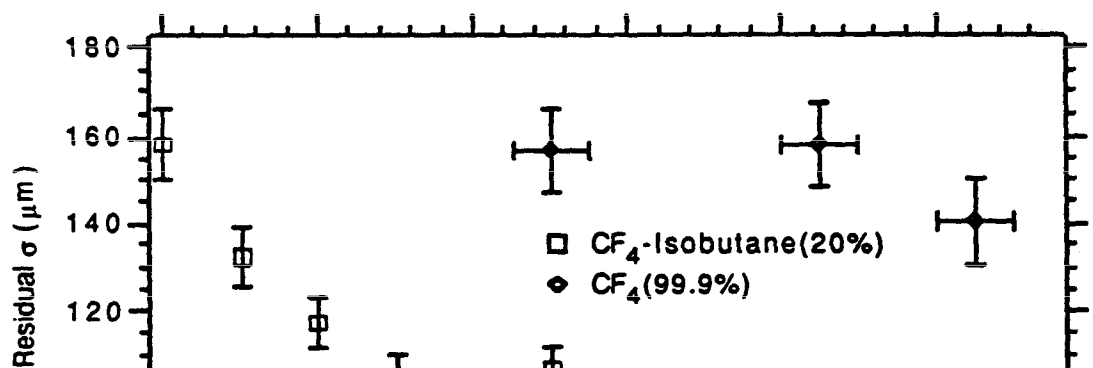

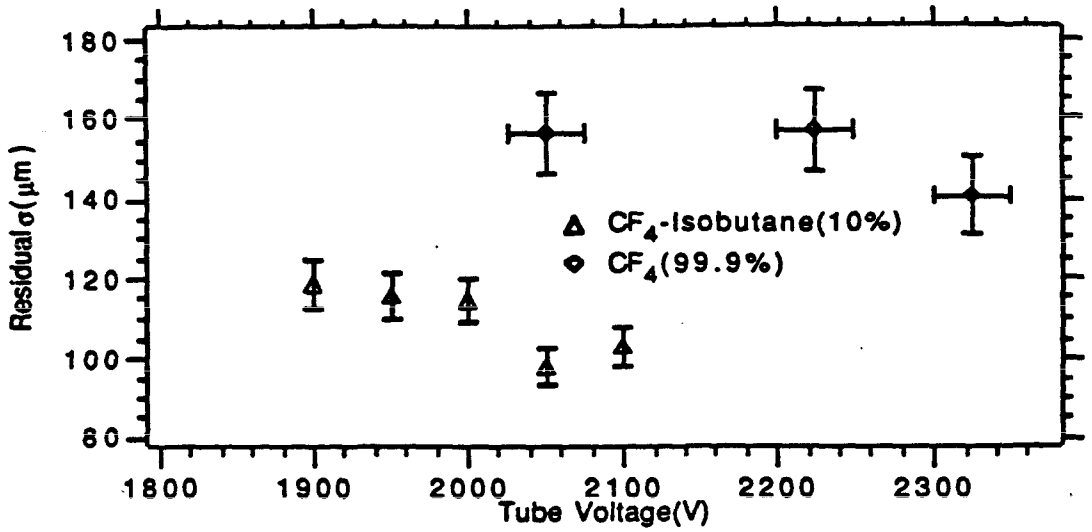

Fig. 8 Resolution for CF_4. Isobutane(10%) and CF_4

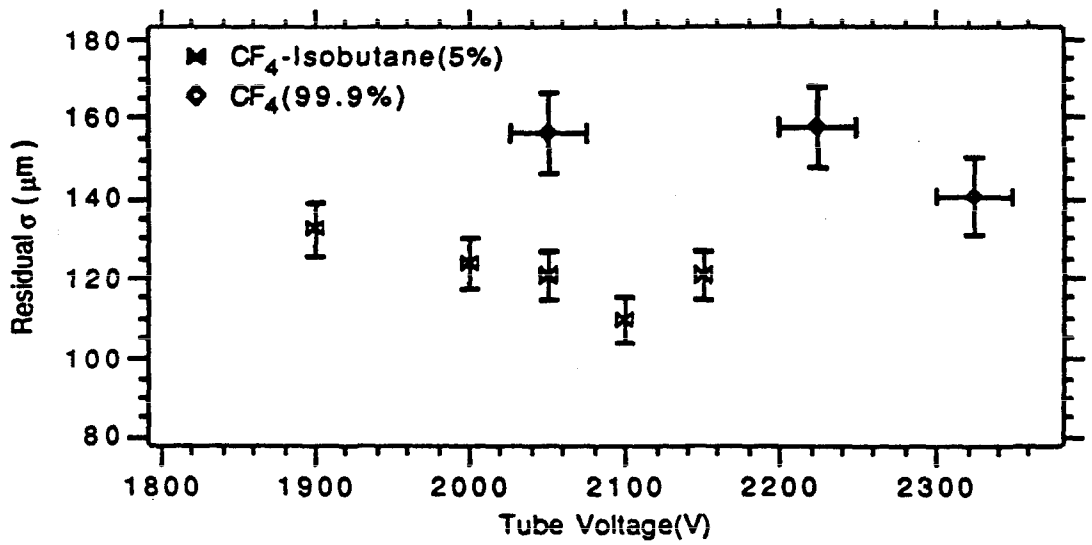

Fig. 9 Resolution for CF_4-isobutane (5%) and CF_4

7) Drift Velocity

The short time (16 nsec) between bunch crossings at the SSC dictates the use of a gas with a high drift velocity. We have looked at a number of gasses which might have the

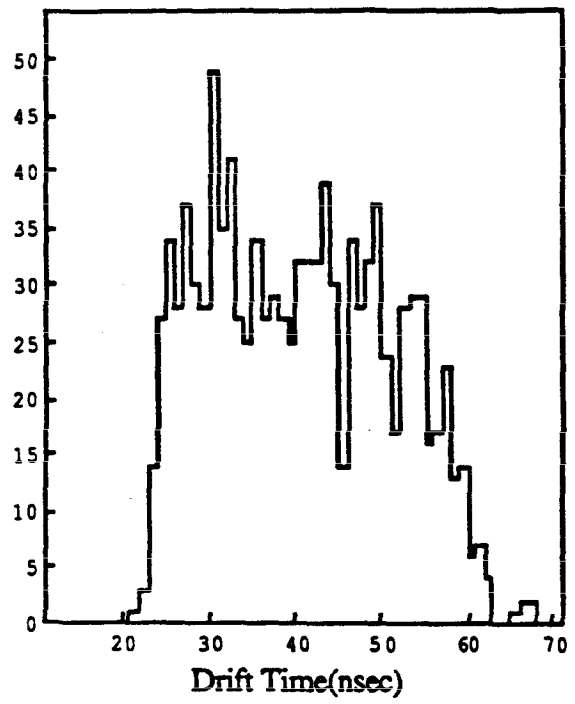

Fig. 10 Ar-Ethane(50%)
1700 V Threshold 0.6 mV

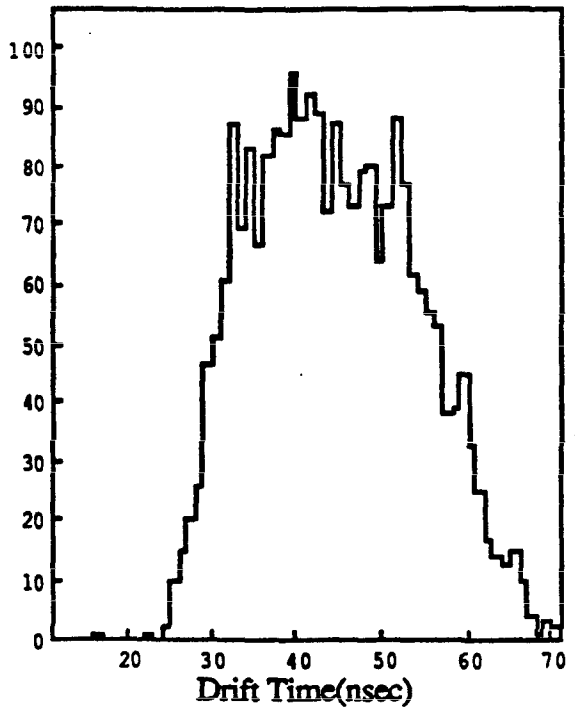

Fig. 11 HRS (Ar-CO_2(10%)-CH_4(1%))
1350 V Threshold 0.6mV

The full widths of CF_4 and CF_4-Isobutane(20%, 10%, 5%) range from 18 to 22 nsec for a 2 mm drift, making any of these gasses suitable for the SSC. They are shown in Figures 12, 13, 14 and 15. We do not yet understand in detail the shape of these distributions.

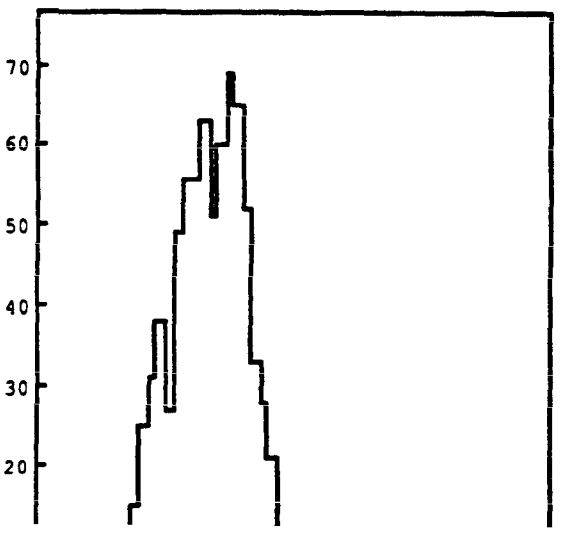

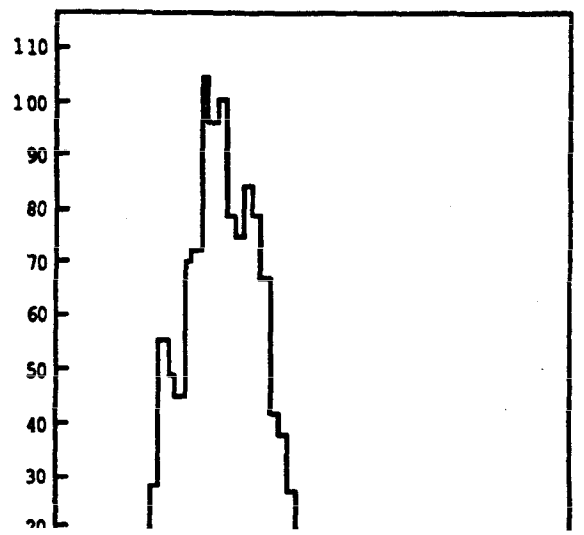

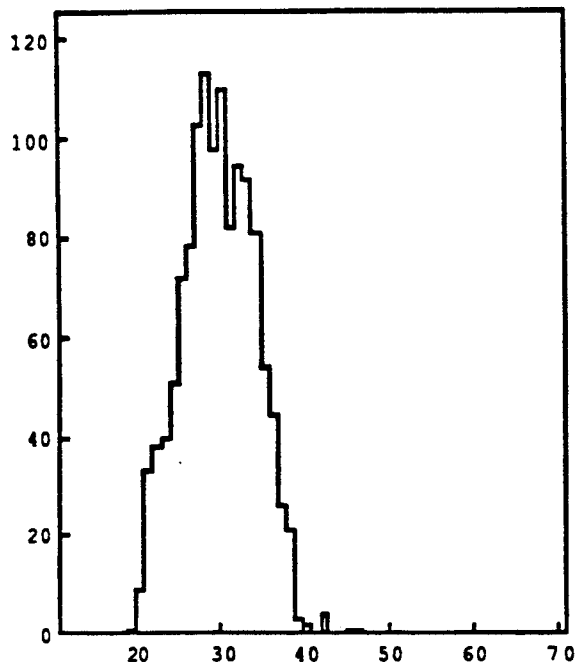

Fig. 14 CF_4-Isobutane(10%)
2300 V Threshold 0.6 mV

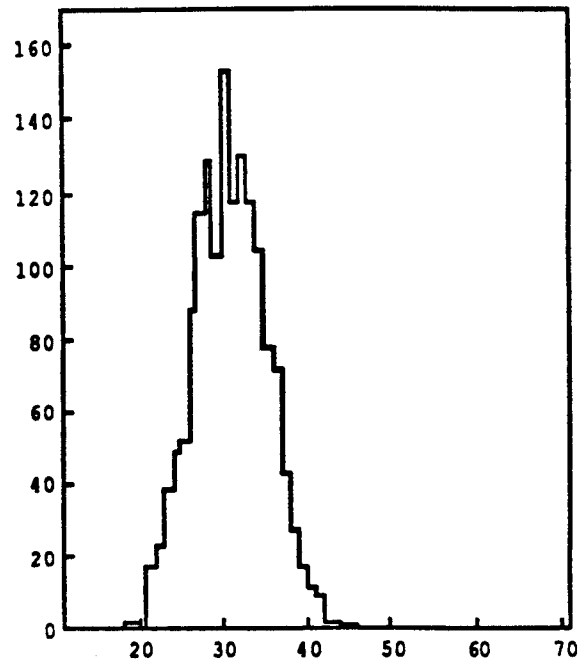

Fig. 15 CF_4-Isobutane(5%)
2100 V Threshold 0.6mV

In addition to the gasses already tested we measured drift velocities. for several other gas mixtures. However, the exact compositions for optimum operation have not yet been determined. One of these gasses tested was HRS-CO_2(50%) this mix was an approximation to Ar-CO_2(50%). As can be seen in Fig. 16 this gas has a long tail which may in part be due to its unsaturated drift velocity.
Another $C0_2$ mix we looked at was CF_4-CO_2(15%). As can seen in Fig 17 this gas has a full width of 28 nsec but like Ar-CO_2(50%) it also has some events at longer drift time.
We also measured Ar-CF_4(50%). This gas has a fast drift time of 24 nsec as can be seen in Fig 18. However this gas didn't plateau, as was shown in Fig 4.

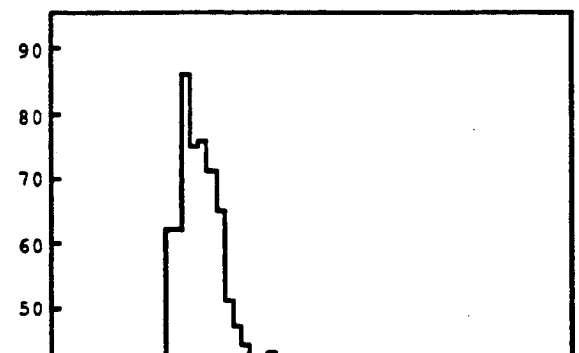

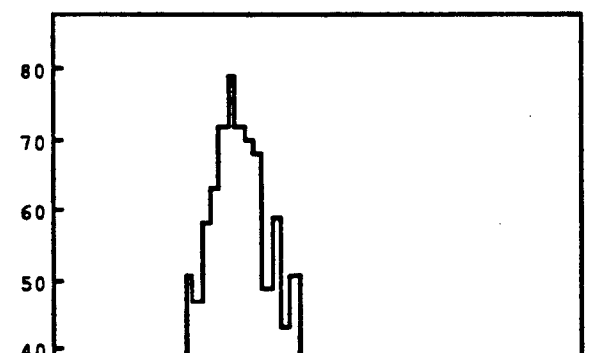

2100 V Threshold 0.6mV

2250 V Threshold 0.6 mV

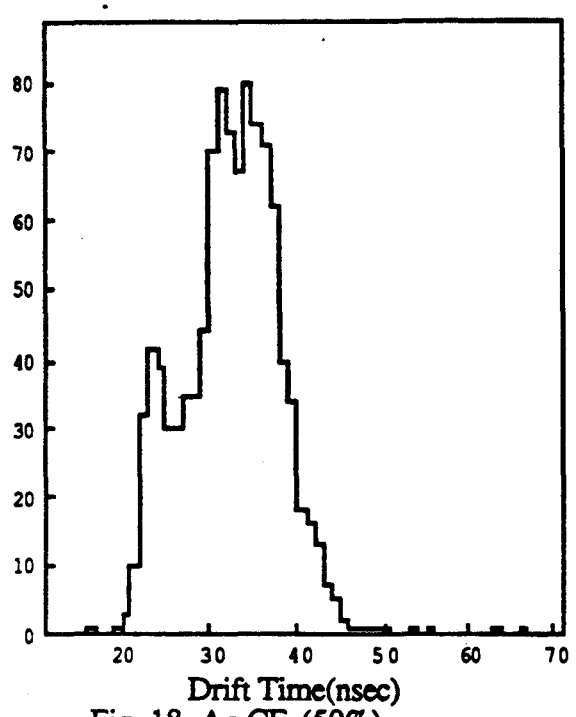

Fig. 18 Ar-CF_4(50%)
2040 V Threshold 0.6mV

8.) Conclusions

We have measured several basic properties of 4 mm diameter straw drift tubes. A gas mixture of CF_4 -Isobutane (20%) would appear to satisfy all the requirements for a fast detector at SSC. This mixture has full eficiency at 2000 V, a gain of 5×10^4, an intrinsic resolution of about 100 μ, and a drift time of less than 20 ns in a 4mm diameter straw. However, we would much rather use a nonflammable gas in the tracking system. We will continue to explore other gas mixtures.

References:

1. J. Fischer, et .al., Nuclear Instruments and Methods A238(1985) 249

February 9, 1990
IUHEE 90-2

Wire Stability tests on 4 mm Straw Chambers

H. Ogren, R. Foster, G. Hanson, B. Martin, C. Neyman, D. Rust

SSC R&D Group
Indiana University

1.) Calculation of Electrostatic forces

The electrostatic stability of a wire in a straw chamber is a function of the tension on the wire. The electrostatic limit can be estimated by using the linear term in the expression for the attractive force per unit length on a wire element displaced by δ from the center line of the cathode :

$$F=\frac{2\pi\varepsilon_0 V^2\delta}{[\ln(\frac{R}{r_0})]^2 R^2}, \qquad (1)$$

where V= voltage, R= cathode radius, r = wire radius, δ= displacement from center. In general this will be balanced by the tensional force of the wire. Therefore, assuming that the wire will have a sinusoidal shape about the central cathode axis, and imposing the boundary conditions that the wire is fixed at both ends , the condition on the wire tension for stability is: [1]

$$T > \frac{2\varepsilon_0 V^2 L^2}{\pi R^2 \ln(\frac{R}{r})^2}, \qquad (2)$$

where L is the wire length (meters).

For a 2 mm radius tube and a 12.5 μ radius wire this condition is

$$T > 5.6\times10^{-6} V^2 L^2 \text{ gm force} \qquad (3)$$

This is the minimum theoretical tension (in grams of force) required for stability for a given length of 4mm diameter straw at a specified voltage.

Δ from the symmetry axis. Assuming the wire distortion is sinusoidal, the total force on the wire can then be expressed as the integral :

$$F_{TOT} = \frac{2\pi\varepsilon_0 V^2}{\ln(R/r)^2 R^2}\int_0^L (A\sin(\pi x/L)+\Delta)dx \qquad (4)$$

The resulting tension in the wire is

$$T = \frac{LF_{TOT}}{2\pi A} = 5.6\times10^{-6}\, V^2L^2(1+\frac{\pi\Delta}{2A}). \qquad (5)$$

Notice that the tension now depends on the amplitude of the wire deflection unlike the first approximation for a well-centered wire. The deflection amplitude now can be solved for:

$$A = \frac{\pi\Delta}{2(\frac{T}{5.6\times10^{-6}\, V^2L^2}-1)} = \frac{\pi\Delta}{2(\frac{V_0^2}{V^2}-1)}, \qquad (6)$$

where V_0 is the stability limit for zero displacement from Eq. 3.

This amplitude function , A ,is shown in Fig.1 for a 1 meter long tube and a wire tension of 40 grams.

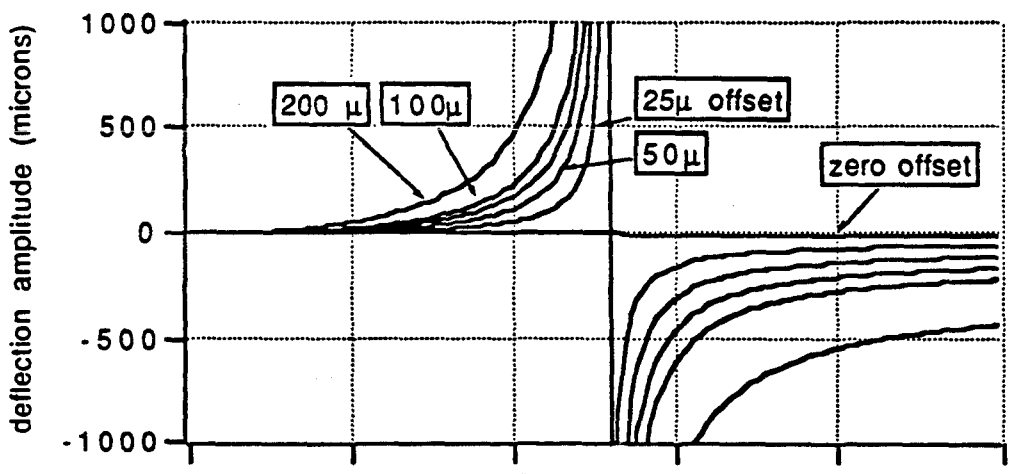

Notice that if we set a limit of 100 μ maximum amplitude , A, then we can find the relationship between the offset error and voltage limit. For instance, suppose we could construct the tube assembly with a maximum offset of 50 μ. This formula then limits the allowable voltage to V/V_0 = sqrt(1/ (50/70+1)=0.7. Since we plan to use a drift gas that requires 2000 Volts for good efficiency, the implies a V_0=3000 V. Then, using Eq. 3, for a maximum free span of 1 meter, we find the required tension = 50 grams.

3.) Measurements of stability

We have attempted to verify these expressions by performing a number of optical and electrical tests. The first test was with a 2.1 m length straw that was tensioned and positioned vertically with a central wire 25 μ in diameter.The tension of the wire was varied and the voltage recorded at the onset of instability, (when the supply tripped!).Oscillations of the straw were observed at instability when the tube was unsupported. Four support points were added to stop the oscillations , but as can be seen from Fig. 2 we were far from the theoretical limit. of 26 grams force at 1000 Volts.

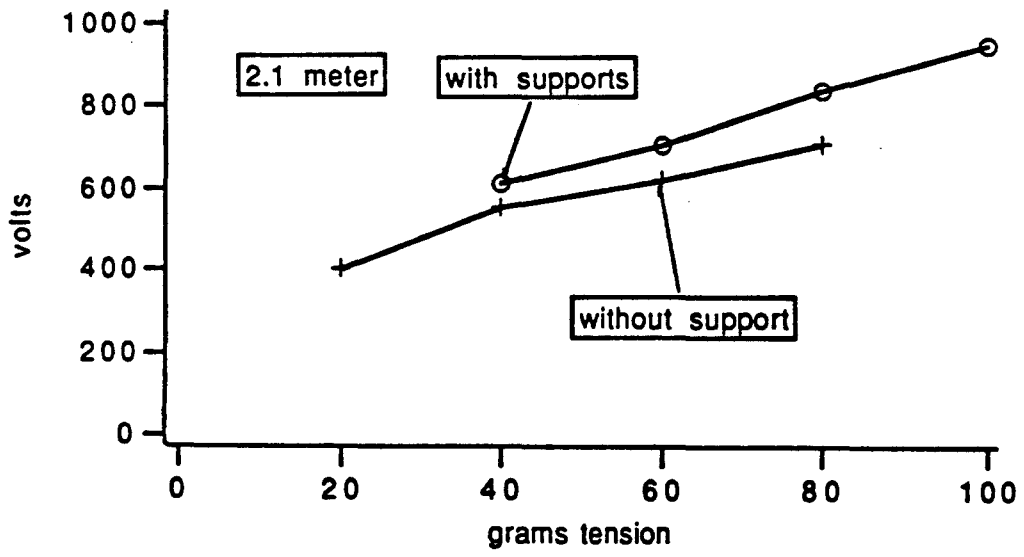

Fig. 2 Stability measurement

We know from further measurements that the problem was in the method of positioning the straw. In our initial tests we had tensioned the straw on a vertical jig and then added up to four glue joint contact points for transverse stability along its length. We now know that a much more accurate method must be used for positioning and holding the

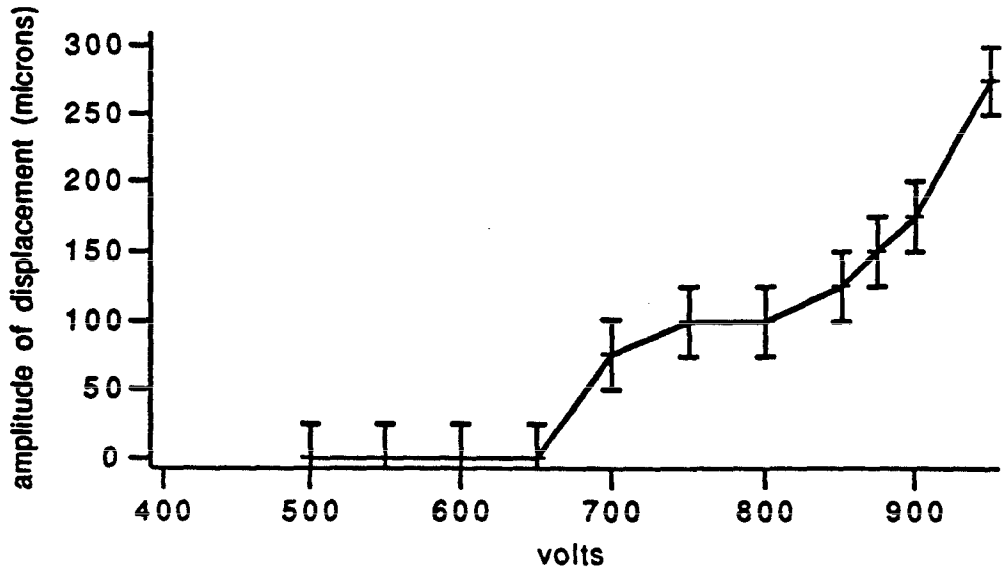

Fig. 3 Measured wire displacement from center vs voltage for a 2 meter straw with unsupported wire at 100 grams tension.

In order to improve our measurements we built a new test system. A 4 mm square groove was machined in an aluminum channel with a linear runout of less than 50 μ. The wire was positioned at each end with x-y translators capable of 25 μ accuracy. The total length of the wire was 1.07 m. The wire tension was set at 40 gm for all the measurements we report here. This results in a catenary sag of 20 μ which we ignore. C02 gas was flushed through the straw to suppress HV discharge.

We first experimentally determined the position of maximum stability. This was done by translating the wire and testing the high voltage limit of stability. This corresponded to a maximum of 2500 volts and was taken to be the central axis of the straw. This is 8% lower that the theoretical limit, but a considerable improvement from the unsupported measurements. It probably reflects the residual misalignments in the straw positioning. Then the wire was translated horizontally in a series of steps to investigate the change in stability. Again the stability point was determined by the wire snapping over to short to the cathode.We found that the maximum voltage point dropped by about 100 volts for every 50 μ of horizontal displacement. of the wire. This is shown in fig. 4.

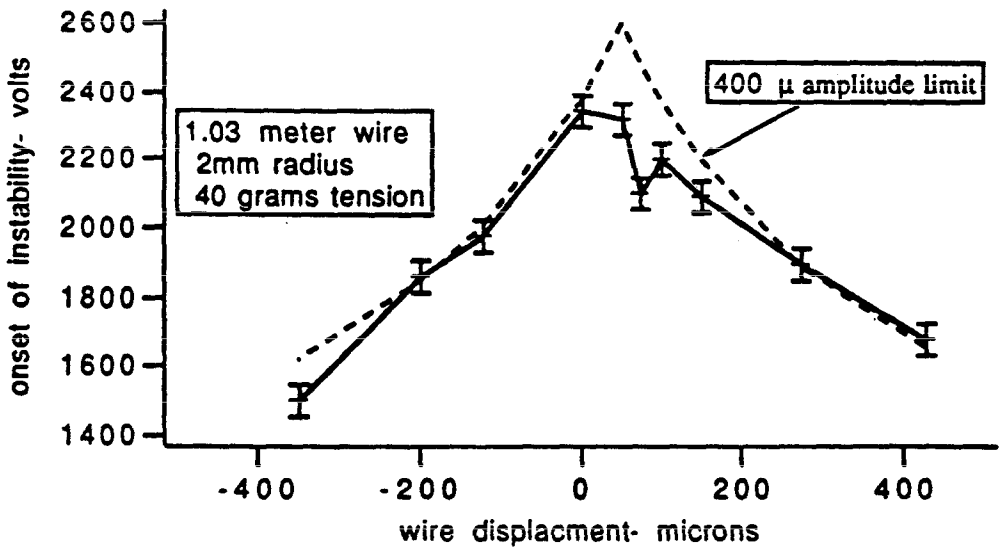

Figure. 4 Electrostatic stability limit vs. radial wire displacement.

We can compare this to the model for instability in Eq. 6 by assuming a maximum amplitude, A= 400 μ, before the sudden nonlinear onset of instability. This plot of the voltage limit vs wire displacement is shown in Fig. 4. The match to the data is reasonable. Thus the model expressed in Eq. 6 can be assumed to be correct up to maximum amplitudes of about 400 μ . After this point the forces are no longer linear and the wire rapidly goes unstable.

4.) Conclusions

One of the conclusions of this study is that for straw tube construction we must align the cathode structures to a precision better than 100 μ if we attempt stable, unsupported wires spans of 1 meter. Thus the requirements on the straw alignment is comparable to the precision required for wire placement.

We should mention that we have developed [2] a wire support mechanism that is simple and easy to implement. It may be that using wire supports every 50 cm would lead to a more conservative design and less restriction on tension and voltage. However we have yet to establish the requirements for gain stability, d vs t, variations. and attenuation.

References:

February 9, 1990
IUHEE 90-3

A wire support design for Straw Drift Chambers

R. Foster, G. Hanson,B. Martin C. Neyman, H. Ogren, D. Rust

SSC R&D Group

Indiana University

1) Introduction

Straw drift chambers have been built and used in experiments for the past eight years. Straw lengths up to 80 cm and straw diameters as small as 4 mm have been used With the smallest diameter straws, and with voltages of more than 2000V , electrostatic stability becomes a problem. The design of 2 and 3 meter straws for SSC will necessitate the use of internal spacers to support the wire. This report is a description of a device for supporting the sense wire precisely in a straw tube. Our design seems close to meeting the following design goals:

- •Center the sense wire within 25 μ
- •Allow free gas flow through straw
- •Insulate without noise at the 2 KV working voltage.
- •Minimize multiple scatter and photon conversion.
- •Minimize detector dead space.
- •Allow low cost , rapid, and, automated assembly.
- •Have long term dimensional stability
- •Allow accurate positioning along the sense wire.

2.) Description of the support spacer

The support, shown in figure 1, is injection molded from acetal plastic,(Celanese Celcon M90). The overall form is a cylinder 3.95 mm diameter and 4 mm long. The central portion which grips the wire is molded as a blank disk 0.3 mm thick and about 0.5 mm diameter. The disk is connected to the wall by three spokes. The wall, which is 0.5 mm thick, is the only high precision part of this support; it must precisely conform to the straw's inner wall allowing a sliding fit within the straw. One end of the cylinder is rounded to allow easy entry into a straw. The mold parting line is placed at the edge on the opposite end. The molding injection hole, located on the outer wall, has been slightly recessed to clear the edge of the cylinder.

3) Wire attachment

the constant tension, (about 50 gm), needed to drive the wire through the melted plastic to the centerline . The wire is heated electrically by current fed through the clamps. A 0.25A current applied for less than 2 sec. is needed to center a 25 μ diameter gold plated tungsten wire. When the wire reaches the center, radial forces vanish and the wire remains centeredwhen the plastic cools (within a second or so).

3.) Tests and applications

Some tests have been made to see how closely this technique reaches our design goals. The molded-in wires have been measured to center within 40 μ. We believe that further improvements such as more careful adjustment of the quartz rods.in the melting fixture will allow this to be better than 25 μ. The centering of the wire in the straw would then be limited by the necessary gap between support and straw tube needed to slide the support into position.

We are in the process of assembling a long straw chamber using these supports. We have tested these supports in a short prototype straw chamber and have not observed any problems with noise or breakdown when operated at the highest normal operating voltage of 2.3KV.

Because of the small size of the attachment point at the center of the support the wires break free from the plastic at about 30 gm. of axial force and then slide freely through the plastic. All supports needed for a straw may be attached with the required separation prior to pulling the wire into the straw. The attachment seems secure enough for the supports to retain their proper separation after the wire is pulled through the straw, yet can be dislodged without damage to wire or spacer if adjustments are needed.

We plan to continue evaluation of these supports. Some of the questions we will try to answer are:

What is the impedance to gas flow?
Are there signal attenuation effects?
How effective are the supports for use in splicing straws?
Is there long-term creep when the supports are subjected to radial forces likely to occur at straw ends?
Can these supports be helpful in centering the wire at the ends of straws and thus be integrated into the end cap design?
Are the supports damaged by the radiation dose in an SSC experiment.

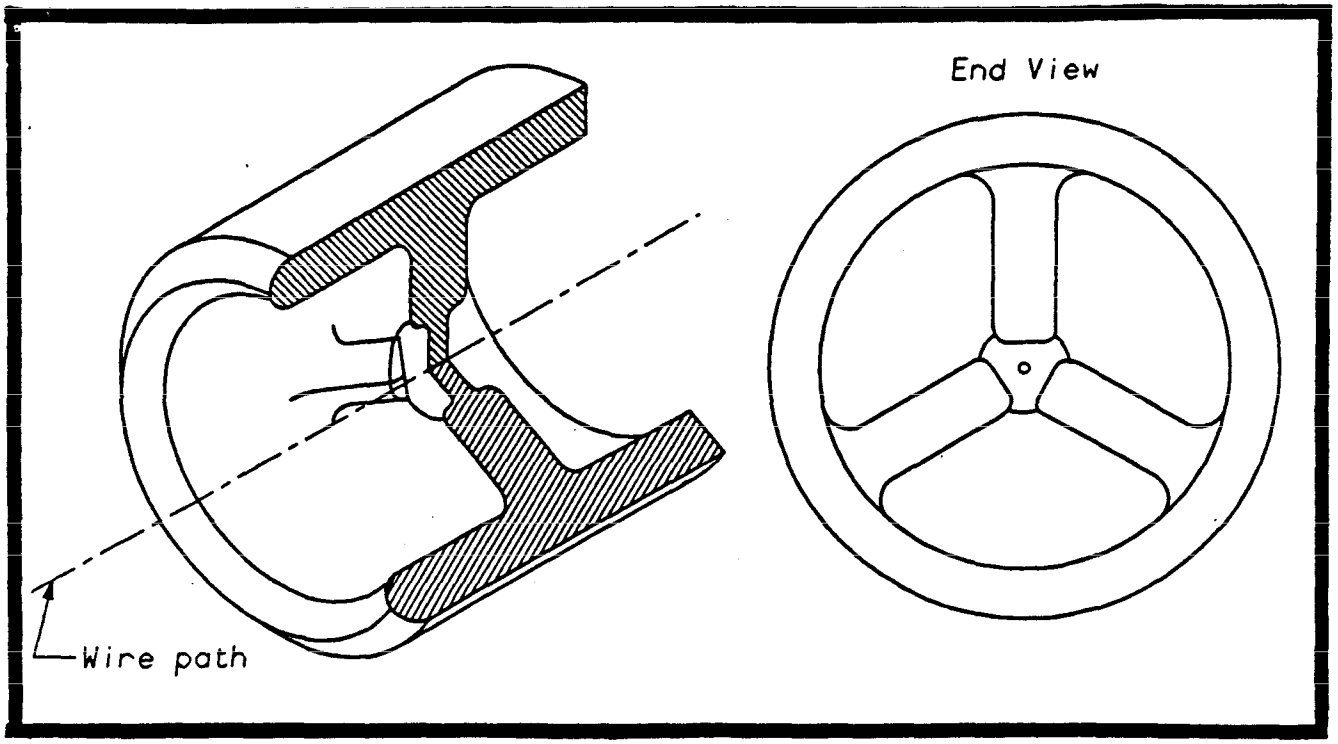

Figure 1 Wire Support

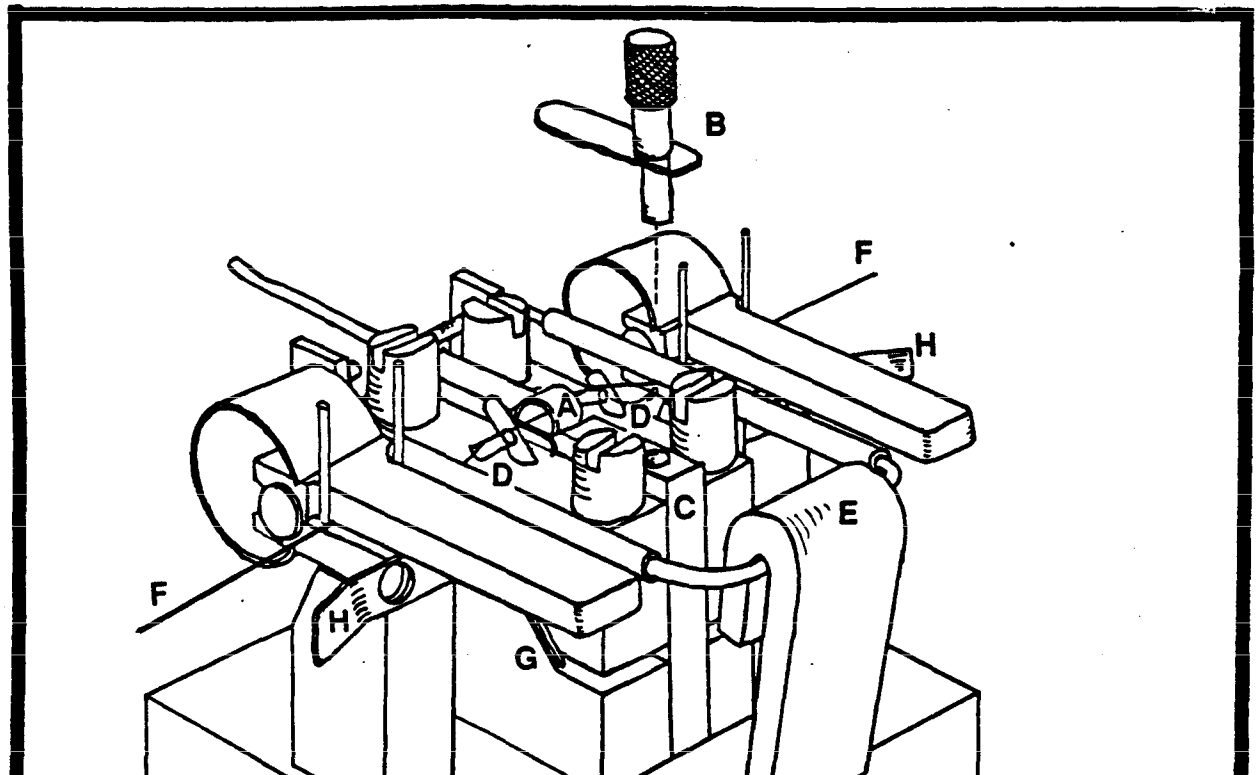

May 30, 1990
IUHEE-90-5

INTEGRATED TRACKING CONFIGURATION I: SILICON AND WIRE CHAMBERS*

GAIL G. HANSON
Indiana University, Bloomington, Indiana 47405 USA

ABSTRACT

A conceptual design of a tracking system for a solenoidal detector is presented. The tracking system consists of silicon pixels and microstrip detectors at small radius and wire chambers at larger radius. The goals for the tracking system design are to provide momentum measurements of all charged particles with p_T above a few GeV/c for $|\eta| \lesssim 2.5$ and to provide a fast trigger for such particles.

1. TRACKING SYSTEM DESIGN

The conceptual design for the tracking system is shown in Fig. 1. It consists of:

- A high-resolution two-dimensional pixel detector to aid in pattern recognition and detect separated vertices from long-lived particles and multiple p-p interactions;
- An array of segmented silicon microstrip detectors to provide a powerful pattern recognition tool even in the cores of jets;
- A wire chamber system to provide the high-precision momentum measurements and trigger information for high-p_T tracks.

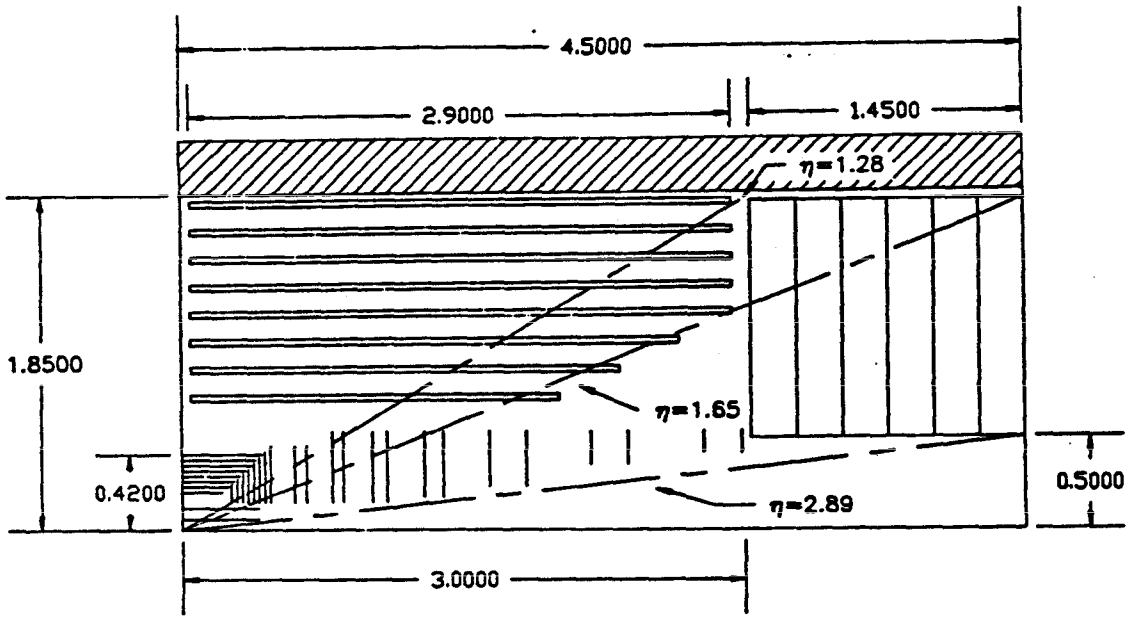

Fig. 1. Conceptual design for a pixel, silicon strip, and wire chamber tracking system for a solenoidal detector.

1.1. Pixel Vertex Detector

The pixel vertex detector[1] provides three-dimensional position measurements. It consists of two concentric cylindrical layers of pixel arrays within a radius of 10 cm from the interaction point and covers a pseudorapidity range $|\eta| \lesssim 2.5$, extending to $|z| = 40$ cm, where z is the distance along the beam line. The pixel sizes are expected to be 30 μm × 300 μm in the ϕ and z directions, respectively. The position resolutions should be better than 10 μm in ϕ and 100 μm in z. The pixel arrays are shingled in both ϕ and z to provide complete coverage. The detectors will be about 300 μm thick, and a particle at normal incidence will traverse about 2% of a radiation length of material.

Because of the high particle rate, a "smart pixel" electronic system architecture is being developed to buffer information and read out events efficiently. A smart pixel signals when it is struck, stores the analog signal, and is read out only if it is associated with a valid trigger event. All circuit functions prior to readout are on the chip. The electronics will either be fabricated directly on

strate. The detectors are arranged in superlayers, each with four measurements, in a cylindrical barrel region and also in planar endcaps. The intermediate angle detectors are spaced along the beam to a distance of nearly 3 m from the interaction point to allow good momentum measurement to large rapidities. About 32 m^2 of silicon are needed. The supports must withstand both thermal and radiation effects and are expected to be made of either a graphite-based composite or beryllium. The goal is to have less than 5% of a radiation length of material at normal incidence.

Double-sided detectors with sizes up to 3 cm × 8 cm may be wire-bonded together to make larger units for electronic readout. The pitch in the barrel modules is 50 μm, whereas in the intermediate angle detectors the pitch varies with distance from the beam line. The heat load is about 1 mW/channel. Heat load is a major concern, and cooling by an evaporation-wick technique is being studied.

The spatial resolution is expected to be 15 μm, and the double-hit resolution is expected to be 150 μm. With such excellent position determination, the silicon microstrip system is expected to provide superior pattern recognition even in the cores of jets with p_T up to about 1 TeV/c. There are about 10 million channels in the system.

The pixel detector and silicon microstrip detector will have a common support system and will form an integrated high-resolution tracking device.

1.3. Straw Tube Central Tracking

Wire chambers are used for tracking for radii between 60 cm and 180 cm. They are suitable for spanning the tracking length needed for precise momentum measurement inside the large magnetic volume. They can also provide a fast trigger for tracks with p_T larger than some minimum value by the requirement that track segments in outer layers point back to the interaction point.

To meet the constraints imposed by radiation damage, current draw, chamber lifetime, gain reduction from large particle flux, hit rate, loss of data because of high occupancy, and pattern recognition in the complex environment, drift cells

half-cell stagger between layers permits resolution of left-right and crossing-time ambiguities. Local track segments found in each superlayer are linked to form tracks.

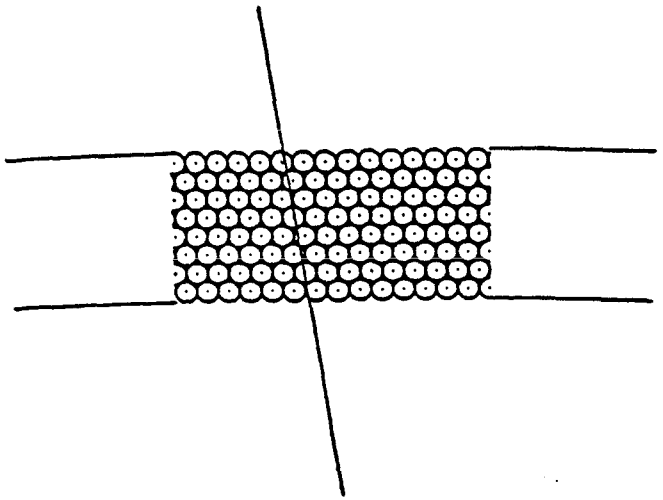

Fig. 2. Cross sectional view of the eight layers of a superlayer of straw tubes.

The coordinate along the wire is measured by means of small-angle stereo. With a spatial resolution of 100-150 μm per wire in the r-ϕ projection, the expected resolution in z is 2–3 mm. The superlayers are ordered axial, $\sim +3°$, axial, $\sim$ -3°, etc., for a total of eight equally-spaced superlayers spanning $70 < r < 180$ cm, as shown in Fig. 1. The double-hit resolution is 2 mm. The maximum straw length is limited by signal attenuation to about 3 m. Straws up to 3.5 m long with wire supports inside the straws every 80 cm for electrostatic stability have been operated at the required voltage.[4] The central tracking system design therefore contains an electrical break near the middle. The current draw per wire at the operating gas gain of 2×10^4 is shown as a function of radius in Fig. 3(a); it is less than 0.35 μA/wire over the entire system and less than 0.15 μA/wire

(a)

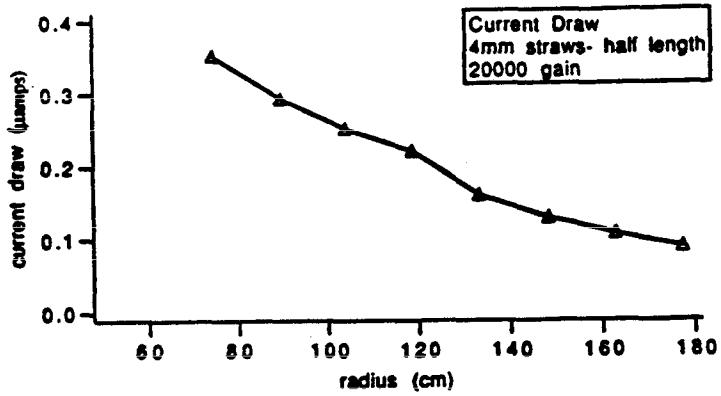

(b)

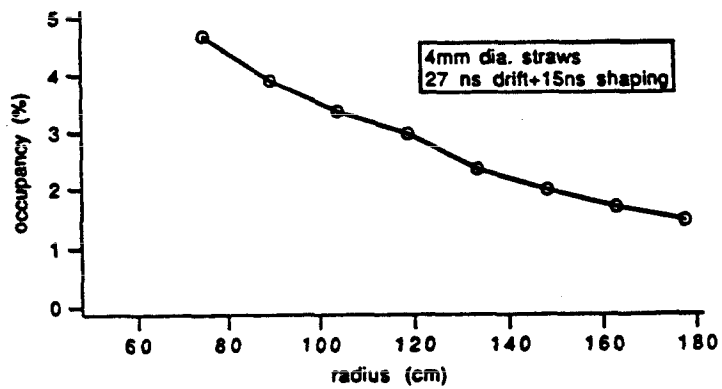

Fig. 3. (a) Current draw per wire *vs.* radius in the straw tube central tracking system for a gas gain of 2×10^4 at the SSC design luminosity. (b) Occupancy *vs.* radius in the straw tube central tracking system at the SSC design luminosity.

carbon-composite framework supporting replaceable modules of straws, as shown in Fig. 4.

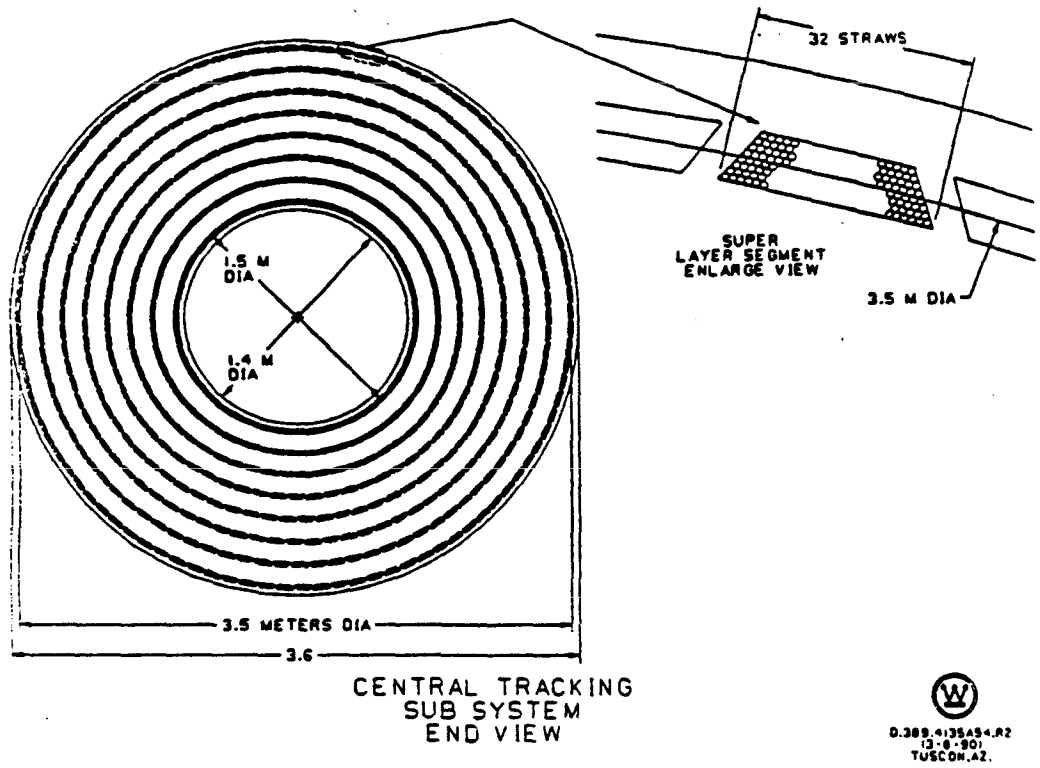

Fig. 4. Support system for replaceable modules of straws.

first employs crossed planar superlayers of straw tubes. The second involves the use of arrays of transverse drift cells which are optimized for fast track finding and reconstruction in a uniform axial magnetic field, much like the intermediate angle track detector in the H1 experiment at HERA[5], shown in Fig. 5(a). In the latter this is efficiently achieved by means of radial sense wires, but the requirements both of a fast gas with large Lorentz angle and of high rate capability at the SSC mean that further consideration of the wire orientation is necessary; work is underway. Such a detector would contain about 300 azimuthal wedges to meet the constraints on current draw and occupancy over the full radial range. The coordinate along the wire will be measured with planes of wires tilted at small angles to the nominal wire direction, as shown in Fig. 5(b). The total number of channels for the intermediate angle tracking system is about 6×10^4. An

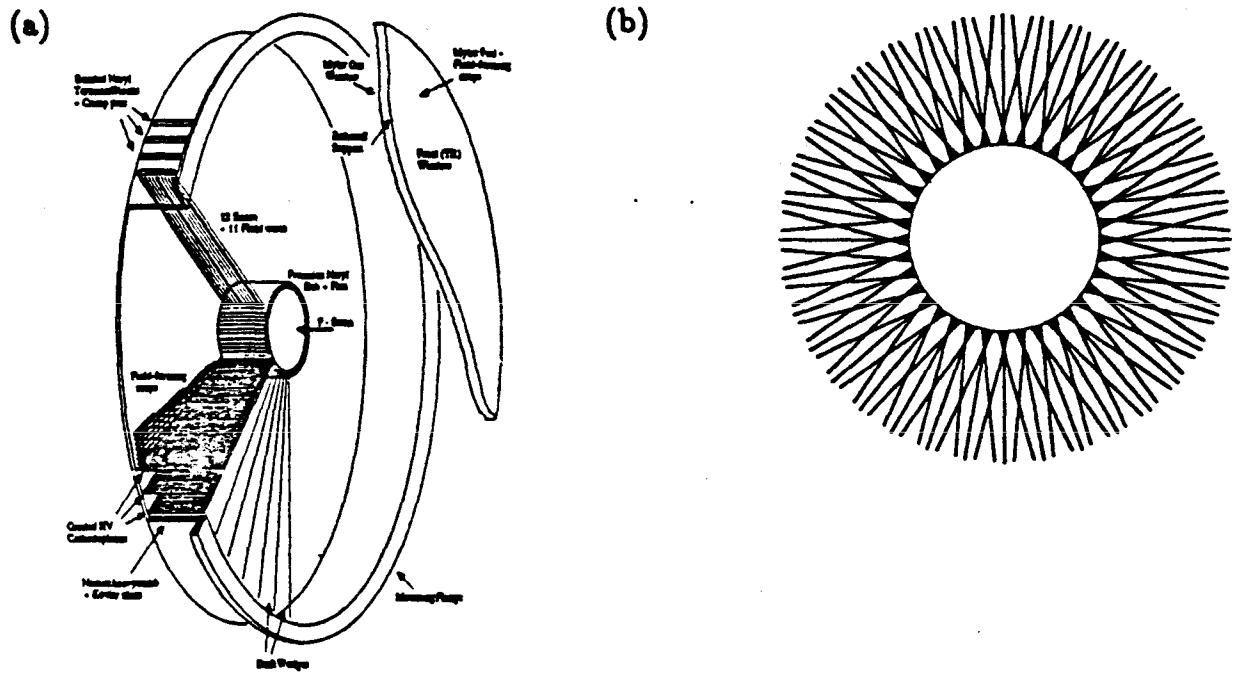

Fig. 5. (a) Schematic view of a radial wire drift chamber, as in the H1 forward tracking system, indicating the principles of construction and function. (b) Schematic view of wires tilted at a small angle to the radial direction in order to measure the coordinate along the radial wires.

figurations, pulse integral readout opens up the possibility of enhancing electron identification by detecting transition radiation X-rays.[6]

1.5. Tracking System Performance

The expected performance of the tracking system is shown in Fig. 7. Figure 7(a) shows the momentum resolution in a 2 Tesla magnetic field as a function of $|\eta|$ for the cases of no beam constraint and no pixels, 20 μm beam constraint

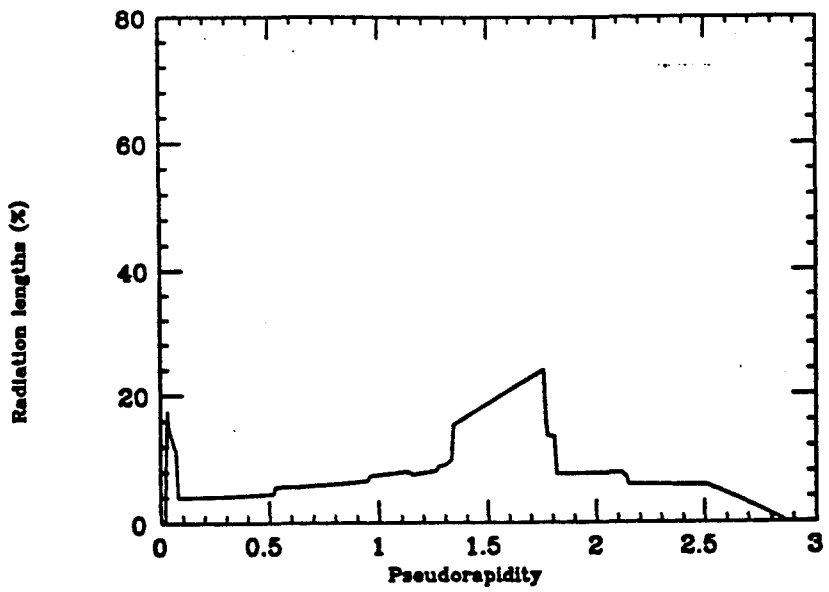

Fig. 6. Estimated percentage of a radiation length of material *vs.* $|\eta|$ for the straw tube central tracking system and the wire chamber intermediate angle tracking system.

2. WIRE CHAMBER ELECTRONICS

2.1. Front End Electronics

The wire chamber front end electronics will use radiation-hardened bipolar and/or CMOS technology. The drift time measurement resolution must be < 0.5 ns. The front end electronics consists of the following components:

- Preamplifier/shaper with signal tail cancellation
- Low power differential discriminator
- Time-to-voltage converter (TMC) and Analog Memory Unit with some trigger control[7]

or

- Time Memory Cell (TMC) digital time measurement[8]
- Data collection chip

Figure 8 shows block diagrams for both the TMC and TVC designs, for both of which prototyping is well underway. Similar electronics can be used for radial

(a)

(b)

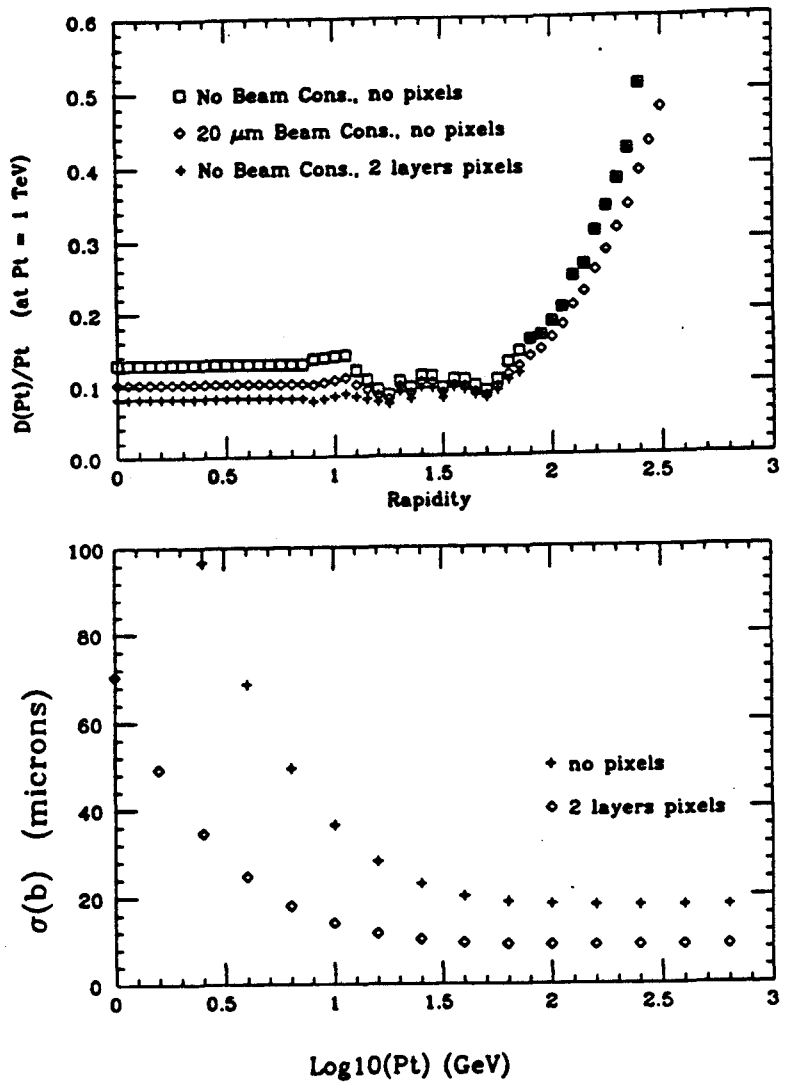

Fig. 7. (a) Momentum resolution in a 2 Tesla magnetic field as a function of $|\eta|$ for the proposed tracking system. (b) Impact parameter resolution as a function of momentum for the proposed tracking system.

of optical fibers. A preliminary cost estimate (not including the trigger) indicates a cost of less than $35 per channel for TVC-based straw tube electronics.[9]

2.2. Track Segment Finding and Triggering

(a)

(b)

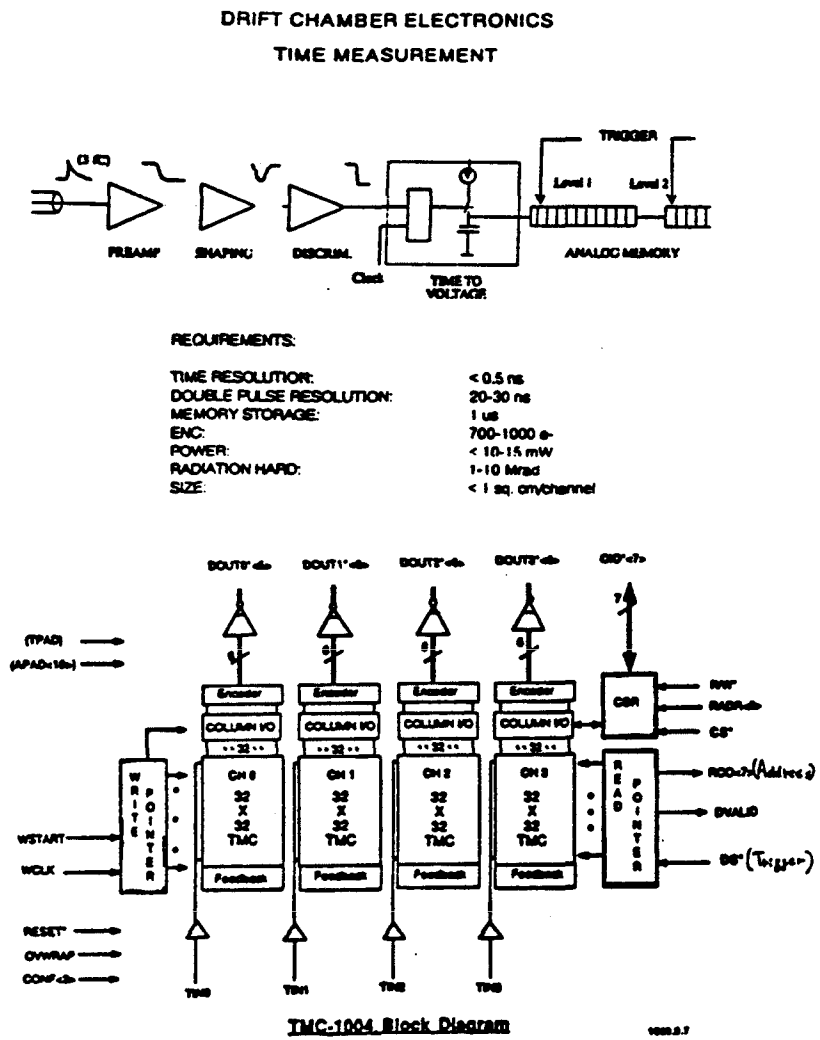

Fig. 8. (a) Block diagram for TMC-1004. (b) Block diagram for TVC-based front end electronics.

needed in the segment finding. An added complication is the need to have an estimate of the position of the track along the length of the wire since the propa-

ments between the axial and stereo superlayers (provided the linking can be accomplished). For this purpose one would not even have to use the drift times, although if the track is subject to a high-p_T cut this would probably be done using the track segments found in the trigger electronics. With 3° stereo, the displacement for a 3-m-long wire would be within ± 7.9 cm. Since the radius of the cell is 2 mm, this technique gives a resolution in z of 3.8 cm, which corresponds to ~ 0.1 ns propagation time.

3. RESEARCH AND DEVELOPMENT ISSUES

The are many questions that must be answered before we can arrive at a final design for an integrated silicon and wire chamber tracking system. Much of the R&D is being carried out in several SSC subsystem and generic programs.[1,2,11,12,13] Some of the relevant research is summarized below.

The viability of the pixel and silicon strip system that occupies the inner part of the tracking volume depends on the resolution of such issues as fabrication technology, circuit design, radiation hardness, mechanical and thermal stability, precision alignment, adequate heat removal and ease of assembly.

For the outer part of the tracking volume, wire chamber technology is mature, although its application in the SSC environment poses unprecedented challenges. Research and development areas include minimizing material in the supports and end regions, incorporation of electronics, gas manifolds and high voltage distribution, precision alignment, and thermal management. Also included are the investigation of a hexagonal cell option, which might decrease the amount of material and improve the assembly procedure, and the R&D specific to the intermediate angle tracking system.

Research and development in the areas of front end, data acquisition and triggering electronics for the various components of the tracking system is advancing.

Engineering design leading to an integrated low-mass support system incorporating the necessary precise alignment is beginning. In addition, engineering design leading to the integration and assembly of the tracking system into the

4. POSSIBILITIES FOR HIGH-LUMINOSITY PERFORMANCE

Computer simulation studies of track segment finding have been carried out for the tracking system design for the "Large Solenoid Detector"[14] at the SSC design luminosity of 10^{33} cm^{-2} s^{-1}. These simulations[15] included background from minimum bias events within the resolving times of the cells, interactions of the particles with the material in the tracking system, curling tracks in a 2 Tesla magnetic field, and loss of hits due to the double-hit resolution. Over 80% of the track segments in the outer superlayers were found for high-p_T e's and μ's from Higgs boson decays with a crude segment-finding algorithm. Since that tracking system was designed, improvements have been made because of detector R&D efforts. These new developments have been incorporated in the design of the tracking system described here:

- The outer radius of the tracking system has increased from 1.5 to 1.8 m.
- Since there is a break in the wires in the middle due to signal attenuation, the rapidity range covered by a wire has decreased by about a factor of two.
- In the previous design, the cell width for the outer superlayers was nearly 7 mm. In the present design 4 mm diameter cells are used throughout.
- The old simulation used a drift velocity of 50 μm/ns. Since that time fast gases with drift velocities $\sim$ 100 μm/ns have been shown to work.[4]

The relevant proportionality factors are given by

$$Occupancy \propto \frac{\eta_{max}\, n_B\, w}{r},$$

where η_{max} is the rapidity coverage of the wire, n_B is the number of bunch crossings during the resolving time of the cell, w is the width of the cell, and r is the radius. For the outer superlayers the largest improvement has occurred in the factor n_B because of both the decrease in the cell diameter and the increase in the drift velocity. A comparison between the old design and the present one shows that n_B has decreased from 4.3 to 1.4. Including the other improvements (two factors of two) we find that the occupancy for the present design is only 8%

there is reason to hope that at a luminosity of 10^{34} cm^{-2} s^{-1} the outer superlayers of the straw tube tracking system will not only survive but also still be usable for finding track segments and providing a trigger.

ACKNOWLEDGMENTS

We would like to thank the organizers of the Workshop, particularly T. Kondo, for providing such a well-organized and congenial environment and for the opportunity to meet and work with so many of our colleagues in Japan. We gratefully acknowledge the support of the Department of Energy for SSC detector research and development.

REFERENCES

1. "SSC Detector R&D Proposal: Development of Technology for Pixel Vertex Detector," D. Nygren, contact person (1989).
2. "Subsystem R&D Proposal to Develop a Silicon Tracking System," A. Seiden, contact person (1989).
3. D. G. Cassel, G. G. Hanson *et al.*, "Report of the Central Tracking Group," *Proceedings of the 1986 Summer Study on the Physics of the Superconducting Supercollider, edited by R. Donaldson and J. Marx, Snowmass, CO, 1986*, p. 377.
4. H. Ogren, "Progress Report from Straw Chamber Subgroup," in these Proceedings.
5. G. A. Beck *et al.*, "Radial Wire Drift Chambers for the H1 Forward Track Detector at HERA: Design, Construction and Performance," *Proceedings of the Wire Chamber Conference, Vienna, Austria, 1989*, Nucl. Instr. and Meth. **A283**, 471 (1989).
6. H. Grässler *et al.*, "Simultaneous Track Reconstruction and Electron Identification in the H1 Radial Wire Drift Chambers," *Proceedings of the Wire Chamber Conference, Vienna, Austria, 1989*, Nucl. Instr. and Meth. **A283**, 622 (1989); S. Ahlen *et al.*, "Proposal to Develop An Integrated High Rate Transition Radiation Detector for the SSC," SSC-PC-011, O-

8. Y. Arai, "Development of TMC Chip and Track Trigger," in these Proceedings; Y. Arai and T. Ohsugi, "TMC – A CMOS Time to Digital Converter VLSI," IEEE Trans. Nucl. Sci. NS-36, 528 (1989); Y. Arai, "A Time Measurement System at the SSC," *Proceedings of the Workshop on Triggering and Data Acquisition for Experiments at the Supercollider, Toronto, Canada, 1989*, SSC-SR-1039, p. 125.

9. F. M. Newcomer and R. Van Berg, "Straw Electronics Cost Summary," unpublished (1990).

10. J. Chapman, "Tracking Trigger," in these Proceedings; S. Kim, "Tracking Trigger Study," in these Proceedings.

11. "SSC Detector Subsystem Proposal: Central and Forward Tracking with Wire Chambers," G. Hanson, contact person (1989).

12. "SSC Detector Subsystem Proposal: A Hybrid Straw Tube/Scintillating Fiber Tracking System," A. Goshaw, contact person (1989).

13. S. Parker, "A Proposal to Develop a VLSI Pixel Device for Particle Detection," (1987).

14. G. G. Hanson, S. Mori, L. G. Pondrom, H. H. Williams *et al.*, "Report of the Large Solenoid Detector Group," *Proceedings of the Workshop on Experiments, Detectors, and Experimental Areas for the Supercollider*, edited by R. Donaldson and M.G.D. Gilchriese, Berkeley, CA, 1987, p. 340.

15. G. G. Hanson, B. B. Niczyporuk and A. P. T. Palounek, "Wire Chamber Requirements and Tracking Simulation Studies for Tracking Systems at the Superconducting Super Collider," *Proceedings of the Wire Chamber Conference, Vienna, Austria, 1989*, Nucl. Instr. and Meth. A283, 735 (1989).

May 29, 1990
IUHEE-6

Notes on straw heating and gas flow requirements

Harold Ogren
Indiana University

For a given gas gain, the current draw in each of the straw drift cells at each superlayer location can be estimated. This is shown in the following figure.

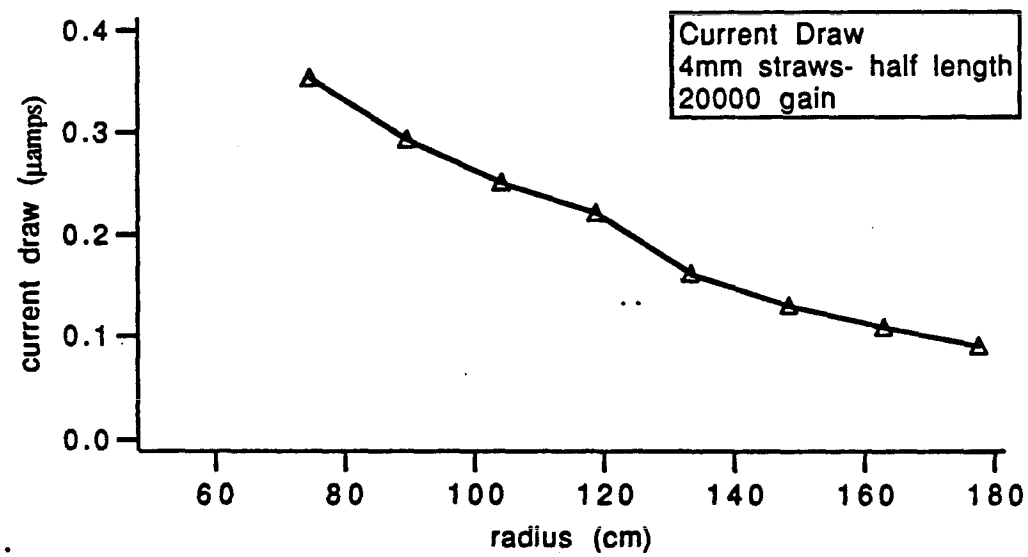

The positive ions, which were produced in the avalanche, drop though the full drift chamber potential and heat the gas. The temperature rise in the gas flowing through the straws can estimated, by assuming that there is no heat loss to the walls. This is obviously not correct, but it will result in a conservative estimate A better calculation is underway by ORNL, and a measurement is planned in the next few months.

I = the current draw.
V_0 = the voltage.between cathode and sense wire
P = pressure (10^5 N/m^2).
A = the straw cross-sectional area (1.25×10^{-5} m^2).
T = the ambient temperature (300 K).
ΔT = is the temperature change.
R = the universal gas constant (8.31 J/mol K).
C_p = the molar specific heat of the gas.

(the original calculation was done by S. Witacker and J. Kadyk at theVancouver Workshop, 1989)

For CF_4 - (20%) isobutane I estimate $C_p/R = 9.1$. Using this value the velocity is found to be

$$v=2.5/\Delta T \quad (\text{K cm/sec}).$$

(this number is smaller than the Vancouver calculation because they used $C_p/R=5$ and $A=1 \times 10^{-5}$ m^2.)

The temperature change that can be tolerated is not very well determined; I have chosen $\Delta T \doteq$ 6 K. (the Vancouver calculation used a 3 K temperature increase). This represents at 2% variation in the temperature, which seems safe in terms of expansion effects. This temperature increase will produce about a 10% variation in the gas gain from one end to the other. Again this seems tolerable. The maximum velocity equired for the gas is the found to be

$$v= 0.4 \text{ cm./sec} \quad (\text{for } 0.5\ \mu \text{ amp of current at } 1900 \text{ V})$$

Using the current draw at each superlayer indicated in the previous figure, the maximum flow velocity required at each superlayer position can be calculated. This is indicated in the following figure.

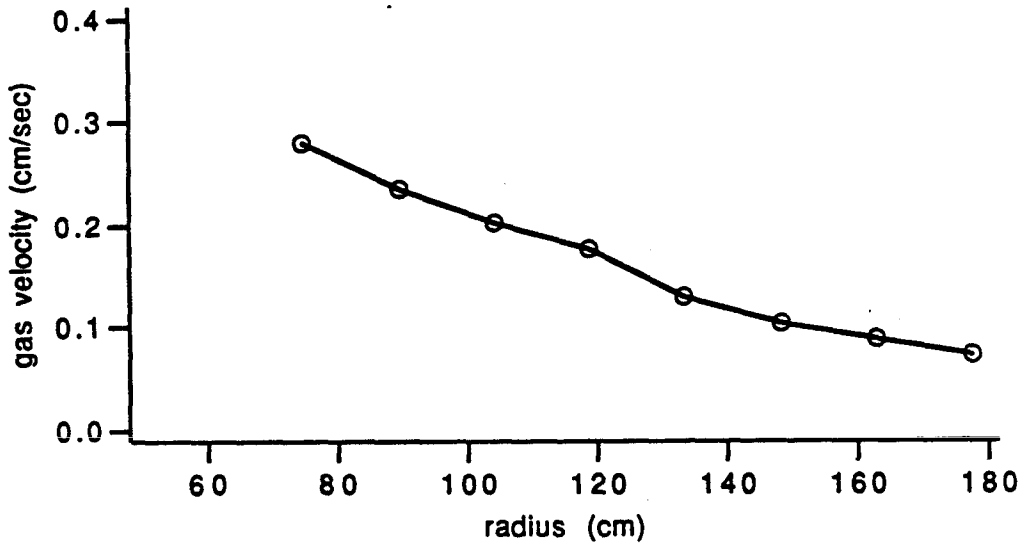

The maximum flow rate is .3 cm/sec. This drops to less than 0.1 cm/.sec at the outer layers. The total gas flow for each superlayer can now be calculated. This is shown in the following figure.

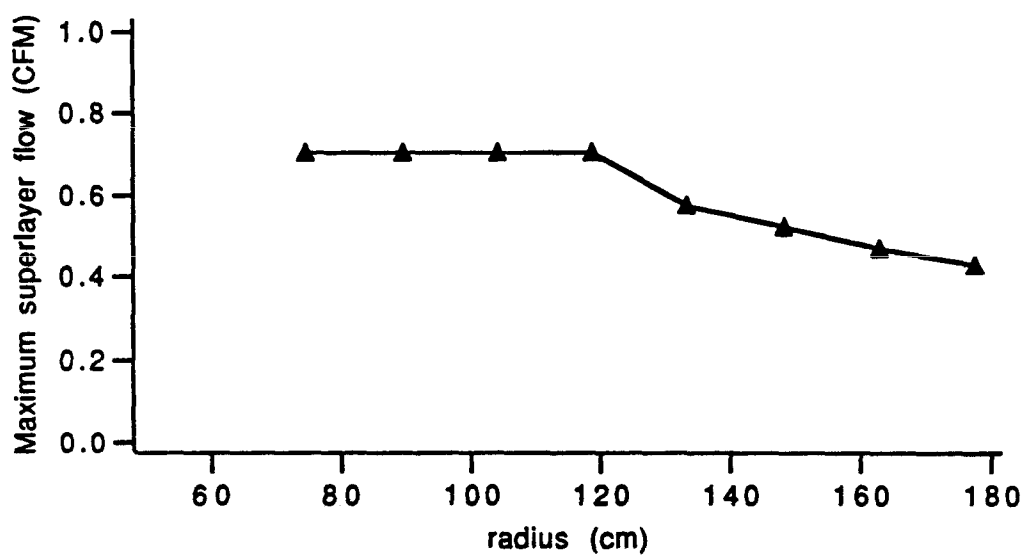

May 31, 1990
IUHEE-7

Attenuation Studies of 3.5m Straw Tubes

C. Neyman, B. Martin, H. Ogren

SSC R&D Group

Indiana University

1) Introduction

The current cylindrical geometry for the central tracking chamber of the SDC calls for the outer most straws to be of 3.5m to 4m in length. The large length of the straws makes it critical to understand their signal transmission properties. As a first step in this process the attenuation length of two straws in a 3.65m (12 ft) chamber was measured.

2) Description of detector

The drift chamber constructed for this series of tests was a six tube array with a length of 3.65m. The large length of the straws was achieved by splicing two 1.8m straws together. The straws were glued to a plastic spacer[1], which was slid half way inside each straw, with a conductive epoxy giving a continuously conductive cathode. The straws were fabricated by Precision Paper Tube Company., Rockville, Ill. Each straw consists of a layer of 0.5 mil polycarbonate film aluminized on the inside surface, covered by an 0.5 mil mylar film. The two films are wound with overlapping pitch and bonded by an application of epoxy resin between them. The resulting tube is gas tight, and robust enough to handle easily. The inside diameter is 0.157 in or 4.0 mm.

The anode is a gold plated tungsten wire 25 μm in diameter. It is tensioned and held centered by two Delrin pins inserted in each end of the straw. The Delrin pins are inserted into an aluminum gas manifold, which positions the wires and provides a robust mechanical support. The triangular gas manifolds sit in a precision V groove that is machined in a long aluminum bar. The V groove aligns both ends and hold the straws in position. Mechanical tolerances for the construction were about ± 50 μm. In addition to these supports the wire was held with 7 Mercedes type spacers[1] every 58 cm that were melted to the wire.

3) Electronics

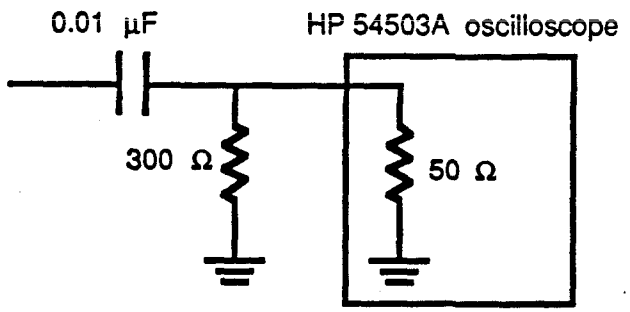
0.01 µF
HP 54503A oscilloscope
300 Ω
50 Ω

Fig 1

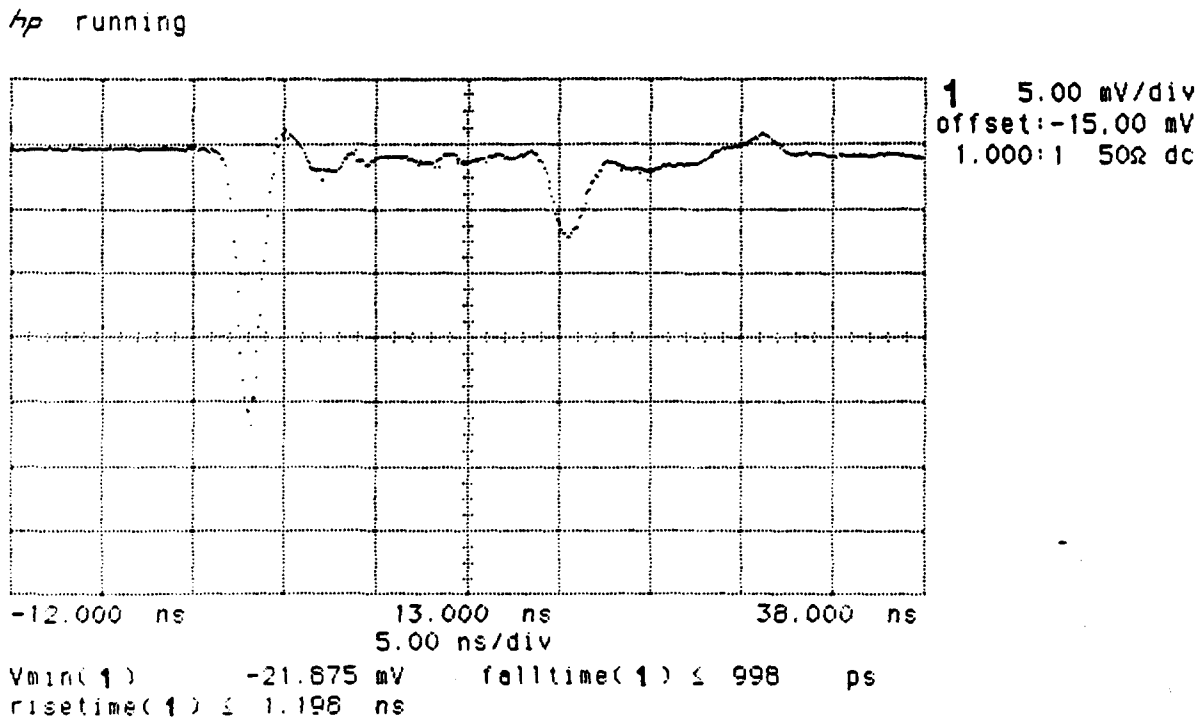
hp running
1 5.00 mV/div
offset:-15.00 mV
1.000:1 50Ω dc
-12.000 ns
13.000 ns
38.000 ns
5.00 ns/div
Vmin(1) -21.875 mV
falltime(1) ≤ 998 ps
risetime(1) ≤ 1.198 ns
1 -7.500 mV

Although we expect no difference the attenuation length was measured both terminated and unterminated. The termination was 34pF capacitor and a 0-300 Ω pot to ground. The pot was adjusted to give the least reflection. This value was measured to be 223 Ω.(see Fig. 3, 4, and 5)

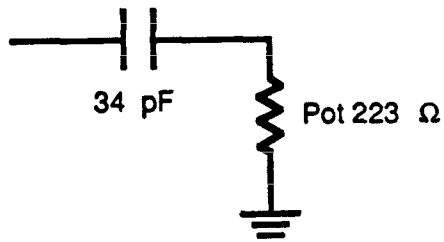

Fig 3
Termination

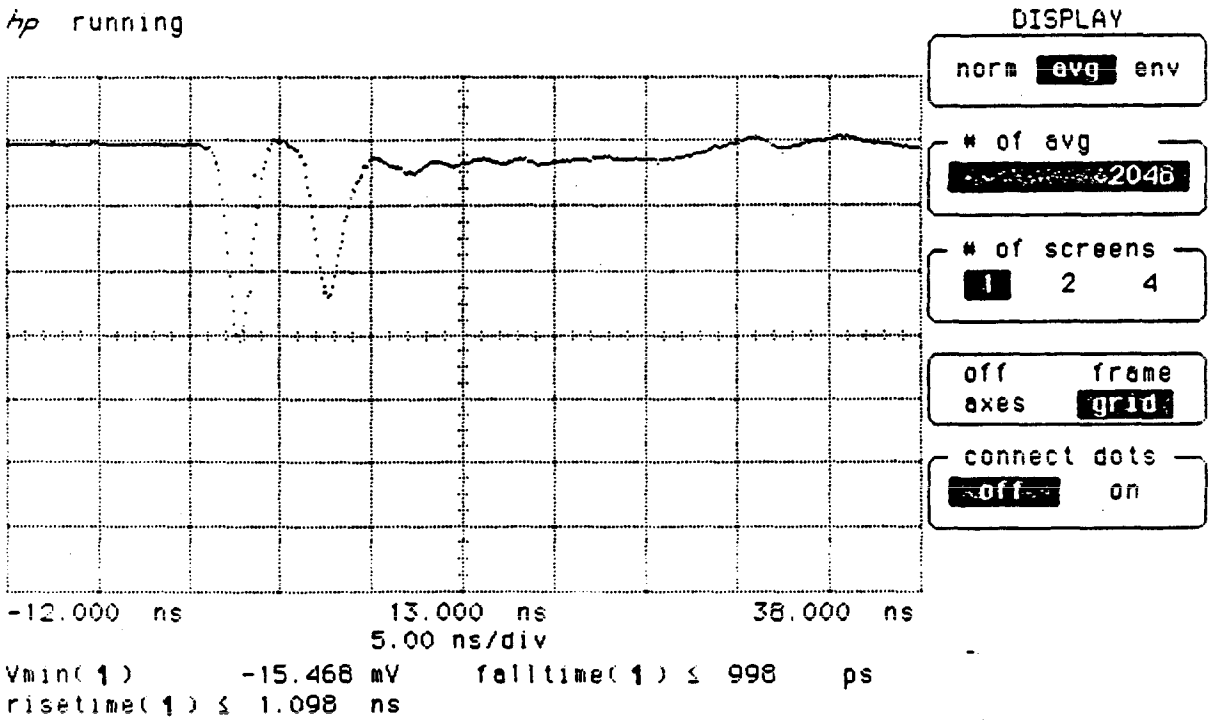

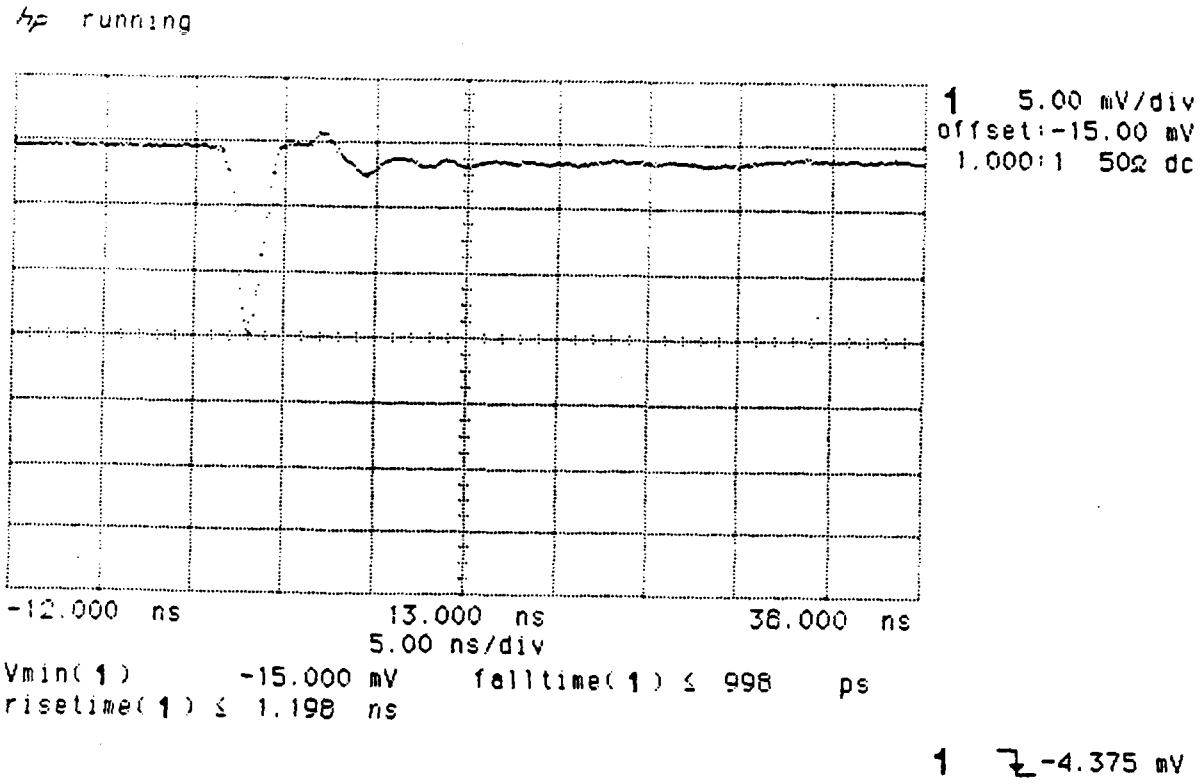

Fig. 5
Pulse terminated (source at L=305 cm)

The signals from an Fe^{55} source were recorded on an HP 54503A digital oscilloscope. The position of the source from the read out end of the tube was also measured. All distances in this paper are measured from the origin at the electronics readout end of the tubes. To reduce the effect of noise we averaged 2048 pulses to give the display from which the pulse height was measured. The pulse height as function of distance along the tube was fit to a decaying exponential of the form:

$$y=A\exp\left(\frac{-x}{L_0}\right)$$

were A in the initial pulse height and L_0 the attenuation length.
The data and the fits can be seen in Fig. 6, 7, 8, and, 9. The data are also summarized below

Table 1. attenuation length

	tube #2	tube#3
terminated	407.3	402.7

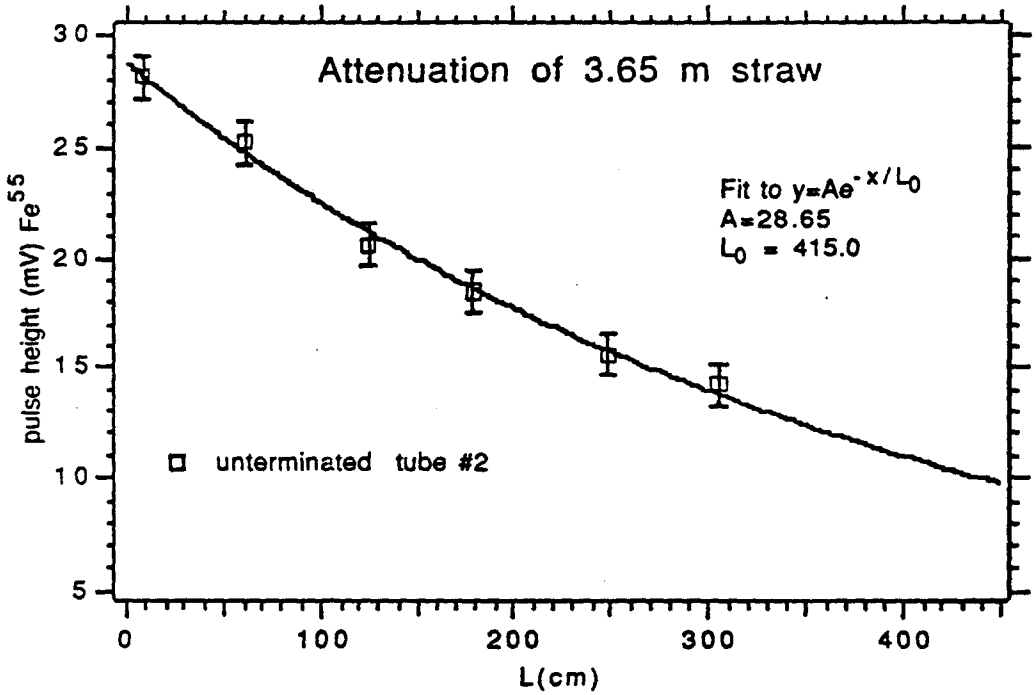

Fig 6
Tube #2 unterminated

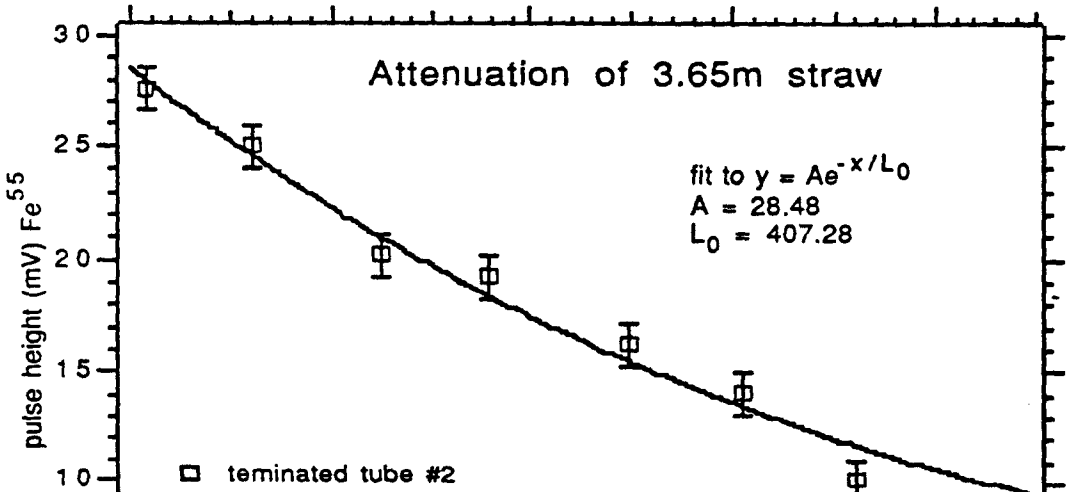

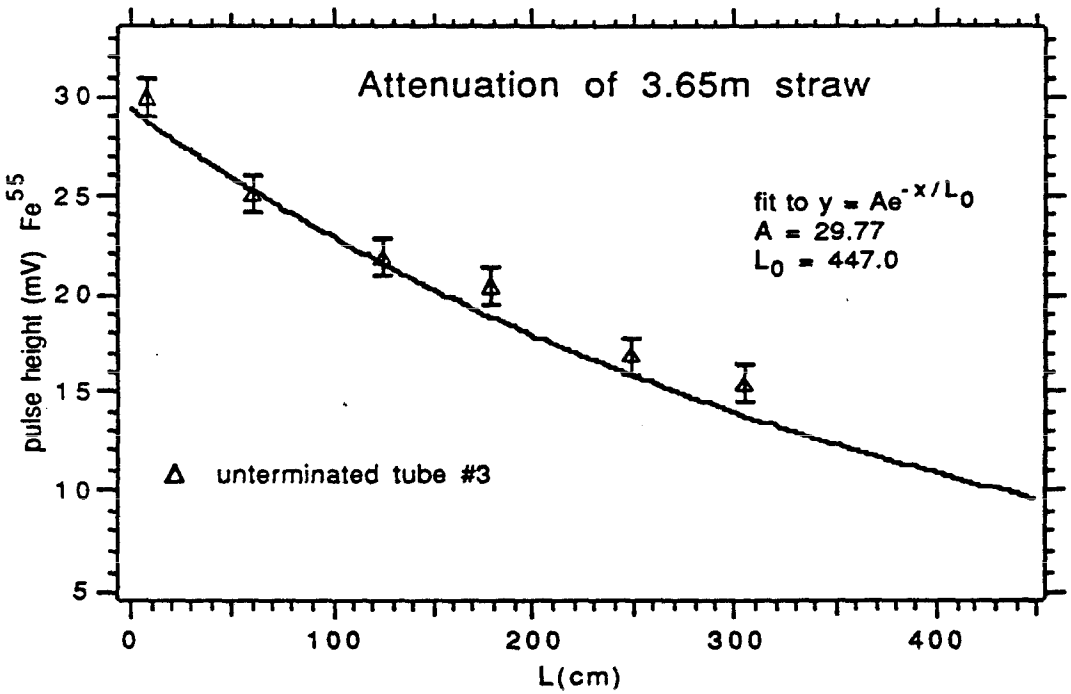

Fig 8
Tube #3 unterminated

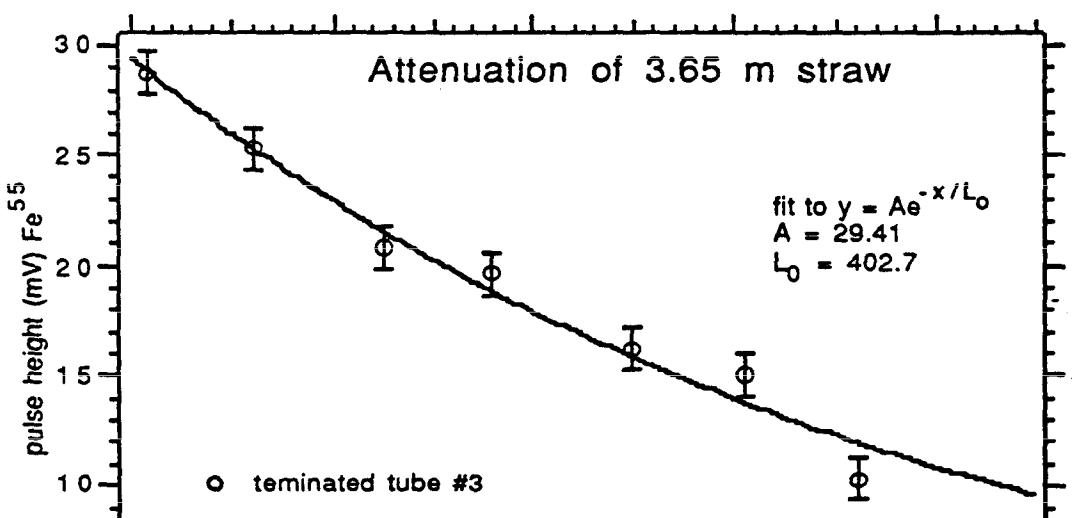

May 29, 1990
IUHEP-90-9

Progress Report on 4 mm Straw Chambers

Harold Ogren
Indiana University
Bloomington , IN 47405

Introduction

Cylindrical drift chambers made with wound mylar cathodes (Straw Chambers) were developed almost a decade ago. I am going to report on recent developments i in the design of these chambers for an SSC detector. This work was carried out at Indiana University under an SSC R&D grant and as part of the Central and Forward Tracking with Wire Chambers Subsystem group [1]

The central tracking system for SDC

The central wire tracking chamber for the SDC will consist of 8 superlayers. Each superlayer consists of two cylindrical sections 3 meters in length. Each superlayer contains 8 layers of straws. The inner radius is 0.7 meters, the outer is 1.8 meters. One quarter of the tracking system is shown in Fig. 1.

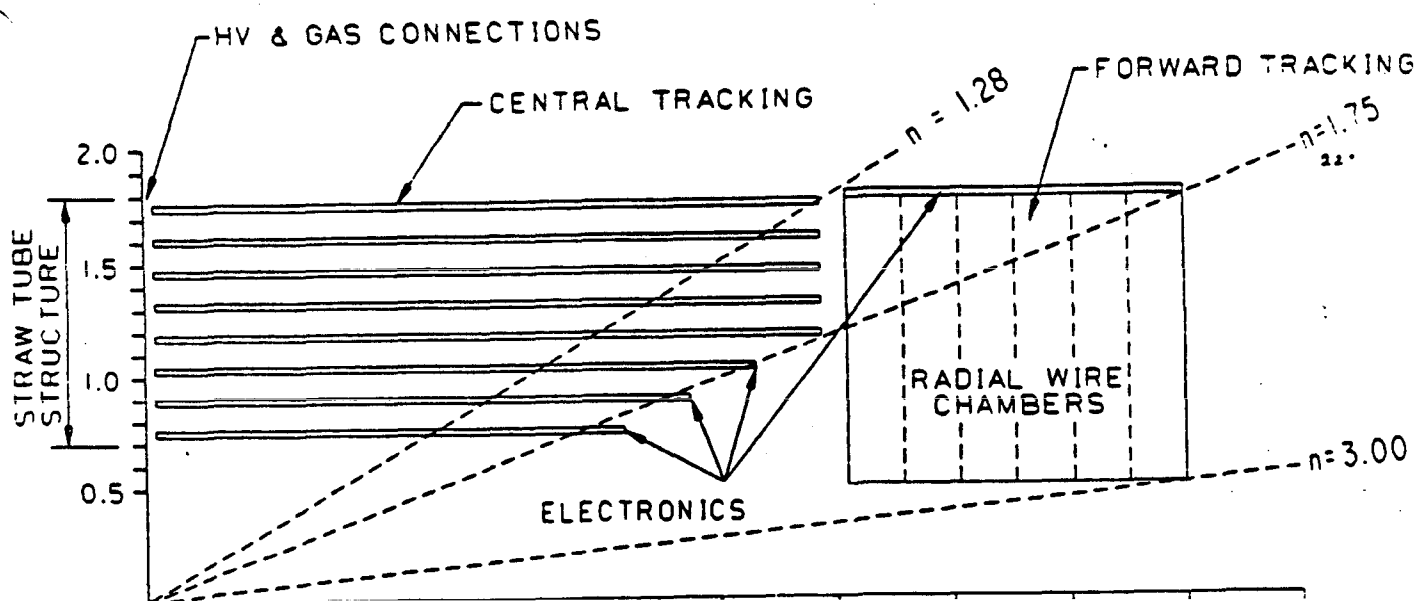

In Fig. 2 we see the end view of the central wire tracking chamber and the the eight super layers. The superlayers are constructed from a ring of identical modules, holding up to 256 straws. Four of the superlayers are stereo and four are axial. The stereo layers are formed by orienting a module of straws at a 3 degree angle. (The modules (and straws) are kept straight).
The total number of module will be about 544*2.
Since straws type detectors have been used in a number of experiments in the past ten years, the primary task is to define the mechanical specification for the superlayers, modules, and straws, and to integrate the system with the silicon tracker.

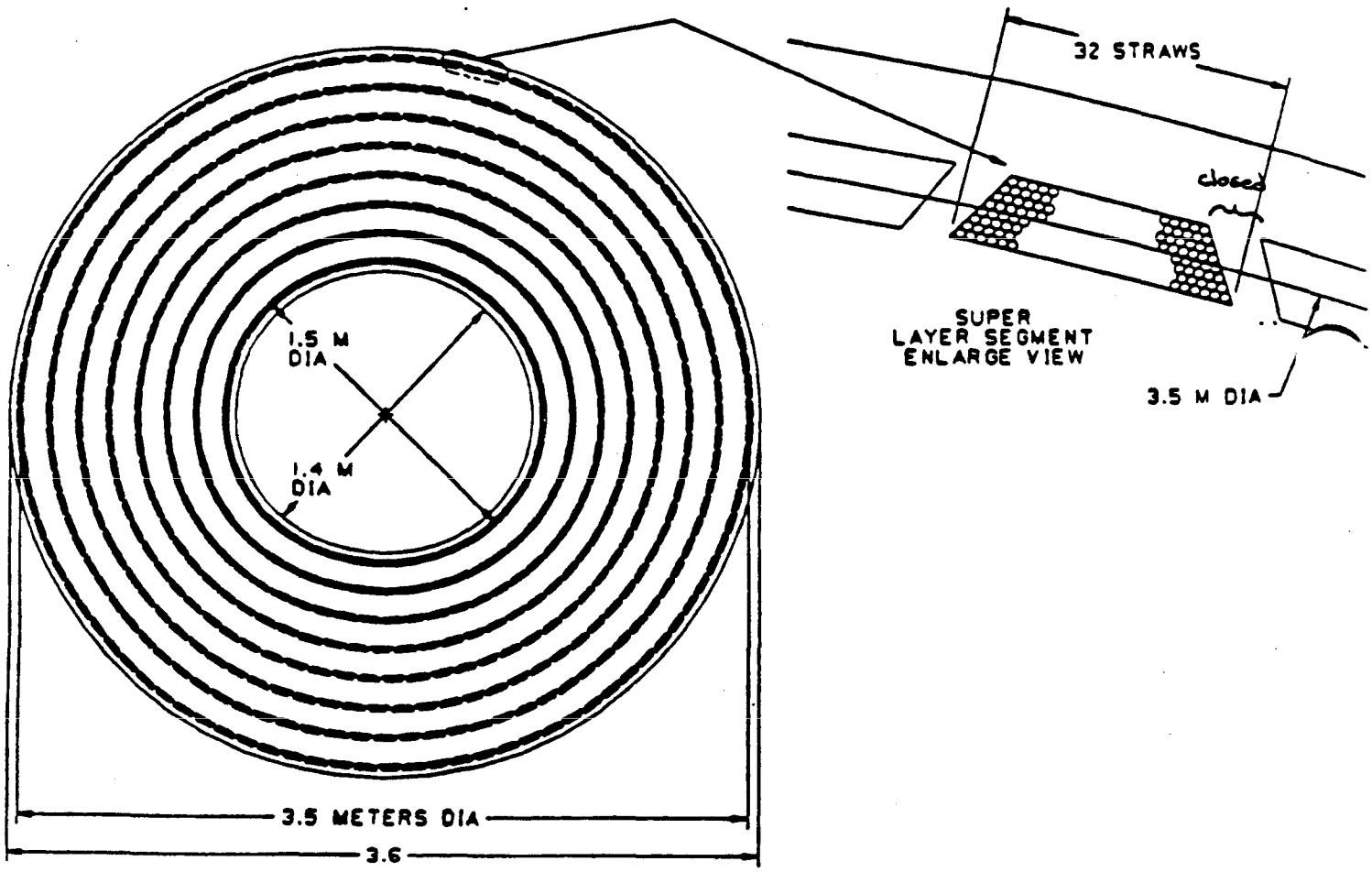

CENTRAL TRACKING

The SSC Environment

The hit rate, current draw, occupancy, and charge/unit length were calculated using the rates predicted by D. Groom at a nominal luminosity of 10^{33} cm $^{-2}$ sec $^{-1}$. They are shown in Fig. 3 a,b and Fig. 4 a,b. The effects of the magnetic field (loopers) will increase these predictions at intermediate radii and decease them for the larger radii, however these the general dependance and are a valuable guide for chamber construction. The current draw for each straw may be the limiting feature for the operation at SSC. It s principally for this reason that the straws are split into two sections axially.

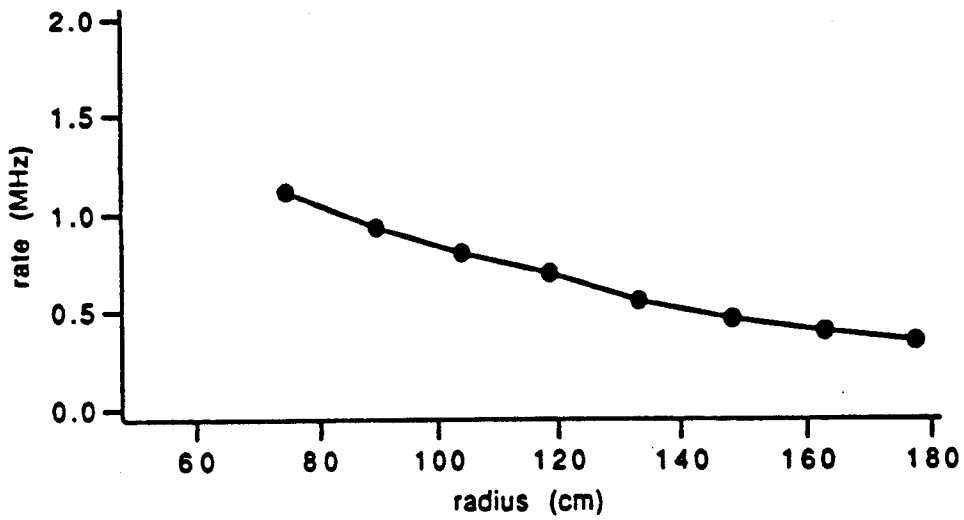

a

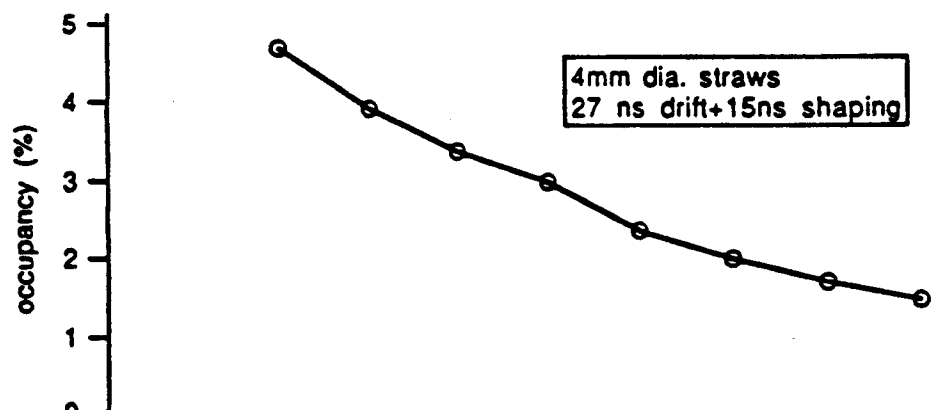

b

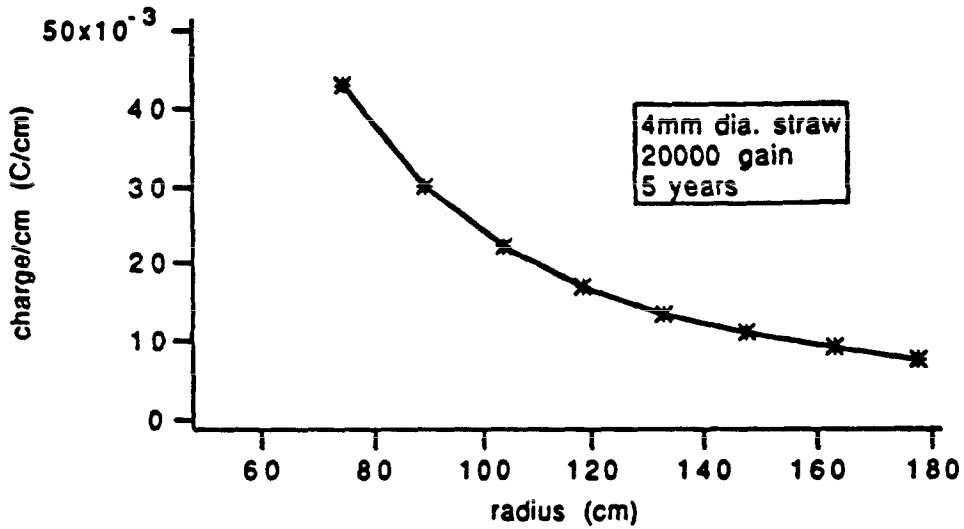
50x10^-3
40
30
20
10
0
charge/cm (C/cm)
60
80
100
120
140
160
180
radius (cm)
4mm dia. straw
20000 gain
5 years

a

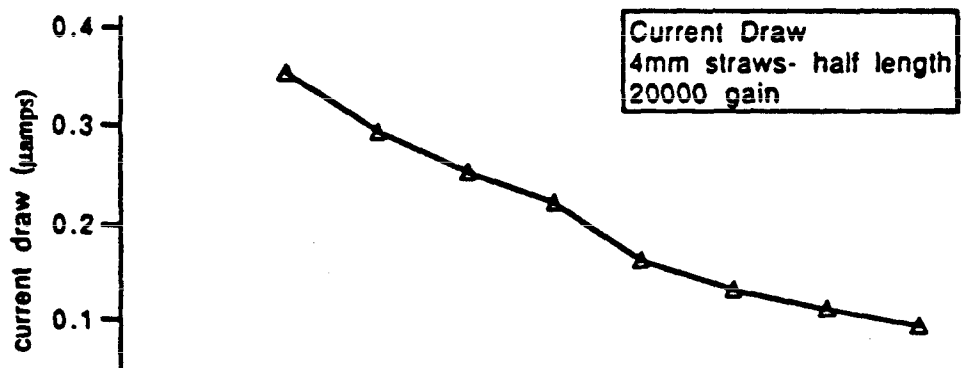
0.4
0.3
0.2
0.1
current draw (µamps)
Current Draw
4mm straws- half length
20000 gain

Modular Design Aspects

We are interested in the design of modular systems for the SSC. We believe that there are several compelling reasons for this:

1) Alignment
- The module's cross section stability aligns the straws internally
- The support structure maintains the modules in position.

2) Compressional Loading
- The compressional loading due to the wire tension (12 Kg for 256 wires) is taken up entirely by the external module.
- Since the module takes up the compression, the end support structure can be very light.

3) Mass Production
- The 240,000 channels of drift tubes is much larger number of wires than past detectors. With a modular approach the 1088 identical modules can be built by industry.
- Endplate design is simplified, HV, gas, electronics card are all identical.

4) Testing
- Each module can be tested, calibrated, and measure before assembly.
- HV and gas tests can be completed before assembly.
- The completed electronics and trigger can be tested before assembly.

5) Repair
- Modules can be repaired both before and after assembly.
- Modules can be replaced during major shutdown periods.

Module construction

As part of our SSC Tracking Subsystem development, we are planning on constructing several smaller modules this summer. The purpose of these smaller test modules is to determine the multi-straw alignment, to workout an endplate design, to begin to understand construction techniques with carbon fiber composites, and to investigate integration of the electronics in the modular design. The first modules will be about 1 meter in length. Fig. 5 shows a endview of a 64 straw prototype chamber.

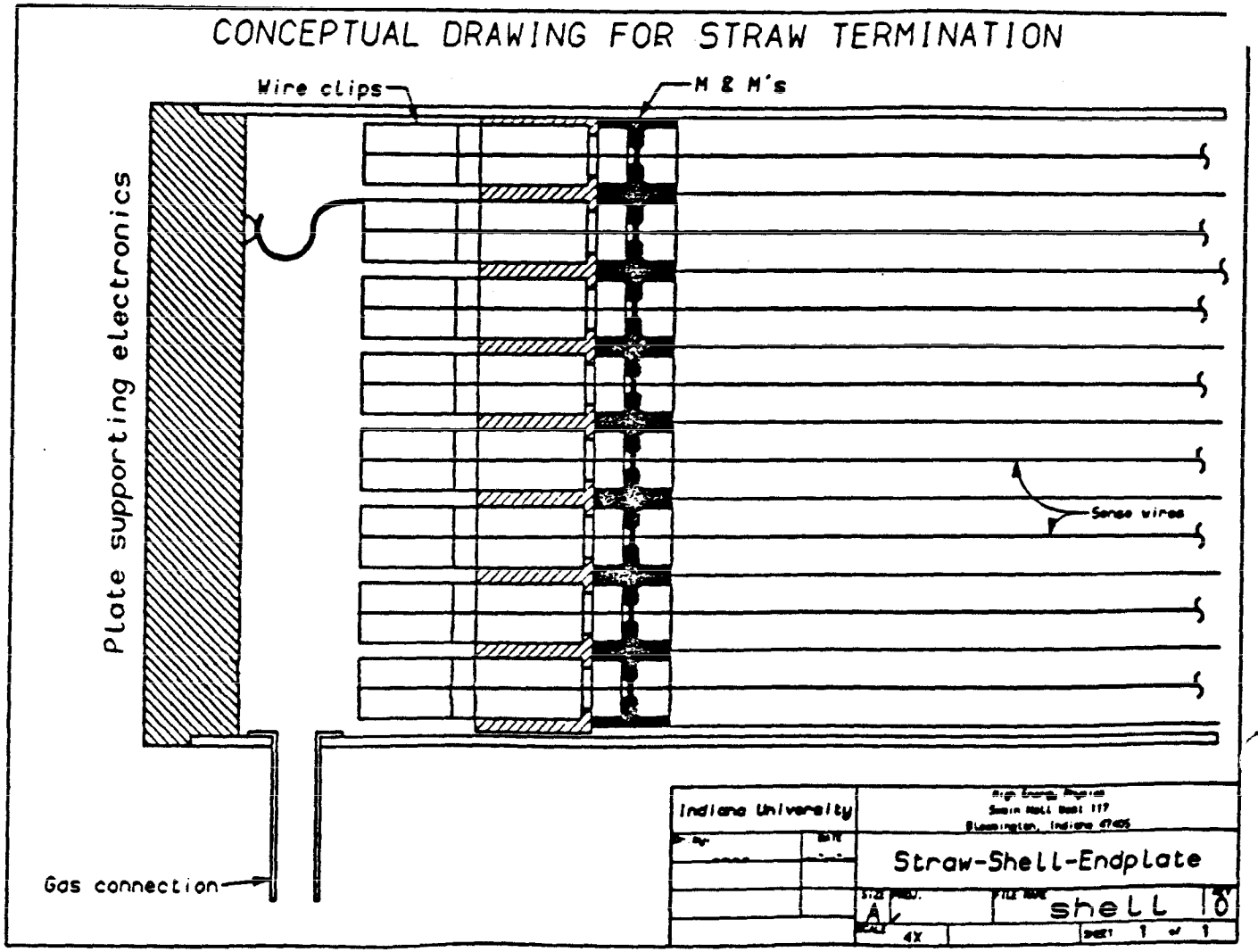

Fig. 5. Side view of a possible small straw test module

We are trying to workout a minimal mass design for the modules . One possibility is to slightly compress the wire supports with the outer shell in order to set the straw spacings. In this case the endplate provides the wire tension, but does not have to position the wire accurately. We have several preliminary designs that utilize this idea. The sideview, showing the end cap and wire attachment pin are shown in Fig. 6. Details of the endplate and the wire connection pin are shown in Fig. 7 and Fig. 8.

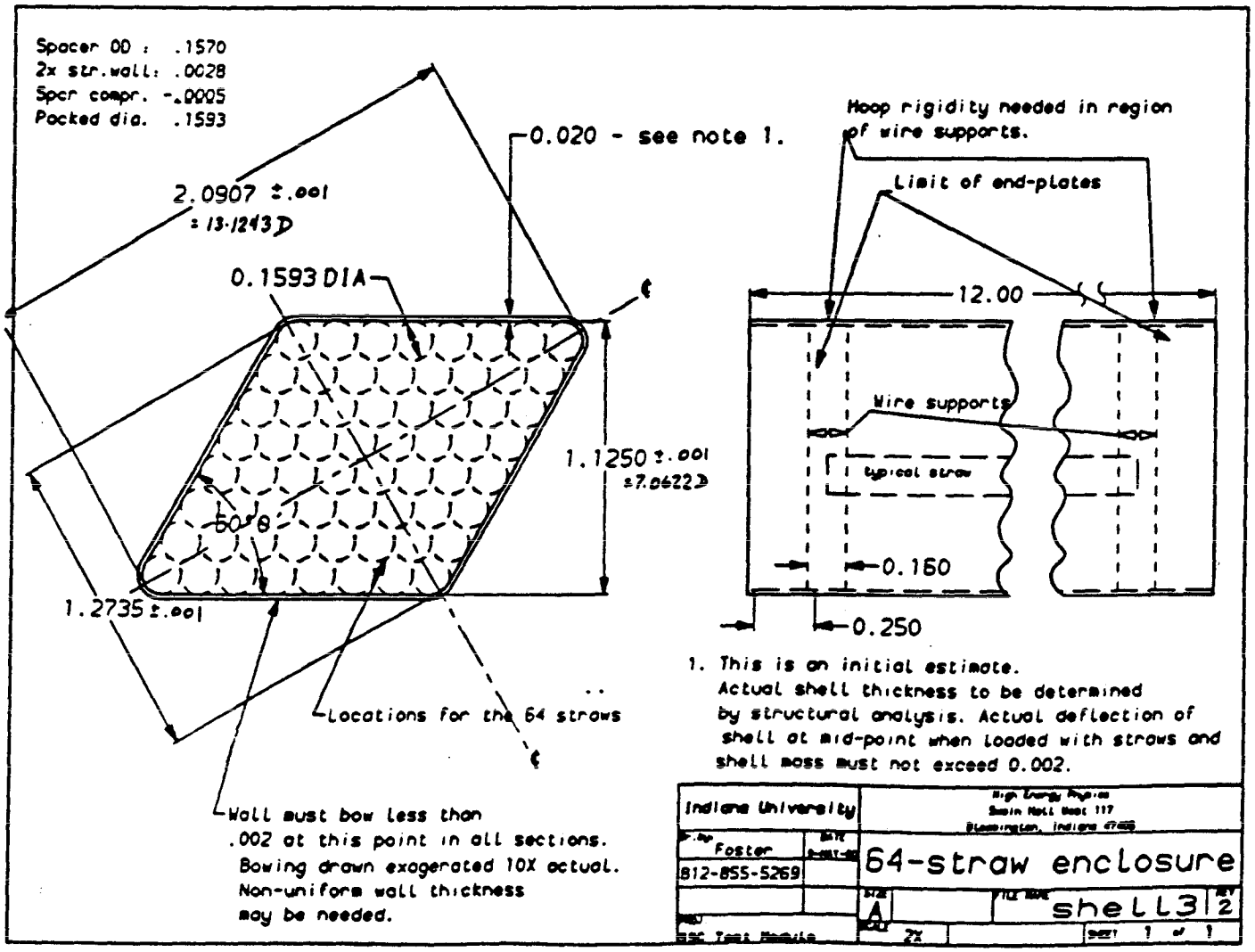

Fig. 6. End view of a possible 64 straw test module

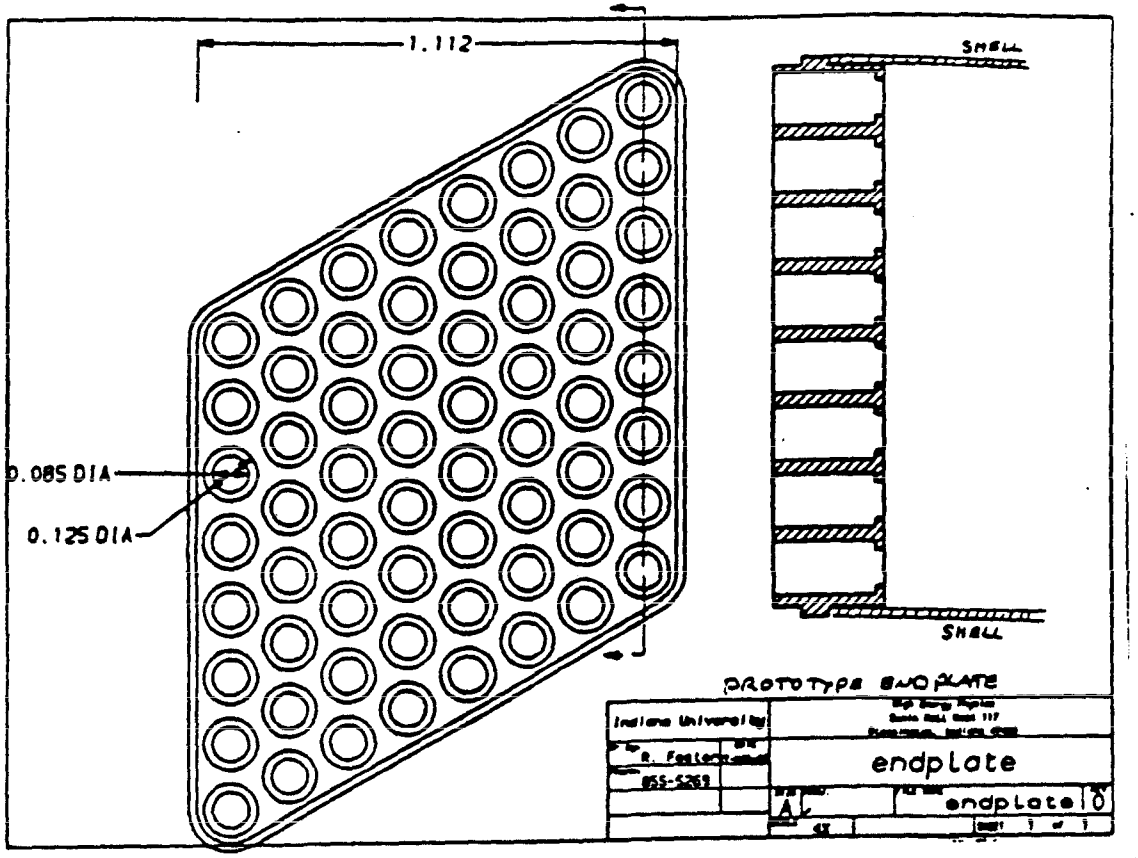

Fig. 7. End view of an endplate for a 64 straw module

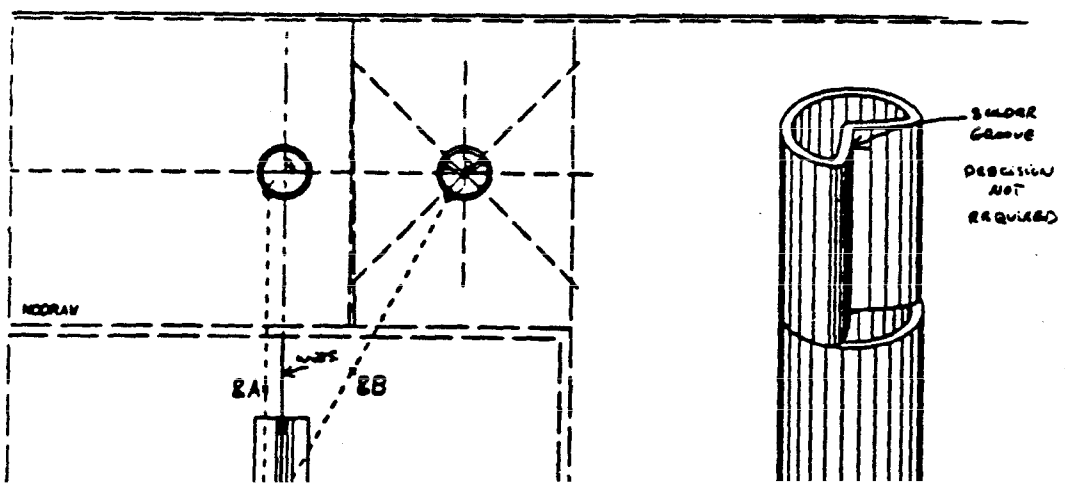

Basic straw cell, design

The straws we are presently using are 2 meters long.[2] Construction of 3 meter straws is not thought to be a problem. The general method is shown in Fig. 9. Two thin films are wound on a precision mandrel. The straws we are using are made with an aluminized (1000A) polycarbonate layer and an outer wrap of mylar. Both films are 12 microns thick.

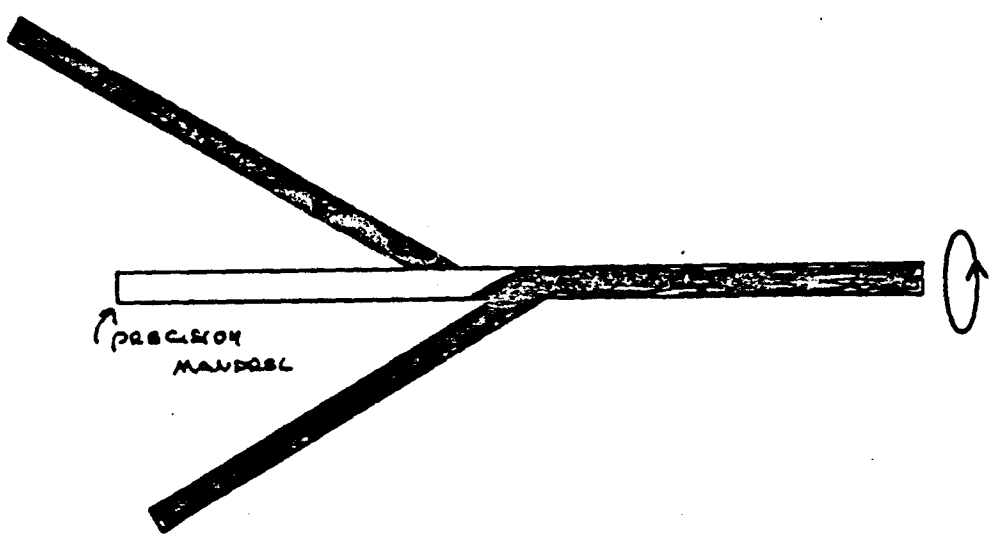

Fig. 9. Schematic of straw construction

Some of the R&D areas we are working on are fabrication of thinner straws, investigating other materials such as Kapton, and increasing the metallic coating to reduce the cathode resistance.

manufactured for use in the prototype modules we are building this summer. It has the advantage over the "M&M" of allowing restringing.

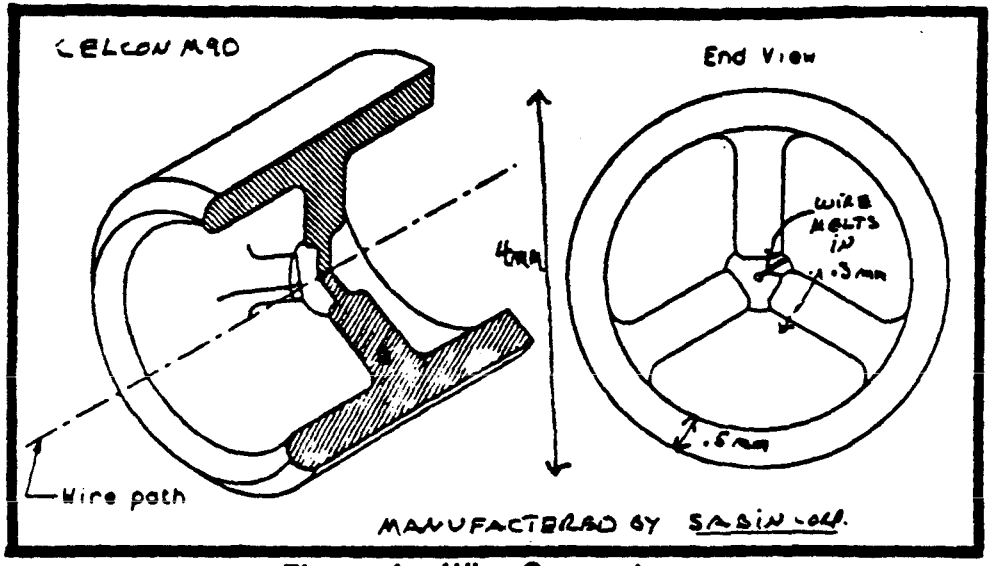

Figure 1 Wire Support

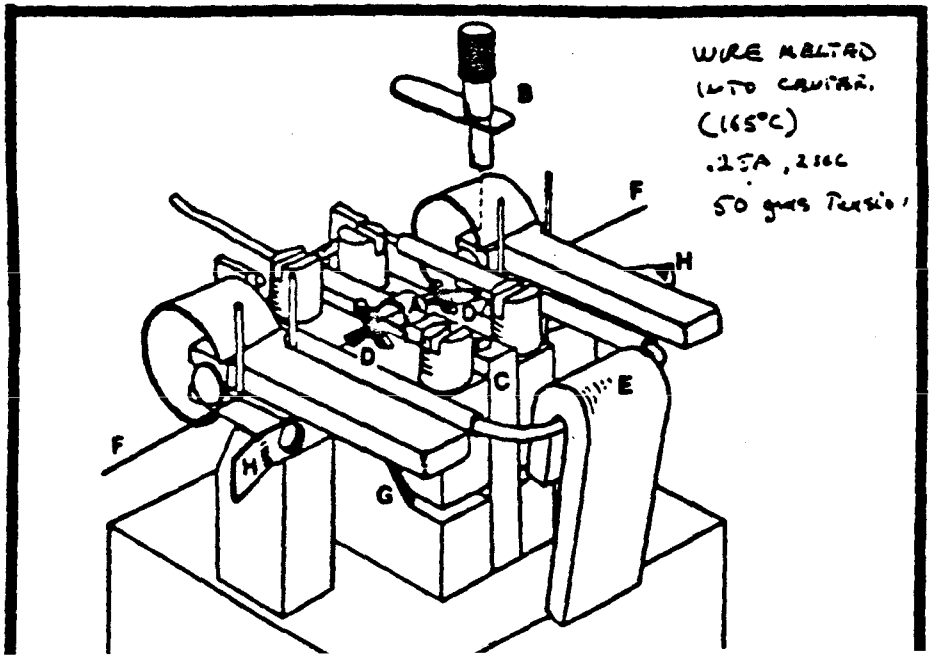

18-APR-90 Sense-wire collar, double "V" design

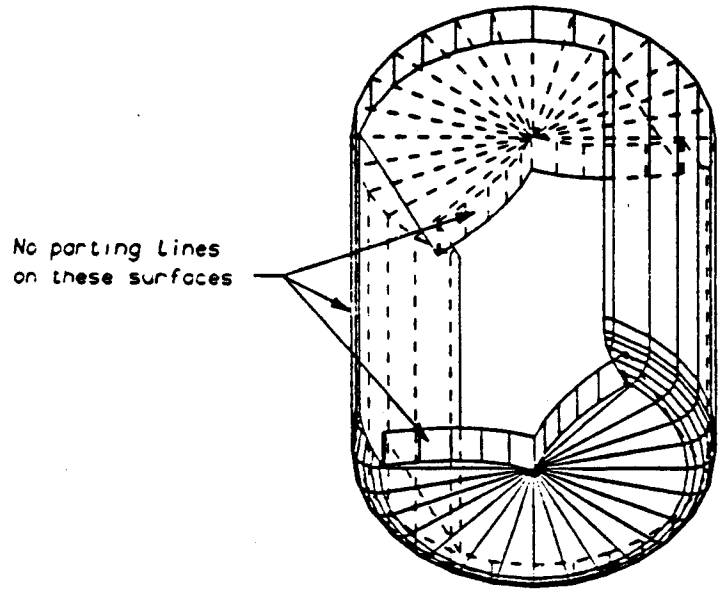

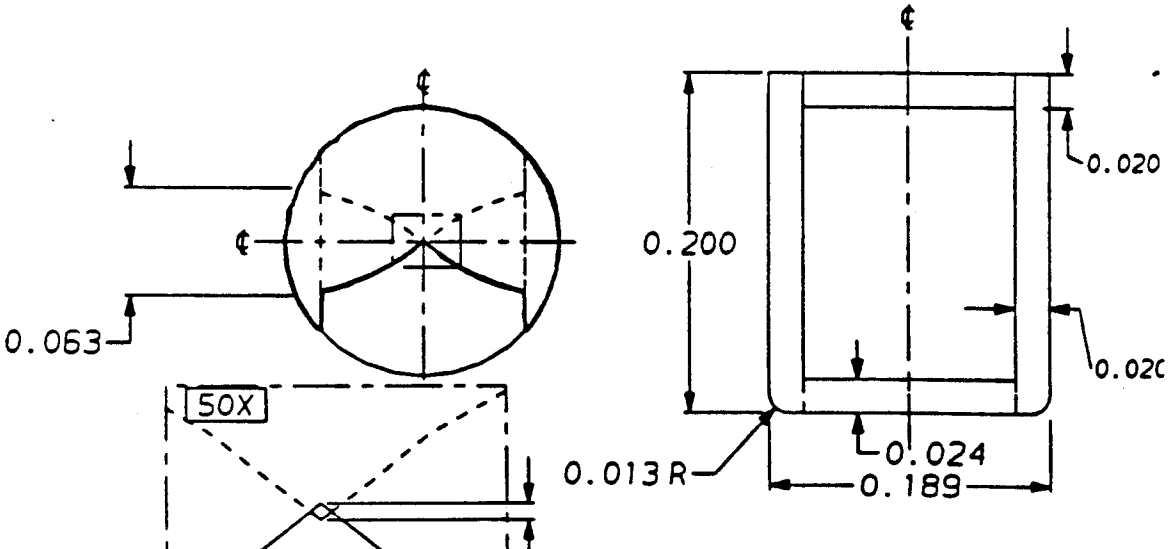

PROPOSED SENSE WIRE SUPPORT FOR WIRE CHAMBER

3-APR-90

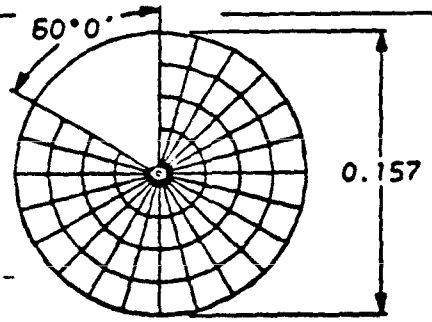

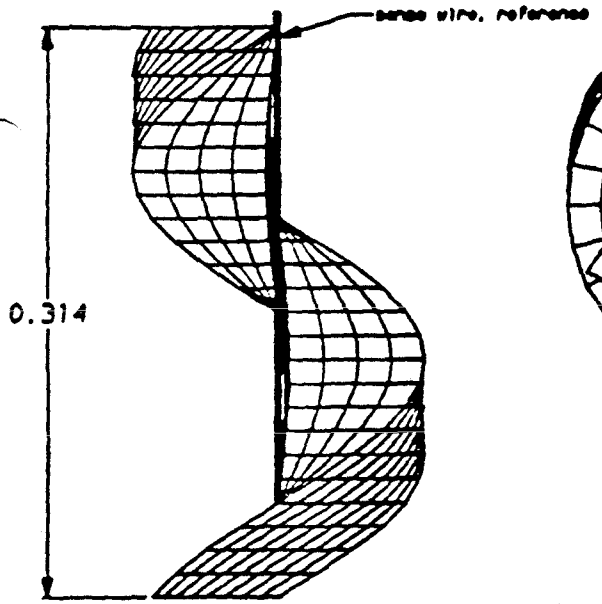

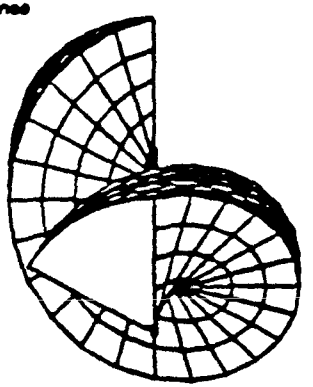

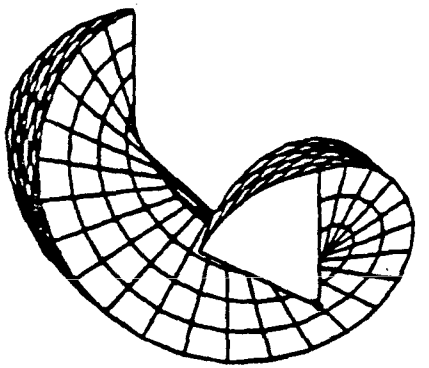

The twister must have a sliding fit in a bore of 4mm, (0.1575")
Intended to allow constraint of wire over 360 deg., yet allow threading wire through bore.

Twister is positioned at 80cm. intervals.

Drift Chamber tests

A number of studies have been done on drift chamber gases. These have been reported[4] previously , so I will mention only a few of the results to show that we have an example of a gas that will work at the SSC. The speeds of various gasses are shown in Fig. 14 a,b,c,d. The fastest gas we have studied is CF_4. with 20% isobutane, shown in 14 d. The drift time with no magnetic field is 19 ns for 2 mm drift.

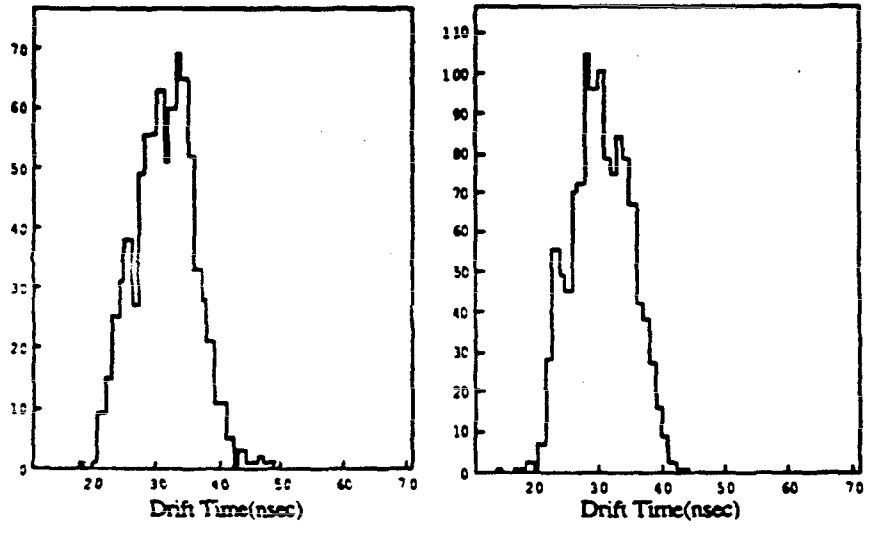

a b

Fig. 14 . a) TDC distribution for Ar-Ethane(50%) b) TDC distribution for HRS gas

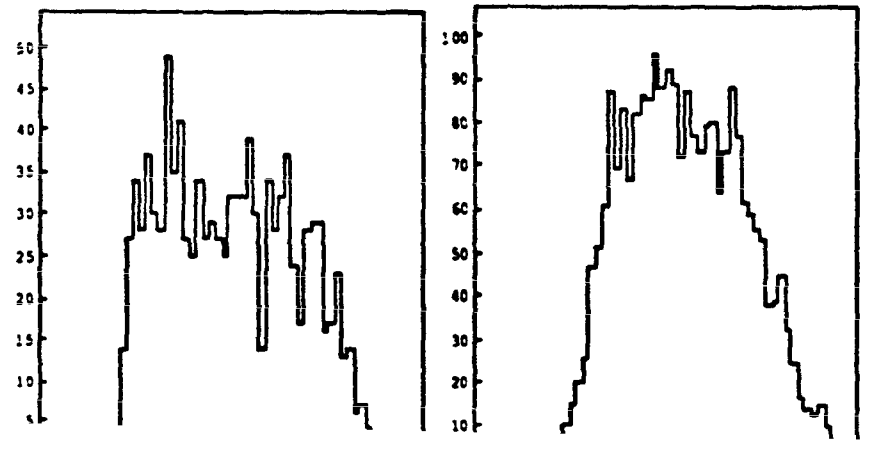

The resolution of this gas, for various isobutane concentrations is shown in Fig. 15
This gas gives us a resolution of about 100 microns and full efficiency at about 2000 Volts. Other gases are still under study.

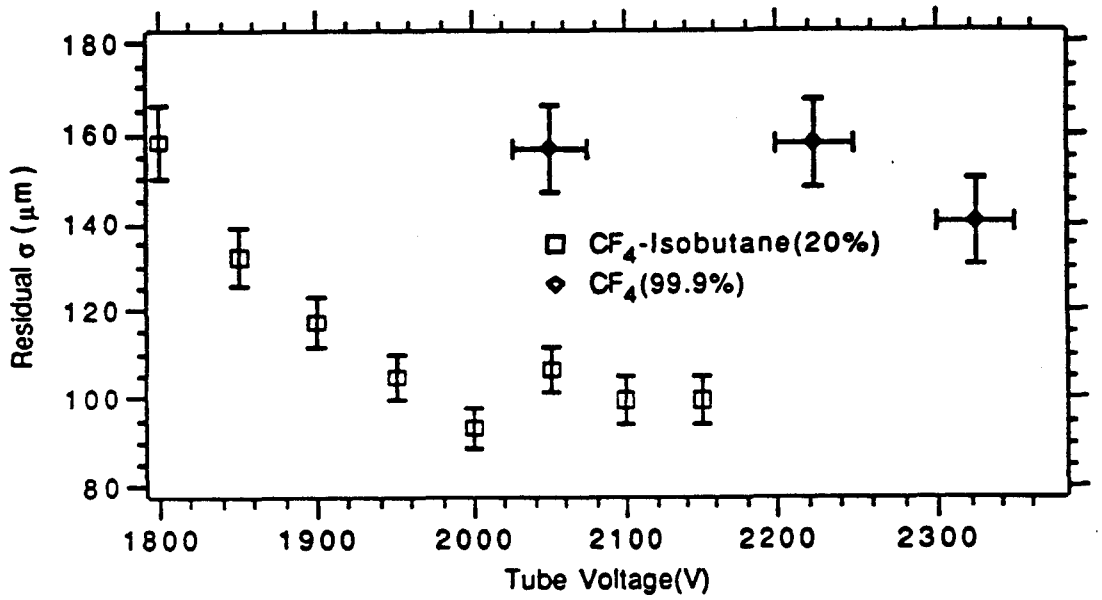

Fig. 15. Wire resolution for CF4 gas mixtures

We have also measure the efficiency of these gas mixtures as a function of voltage. These measurements, shown in Fig. 16, will depend rather importantly on the noise immunity of the electronics and the resulting threshold level, so they should only be taken as an indication of the signal size for this particular gas.

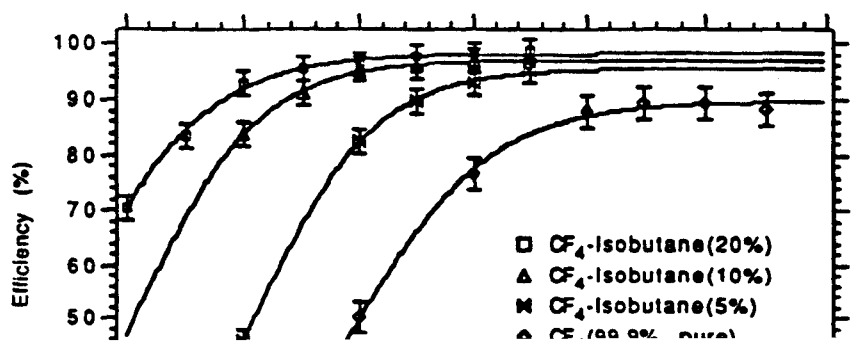

Long straw tests at Indiana University

In addition to the basic chamber operation studies that I reported above, we have begun a program for directly measuring the properties of long straw systems- chambers as long as those required for SSC. The goals of this program are:

- •Establish construction techniques
- •study signal attenuation
- •Study termination
- •Verify short straw performance
- •verify support-stability calculations

As part of this program we have constructed a 2 meter, six straw array and completed a 3.5 meter, six straw array. The six straws are held in a precision machined V groove 3.6 meters in length. The basic test system for cosmic rays in shown in Fig. 17.

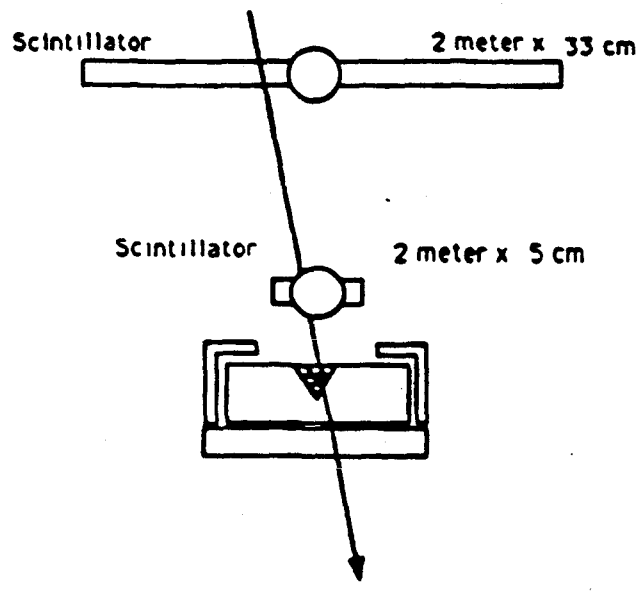

Fig. 17. Layout for 6 straw chamber cosmic ray tests

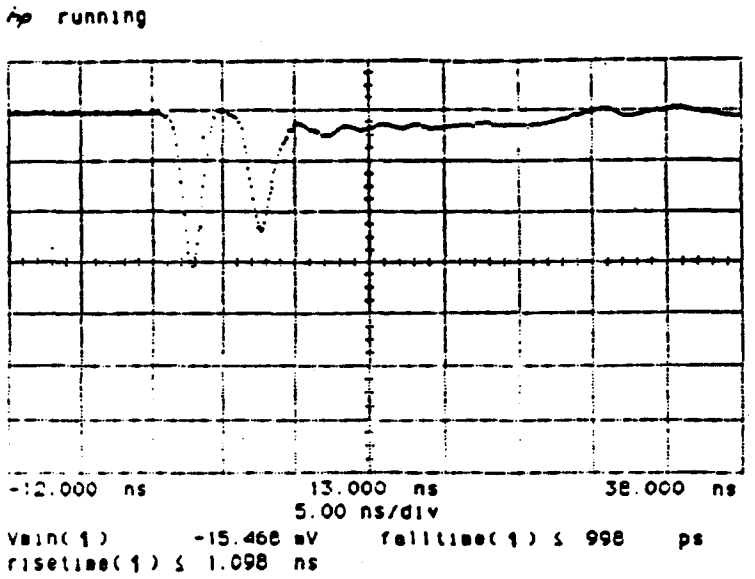

Fig.18. Direct signal from Fe^{55} source with reflection pulse

The far end of the straw was satisfactorily terminated with 223 ohms through 34 Pf. This is consistent with the calculated value of 310 ohms for the impedance of the straw transmission line. The terminated pulse is shown in Fig. 19.

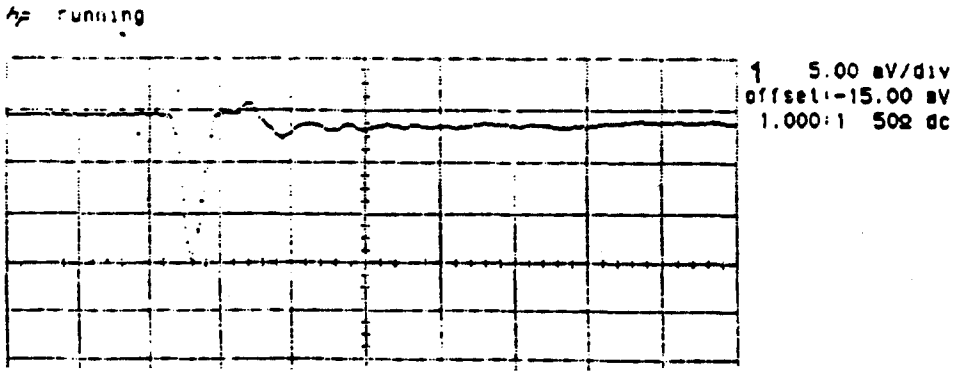

Using the terminated pulse we were able to measure the attenuation of the Fe^{55} signal in the straw chamber. This is shown in Fig. 20. We find an attenuation length of somewhat over 4 meters. This would be satisfactory for the 3 meter length chambers foreseen at SSC, but is somewhat shorter than a simple calculation would predict. We are investigating the effects of the splice resistance and the total cathode resistance.

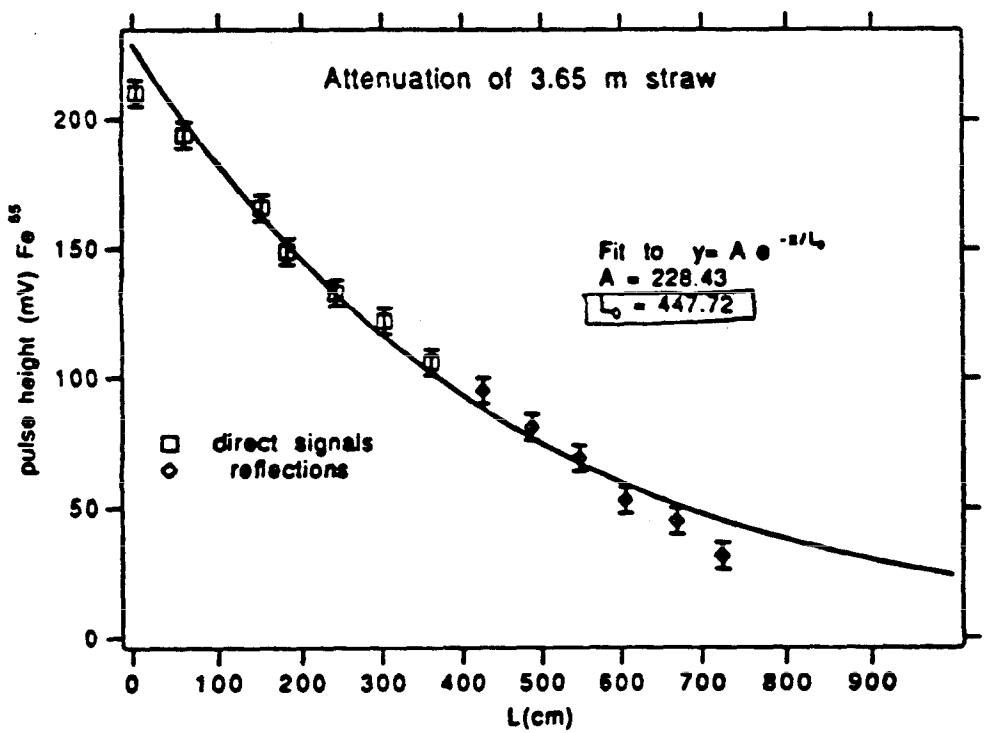

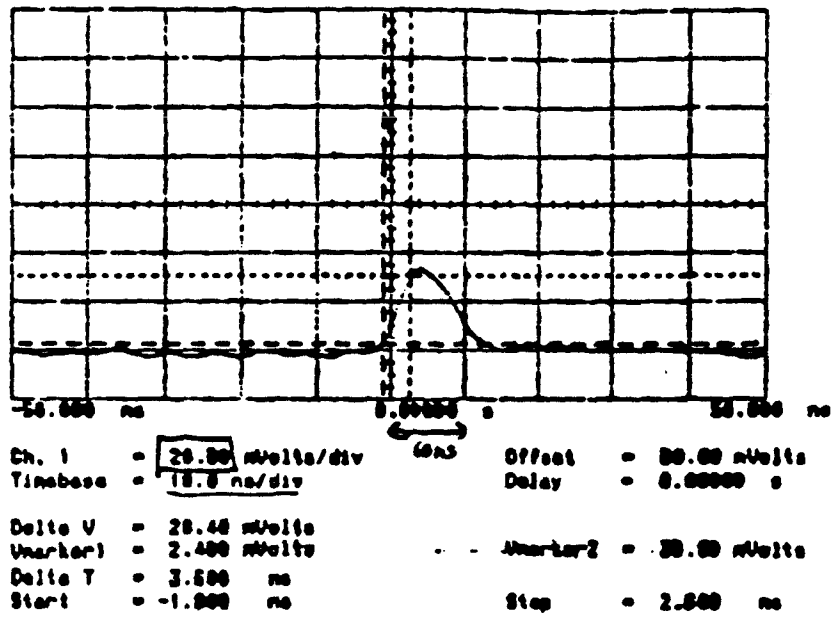

Fig. 21. A "typical" cosmic ray signal after amplification and tail cancelation

Signal Calculations

We have calculated the signal characteristics of the 4 mm straws based on the work done by Iwasaki.[5] We note that there is an impressive gain in signal size going to a fast gas at higher voltage. Figure 22 shows the calculated signal from a 3 meter straw for both 7 mm and 4 mm diameters. The 4 mm straw gives almost twice the signal, and has a much faster rise time. We feel that both jitter and walk errors will be tolerable in 4 mm straws. of 3 meter length.

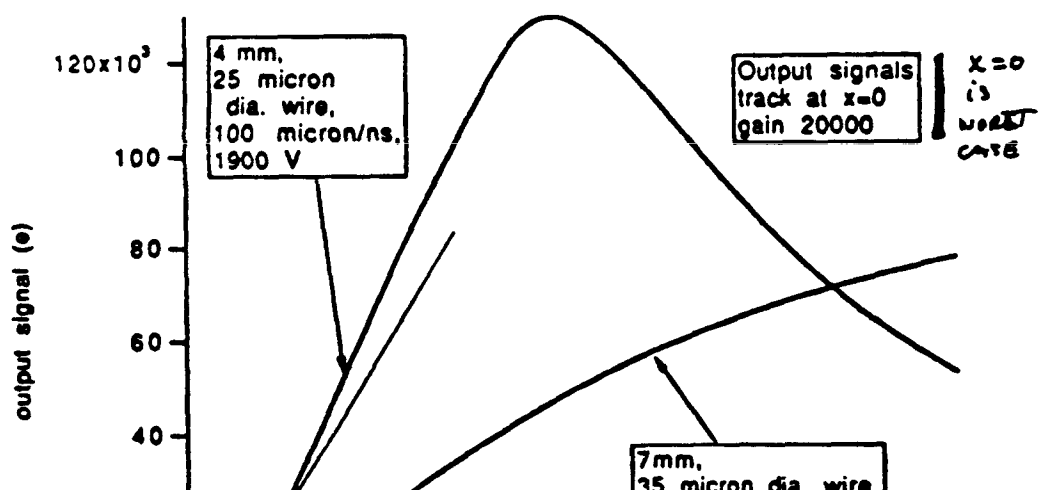

Summary

Large scale mechanical design of a modular straw system is underway by Westinghouse. This design will include the integration with Si system , the module support , and a study of the alignment and stability of the system.

The modular approach to constructing a tracking system will be studied this summer with the construction of several 64 straw modules. These will be available for testing by collaboration. Tests might include :

- electronics evaluation
- High rate beam studies
- Trigger electronics
- Gas flow and heating studies
- Radiation testing
- precision track linking and resolution

We would like to stress that basic R&D still very useful by any group. We would like to help you get started if you are interested. Some areas of useful activity might be:

- Straw tube materials
- wire studies
- spacer designs
- fast gases- response in B fields
- endplate design- signal coupling
- termination- capacitors

References

1. Central and Forward Tracking with wire chambers, SSC Detector subsystem,
   Indiana University
   D. Blockus, R. Crittenden, A. Dzierba, R. Foster,G. Hanson, C. Neyman, H. Ogren, D. Rust
   University of Colorado
   G. Baranko, H. Cheung, J. Carr, J. Cumalat, E. Erdos, W.T. Ford, J. Ginkel, U. Nauenberg, P. Rankin, G. Schultz, J. G. Smith
   University of Pennsylvania
   F. Newcomer, R. Van Berg, H.H. Williams
   KEK National Laboratory
   Y. Arai
   Lawrence Berkeley Laboratory
   A. Palounek
   University of Michigan
   J. Chapman
   University of California, Davis
   R. Breedon, W. Ko, R. Lander, K. Maeshima, J. Smith
   Rutherford Appleton Laboratory
   J.C. Hart, N. McCubbin, D. Saxon, P. Sharp
   University of Liverpool
   P. Booth, J. Dainton, E. Gabathuler
   Westinghouse Science and Technology Center
   D.Hackworth, J. Hendrickson, J. Barkel, R. Svendrud
   Oak Ridge National Laboratory
   T. Shannon

2) The 4 mm straws we used were made by Precision Paper Tubes, Wheeling Ill.

3) Wire Stability tests on 4 mm straw chambers, H. Ogren, et. al., IUHEE 90-2

4) Gas Studies on 4 mm diameter straw drift chambers, C. Neyman, IUHEE 90-1

5) A study of Time resolution for a Straw Chamber, H. Iwasaki KEK 89-158

IUHEE-90-11

Some Facts Concerning the Electrical Resistance of Straw tube Chambers

David R. Rust

I. The Cathode Resistance

The resistance is determined by the thickness and composition of the coating. We have always used aluminum for the coating material. Early in our experience with straw tubes we found that we could not use standard aluminized mylar because the coatings were too thin and the material was usually coated on both sides. We wanted to obtain as much electrical conductivity as we could but we found that we could not obtain coatings on mylar or polycarbonate that were thicker than about 1000 Angstroms. This limit is apparently set by the amount of heating that the plastic film can withstand during the metalization process. The resistance of these coatings is about 1 ohm/sq.

There is no conductivity across the gaps in the spiral wound straws as far as we know. The effective length of the straw when calculating the total resistance is therefore the length of the strip that forms the inside layer. It is about 0.45 in wide and perhaps 15% longer than the length of the tube itself. Thus a 1 meter long tube has a resistance of about 100 ohms. This is confirmed by measurements on the tubes.

The new Kapton material has 2500 Angstroms of aluminum and the measured resistance is 0.25 ohms/sq. This is 4 times lower than the resistance of the old material but the thickness is only 2.5 times thicker. This is probably because the coating is not uniform at a microscopic level and with the thicker coating there are more connections between islands of aluminum.

II. The Wire Resistance.

We have several possibilities for wire material and wire size as well as for coating the wire with a different material. Moreover the losses to the pulse amplitude after transmission along the wire depend on the rise time of the pulse because of the skin effect

Cu	1.75 microhm-cm	7.1 micron
Au	2.4	8.3
Al	2.6	8.5
Mo	4.8	11.8
W	5.6	12.7
Be-Cu 25 Alloy	7.7	15

Resistivities and skin depth at 100MHz for a few materials.

Our standard gold plated tungsten wire with 0.00100 in diameter has a measured resistance of 113 ohms/m. The amount of gold is 3 to 5% by weight which is the same as 3 to 5% of the area because the densities of gold and tungsten are about equal. This corresponds to 1.5 to 2.5% of the radius being gold so that the gold coating is about 1/4 micron thick on the 25 micron wire. Using a radius of 12.5 micron and the resistivity in the table the tungsten part of the wire has a resistance of 115 ohms/m. A gold wire with 4% of the area of the tungsten has a resistance of 1230 ohms/m and the parallel combination of the two is 105 ohms/m. This is in fair agreement with the measured value. The resistivity of the very thin drawn wire may differ from the bulk value quoted in the tables of resistivity. The gold lowers the resistance of the wire by only a small amount.

A reduction in the resistance of the wire can be achieved by increasing the size of the wire or by using a material with lower resistivity. Be-Cu of the type with high tensile strength has a higher resistivity and so is not desireable. Molybdenum wire has sometimes been used for chamber sense wires and has about a 15% lower resistivity than tungsten. Its Z is 42 as compared to 74 for tungsten

The skin depth is inversely proportional to the square root of the frequency. As the table shows the typical skin depth at the typical frequency of 100 MHz is of the same order as the wire radius. Although the exact form of the dependence of the resistance on the frequency is complicated, a simple approximate relationship can be used. For values of the wire radius r and skin depth d such that r/d is less than or equal to 1, the effective resistance is within a few per cent of the D.C. value. For r/d = 1.5 the effective resistance is about 10% larger than the D.C. value. For r/d more than or equal to 2 the ratio of the effective resistance to the D.C. resistance is 1/4+r/2d.

For pulses from charged particle tracks where the rise time corresponds to a frequency of 100 MHz or less, the ratio r/d is about 1 so that we can just use the D.C. resistance. For pulses from the Fe-55 source (frequency of about 300 MHz) there is an increase in the resistive loss by 15-20% over the D.C. value. Losses will still scale inversely with the area of the wire. The gold plating on the wires is too thin to change the current distribution at high frequency.

August 30, 1990
IUHEE-90-13

Depenence of Straw Tube Gain on Wire Diameter

C. Neyman, B. Martin, H.Ogren

SSC R &D Group

Indiana University

It would be advantageous for the electical characteristics of staw tubes if the wire resistance was decreased. One way to achieve this is to use a larger wire diameter (2mil as opposed to the current wire size of 1 mil). However the trade off is a lower electric field at the wire surface with the corresponding drop in signal gain. All else being equal this requires runing the tubes at a higher voltage. To understand the required increase in voltage the gain was measured for both 1mil diameter gold plated tungsten and a 2mil gold plated molybdenum wires.

The drift chamber constructed for this series of tests was a single tube with a length of 25 cm. Our straws were fabricated by Precision Paper Tube Company., Rockville, Ill. The straws consists of a layer of 0.5 mil polycarbonate film aluminized on the inside surface, covered by an 0.5 mil mylar film. The two films are wound with overlapping pitch and bonded by an application of epoxy resin between them. The inside diameter is 0.157 in or 4.0 mm.The anode is a gold plated tungsten wire 25 μm in diameter. It is tensioned and held centered by two Delrin pins inserted in each end of the straw. The Delrin pins are inserted into a plastic gas manifold, which positions the wires and provides a robust mechanical support. These gas manifolds are designed to allow quick changes of the wire. The single tube sits in a groove that is machined in a aluminum bar. The groove aligns both ends and hold the straws in position. The tubes were at ground potential with the wire at positive high voltage. A 47 pF bocking capacitor was used to couple the signal to the amplifier.

into the input of the amplifier The signal was displayed on an HP digital scope. 2048 signals were averaged to give the display from which the pulse height was read. The pulse output verses charge is plotted in fig 1 only the first six point were used in the fit. The amplifier seems to be non linear in the region above 400 mV. This is alright because the signals from the chamber are much smaller.

fig 1

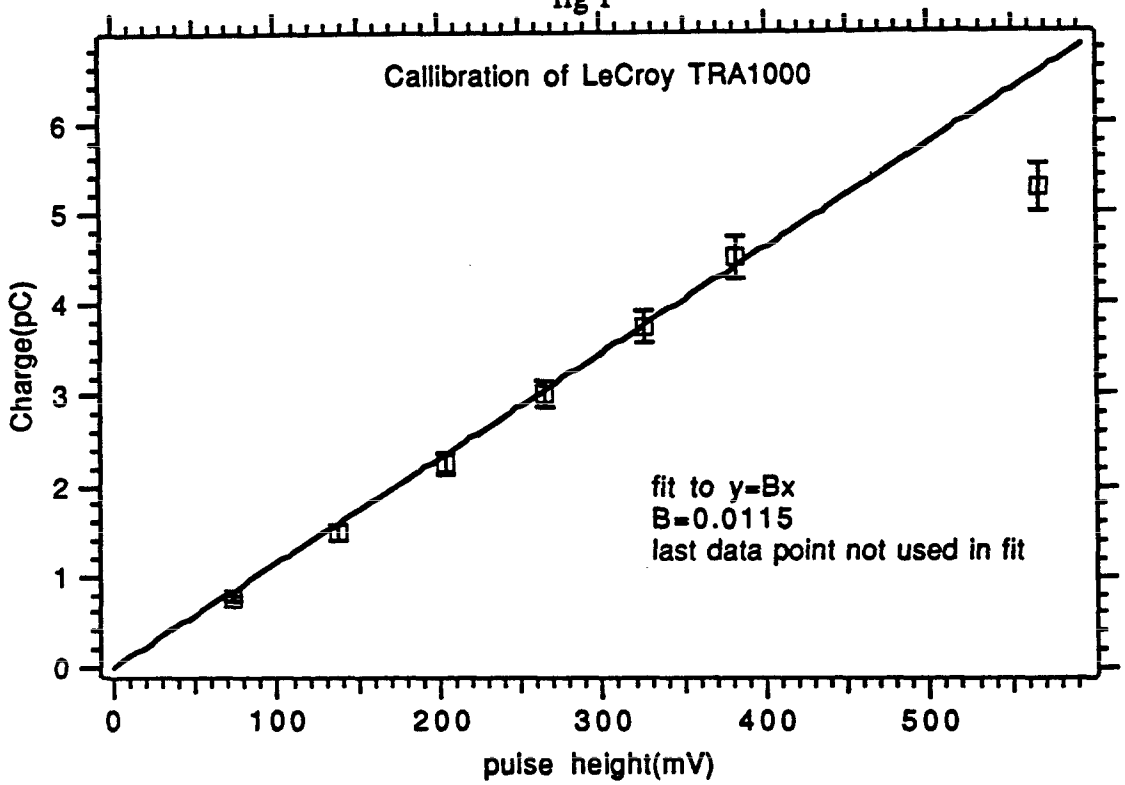

The gain of the tube was measured on the digital scope in the same manner as the calibration. Measurements were made with both 1mil and 2mil wires. The data are ploted in fig. 2 In order to operate with a 2mil wire the tubes potential would have to be increased approximately 300V over the potential for a 1mil wire

Fig 2

Gain of 1mil and 2mil Diameter Wires

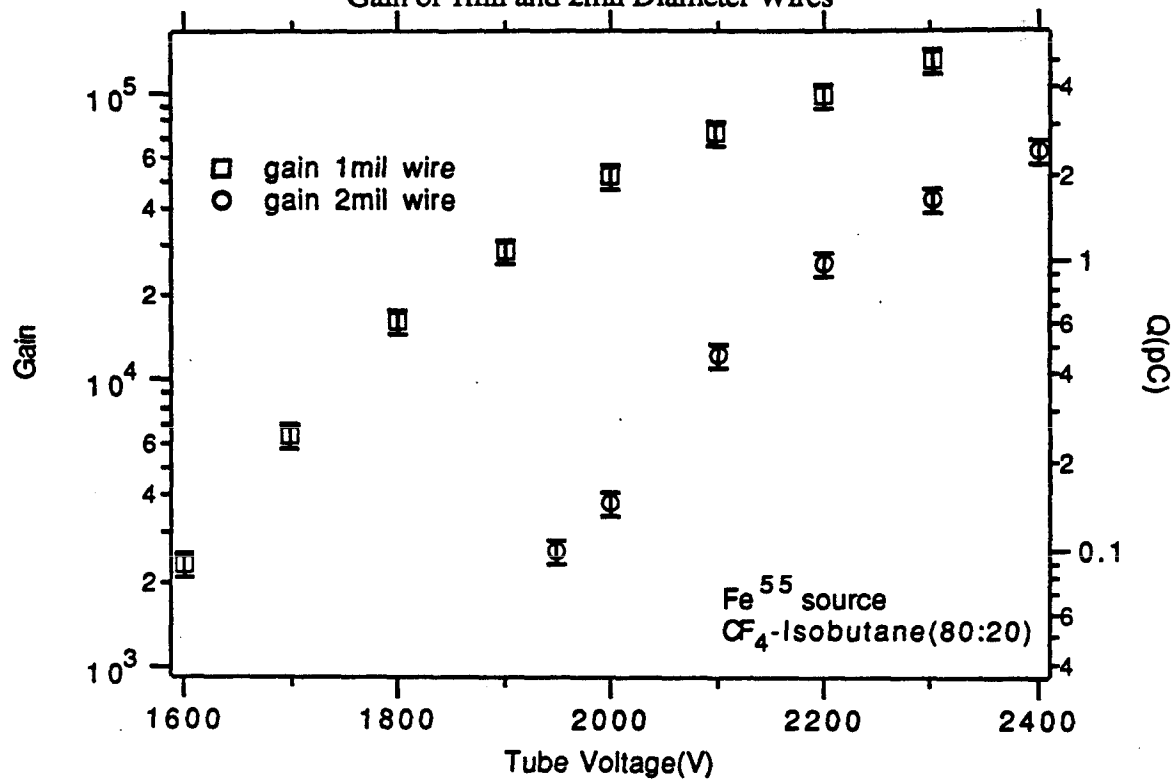

August 30, 1990
IUHEE-90-14

Dead Space of an M&M Wire Support and a Doped Wire

C. Neyman, B. Martin, H.Ogren

SSC R &D Group

Indiana University

M&M Dead Space)

The dead space of any potential wire support device is an important quantity to know as it has direct impact on the efficiency of any potential central tracking chamber at SSC.

The drift chamber constructed for this series of tests was a single tube with a length of 25 cm. The straws were fabricated by Precision Paper Tube Company., Rockville, Ill. The straw consists of a layer of 0.5 mil polycarbonate film aluminized on the inside surface, covered by an 0.5 mil mylar film. The two films are wound with overlapping pitch and bonded by an application of epoxy resin between them. The inside diameter is 0.157 in or 4.0 mm.The anode is a gold plated tungsten wire 25 μm in diameter. It is tensioned and held centered by two Delrin pins inserted in each end of the straw. The Delrin pins are inserted into an plastic gas manifold, which positions the wires and provides a robust mechanical support. These gas manifolds are designed to allow quick changes of the wire. The single tube sits in a groove that is machined in a aluminum bar. The groove aligns both ends and hold the straws in position.

The Counting rates were measured from an iron Fe^{55} source. A special translational stage with micrometer movement allowed the source to be scanned along the tube in 1mil increments. To better collimate the x rays the source was placed on 1/8 in thick aluminum sheet with a 2mm hole. The counting rate as a function of distance is plotted in fig. 1. The full width half maximum corresponds to dead region of the M&M wire support of 5mm . The physical length of the M&M is 4mm

Fig. 1
M&M Dead Space

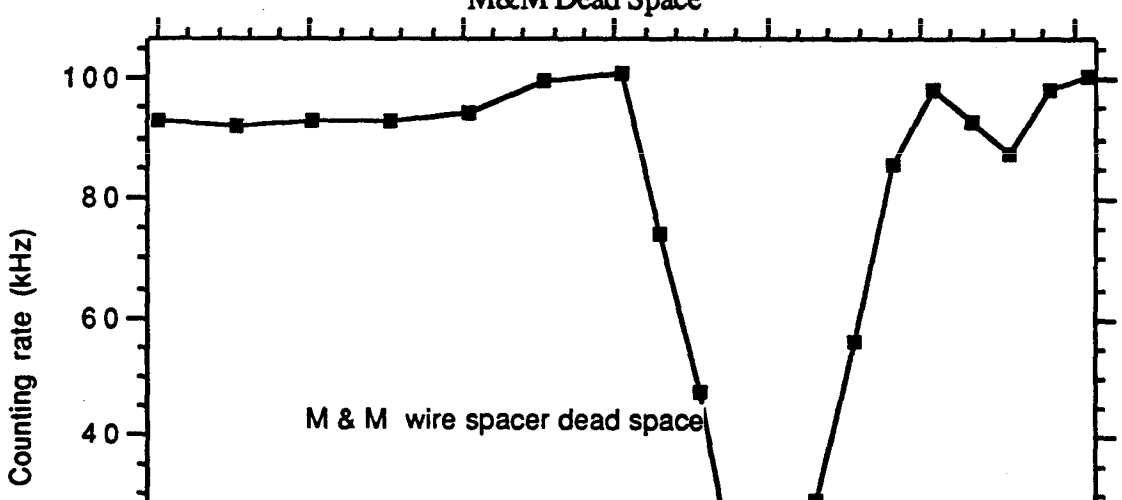

Deadening Sense Wires)

Westing House engineers have suggested that the central tracking chamber mechanical support could be greatly simplified if all the straw were the same length . One way to achieve this is make all straws of longest length required and deaden the ends of the wires of the inner straws. To test the feasibility of this idea the wire of the one straw test setup was painted with Corona Dope an anti arcing paint used in television repair.

The same apparatus and methods were used as above to measure the M&M dead space The counting rate verses position is plotted in fig. 2 The wire has 58 mm dead space. The physical size of the doped region was approximately 53 mm

Fig 2

Doped Wire Dead Space

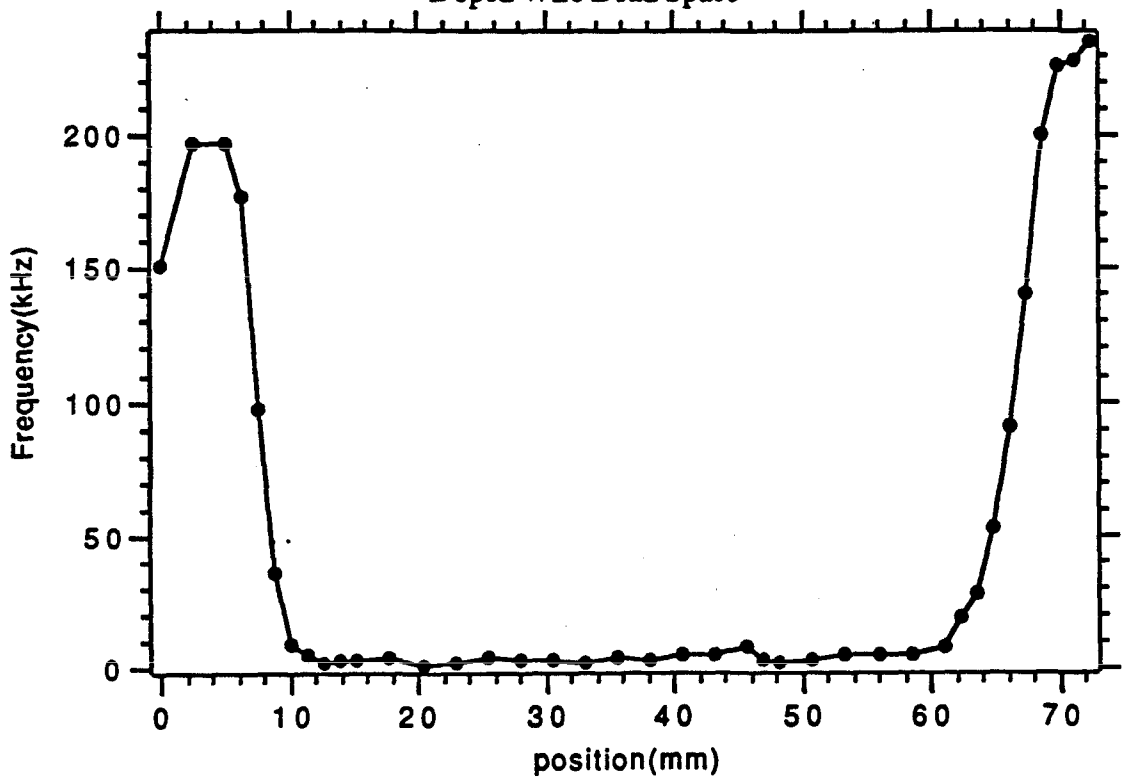

August 30, 1990
IUHEE-90-15

Gain of a 3.65m Straw Drift Tube

C. Neyman, B. Martin, H.Ogren

SSC R &D Group

Indiana University

The gain of the long straw prototype located in in the Swain West basement was measured to be compared with previous results from the 25 cm chamber. The specification of this chamber are given in IUHEE-7(May 90). An Fe^{55} source was used to produce a constant pulse height signal. The Fe^{55} x-ray has an energy of 5.9 keV. Assuming an average energy to produce an ion-electron pair of 24.5 eV, the primary ionization of the x-ray gives 240 electron-ion pairs.

The total charge from each x-ray was measured with a LeCroy TRA1000 amplifier. The feed back of the amplifier was 10pF in parallel with 10MΩ(22MΩ) this gives a time constant of 100(220)μsec, the effective integration time is about 10μsec. The amplifier was calibrated by discharging a capacitor into the input of the amplifier The signal was displayed on an HP digital scope. 2048 signals were averaged to give the display from which the pulse height was read. The pulse output verses charge is plotted in fig 1 only the first six point were used in the fit. The amplifier seems to be non linear in the region above 400 mV. This is alright because the signals from the chamber are smaller.

fig 1

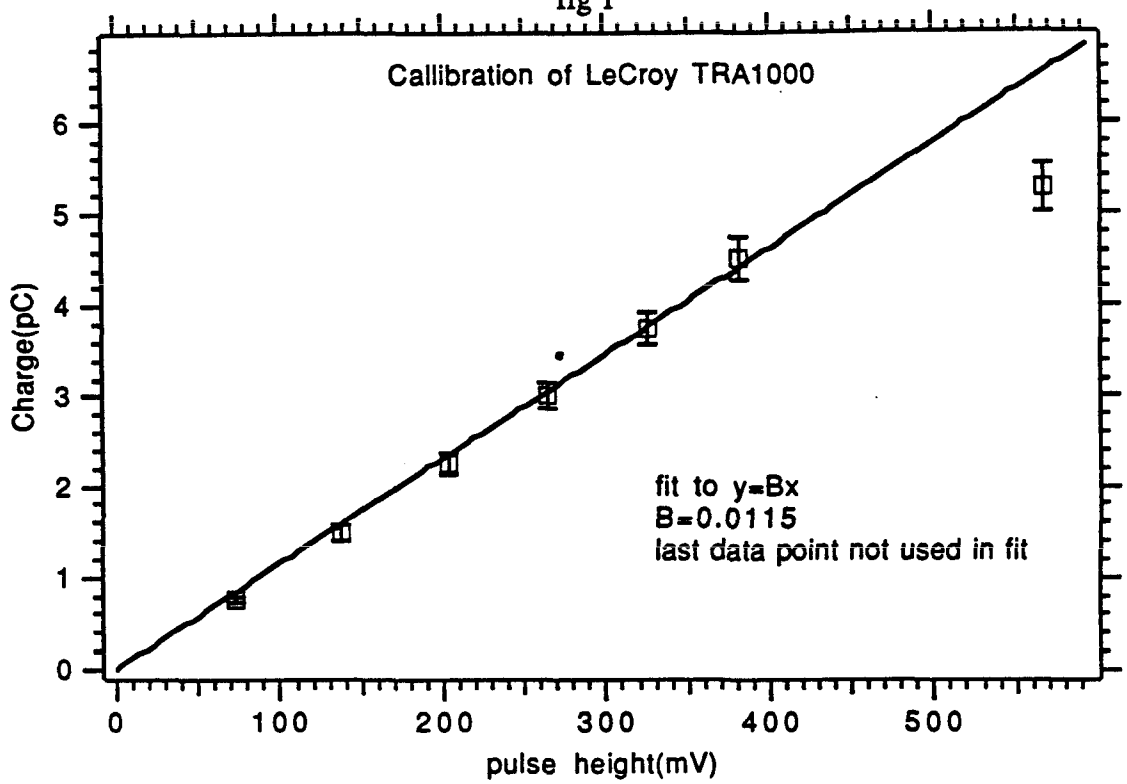

The gain of the tube was measured on the digital scope in the same manner as the calibration. Measurements were made with both 10MΩ and 22 MΩ resistors the larger resistor gives a longer time constant allowing more of the charge from positive ion drift to be collected. As one can see from fig 2 it is is hard to distinguish this effect. Apparently we are being dominated by other systematic errors that we do not understand at this time. These results agree to within errors of our results from the 25cm chamber.

Fig 2

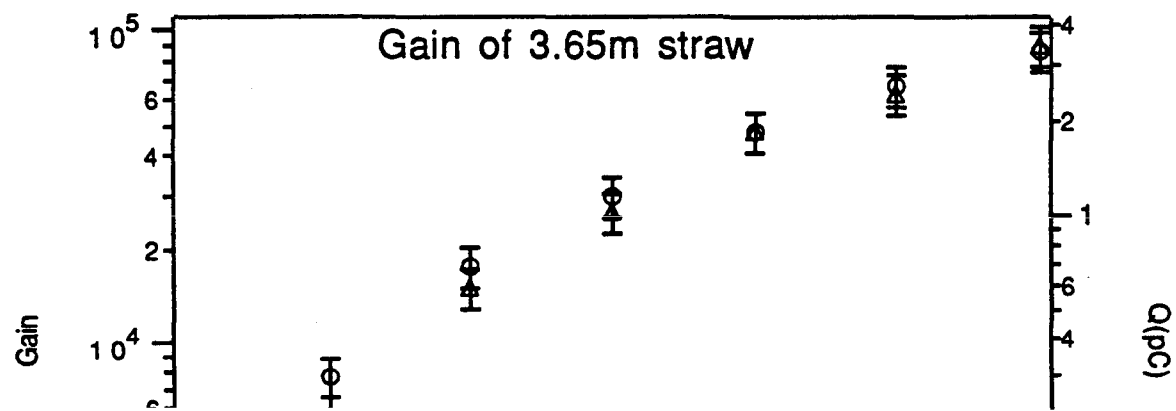

INHIBITION OF WIRE AGING USING CF_4-BASED GASES

J.A. Kadyk,[1] J. Wise,[1,2] and D.W. Hess[1,2]

[1]Lawrence Berkeley Laboratory
[2]University of California, Berkeley

CF_4/isobutane gases are found to restore aged wires with silicon-based deposits to their initial condition and also to prevent formation of the silicon deposits. The effect of molecular oxygen on these gases is investigated. Similarities to low-pressure rf-discharge plasmas, in which CF_4 is known to etch silicon, are discussed.

Corresponding Author:
J. Wise, Lawrence Berkeley Laboratory, MS 50A-2160, 1 Cyclotron Rd., Berkeley, CA 94720, ph. 415-486-7187.

J.A. Kadyk, Lawrence Berkeley Laboratory, MS 50A-2160, 1 Cyclotron, Rd., Berkeley, CA 94720, ph. 415-486-7189.

D.W. Hess, Department of Chemical Engineering, University of California, Berkeley, CA, 94720, ph. 415-642-4862.

The very good aging properties of wire chamber gases containing CF_4 have been known for some time [1,2]. There has recently been a report that hydrocarbon deposits were etched away using a CF_4/isobutane (80/20) mixture, adding additional support for the use of this gas [3]. We use this same gas to remove silicon-based deposits and to show that an established technique for formation of the silicon-based deposits on wires does not operate in the presence of the CF_4/isobutane mixture.

Wires are damaged by bubbling argon/ethane (50/50) through Dow 704 silicone oil [2]. Aging rates in such instances are typically $R \sim 100$ %/C/cm, and ^{55}Fe pulse-height spectra of the aged wires are degraded significantly. FTIR surface analyses of these wires reveals the presence of Si-O bonds, suggesting that the silicone oil is responsible for the aging in this instance. This technique has been used repeatedly to create wire deposits and is quite reproducible.

When the wire has been aged in the above-mentioned way until the initial current has dropped to a small fraction (~30%) of its initial value, the gas is changed from the argon/ethane to the CF_4/isobutane mixture. At first the current continues to fall, and periodic large current surges suggestive of Malter-type breakdowns also occur, indicating that cathode coatings may be present as well. However, the current soon begins to rise in a somewhat erratic manner, and the discharges become less frequent and finallly cease. The current (gain) ultimately reaches a constant value corresponding to the gain of a new, "clean" wire, and no longer fluctuates. Approximately 0.6 C/cm were required to restore the wire to full

CF_4/isobutane was used instead of argon/ethane. In this test, a total of 1.0 C/cm of charge was collected and the measured aging rate was only $R \sim 3$ %/C/cm.

We suggest that such behavior is an example of competitive ablation and polymerization (CAP) [4], a situation in which a steady-state between polymer etching and deposition is achieved. It is known that CF_4/hydrocarbon plasmas tend to be polymerizing [5]. That the CF_4/isobutane mixture does not age suggests that this gas mixture is well balanced. Indeed, it has been suggested that proper "tuning" of gas mixtures from a chemical standpoint may be an important factor in reducing aging [6].

We report tests of CF_4/isobutane mixtures of varying compositions and of CF_4/isobutane mixtures with molecular oxygen, added to determine possible similarities between the low-pressure rf-discharge plasma regime and that of wire chambers.

References

[1] (a) R. Henderson *et al*, *IEEE Trans. Nucl. Sci.*, NS-35 (1988) 477, (b) R. Openshaw *et al.*, *IEEE Trans. Nucl. Sci.*, NS-36 (1989) 567.

[2] J. Kadyk *et al*, accepted for publication in *IEEE Trans. Nucl. Sci.*, NS-37 (1990).

[3] R. Openshaw, private communication (1990).

[4] H. Yasuda, Plasma Polymerization (Academic Press, New York, 1985), p. 178.

[5] H. Yasuda, p. 180.

[6] J. Va'vra, *Nucl. Instr. Meth.*, A252 (1986) 547.

LBL-29354
Preprint

Lawrence Berkeley Laboratory

UNIVERSITY OF CALIFORNIA

Physics Division

Submitted to Nuclear Instruments and Methods
in Physics Research A

Use of Straw Tubes in High-Radiation Environments

J.A. Kadyk, J. Va'vra, and J. Wise

July 1990

DISCLAIMER

This document was prepared as an account of work sponsored by the United States Government. Neither the United States Government nor any agency thereof, nor The Regents of the University of California, nor any of their employees, makes any warranty, express or implied, or assumes any legal liability or responsibility for the accuracy, completeness, or usefulness of any information, apparatus, product, or process disclosed, or represents that its use would not infringe privately owned rights. Reference herein to any specific commercial products process, or service by its trade name, trademark, manufacturer, or otherwise, does not necessarily constitute or imply its endorsement, recommendation, or favoring by the United States Government or any agency thereof, or The Regents of the University of California. The views and opinions of authors expressed herein do not necessarily state or reflect those of the United States Government or any agency thereof or The Regents of the University of California and shall not be used for advertising or product endorsement purposes.

Lawrence Berkeley Laboratory is an equal opportunity employer.

LBL-29354
SLAC-PUB-5306
July 1990

USE OF STRAW TUBES IN HIGH-RADIATION ENVIRONMENTS*

J.A. Kadyk,[1] J. Va'vra,[2] and J. Wise[1]

[1]Lawrence Berkeley Laboratory, University of California, Berkeley, CA 94720, USA

[2]Stanford Linear Accelerator Center, Stanford University, Stanford, CA 94309, USA

Abstract

We have investigated several aspects of straw tubes relating to their viability for use in SSC detectors. Gas temperature changes and the consequent gain changes resulting from the power dissipated in the tube at high rates are found to be relatively minor effects. Conduction through the gas between the wire and the wall is found to be the major mechanism by which heat is removed. Little aging is observed in straw tubes operating with any of several different gas mixtures. The dependence of aging on gas flow rate is found to be small. Water vapor at low concentrations (1000 ppm) is found to prevent breakdowns. Design and construction of straw tubes are discussed.

1. Introduction

Straw tubes have received attention as candidates for use in detectors at the proposed Superconducting Super Collider (SSC), where they would be expected to be exposed to high-radiation environments. Before straw-tube wire chambers can be implemented, however, a number of issues, including (1) design and construction of the tubes, (2) aging behavior of the tubes, (3) possible gain fluctuations or nonuniformities due to temperature changes caused by the power dissipated in the gas, (4) signal attenuation in long tubes, and (5) optimal operating gain need to be addressed.

There are four parts to this investigation: (1) study of aging effects in straw tubes, including straw tubes previously damaged by discharges; (2) use of straw tubes equipped with carbon wires to study the thermal effects of avalanches; (3) study of the effects of various cathode materials; (4) study of tracking resolution and correlation with the rate of aging and with other aging effects. This report discusses only the first two parts.

2. Construction Techniques

A novel feature of the tubes used in these tests is that their inside diameter is only 4 mm, whereas previously-used straw tubes had 7-10 mm inside diameters [1].

Since it is known that it an efficient gas flow through the tube is necessary [2,3,4], a feedthrough was designed to ensure such a flow. Fig. 1 shows our design of a feedthrough pin made of Delrin [5]. This design assumes that the end flange has a gas manifold that allows the gas to enter the tube through four rectangular grooves, each of cross-section of about 0.5 x 1.0 mm. The grooves are machined into the pin and are located near the cathode wall.

A brass tube, shown in Fig. 1, is set into the Delrin pin and is used to support the wire. A sapphire jewel [6]

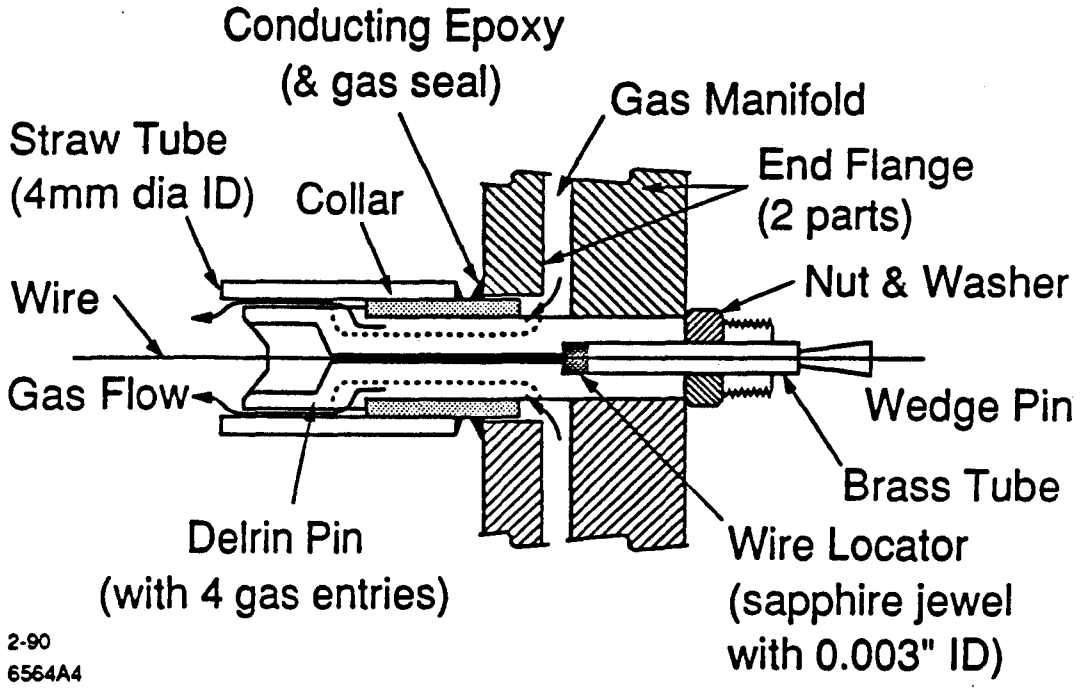

Fig. 1. Our design of the feedthrough pin.

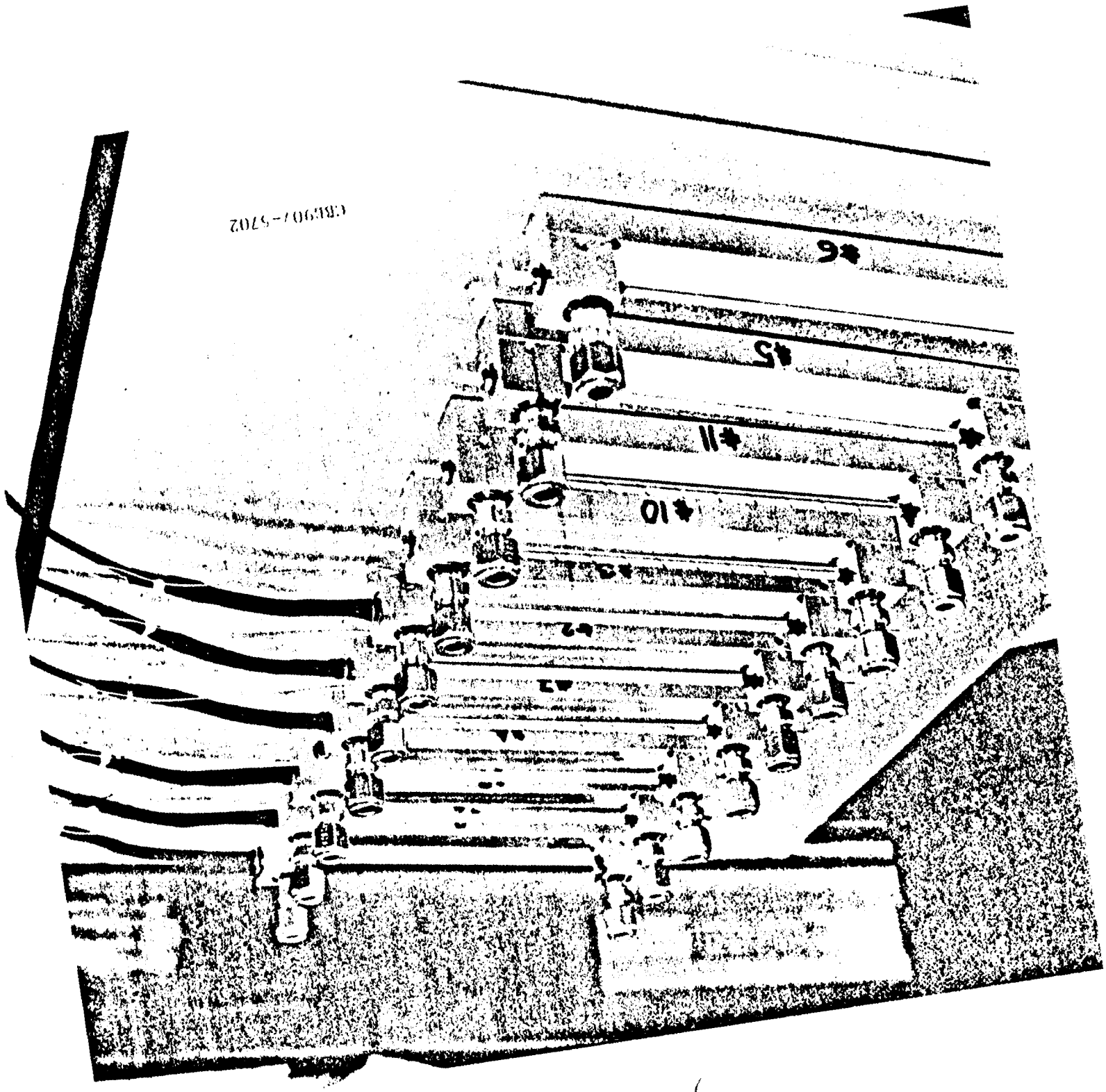

CB690/-5702

3

friction fit and had to be secured by gluing. Wire tensions were 140 g for the 38 μm-diameter gold-plated tungsten and 32 g for the 33 μm-diameter carbon wires. The unsupported wire length was only 17.5 cm and therefore electrostatic instability was not an issue in these tests.

The straw tube walls were constructed by bonding together four layers. The innermost layer is 9 μm-thick aluminum and the three outer layers are each 25 μm-thick Mylar [5]. Polyethylene of 7.6 μm thickness is used as the bonding medium between layers. The bonding was done at high temperature to create the straw tube body [8]. The relatively thick aluminum layer was used to prevent "etching" of the cathode surface in a high-radiation environment [9]. The thicker aluminum also helps to keep the tube straight [10]. The total thickness of the tube wall was about 107 μm in this test, although this can be reduced for applications at the SSC. (We considered the choice of wall material to be the most important variable in these tests.) The electrical contact to the cathode was made with conducting epoxy [11], which was cured at room temperature. We used DP-190 epoxy [12] for the other gluing operations. Fig. 2 shows the straw tube test chambers used for the studies described in this paper.

Prior to use, the tubes were washed in ethanol for a few minutes using an ultrasonic cleaner, and then dried under a gaseous nitrogen flow. The wires were cleaned during stretching with a lint-free tissue moistened in ethanol. All parts were handled with rubber gloves to prevent contamination of the surfaces.

The gas was in contact with the following materials in these chambers: carbon or gold-plated tungsten (anode wires), aluminum (straw tube body), brass, Delrin, Mylar, polyethylene, DP-190 epoxy, conducting epoxy, and T-6061 chemically etched aluminum (end flanges).

towards further breakdown. This phenomenon has been studied with a straw tube that had portions of its wire damaged accidentally (by operating with excessive gain and/or current). The point at which breakdown occurs was found to depend upon both the gain and current at which the tube was operated, and upon the condition of the portion of the tube irradiated. If the gain and/or current is large, or if the tube has been previously damaged by aging, the threshold for breakdown is decreased.

When using argon (Ar)/ethane (50/50) or carbon tetrafluoride (CF_4)/dimethyl ether (DME) (90/10), the straw tube was found to operate stably when water at the 1000 ppm level was added directly to the gas with a gas bubbler. Water could also be introduced indirectly, by outgassing from the walls of the plastic tubing used for the gas plumbing and/or by diffusion through the tubing. The concentration of water added indirectly in this way is not known. Breakdown occurred within minutes after startup when using electropolished stainless steel tubing, which is impermeable to air and is known to have little outgassing [13]. No breakdown was observed up to current densities of about 400 nA/3 mm when nylon tubing was substituted for the stainless steel under otherwise identical conditions. This dependence on tubing material was quite reproducible. Based on these results, nylon tubing was used for all subsequent tests.

The exact mechanism by which water arrests or prevents Malter breakdowns is not clearly understood. We mention briefly two possible mechanisms. (1) Water may make an insulating cathode deposit slightly conducting. In this way, accumulated positive charge on the cathode, which is a precursor of the Malter breakdown, can be bled off. (2) If hard UV photons from carbon excitations [14] are responsible for photoionization at the cathode, the effect of water is can be explained by its absorption of these photons [15]. The absorption by water is plotted in Fig. 3. Although

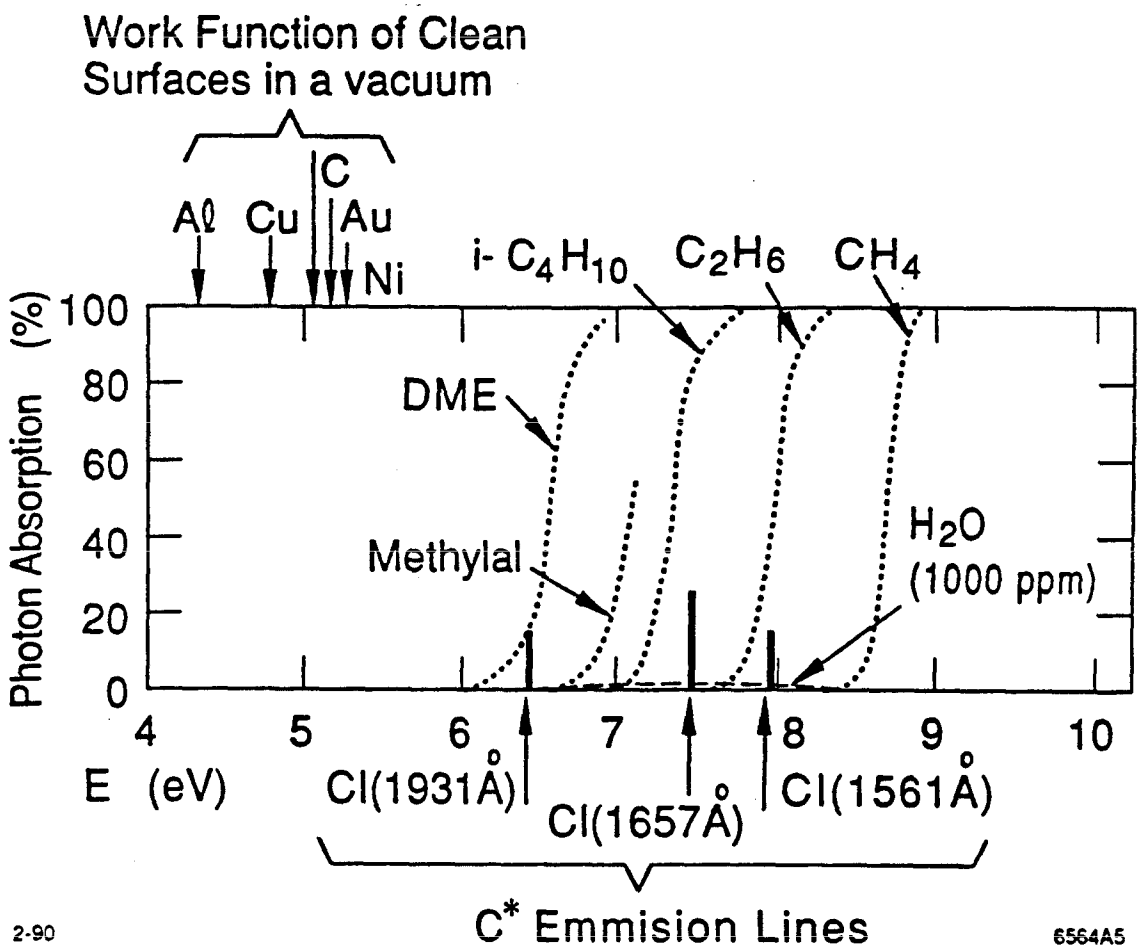

Fig. 3. Qualitative theory explaining the effect of water in arresting Malter breakdowns by hard UV photon absorption.

concentrating water molecules, e.g. on the cathode, would therefore be required for this mechanism to be effective.

It is clear that the effect of water needs to be investigated further, including its effect on drift velocities in so-called fast gases, such as those with a CF_4

CF_4/dimethyl ether (90/10). Argon/ethane was tested because it is a commonly used gas. The CF_4/isobutane (80/20) mixture was tested because it possesses several attractive properties: (1) it has been tested to 8 C/cm with no apparent aging [16]; (2) it has a high drift velocity (in excess of 10 cm/μsec) [17,18], a feature that may be quite important at the SSC and in other high luminosity colliders; (3) it has a relatively high ionization density for minimum ionizing tracks (180 ion pairs/cm) [19]; and (4) it has a low electron diffusion constant [18]. These properties make CF_4/isobutane (80/20) an attractive choice for use in high-resolution drift chambers in high-radiation environments. The CF_4/dimethyl ether mixture was tested in the belief that it may have similar properties.

The techniques used to collect aging data have already been described [20]. The 5.9 keV photons emitted by an ^{55}Fe source (1 or 2 mCi) were used to simulate particle radiation. The irradiated region of the wire was about 3 mm. Results of these tests are shown in Table 1.

As can be seen, the rate of gain loss, R, was determined to be small or consistent with zero in nearly every case ($R \leq 10$ %/C/cm). As little as 1000 ppm of water vapor, added to the argon/ethane by means of a gas bubbler, was found to be sufficient to avoid the electrical breakdown, and tests were not made with smaller amounts of water added in this way.

Measurements of R vs. gas flow rate were made with argon/ethane at relatively low flow rates to find the minimum acceptable flow rate. As shown in Table 2, negligible aging rates were observed for gas flow rates as low as 1.0 cm^3/min, corresponding to an average linear gas velocity of ~1.3 mm/sec. Indeed, no gain change was observed until the gas flow was completely interrupted.

Although the above results indicate that straw tubes are or can be made resistant to wire aging, it is important to realize that under less-well-controlled conditions, aging

Table 1
Summary of aging results in straw tubes. Gold-plated wires were 38 μm diameter; carbon wires were 33 μm diameter. The aging rate, R, is defined as $R = -(1/G_0)(dG/dQ)$, where Q is the collected charge per length of wire and G is the gas gain. The total gain was ~5x10⁴ for tests with gold-plated wires and ~2x10⁴ for tests with carbon wires. Nylon tubing was used for the gas plumbing in all tests.

gas	R %/C/cm	accumulated charge C/cm	anode voltage V	wire surface material	average gas velocity mm/sec
Ar/C_2H_6 (50/50)					
+1000 ppm H_2O	15	0.4	1600	Au	53
CF_4/iC_4H_{10} (80/20)					
+1000 ppm H_2O	3	0.5	2240	Au	53
w/out added H_2O	5	0.25	2240	Au	53
CF_4/DME (90/10)	3	0.7	2200	Au	26.5
Ar/C_2H_6 (50/50)	~0	0.8	1590	carbon	26.5

Table 2
Summary of aging results in straw tube with a 33 μm diameter carbon wire as a function of the gas flow rate. Argon/ethane (50/50) was used for all tests. The anode wire voltage was 1590 V. All measured values of R are consistent with zero within our estimated systematic uncertainties.

gas flow rate cm^3/min	average gas velocity mm/sec	R %/C/cm	accumulated charge C/cm
20	26.5	−2	1.0

5. Heating Effects

Possible limitations to the use of straw tubes in high radiation environments are gas temperature changes and the consequent gain changes. Indeed, temperature changes as small as 6°C, corresponding to ~10% gain variations, may be unacceptable in some applications. The potential difficulty arises in removal of the power dissipated as heat in the tubes.

To illustrate the potential difficulty caused by heating effects on gain, we consider the following hypothetical case in which heat removal from the straw tube occurs solely by the gas flow. In this case, the temperature rise is determined by the gas heat capacity, gas flow rate, and power input. For the latter, we will assume 2 mW of power generated over a 1 m length of wire (2000 V * 1 μA/m). The heat is deposited mainly by drifting positive ions produced in the avalanche, and not by the electrons, since the former charges traverse a much larger potential difference (nearly the full anode-cathode voltage). However, the heating is concentrated near the anode wire because the potential difference, and hence the power deposited, is logarithmic with the radius. For a 4 mm-diameter tube with a 33 μm-diameter wire, one-half of the power is produced within a radius of about 260 μm. Since the gas velocity is relatively small (low Reynolds number), we expect laminar flow, and the power deposited within this radius will heat the gas in a corresponding volume. For a 1 m-long tube, we calculate that the heated volume of 0.053 cm^3 contains 2.4×10^{-6} moles of gas. At an assumed flow velocity of 1 mm/sec, there would be a volume change every 1000 sec. For the case of argon/ethane (50/50), which has a heat capacity of about 40 J/mol-K, this volume will experience a temperature rise of:

$$(1\ mW)(1000\ sec)/((40\ J/mol\text{-}K)(2.4 \times 10^{-6}\ mol)) = 10^4\ °K$$

temperature rise is inconveniently large: average linear gas velocities of several centimeters per second are needed to achieve the assumed 6°C maximum allowable temperature rise. We note, however, that even at these velocites, the Reynolds number is on the order of ten, far below the values corresponding to turbulent flow [21], suggesting that uniform heat distribution would not be achieved.

There are, however, other mechanisms by which heat can be removed, namely radiation and conduction. At the small temperature increase allowable for acceptable operation, radiant heat transfer is negligible. This is not the case, however, for conduction.

The heat, Q, transferred by conduction between concentric cylinders is given by

$$Q = 2\pi L k \Delta T / [\ln(r_2/r_1)], \qquad (1)$$

where L is the length of the cylinders, k is the thermal conductivity of the medium between the cylinders, ΔT is the temperature difference between the cylinders, and r_2 and r_1 are the radii of the outer and inner cylinders, respectively. For the above-mentioned example of the 4 mm-diameter straw tube with the 33 μm-diameter wire, a temperature difference of only about 0.1°C is needed to conduct all of the heat from the wire to the wall through an argon/ethane (50/50) gas mixture. A smaller temperature difference is needed to conduct the heat from the wall into a surrounding gas environment.

For the purpose of investigating the heat transfer mechanisms in detail, we used a straw tube of the above-mentioned design with a 33 μm-diameter carbon anode wire through which current was passed to produce ohmic heating, and in this fashion to simulate the heat produced in a tube in a high-radiation environment. We believe this method simulates closely the gas heating near the surface of the

function of temperature. To estimate the temperature, we used the coefficient for carbon resistance as a function of temperature [22]. Fig. 4 shows the estimate of the anode wire temperature as a function of voltage across the wire. A similar method was previously used to estimate the surface temperature of 7-μm-diameter carbon wires [23].

A second method of estimating the temperature near the wire surface was measurement of the gain increase observed in the pulse-height spectrum of ^{55}Fe when the wire was heated. The dependence of gain on temperature has been well established from ambient pressure and temperature changes during many wire aging tests performed with this system.

A third method of determining the wire temperature follows from an analysis of the heat transfer. Estimates show that all except one of the potential channels for heat flow are small enough to be neglected: conduction through the gas along the radial direction between the anode and the cathode dominates the heat flow. With this simplification, an estimate of the temperature change is obtained directly from the conduction equation (eqn. 1), using the known heat input to the wire.

Measurements of the temperature were made using all three methods, by varying the battery voltage up to about 100 V. Two specific cases, 9 V and 46 V, are summarized in Table 3. The agreement between the three methods for the 46 V case is good. In the 9 V case, there is considerable uncertainty in the measurement of resistivity at low voltage, due to the apparent non-linearity of the curve in this region (Fig. 4). Therefore, Table 3 does not include a value determined by this method for the 9 V case. Estimates, however, give a temperature value close to that found by the other two methods.

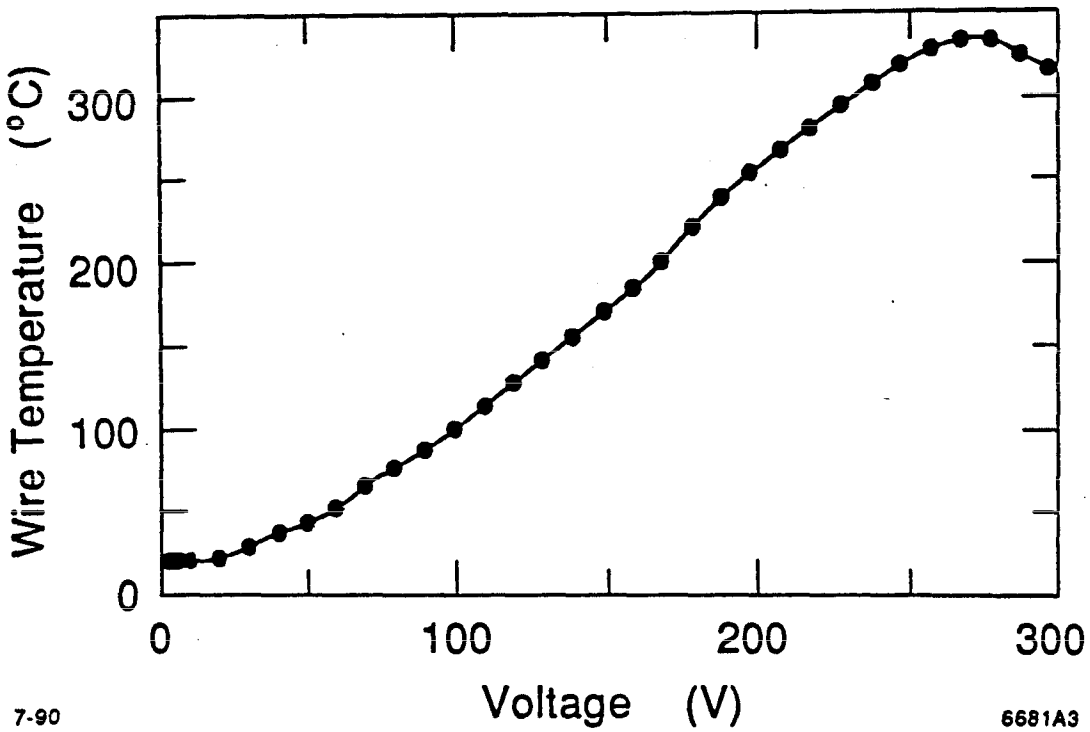

Fig. 4. Estimate of the carbon-wire anode temperature as a function of the applied voltage. The temperature dependence of carbon resistivity was taken to be -5×10^{-4}/°C [22]. The resistance of the wire was 9.24 kΩ at 21°C. The wire fails near 300°C in air.

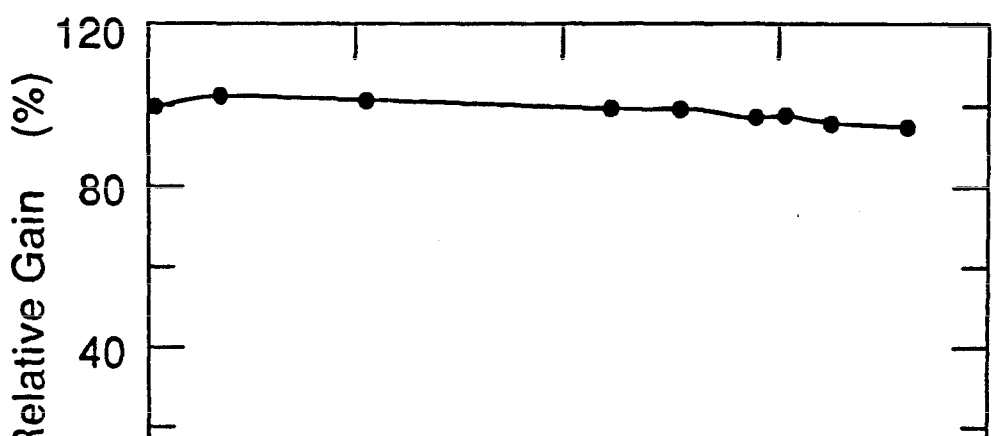

Table 3
Measurements of heating effects in straw tube with 33 μm diameter carbon filament anode: 9 V and 46 V cases. Temperature dependence of carbon resistivity: $(1/R_o)dR/dT = -5\times10^{-4}/°C$. The resistance of the filament was 9.24 kΩ at 21°C. The electrical length of the wire was 22.9 cm; the active length was 12.2 cm.

	9 V	46 V
Voltage across filament (V)	9.0	45.8
Current through filament (mA)	0.98	5.0
Resistance of filament (kΩ)	9.23	9.13
Power input (mW)	8.8	230
Power input to active region (mW)	4.7	123
Gas flow (cm^3/min)	20	18
^{55}Fe: Pulse-height of principal peak, pedestal subtracted (channel)		
Base case* (0 V)	400	376
With voltage applied	423	769
Gain ratio G(V)/G(0):	1.06	2.04
Computation of temperature rise (°C) (estimated error)		
From filament resistance (±10%)	—	43
From fractional gain change (±5%)	2.4	45
From power and radial conduction Eq. (±5%)	1.6	41

*The tests were made on different days, and the differences in the pulse heights of the base cases are due to barometric pressure changes.

The level of agreement between these two cases gives some confidence that this procedure can be extrapolated to the still lower power levels appropriate to an SSC experiment. In any event, even though the power corresponding to the 9 V case is ~60 mW/m, perhaps 100 times the maximum expected in normal SSC operation, the temperature rise is nevertheless sufficiently small to be

observed for flow rates of 1.5 to 120 cm^3/min, indicating that the gas temperature in the avalanche region is largely unaffected by the gas flow rate, as expected if radial conduction is the dominant heat transfer mechanism. Some change in the gain was observed for flow rates in the 120 to 150 cm^3/min range, however (Fig. 5). We believe that this was where the transport of heat by gas flow through the tube at higher flow rates began to compete with removal of heat by conduction radially.

Since conduction is the dominant heat transport mechanism, the gas flow rate is not dictated by heat removal, and can be as low as consistent with acceptable aging. We obtained good aging results with gas flows as low as ~1.0 cm^3/min, corresponding to an average linear gas velocity of only 1.3 mm/sec (Table 2).

For isolated straw tubes, conduction alone is sufficient to remove the heat from the tube wall; some convection is expected to be necessary to remove heat from an array of tubes such as in a full-scale detector. If tubes are arranged in layers with a small number of tubes per layer, as in some current designs [24], there will still be only negligibly small temperature rises within each layer according to our estimate, with heat being carried away efficiently by the gas between layers.

6. Conclusions

The simple prototype straw tube proportional counters described here were used for studies of aging and heating under conditions that are expected to be encountered at SSC experiments. Two major concerns investigated were the aging rates with several gases and the proportional gain fluctuations due to avalanche heating.

We have tested the aging of straw tubes having aluminum cathodes with several gases: argon/ethane (50/50) and

least one case (CF_4/DME), however, use of stainless steel tubing resulted in immediate electrical breakdown, which we believe to have been due to the lack of water vapor. All of the gases tested were found to give satisfactory aging rates. In addition, argon/ethane gave satisfatory aging with gas flow rates as low as 1.0 cm^3/min.

The investigation of heating effects used a 33 μm-diameter carbon anode wire to model the avalanche gas heating by ohmic heating from small electric currents. It was found that the heat transfer from the wire is essentially all by conduction through the gas along the radial direction. The recognition of this may simplify considerably the design of large straw-tube detectors.

The construction details of the straw tube prototype and the associated feedthroughs are also described.

Acknowledgements

We thank O. Millican for technical help with this project and J. Broeder for discussions and assistance.

References

[1] HRS: D. Rust, SLAC-PUB-3311 (1984).
MAC: W.W. Ash *et al.*, SLAC-PUB-4047 (1986), and *Nucl. Instr. and Meth.*, **A261** (1987) 399.
MARK II: W.T. Ford, *et al.*, *Nucl. Instr. and Meth.*, **A255** (1987) 486.
MARK III: J. Adler *et al.*, *Nucl. Instr. and Meth.*, **A276** (1989) 42.
TPC: (a) Proc. AIP Conference on Heavy Quark Physics, No. 196, Cornell Univ., Ithaca, NY (1989), p. 130, (b) M.T. Ronan *et al.*, *IEEE Trans. Nucl. Sci.*, **NS-35** (1988) 329.
KEDR: V.M. Aulchenko *et al.*, *Nucl. Instr. and Meth.*, **A283** (1989) 528.
CLEO: H. Kagan, to be published in Proc. Fifth International Conference on Instrumentation for Colliding Beam Physics, Novosibirsk, USSR, March 15-21, 1990.

[5] Registered trademark of E.I. DuPont de Nemours & Co., Inc.

[6] Bird Precision Jewels, Waltham, MA 02154, USA; p/n 24319.

[7] Avco Specialty Materials - Textron, Lowell, MA 01851, USA. This particular carbon wire is made of pure homogeneous glassy-phase carbon, and not from an acrylic fiber, which is more typical in the industry.

[8] Euclid Spiral Paper Tube, Applecreek, OH 44606, USA.

[9] H. Nelson, Reference 2, p. 131.

[10] G. Godfrey, private communication.

[11] Chomerics, Woburn, MA 01801, USA; p/n 50-02-0584-0029.

[12] 3M, St. Paul, MN 55144-1000, USA.

[13] J. Wise, J.A. Kadyk, D.W. Hess, and M.C. Williams, *IEEE Trans. Nucl. Sci.*, NS-37 (1990) 470.

[14] H.D. Morgan and J.E. Mentall, *J. Chem. Phys.*, 60 (1974) 4734.

[15] J. Va'vra, SLAC-PUB-5207 (1990).

[16] R. Openshaw *et al.*, *IEEE Trans. Nucl. Sci.*, NS-36 (1989) 567.

[17] (a) T. Yamashita *et al.*, *Nucl. Instr. and Meth.*, A283 (1989) 709, (b) L.G. Christophorou *et al.*, *Nucl. Instr. and Meth.*, 163 (1979) 141.

[18] B. Schmidt, HD-PY/86/06, Univ. of Heidelberg.

[19] J. Fehlmann and G. Viertel, Compliation of Data for Drift Chamber Operation, ETH Zurich (August 1983).

[20] J. Kadyk, J. Wise, D. Hess, and M. Williams, *IEEE Trans. Nucl. Sci.*, NS-37 (1990) 478.

[21] R.B. Bird, W.E. Stewart, and E.N. Lightfoot, Transport Phenomena (Wiley, New York, 1960), p. 54.

LBL 21633

ANODE WIRE AGING TESTS WITH SELECTED GASES*

J. Kadyk

Lawrence Berkeley Laboratory, Berkeley, California

and

J. Wise, D. Hess, M. Williams

University of California, Berkeley, and Lawrence Berkeley Laboratory

Abstract

As a continuation of earlier wire aging investigations, additional candidates for wire chamber gas and wire have been tested. These include the gases: argon/ethane, HRS gas, dimethyl ether, carbon dioxide/ethane, and carbon tetrafluoride/isobutane. Wires used were: gold-plated tungsten, Stablohm, Nicotin, and Stainless Steel. Measurements were made of the effects upon wire aging of impurities from plumbing materials, or contamination from various types of oil. Attempts were made to induce wire aging by adding measured amounts of oxygen and halogen (methyl chloride) with negative results. Finally, the possible role of electronegativity in the wire aging process is discussed, and measurements of electronegativity are made with several single carbon Freons, using both an electron capture detector and a wire chamber operating with dimethyl ether.

I. Introduction

Wire chambers are in common use for particle detection and tracking and yet the aging effects due to radiation are only partially understood. In the field of high energy physics, a very large wire chamber ($\sim 10^4$ - 10^5 wires) is normally a component of the experimental detector, and the demands on wire chambers are becoming increasingly severe, due to operation at higher gains and in more intense radiation environments.

Effects of radiation damage to wire chambers have been published both in terms of observations and experiences in actual experiments, and also as systematic laboratory aging tests done to prove the robustness against aging of specific wire chamber conditions. A summary of principal results

II. Procedures and Techniques

Since earlier results were reported,[2] a variety of improvements in techniques and procedures have been made. Perhaps the most important of these is the appreciation of the aging associated with even small amounts of certain gas contaminants. These may be already present in the supply gas, or be introduced into the gas stream through desorption from the materials in contact with the gas, such as the supply gas container, the plumbing system, or the wire chamber itself. Therefore, care was exercised in the selection and/or cleaning of components in contact with the gas, and in the purity of the source gas. In the case of dimethyl ether (DME) gas, it was found that poor results were obtained with any of several types of plastic upstream of the wire chamber under test, even in the form of a small plastic valve seal. For this reason, recent tests on DME were done with only certain metals upstream (e.g., electropolished stainless steel, hydrogen-fired copper), which required careful selection and, in the case of the control of gas flow, we used a valve of our own design and construction.[3]

The aging tests were done with proportional tube wire chambers of two varieties. The earlier tests used aluminum tubes, each of which was used for only one test; later tests used the copper tube shown in Figure 1, and these tubes are cleaned and rebuilt for each subsequent test. The reason for changing to a copper tube was the rather high rate of electrical breakdown failures encountered with aluminum tubes. This failure mode may be associated with the insulating property of aluminum oxide on the cathode wall inducing a self-sustained current by a mechanism similar to the well-known Malter dis-

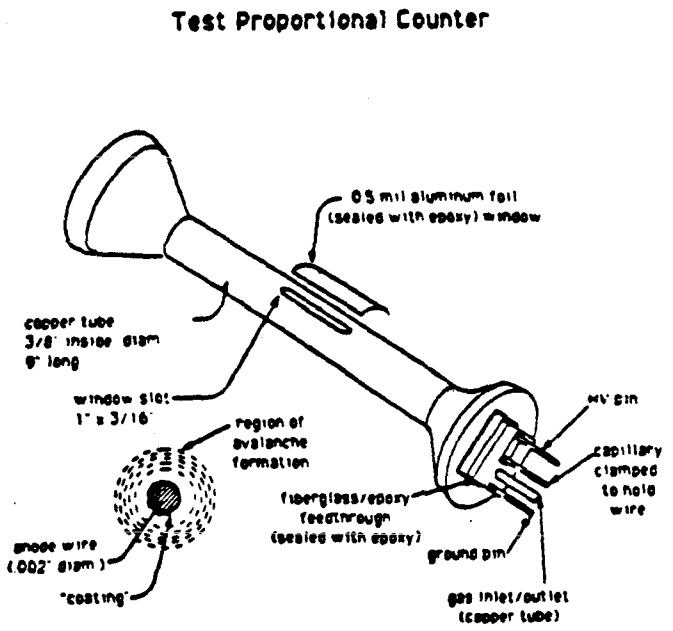

Fig. 1: Sketch of a copper tube used for anode wire lifetime tests, with a simple representation of wire cross-section and coating from deposits, and equipotential lines. Wire diameters are typically fifty microns. Aluminum tubes used in early tests were of rectangular cross-section, but otherwise similar in concept to the one pictured here.

The testing and analysis system is shown schematically in Figure 2. There are four independent test systems (of which two are shown in Figure 2), and each system has its own monitors of high voltage, current, temperature and gas flow. All gases exhaust at atmospheric pressure, and a single precision barometer, Setra model 270, monitors this pressure. All currents are digitized by Keithley 485 autoranging digital picoammeters. All other monitors are scanned sequentially by a Hewlett-Packard 3495A scanner and digitized by a Keithley 196 digital multimeter. Communications between the IBM PC/AT computer and the digital meters is via an IEEE 488 bus. Data are recorded on hard disks.

Programs controlling data retrieval, graphing and analysis were written specifically for this system, in FORTRAN (Microsoft,

only a very small pressure change at the small flow rate used, about 20 cc/min. A permeation device (Model 570-C Generator, Kintek Precision Gas Standards) is available to introduce metered amounts of known contaminants in order to determine their effect on the aging rate.

Usually the tests were performed with initial current densities of about 0.3 or 0.6 μA/cm, corresponding to currents of about 200 or 400 nA over a wire length of a few mm, depending on the type of test counter [6]. Small Fe^{55} sources of several hundred microcuries strength, placed close to the window, were used to irradiate the counter. Test runs usually accumulated at least several tenths of coulombs/cm, and have collected up to 2 C/cm. Gains are known only approximately, and are about 20,000 - 50,000. All tests were performed with a gas flow rate of approximately 20cc/min.

III. Aging Test Results

A. *Parameterization of Aging Tests*

Recent results are summarized in Table I, along with three tests previously published[2] with different types of plastic tubing upstream. The parameterization of gain loss is fractional gain loss per coulomb/cm of collected charge:

$$-(1/Q)\ dG/G \quad (\%/C/cm)$$

Gain loss can be caused by deposits (e.g., polymers condensed from the avalanche plasma), that function by increasing the diameter of the anode wire or by forming an insulating coating on the wire, or both. In either case, the surface electric field is decreased, reducing the gain. There is positive evidence for each of these effects. Another mechanism for gain loss is chemical attack of the wire surface by the gas (or species in the plasma) causing, for example, oxidation of some active elements in the wire material: this is only a problem for wires that are not gold-plated. The other important effect of aging is self-sustained current discharge, or Malter breakdown, which has not been investigated explicitly here, but is seldom a limiting factor in the present tests.

B. *Results*

The aging test results will be discussed according to the type of gas or gas mixture used. Plots of recorded current vs. collected charge for various tests are shown in Figure 3.

1. Dimethyl Ether

This gas has a quite low diffusion constant and high linear ionization density which makes it an excellent choice for high resolution drift chambers, e.g., vertex detectors. In some tests using DME, no measurable aging could be found, while in other tests, very poor aging results were obtained. [2,7,8] The differences in these results can be attributed to contaminants at

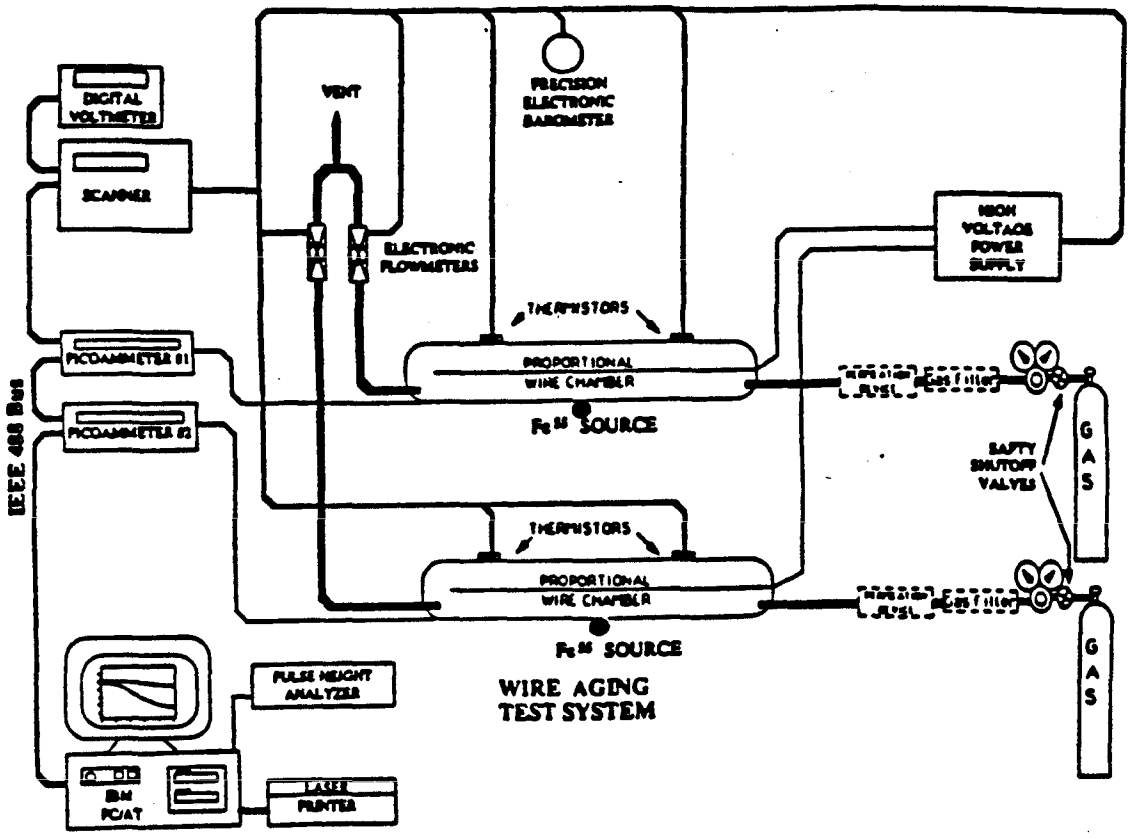

Fig. 2: Schematic of the wire aging test system. The system has recently been expanded from two to four independent test channels.

and needle valves (see e.g., Fig. 3a). For the last two DME results listed, and shown in Fig. 3b all plastics were eliminated on the upstream side by removing the pressure regulator and by constructing our own "needle valve" entirely from stainless steel tubing [3]. These two results using resistive [10] wire indicate that wire chamber operation with negligible aging can be achieved with DME, even if the wire is not gold-plated, when the gas plumbing system is rigorously clean and inert and free from contamination originating in commercial plastic components. The tests were done without the use of any filter ahead of the wire chamber.

2. Argon/Ethane (50/50)

This gas mixture is very popular because of its good properties of drift velocity saturation, good quenching and relatively high gain. However, there have been many reports of rapid wire the purity grade of gas is only moderately high (Matheson HP grade), and conventional gas regulators, needle valves, and plastic tubing (nylon) were used upstream of the test counter. However, such results may well depend upon the operating gain and geometry of the wire chamber.

3. Argon/Carbon Dioxide/Methane (89/10/1)

The presence of carbon dioxide in this gas ("HRS" gas) may be responsible for the moderate aging observed with Stablohm[10] resistive wire, perhaps due to surface oxidation, while negligible aging is found with gold-plated wire (Fig. 3a).

4. Carbon Dioxide/Ethane (95/5)

The large fraction of carbon dioxide in this gas contributes to the good spatial resolution obtained (low electron diffusion) in drift chamber operation. However, there does not seem to be much degradation of the resistive wires tested here (cf. with 3.

cm/μsec; (3) the ionization density along a minimum ionizing particle track is high (>200/cm total ion pairs); (4) the diffusion constant is low. These are the properties one would seek for operating a high resolution wire chamber ("vertex detector") near the beam pipe in a high luminosity collider (e.g., the proposed Superconducting Supercollider). The test result shown in Table I and Fig. 3c is a confirmation of the original tests at TRIUMF[14], although at smaller collected charge and somewhat lower gain.

6. Isopropanol Additive with Resistive Wire

As indicated in 2 above, additives of ethanol (~1.5%) or water (~1000 ppm) are known to be effective in suppressing wire aging, using gold-plated wires. Subsequently it was found that such a technique does not work with certain resistive wires (e.g., Stablohm),[13] apparently due to chemical action by these additives on certain constituents in the wire.[5] However, a substitute additive was found which does appear to inhibit aging even on resistive wire,[5] and the present result is a confirmation: negligible aging was observed on Stablohm 800 wire with 0.7% isopropanol added to the argon/ethane gas mixture by bubbling.

7. Tests of Gas Tubing.

The next six tests are directed at a partial understanding of the effects of potential contaminants introduced into the gas stream by outgassing from plumbing components: tubing, regulators, valves, etc. Three types of commonly used plastic tubing, 20m long, one tubing for each test, have been introduced upstream of the test chamber in an otherwise clean plumbing system and the aging measured using an argon/ethane (50/50) gas mixture. This result has been published previously[2] but is included here because the results may be compared with analyses using gas chromatographic techniques (in accompanying paper). As can be seen from Table I, there was very little aging observed for any of the three tubings. What is not apparent from these results is that several subsequent tests attempted on the same plumbing system in which the PVC tubing had been used, and then removed, all failed due to Malter breakdown (self-sustaining currents), a phenomenon which did not occur on a different plumbing system where the other plastic tubings (nylon, polyethylene) had been tested. Evidently, the PVC had introduced some pernicious contaminants into the adjacent (probably downstream) plumbing which interrupted later testing even though the original PVC tubing had been removed. A similar test was done earlier by Kotthaus, but with rather different results.[12] There, a substantial rate of gain loss was observed, ~140%/C/cm, when 10m of PVC tubing was inserted, and a

8. Effects of Oil Vapors

Sources of contamination often implicated in wire aging a oils or greases not rigorously excluded from the gas system. they are present as mold release agents, and as lubricants in pump systems, seals, etc. A simple set of tests was done to test the effects of three commonly-used oils: 1) a silicone diffusion pump oil (Dow 704), a mineral oil (Squibb), and a mechanical pump oil (Duo-Seal). For each test, the argon/ethane was bubbled into a column of oil through a gas dispersion element to saturate completely the gas (at room temperature) with oil vapor; then this gas was fed directly into the test chamber. Only in the case of the silicone oil was any significant aging observed and in this case it was moderate. However, the vapor pressure of this oil at room temperature is only 1.4×10^{-8} torr, resulting in a very low concentration in the gas (~18 ppb). That moderate aging can occur at such low levels of contamination is of interest, since silicon has been strongly implicated in anode wire coatings, even when a source of the silicon could not be readily identified.[1]

9. Attempts to Induce Aging

As part of a program to understand causes of wire aging, certain contaminants have been added to the argon/ethane (50/50) gas mixture to induce aging. Two of these result are listed in Table I. Using the permeation device mentioned earlier, small quantities of methyl chloride were added in one test, and oxygen in another test (Fig. 4). The first test was motivated by the suspicion that chlorine-containing compounds may be involved in aging processes, and the second test by some reports of aging when the gas system is not leak-free. As can be seen, no significant gain loss v observed in either case. However, in the case of meu chloride, a series of upward current "spikes" was observed in the latter part of the tests. This phenomenon is not understood at present, and may result from electrode coating.

IV. Electronegativity of Gases

Gas molecules can vary greatly in their propensity to capture electrons and become negative ions. Because of the possibility that negative ions may concentrate near the anode wire where the plasma is most concentrated, some simple measurements were made to establish the scale of such an effect.

A. *Relative Measurements of Electron Attachment Using an ECD*

Using an electron capture detector (ECD) coupled to the gas chromatograph, the relative signal due to electron capture in the ECD was measured for six common single-carbon (methyl) Freons, and the results are given in Table II. It is interesting

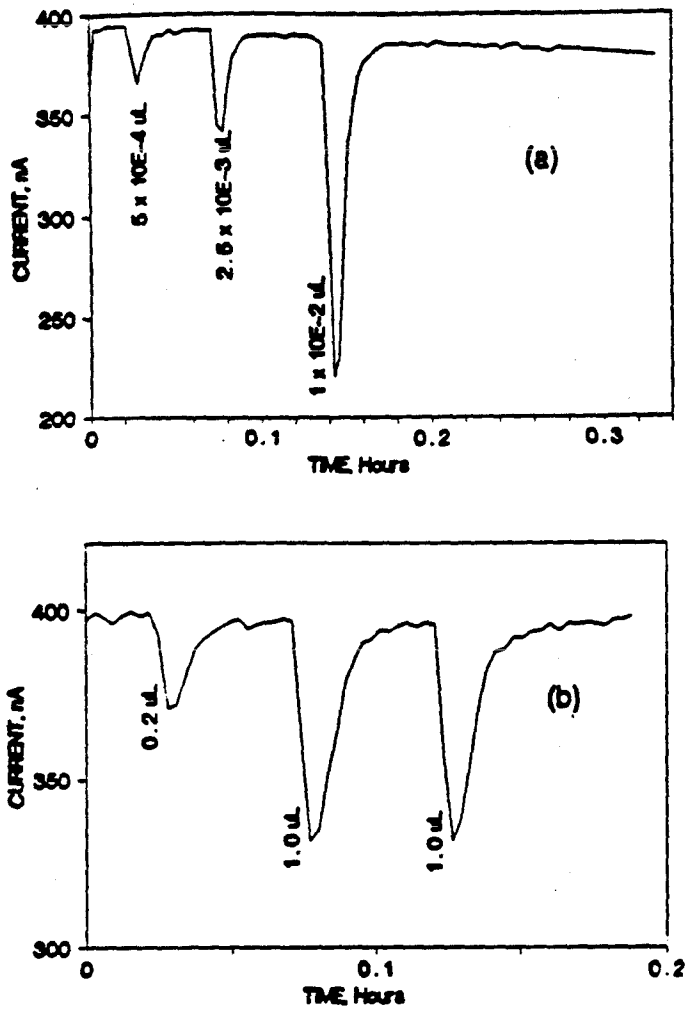

Fig. 5: Response to injections of Freons into the DME gas stream just ahead of a copper test chamber. (a) 50μL, 250μL, and 1000μL injections of Freon 11 diluted to 10 ppm in helium; (b) 100μL and 500μL injections of Freon 12 diluted to 2000 ppm in helium. The equivalent amounts of pure (undiluted) Freon gas injected are noted on each graph next to the corresponding dip in current.

V. Conclusions

Some new candidates for wire chamber gases have been tested under laboratory conditions, with control and monitoring of purity, materials, plumbing, etc., and some previously known gases have been more thoroughly investigated. Special emphasis has been given to the testing of very pure dimethyl ether (DME), and the conditions necessary to maintain good aging stability. It is found that this gas appears to be extraordinarily sensitive to materials in the gas stream, especially to certain plastics. However, with sufficient precautions, very good stability against aging was found with the resistive wires Stablohm and Nicotin. Another, newer, gas that appears to be promising for future, more demanding operation, is CF_4/iC_4H_{10} (80/20). This gas has been tested at TRIUMF, and confirmed here to have excellent aging properties, to quite high levels of collected charge/wire length. It also has the advantages of high drift velocity, high linear ionization density, and low diffusion. Another gas exhibiting good aging and low diffusion, and perhaps less sensitive to contaminants than DME is CO_2/C_2H_6 (95/5). Also tested are conventional gases Ar/C_2H_6 (50/50) and $Ar/CO_2/CH_4$ (89/10/1), which have negligible anode aging when used with gold-plated wire. However, the latter gas seems to attack somewhat the resistive wire Stablohm.

An investigation of three types of oil vapors showed that only silicone oil caused any appreciable aging, but that was at a concentration of ~ 18 ppb! Studies were made of various types of tubing commonly used for gas plumbing or implicated in bad results. In one study, nylon, polyethylene and polyvinyl chloride (PVC) tubings were tested, and only the PVC tubing exhibited aging effects. In that case the aging was not in the form of gain loss, but rather sustained current breakdowns experienced in subsequent tests using the same plumbing system which was exposed to the PVC, even though the PVC tubing itself had been removed.

The response of an electron capture detector (ECD) to six Freons showed a very wide range of electron attachment cross-sections, by a factor of more than 10^6, under the conditions of the ECD operation. Test injections of two Freons in a DME gas stream confirmed qualitatively the ECD results; however, no induced aging was observed from this brief exposure. The possible role of electronegative components in anode wire aging was examined. Further study is needed to establish (or disprove) any connection between electronegativity and potential mechanisms of wire aging.

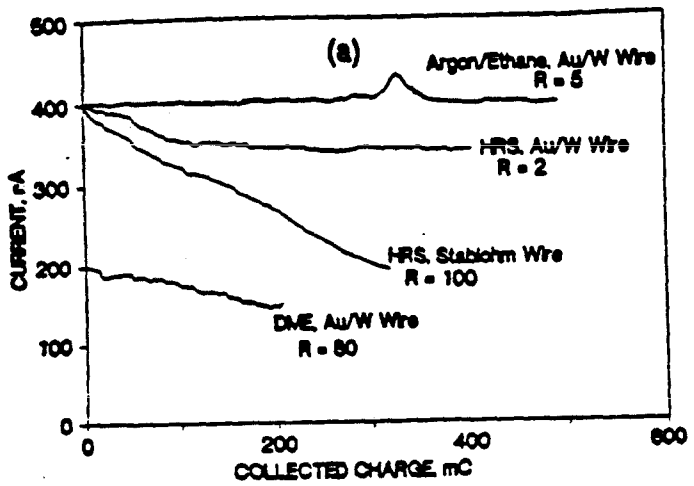

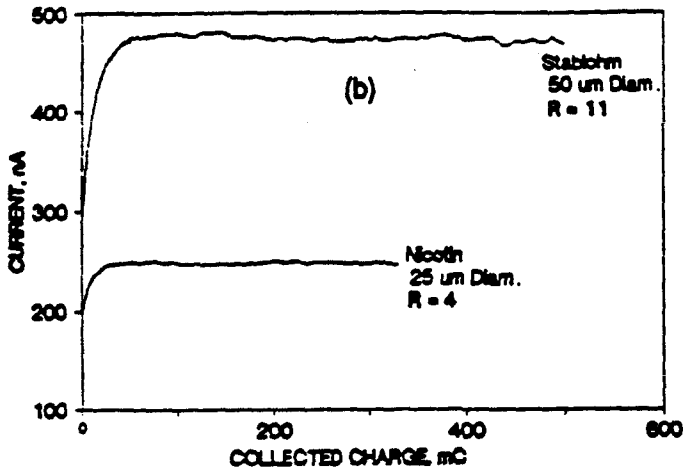

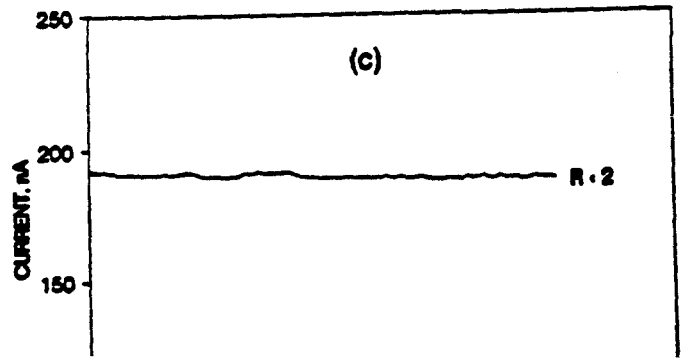

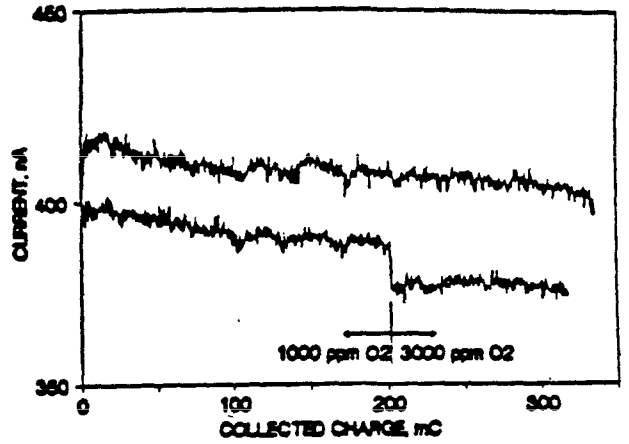

Fig. 4: Plot of current vs. collected charge for aging test, using a permeation device to add oxygen to the argon/ethane (50/50) gas flow, in the amounts 1000 ppm and 3000 ppm, as indicated on the lower curve. The upper curve shows current in a control test in which the same argon/ethane gas was used, but without oxygen being added. A slight aging is observed in both tests and the electronegativity of oxygen results in a slight drop in gain, but no effect of aging due to addition of oxygen is apparent.

DME may be due to a progressively larger amount of Freon in the gas as the DME "distills" from the gas cylinder, leaving behind an increasingly larger concentration of the Freon 11 contaminant. Of course, the relative signal responses in a wire chamber may be different than measured with an ECD, hence the test described below in B. was done.

B. *Test Chamber Response to Freon Injection Into Gas Supply*

Small injections of Freons 11 and 12 were made through a septum just upstream of a test chamber operating on DME. The response is shown in Figure 5 (a) and (b) for the two different Freons, and the peak amplitude of response is indicated in Table II. Again, there is a larger response observed for Freon 11, but not by the factor seen using the ECD. In each case, the current appeared to fully recover, indicating no aging effects due to such a short exposure to Freons.

C. *Discussion*

The large cross-section for electron capture of certain molecules, e.g. those containing halogens, may have a

Table I: Aging Test Results

Gas	Approx Gain Loss $-(1/Q)dG/G$ (%)/C/cm	Approx Charge Collected (C/cm)	Approx Gain	Approx Anode Current Density (μA/cm)	Anode Wire Diameter (μm)	Wire Surface Material	Comment
Dimethyl Ether (DME) (<1ppm of Freon 11)	120	0.1	5×10^4	0.3	50	Au	Nylon tubing
	80	0.2	5×10^4	0.3	50	Au	Polyethylene tubing
	80	0.3	5×10^4	0.6	50	Au	Stainless steel tubing
	170	0.1	5×10^4	0.6	50	Stablohm	
	11	0.6	5×10^4	0.4	50	Stablohm	Semiconductor grade DME, all inert metal plumbing. Epoxy seals.
	4	0.6	5×10^4	0.4	25	Nicotin	
Ar/C_2H_6 (50/50) HP Grade Ar*	<5	2.0	2×10^4	0.6	50	Au	
$Ar/CO_2/CH_4$ (89/10/1) (HRS gas)	2	0.3	2×10^4	0.6	50	Au	
	100	0.5	2×10^4	0.6	50	Stablohm	
CO_2/C_2H_6 (95/5)	46	0.1	5×10^4	0.3	25	Stainless Steel	
	36	0.4	5×10^4	0.3	25	Nicotin	
+0.5% iC_3H_7OH	97	0.08	5×10^4	0.3	25	Stainless Steel	Gas Bubbled Through iC_3H_7OH
	102	0.3	5×10^4	0.3	25	Nicotin	
CF_4/Isobutane (80/20)	<2	1.2	2×10^4	0.3	50	Au	
Ar/C_2H_6 (50/50)	<10	0.4	2×10^4	0.6	50	Stablohm	

Table I: Aging Test Results (continued)

Gas	Approx Gain Loss -(1/G)dG/G (%)/C/cm	Approx Charge Collected (C/cm)	Approx Gain	Approx Anode Current Density (μA/cm)	Anode Wire Diameter (μm)	Wire Surface Material	Comment
Ar/C_2H_6 (50/50) HP Grade Ar*							
+Silicone Oil (Dow 704)	-50	0.15	2×10^4	0.6	50	Au	Gas bubbled through oil
+Mineral Oil (Squib)	2	0.15	2×10^4	0.6	50	Au	
+Mech. Pump Oil (Duo-Seal)	1	0.18	2×10^4	0.6	50	Au	
Ar/C_2H_6 (50/50) +530 ppm CH_3Cl	7	0.4	2×10^4	0.6	50	Au	Gas bubbled through CH_3Cl
Ar/C_2H_6							
+1000 ppm O_2	14	0.3	2×10^4	0.6	50	Au	
+3000 ppm O_2	2	0.2	2×10^4	0.6	50	Au	

*Gases obtained from Matheson Gas Products. There are several grades of argon available. Grades used here are (highest to lowest purity): Matheson grade, Ultra High Purity (UHP), Prepurified (PREP), and High Purity (HP).

Table II: Effects of Methyl Halogens (Freons)

Equal volumes of Gas (Or Vapor) Injected Into ECD
or Into DME Gas Stream

Name	Formula	-Response- DME (% /mL)	ECD (normalized to CF_4)
Carbon Tetrachloride	CCl_4	---	200,000

Table I: Aging Test Results

Gas	Approx Gain Loss -(1/Q)dG/G (%)/C/cm	Approx Charge Collected (C/cm)	Approx Gain	Approx Anode Current Density (μA/cm)	Anode Wire Diameter (μm)	Wire Surface Material	Comment
Dimethyl Ether (DME)	120	0.1	$5x10^4$	0.3	50	Au	Nylon tubing
	80	0.2	$5x10^4$	0.3	50	Au	Polyethylene tubing
(<1ppm of Freon 11)	80	0.3	$5x10^4$	0.6	50	Au	Stainless steel tubing
	170	0.1	$5x10^4$	0.6	50	Stablohm	
	11	0.6	$5x10^4$	0.4	50	Stablohm	Semiconductor grade DME, all inert metal plumbing. Epoxy seals.
	4	0.6	$5x10^4$	0.4	25	Nicotin	
Ar/C_2H_6 (50/50) HP Grade Ar*	<5	2.0	$2x10^4$	0.6	50	Au	
$Ar/CO_2/CH_4$ (89/10/1) (HRS gas)	2	0.3	$2x10^4$	0.6	50	Au	
	100	0.5	$2x10^4$	0.6	50	Stablohm	
CO_2/C_2H_6 (95/5)	46	0.1	$5x10^4$	0.3	25	Stainless Steel	
	36	0.4	$5x10^4$	0.3	25	Nicotin	
$+0.5\% iC_3H_7OH$	97	0.08	$5x10^4$	0.3	25	Stainless Steel	Gas Bubbled Through iC_3H_7OH
	102	0.3	$5x10^4$	0.3	25	Nicotin	
CF_4/Isobutane (80/20)	<2	1.2	$2x10^4$	0.3	50	Au	
Ar/C_2H_6 (50/50) $+0.7\% iC_3H_7OH$	<10	0.4	$2x10^4$	0.6	50	Stablohm	

Acknowledgements

It is a pleasure to acknowledge the support of Physics Division directors George Trilling, who recognized the importance of beginning a program to study wire aging, and Pier Oddone, who has continued the interest and encouragement so essential to the program. Our many mechanical needs and problems have been superbly managed by Doug Shigley, whose original idea for a completely inert flow control valve has solved a major difficulty. Thanks also to Ron Jones who has helped with the electronics and programming aspects of the project, and to Ketan Desai, who first set up the computer data retrieval system. Thanks go also to Stan Majewski, University of Florida, and Jaroslav Va'vra, Stanford Linear Accelerator Center, for their helpful advice and interest in the project.

References

1. Proceedings of the Workshop on Radiation Damage to Wire Chambers, Lawrence Berkeley Laboratory, April 1986; LBL 21170.

2. I. Juricic and J. Kadyk, IEEE Tran. on Nucl. Sci., Vol. NS-34, No. 1, (1987) 481.

3. A simple "needle valve" for control of gas flows was devised and constructed by Douglas Shigley. It is made entirely of electropolished stainless steel, operates over a wide range of gas flows and is quite stable in operation.

4. L. Malter, Phys. Rev. 50, 48 (1936).

5. M. Atac, IEEE Trans. on Nucl. Sci., Vol. NS-34, No. 1, (1987) 476.

6. The irradiated length of wire is not well known. It has been taken to be 6 mm for the aluminum tube and 3 mm for the copper tube, based on some visual estimates of coatings.

7. M. Jibaly, et al., IEEE Trans. on Nucl. Sci., Vol. 36, No. 1, (1989) 552; M. Jibaly, et al., NIM A273, (1988) 161.

8. G. Bari, et al., CERN-EP/86-56 (1986).

9. J. Adler, et al., SLAC-PUB-4578 (1988).

10. Stabilohm 800 wire used here consists of 75% nickel

12. For example, R. Kotthaus, ref. 1, pp. 161-193; other examples of water as an additive may be found in reference 1.

13. I. Juricic and J. Kadyk, ref. 1, pp. 141-151.

14. R. Openshaw, et al., IEEE Trans. on Nucl. Sci., Vol. 36, No. 1, (1989) 567.

15. H. Kobayashi, et al.; J. Macromol. Sci.-Chem. A8(8), 1345 (1974).

Ar/C_2H_6 (50/50) HP Grade Ar* +Silicone Oil Dow 704)	~50	0.15	$2x10^4$	0.6	50	Au	Gas bubbled through oil
Mineral Oil (Squibb)	2	0.15	$2x10^4$	0.6	50	Au	
+Mech. Pump Oil (Duo-Seal)	1	0.18	$2x10^4$	0.6	50	Au	
Silcone Oil (Dow 704)	43	0.4	$2x10^4$	1.2	50	Au	Repeat of result above
RTV (GE, 108)	~100	0.1	$4x10^4$	1.5	50	Au	
Ar/C_2H_6 (50/50) +530ppm CH_3Cl	7	0.4	$2x10^4$	0.6	50	Au	Gas Bubbled through CH_3Cl
Ar/C_2H_6 +1000 ppm O_2	14	0.3	$2x10^4$	0.6	50	Au	
+3000 ppmO_2	2	0.2	$2x10^4$	0.6	50	Au	
Ar/C_2H_6 (50/50) +1000 ppm H_2O	~30	0.4	$5x10^4$	0.6	38	Au	4 mm Dram. Straw Tube
CF_4/iC_4H_{10} (80/20)	10	0.2	$5x10^4$	0.6	38	Au	
F_4/DME (90/10)	3	0.7	$5x10^4$	0.6	38	Au	

* Gases obtained from Matheson Gas Products. There are several grades of argon available. Grades used here are (highest to lowest purity): Matheson grade, Ultra High Purity (UHP), Prepurified (PREP), and High Purity (HP).

Updated: Jan. 1970

Table I: Aging Test Results

Gas	Approx Gain Loss -(1/Q)dG/G (%)/C/cm	Approx Charge Collected (C/cm)	Approx Gain	Approx Anode Current Density (μA/cm)	Anode Wire Diameter (μm)	Wire Surface Material	Comment
Dimethyl Ether (DME)	120	0.1	5×10^4	0.3	50	Au	Nylon tubing
	80	0.2	5×10^4	0.3	50	Au	Polyethylene tubing
(<1ppm of Freon 11)	80	0.3	5×10^4	0.6	50	Au	Stainless steel tubing
	170	0.1	5×10^4	0.6	50	Stablohm	
	11	0.6	5×10^4	0.4	50	Stablohm	Semiconductor grade DME, all inert metal plumbing. Epoxy seals.
	4	0.6	5×10^4	0.4	25	Nicotin	
Ar/C_2H_6 (50/50) HP Grade Ar*	<5	2.0	2×10^4	0.6	50	Au	
$Ar/CO_2/CH_4$ (89/10/1) (HRS gas)	2	0.3	2×10^4	0.6	50	Au	
	100	0.5	2×10^4	0.6	50	Stablohm	
CO_2/C_2H_6 (95/5)	46	0.1	5×10^4	0.3	25	Stainless Steel	
	36	0.4	5×10^4	0.3	25	Nicotin	
+0.5% iC_3H_7OH	97	0.08	5×10^4	0.3	25	Stainless Steel	Gas Bubbled Through iC_3H_7OH
	102	0.3	5×10^4	0.3	25	Nicotin	
CF_4/Isobutane (80/20)	<2	1.2	2×10^4	0.3	50	Au	
Ar/C_2H_6 (50/50) +0.7% iC_3H_7OH Matheson and PREP	<10	0.4	2×10^4	0.6	50	Stablohm	

Ar/C_2H_6 (50/50) HP Grade Ar* +Silicone Oil (Dow 704)	~50	0.15	$2x10^4$	0.6	50	Au	Gas bubbled through oil
+Mineral Oil (Squibb)	2	0.15	$2x10^4$	0.6	50	Au	
+Mech. Pump Oil (Duo-Seal)	1	0.18	$2x10^4$	0.6	50	Au	
Silcone Oil (Dow 704)	43	0.4	$2x10^4$	1.2	50	Au	Repeat of result above
RTV (GE, 108)	~100	0.1	$4x10^4$	1.5	50	Au	
Ar/C_2H_6 (50/50) +530ppm CH_3Cl	7	0.4	$2x10^4$	0.6	50	Au	Gas Bubbled through CH_3Cl
Ar/C_2H_6 +1000 ppm O_2	14	0.3	$2x10^4$	0.6	50	Au	
+3000 ppmO_2	2	0.2	$2x10^4$	0.6	50	Au	
Ar/C_2H_6 (50/50) +1000 ppm H_2O	~30	0.4	$5x10^4$	0.6	38	Au	4 mm Dram. Straw Tube
CF_4/iC_4H_{10} (80/20)	10	0.2	$5x10^4$	0.6	38	Au	
CF_4/DME (90/10)	3	0.7	$5x10^4$	0.6	38	Au	

* Gases obtained from Matheson Gas Products. There are several grades of argon available. Grades used here are (highest to lowest purity): Matheson grade, Ultra High Purity (UHP), Prepurified (PREP), and High Purity (HP).

STUDY OF PLASMA CHEMISTRY IN WIRE CHAMBERS BY GC/MS†

J. Wise,[1,2] J. A. Kadyk,[1] D. W. Hess,[1,2] and M. C. Williams[1,2]

[1]Lawrence Berkeley Laboratory
University of California
Berkeley, CA 94720

[2]Department of Chemical Engineering
University of California
Berkeley, CA 94720

Abstract

We have constructed an apparatus to allow systematic and detailed study of radiation-induced plasma-chemical reactions that may lead to wire aging. A proportional counter tube irradiated by an ^{55}Fe source is used as a model wire chamber. Less-volatile components in the tube effluent gas are concentrated by several orders of magnitude in a cryotrap to provide the sensitivity needed for detection. Separation and analysis are performed by gas chromatography/mass spectrometry. A strong signal from many products formed in the avalanche by plasma-chemical reactions has been observed.

I. Introduction

To understand better the chemistry of plasma reactions thought to be responsible for aging processes in wire chambers, a system has been developed for detection and identification of trace components in gases. By correlating wire aging with the reaction products in the effluent gas of a wire chamber, modeled by a proportional counter tube, it is hoped that the dominant reactions responsible for wire aging can be identified, and appropriate measures taken to prevent polymer deposits in full-scale wire chambers.

II. Apparatus

The experimental apparatus consists of a Varian 3400 Gas Chromatograph and a Finnigan Ion Trap Mass Spectrometer, which are used to perform a gas chromatography/mass spectrometry (GC/MS) analysis of condensible species in a gas stream. Cryotrapping is used to isolate from the major gas stream a sample of trace species sufficiently large that detection and identification can be made. A sample is created by maintaining the

The cryotrap is a nickel tube 10 in. x 1/16 in. OD x 0.040 in. ID connected to a six-port, two-position sampling valve (Valco 6UWT), the "sample valve." A four-port, two-position valve (Valco 4T), the "purge valve," is used to select between two inlet streams: a helium purge stream and a sample stream (Fig. 1). The valves and all associated tubing are heated (150°C) to prevent both loss of the sample by adsorption and contamination of the sample by desorption of previous samples.

A cryotrapping cycle consists of five parts, starting with the valves in their standby positions (Fig. 1a). (1) The cryotrap is baked while under pure helium flow to remove residual impurities. (2) The cryotrap, still under helium flow, is cooled with liquid nitrogen and its temperature allowed to stabilize at the setpoint. Temperature control is achieved by computerized regulation of the coolant flow. (3) The purge valve is rotated (Fig. 1b), allowing a sample gas to flow through the cryotrap for a preset cryotrapping period. (4) At the end of the cryotrapping period, the purge valve is returned to its standby position (Fig. 1a), allowing helium to displace the remaining sample gas. (5) The sample valve is rotated (Fig. 1c), causing the cryotrap to be in the flowpath of carrier gas (helium) that enters the GC column. The cryotrap is electrically heated by passing a current through the nickel tube, thereby driving the previously condensed species into the carrier gas. These species are recondensed (focused) with a liquid nitrogen spray on an ~5 mm. column segment near the beginning of the GC column so that standard GC analysis techniques can be used. After the sample is transferred and focused, both valves are returned to their standby positions and the GC/MS analysis cycle is initiated. Operation of the entire system is under the control of two PC-AT computers: one to drive the cryotrapping/cryofocussing cycle and to

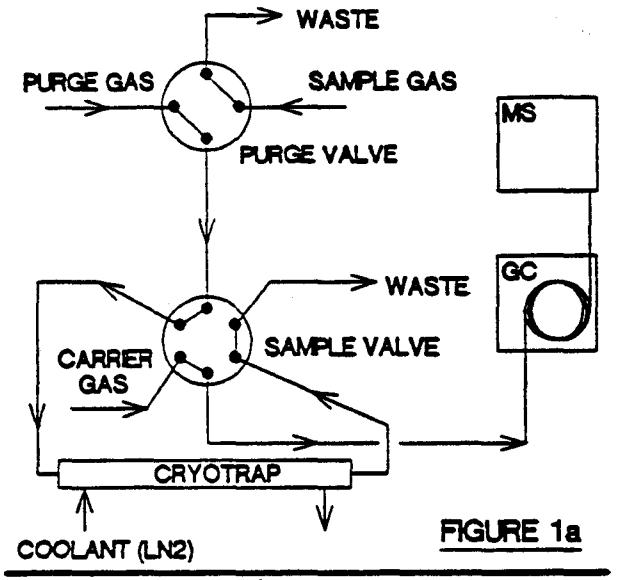

FIGURE 1a

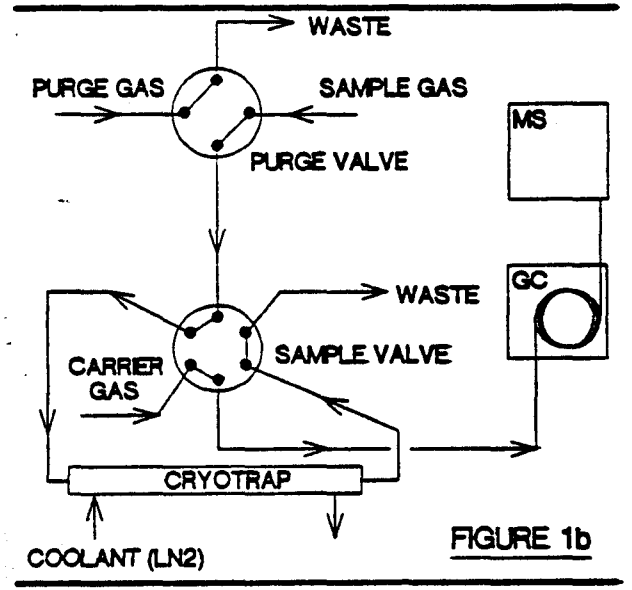

FIGURE 1b

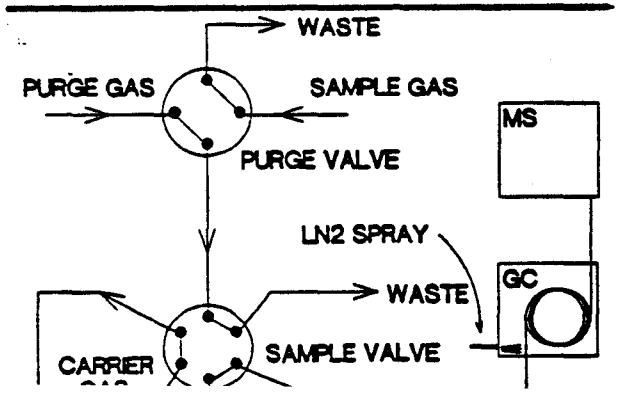

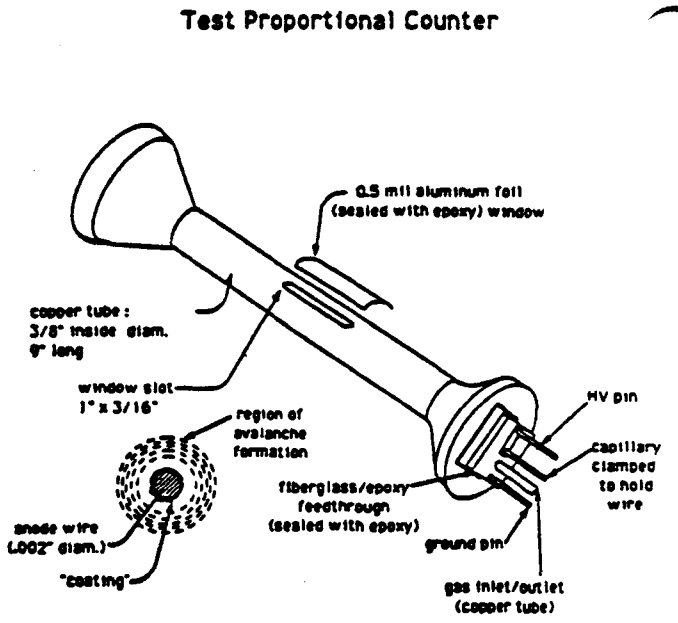

Fig. 2. Sketch of a copper tube and fittings used for anode wire lifetime tests; a simple representation of wire and coating, and equipotential lines.

chemical reactions thought to occur during typical wire chamber operation. A 50 micron diameter, gold-plated tungsten wire is used. Relevant parameters (current and voltage, and gas pressure, temperature and flowrate) of the tube under test are monitored to determine the aging rate and thus establish a correspondence between aging and the observed reaction products.

III. Calibration

The GC/MS system has a sensitivity on the order of 1 ng., and the cryotrapping system is estimated to concentrate samples by at least three orders of magnitude (by volume) over what could be introduced directly into the column. For alkanes with six to twelve carbon atoms, the system response, measured as the ratio of peak area to number of molecules, is roughly constant. For hydrocarbons with five or fewer carbon atoms, however, the response is about one order of magnitude lower when

IV. Analysis of Common Gas Plumbing Materials

A. *Analyses of Tubing Outgas Components*

Several different tubing materials have been analyzed for outgassed or desorbed vapors. Table II and Fig. 3 show results of these analyses. In all cases, the cryotrapping was performed at -70°C using helium (Matheson Grade, Matheson Gas Products, Inc.) flowing at 20 cc./minute for ten minutes. The GC temperature program was: hold the temperature at -50°C for three minutes, ramp to 250°C at 10°C/minute, and hold at 250°C for three minutes. The carrier gas pressure was 15 psig. A 30 m. by 0.25 mm. diameter J&W DB-5 capillary column was used.

The baseline test (Fig. 3a) was run using an 18 in. length of copper tubing, and shows some simple structures that are artifacts of the cryotrapping system, but no major peaks. To some extent, the tests of other tubings show trapped outgas components, most of which can be specifically or at least qualitatively identified. In most cases there is a significant "water peak," manifested by the structure in the chromatograms beginning near scan 1000, which corresponds to 0°C. This water peak can "mask" components that elute before ~scan 1200 (~20°C), resulting in lack of knowledge of quantity and chemical character of eluents in this region. Hygroscopic filters have been used to remove water vapor from the main gas, but they appear to have also removed some of the trapped components under investigation.

Fig. 3 and Table II clearly show quantitative and qualitative differences in the desorbed materials. Although water vapor was found in all other tubings, electropolished stainless steel tubing (Fig. 3a) is essentially free of any water (or other) outgassing. Nearly as clean is the copper refrigeration tubing (Fig. 3b), although water and, frequently, polynuclear aromatics are found. Among the plastic tubings, nylon and polyethylene are relatively clean, while many compounds, including some containing chlorine and fluorine, are observed in the samples from the PVC (Fig. 3c) and the Teflon tubings. It is interesting to note that the peaks observed for TFE Teflon (Fig. 3d) are principally, if not entirely, hydrocarbon in nature, while for PFA Teflon, there are many peaks associated with fluorinated compounds. As has been discussed [1], there may be sound reasons for implicating halogens in the mechanisms of gain loss and wire aging.

B. *Analyses of Other Materials*

Outgassing of silicone compounds from valve grease,

TABLE I. SYSTEM RESPONSE TO SOME CLASSES OF COMPOUNDS

COMPOUND	RESPONSE (PEAK AREA/NANOMOLE)
C_6 - C_7 alkanes	700,000
C_8 alkanes	1,300,000
C_{10} - C_{12} alkanes	1,000,000
halogenated methanes	100,000
methylal, acetone	100,000

chromatograms in which the sample gas was passed through the permeation device even though the Freon supply had been removed for many days. Although Freon 11 may or may not be directly implicated in wire aging [1], a similar situation could be envisioned for other contaminants that do cause aging. This suggests that some tubings may be easily and essentially irreversibly contaminated and that considerable care should be exercised in the selection of tubing and other materials in contact with the wire chamber gas.

V. Aspects of Plasma Chemistry

A. *Experimental Methods*

A proportional tube irradiated by a ten millicurie ^{55}Fe source six cm. long was used to produce samples of the products of plasma-chemical reactions, such as might be produced in an operating wire chamber. Such a tube is similar to the ones used for wire aging tests (Fig. 2), except that it is shorter (4.5 in.) and has a longer window to accommodate the ^{55}Fe line source. A 50/50 (volume basis) argon/ethane mixture (Matheson grade argon, CP grade ethane, Matheson Gas Products, Inc.) was used as the counter gas. Cryotrapping was performed at -70°C by flowing gas at 20 cc./minute for ten minutes. The GC temperature program was: hold the temperature at -50°C for three minutes, ramp to 250°C at 10°C/minute, and hold at 250°C for three minutes. The carrier gas pressure was 15 psig. A 30 m. by 0.25 mm. diameter J&W DB-5 capillary

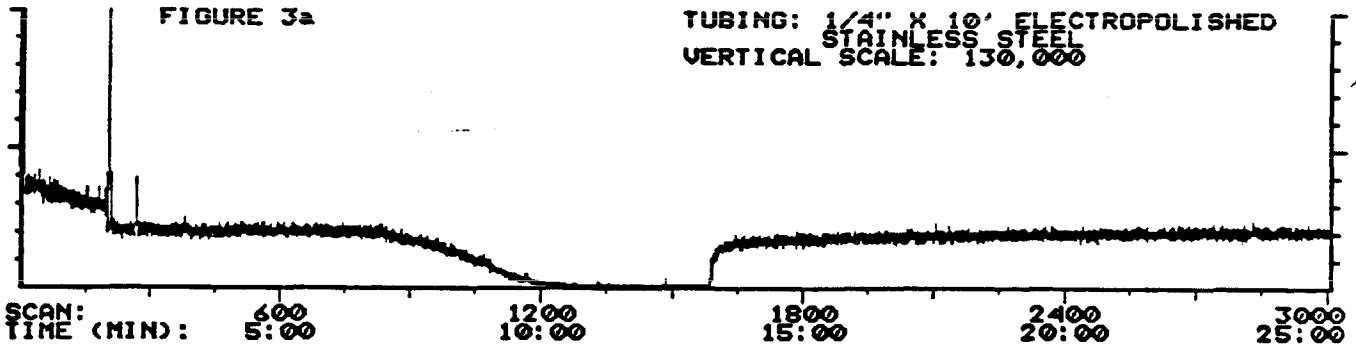
FIGURE 3a
TUBING: 1/4" X 10' ELECTROPOLISHED STAINLESS STEEL
VERTICAL SCALE: 130,000
SCAN: 600 1200 1800 2400 3000
TIME (MIN): 5:00 10:00 15:00 20:00 25:00

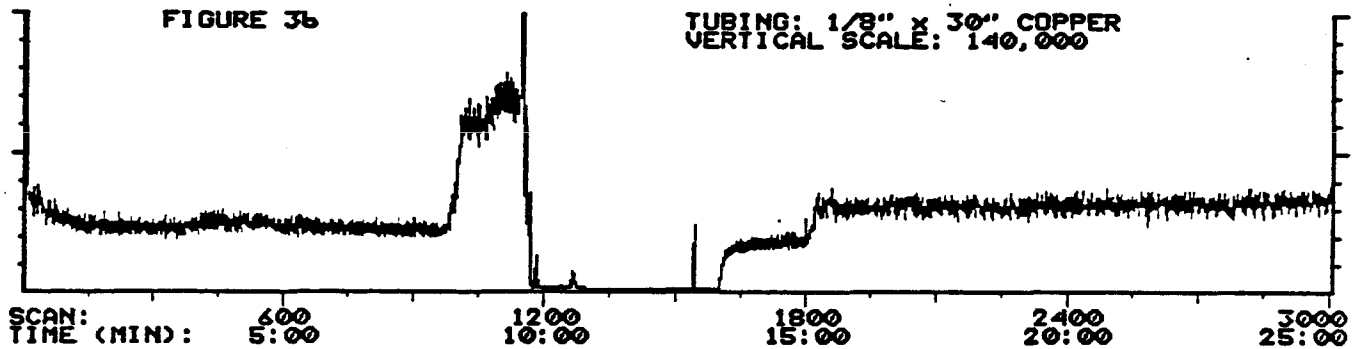
FIGURE 3b
TUBING: 1/8" x 30" COPPER
VERTICAL SCALE: 140,000
SCAN: 600 1200 1800 2400 3000
TIME (MIN): 5:00 10:00 15:00 20:00 25:00

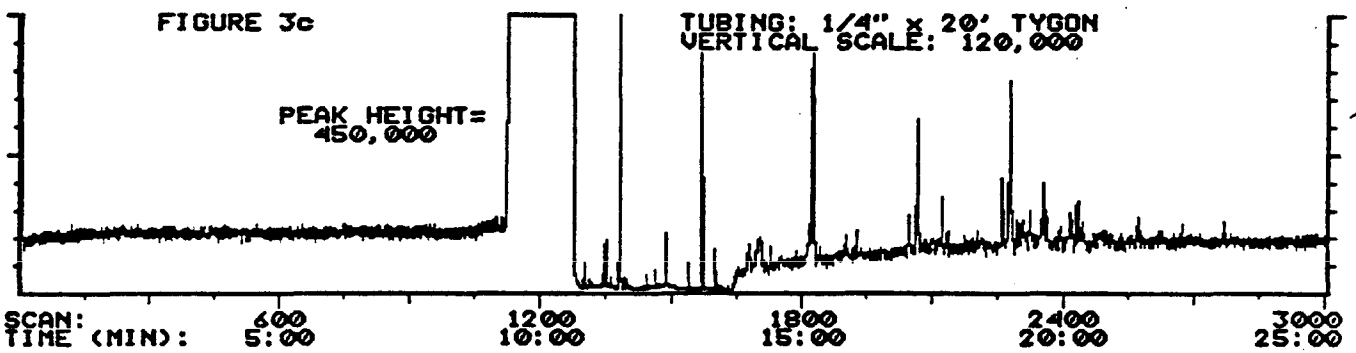
FIGURE 3c
TUBING: 1/4" x 20' TYGON
VERTICAL SCALE: 120,000
PEAK HEIGHT= 450,000
SCAN: 600 1200 1800 2400 3000
TIME (MIN): 5:00 10:00 15:00 20:00 25:00

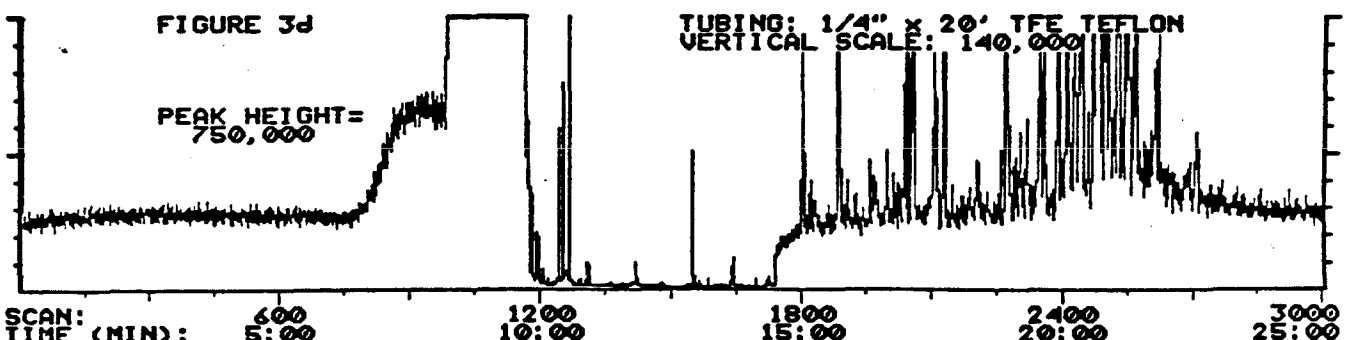
FIGURE 3d
TUBING: 1/4" x 20' TFE TEFLON
VERTICAL SCALE: 140,000
PEAK HEIGHT= 750,000
SCAN: 600 1200 1800 2400 3000
TIME (MIN): 5:00 10:00 15:00 20:00 25:00

TABLE II. TUBING OUTGAS COMPONENTS

Tubing outside diameters are 0.25 inch unless otherwise noted.

TYPE OF TUBING	LENGTH (ft)	TRAPPING TIME (min)	CHEMICAL CHARACTER OF TRAPPED EFFLUENTS
Electropolished Stainless Steel	10	20	Trace components only, no water
1/8" Copper Refrigeration tubing	10	10	Water, polynuclear aromatics
Nylon (Nylo-Seal)	10	10	Water
Polyethylene (Poly-flo)	10	10	Water, large alkanes, substituted aromatics
Polyvinyl chloride (Tygon)	10	10	Water, alkanes, polychlorinated alkanes and aromatics
Polyvinyl chloride (generic)	10	10	Water, alkanes, polychlorinated alkanes, substituted aromatics
Teflon (TFE)	12	20	Water, linear and branched alkanes
Teflon (PFA)	12	20	Water, fluorinated alkanes, small alkanes
Teflon (FEP)	12	20	Water, small alkanes

When the high voltage (~2300 v) was applied and the ^{55}Fe source was present, so that the tube was drawing ~6.0 μA, a multitude of peaks are seen (Fig. 4b). These peaks display good reproducibility, in terms of both chromatographic retention times and relative peak areas. Certain peaks can be specifically identified, and many others can be assigned a structural family classification. Singly unsaturated hydrocarbons (alkenes) and branched alkanes are the most common species, but some peaks appear to contain oxygen, primarily in the form of alcohols and ethers. While the hydrocarbon nature of these species would be expected from an ethane plasma, the presence of oxygen is somewhat puzzling. Possible oxygen sources include air leaks (although these are eliminated before testing), water and air outgassing from plumbing, small amounts of oxygen in the supply gas cylinder, and surface oxides.

Chromatographic peaks in Fig. 4b are seen primarily in the region with retention temperatures from 20°C to condensed on the outer wall of the proportional tube, which is not heated.

C. *Discussion*

1. Heating Effects

Many of the species observed in the proportional tube effluent have boiling points higher than room temperature, and the question arises why these species do not condense onto the wire. The temperature of the gas in the avalanche region cannot be measured easily, but is almost certainly affected by the power dissipated in the avalanche. For the tube used in our experiments, the gas temperature rise due to this power is calculated to be between 2°C and 20000°C, depending on whether the resulting heat is distributed uniformly though the entire gas volume, or is taken to be localized in the avalanche region. For this calculation, the avalanche region is assumed to extend one wire diameter beyond the surface of a 50 micron diameter wire.

These heating effects may have important

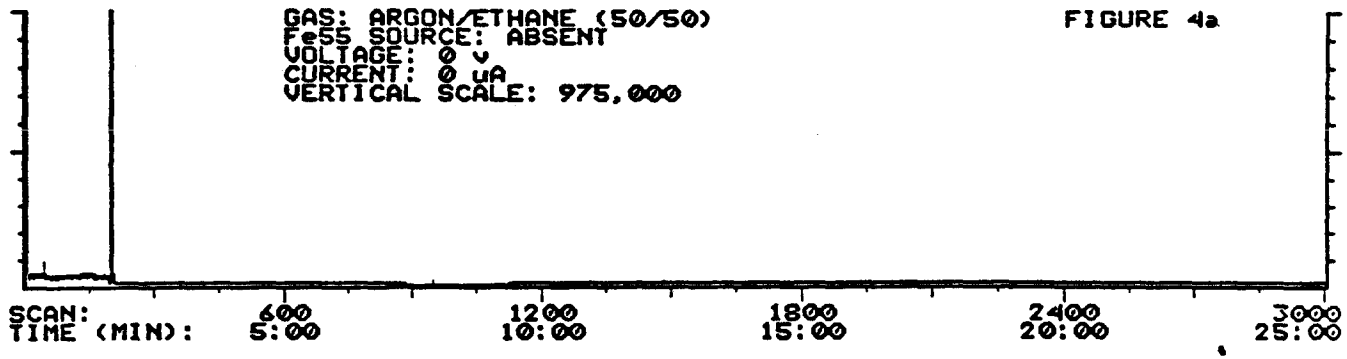

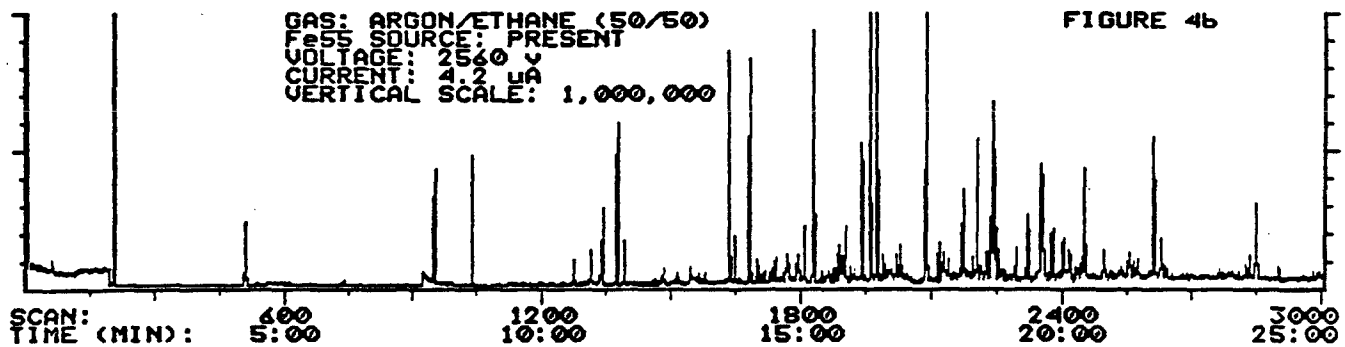

Fig. 4. Chromatograms of analyses of plasma chemistry reaction products. Pictured are: (a) result with no irradiation, (b) result when plasma-chemical reactions occur. The vertical scale is the total ion response of the mass spectrometer.

condensation. To the extent that such effects exist, they may affect the product distribution observed in the chromatograms. There is expected to be a temperature dependence of reaction rates, with the rates, and therefore product concentrations, increasing with temperature. On the other hand, the sticking coefficients of these products on the wire vary inversely with temperature. It is therefore difficult to predict the overall effect of localized heating upon wire coating, and investigations into such effects are planned.

2. Product Formation Rate

plasma polymerization. We note, however, 1) Many radicals that may have been formed could have recombined to form ethane, or other light products that we have not observed; 2) The temperature (150°C) in parts of the cryotrapping system biases it against heavier species (see discussion in section V.B.), and may be causing us to measure a systematically low rate of product formation. For these reasons, we believe that the products of plasma reactions fail to be accounted for by ions by substantially more than the factor of two mentioned above, and that neutral species (radicals) are responsible for the bulk of the reaction occurring.

intentional polymer deposition, and have been extensively studied [3,4]. Although wire chambers operate at higher pressure (~1 atm.) and under dc rather than rf discharge conditions, there is no *a priori* reason to expect that the overall reaction mechanisms should be different, although the kinetics may vary. Indeed, the electron energies for the two situations are expected to be similar [5]. A further suggestion to the possible similarity of these two regimes comes from mass spectral analysis of anode-wire deposits from a failed wire chamber, in which the wire coating was predominantly linear hydrocarbons [6]. This result is in agreement with the observed products in the gaseous effluent of our proportional tube.

A qualitative picture of typical plasma-chemical reactions can be used to describe how some of the observed eluents might be formed. Polymerization is comprised of three types of reactions: initiation, propagation, and termination. Due to the expected large abundance of radicals over ions in wire chamber plasmas, a free-radical mechanism seems most appropriate. A representative, but by no means unique, polymerization scheme might be constructed as follows:

Initiation: These reactions produce active species, radicals in this case, that, due to their unpaired electron(s), are highly reactive.

$$e + C_2H_6 \rightarrow C_2H_4 + H_2 + e$$
$$e + C_2H_4 \rightarrow C_2H_2 + H_2 + e$$
$$\rightarrow 2\ CH_2{:} + e$$
$$\rightarrow C_2H_4^{\cdot +} + 2e$$
$$H^{\cdot} + C_2H_4 \rightarrow C_2H_5^{\cdot}$$
$$H^{\cdot} + C_2H_5^{\cdot} \rightarrow 2\ CH_3^{\cdot}$$
$$H^{\cdot} + C_2H_2 \rightarrow C_2H_3^{\cdot}$$

"e" represents a free electron in the avalanche and the "·" represents an unpaired electron in a radical.

Propagation: These reactions produce species of increasing molecular weight by repeatedly adding small units. The unpaired electron from the initiator is left unpaired in these reactions, and thus can continue to react. It is during this stage, as molecules get heavier, that they may begin to condense onto the wire.

$$R_n^{\cdot} + C_2H_6 + M \rightarrow R_{n+2}^{\cdot} + M$$
$$R_n^{\cdot} + C_2H_6 \rightarrow R_{n+2}^{\cdot} + H_2$$
$$R_n^{\cdot} + H^{\cdot} \rightarrow P_n$$
$$R_n^{\cdot} + CH_3^{\cdot} \rightarrow P_{n+1}$$
$$R_n^{\cdot} + R_m^{\cdot} \rightarrow P_{n+m}$$

The type of reaction scheme described above, expanded to include all possible reactions, has been used to describe the observed polymerization kinetics of ethane in a low-pressure rf discharge [7].

The results presented here demonstrate the capability of probing the chemistry of a wire chamber avalanche. It is hoped that further investigation will lead to identification of the specific reactions responsible for wire aging and will suggest techniques to avoid or eliminate those reactions.

V. Summary and Conclusions

Construction and successful operation of a system to analyze trace components in gases is reported. A study of the outgassed components from several different tubings has been made, and the observed products qualitatively identified. Two possible source of silicon have been identified: incompletely cleaned parts that were once in contact with silicone oils or greases, and parts that may have had transient exposure to silicone vapors.

A proportional tube has been used to model the plasma-chemical reactions that may occur in wire chambers, and a strong, reproducible signal has been observed. Many of the reaction products can be identified either specifically or by family classification. The question of localized heating in the avalanche region and its effect on the general validity of accelerated aging tests is raised.

A series of reactions that may represent the chemistry occurring in wire chambers is discussed in the context of relating wire chamber plasmas to other, better-understood plasmas.

Acknowledgements

Special thanks are due to Doug Shigley for his outstanding help in supplying our mechanical needs. Thanks also to Ron Jones, who has met all of our often-unreasonable demands for electronic equipment, and to Ketan Desai, who set up the computerized data sampling system and made it easily expandable. We also acknowledge the help received from experienced chromatographers Amos Newton and Al Hodgson in the early stages of this project. This work was supported by the Director, Office of Energy Research, Office of High

[3] Yasuda, H., Plasma Polymerization, Academic Press Inc., (New York, 1985).
[4] Shen, M., and A.T. Bell, eds., Plasma Polymerization, ACS Symposium Series, No. 108, Amer. Chem. Soc., Washington, D.C. (1979).
[5] Va'vra, J., *Nucl. Instr. Meth.*, A252, 547 (1986).
[6] (a) Williams, M.C., ref 2, pp. 25-46. (b) Kwong, K., et al., *Nucl. Instr. Meth.*, A238, 265 (1985).
[7] Jensen, R.J., A.T. Bell, and D.S. Soong, *Plasma Chem. Plasma Proc.*, 3, 163 (1983).

LBL-29252

EFFECTS OF FREONS ON WIRE CHAMBER AGING*

Jonathan Wise,[1,2] John A. Kadyk,[1] Dennis W. Hess,[1,2]
and Michael C. Williams[3]

[1]Lawrence Berkeley Laboratory, University of California,
Berkeley, CA 94720, USA

[2]Department of Chemical Engineering, University of California,
Berkeley, CA 94720, USA

[3]Department of Chemical Engineering, University of Alberta,
Edmonton, Alberta T6G 2G6, Canada

Abstract

Data are presented to suggest that trace amounts of Freons do not affect the rate of gain loss in wire chambers filled with either dimethyl ether or argon/ethane. Apparent gain loss in dimethyl ether is explained by attachment of primary electrons to a continuously increasing concentration of Freon 11 in the counter gas. An increase in the concentration of Freon 11 in dimethyl ether is caused by a distillation process in the gas supply bottle and is a natural consequence of the unequal volatilities of the two compounds. Degradation of ^{55}Fe pulse-height spectra obtained

1. Introduction

There are at least two reasons why Freons might be expected to cause aging in wire chambers. (1) Freons contain halogens, which are known to catalyze plasma polymerization of hydrocarbons in the low-pressure rf-discharge regime [1]. It has been suggested that there may be similarities between the low-pressure rf-discharge plasma regime and that of wire chambers [2]. (2) Some Freons are very electronegative and are therefore expected to attach electrons and be drawn to the anode, where, if they do catalyze polymerization, they could most easily affect the aging rate.

Since the primary electrons lost by attachment to electronegative species are not available to initiate avalanches, however, the observed wire current can change if the concentration of electronegative species in the gas changes. It is possible that an increase in the concentration of a highly electronegative species such as Freon 11 may cause the wire current to drop, a result which may be interpreted as aging [3]. In this report we discuss a mechanism by which trace species that are less-volatile than the main gas may be concentrated in a gas bottle.

2. Experimental

to collect aging data have already been described [3]. The 5.9 keV photons emitted by an ^{55}Fe source were used to simulate particle radiation. Initial current densities were ~1.3 μA/cm, corresponding to wire currents of ~400 nA for an irradiated region 3 mm long. The gas gains were known only approximately, and were in the 20,000-50,000 range. The gas flow rate in all tests was approximately 20 cm^3/min, corresponding to 1.25 chamber volumes/min, or an average linear velocity of 0.47 cm/sec.

We express the aging rate, R, as the normalized rate of gain loss:

$$R = -(1/G_o)(dG/dQ), \tag{1a}$$

where G_o is the initial gas gain, G is the gas gain at a subsequent time, and Q is the accumulated charge per length of wire. If the ionization initiating the avalanches does not change, the current on a wire is linearly proportional to the gas gain, and R can be measured as the normalized rate of current decrease:

$$R = -(1/I_o)(dI/dQ), \tag{1b}$$

where I_o is the initial wire current, I is the wire current at a subsequent time, and R and Q are as defined above. We express R in units of %/C/cm.

3. Aging Tests with Freons in Argon/Ethane

of aging tests was performed in which gas permeation [4] was used to add halogenated (Freon) contaminants to the argon/ethane. Permeation was effected with a Kin-Tek Precision Gas Standards Generator Model 570-C (Kin-Tek Laboratories, Texas City, TX). The aging tests discussed below were run only for relatively short periods in an exploratory mode, looking for easily-observed increases in aging rates. In no case was there evidence that Freon addition resulted in significant aging rates. These results are summarized in Table 1.

A test in which $CFCl_3$ (Freon 11) was added to argon/ethane is shown in Fig. 1. In this test, the concentration of Freon 11 was set at several different levels; at each level the current was stable. The test was initially run without Freon 11 added to the gas (segment A of Fig. 1); 100 mC/cm of charge was collected during this period and the measured aging rate was R~7 %/C/cm. When Freon 11 was added to the gas at varying levels (segments B-F), the current dropped from its initial value due to attachment of primary electrons, but then stabilized. Meaningful values of R could not be calculated for these segments because only small amounts of charge were collected at the reduced currents. The transient spikes between levels

the establishment of that level. After the Freon source was removed from the system, the current returned to its initial level (segment G), indicating that little or no deposit had been formed on the wire. A total of about 0.12 C/cm of charge was collected during the exposure to Freon 11. These results were reproduced in subsequent tests.

4. Dimethyl Ether

Dimethyl ether (DME) is an attractive gas with good quenching, a high linear ionization density, a low drift velocity and a low electron diffusion constant [5], properties which make it a good choice for use in high-resolution drift chambers (e.g., vertex detectors). There are, however, several reports [6,7] suggesting that Freon 11 contamination in DME causes rapid aging. Since Freon 11 is a commonly observed [6,7] contaminant in DME, the viability of DME as a useful wire chamber gas has been questioned.

A possible alternative explanation of the above-mentioned observations is that the "aging" is due to a loss of primary electrons by attachment to the very electronegative Freon 11 [3]. If Freon 11 is present in the DME supply, it will be concentrated as the DME, which is more volatile (i.e., has a lower boiling point), evaporates

5. Rayleigh Distillation

Rayleigh distillation describes the equilibrium vaporization process of an initial mass of a binary liquid mixture in a vessel to which heat is added continuously. It is assumed that the liquid is well mixed (i.e., is of uniform composition throughout) and that vapor in equilibrium with the liquid is generated and removed continuously from the vessel. Clearly, the continuous generation and removal of vapor is a valid description of the vaporization of DME in the gas supply bottle. Further, we believe it reasonable to assume that the liquid is well mixed since liquid diffusivities are high.

To describe a Rayleigh distillation, it is necessary to relate the amount of liquid remaining to its composition. This is done by means of a mass balance relating changes in the amount and composition of the liquid to the amount and composition of the vapor removed. In its most general form, the Rayleigh equation (for component i) is

$$\ln(L/L_o) = \int_{x_{io}}^{x_i} dx_i/(y_i - x_i), \qquad (2)$$

where L_o and x_{io} are the initial number of moles of liquid and liquid mole fraction, and L, x_i, and y_i are the remaining number of moles of liquid, liquid mole fraction, and vapor mole fraction at any subsequent time. Integration

The relative volatility, or separation factor, α, between two phases in equilibrium is defined as

$$\alpha = (x_A/x_B)_{\text{phase 1}}/(x_A/x_B)_{\text{phase 2}}. \tag{3a}$$

It is conventional to choose the phases so that $\alpha>1$. For the case at hand, this means that phase 1 is the gas, phase 2 is the liquid, the subscript A refers to the light component (DME), and the subscript B refers to the heavy component (Freon 11). Following the common usage that x_i refers to a liquid-phase mole fraction and y_i to a gas-phase mole fraction,

$$\alpha = (y_A/y_B)/(x_A/x_B). \tag{3b}$$

Because we are interested in very dilute solutions (Freon mole fractions less than 10^{-4}), we can assume ideal behavior. This means that the solution obeys Raoult's law, which states that the vapor pressure exerted by a component in the solution is equal to the vapor pressure of the pure component weighted by the mole fraction of that component in the solution, and that the vapor phase obeys Dalton's law, which states that the partial pressure of a component in a gas mixture is equal to the total pressure of the gas weighted by the mole fraction of that component in the gas. Combining Raoult's and Dalton's laws,

$$y_i P = p_i = x_i P_i^{\circ}, \tag{4}$$

A consequence of Raoult's and Dalton's laws is that α is simply the ratio of the vapor pressures of the two pure components at a given temperature:

$$\alpha = P_A^\circ/P_B^\circ. \tag{5}$$

It can be seen that α is independent of pressure and composition. For this situation, it is further argued that α is only a weak function of temperature [9]. As the temperature of the gas supply bottle is expected to undergo little or no fluctuation, we are justified in treating α as a constant.

Making use of the fact that $x_A + x_B = y_A + y_B = 1$ for a binary mixture, equation (3b) can be rewritten as

$$y_A = \alpha x_A/[1 + (\alpha-1)x_A]. \tag{6}$$

Substituting equation (6) into equation (2), using the fact that α is constant, and integrating with respect to component A gives

$$\ln(L/L_o) = (1/\alpha-1)\ln[((1-x_B)/x_B)/((1-x_B)/x_B)_o] - \ln(x_B/x_{Bo}). \tag{7}$$

With an appropriate value for α (see the following section), this equation can be used to predict the Freon 11 concentration as a function of the amount of liquid DME remaining in the bottle.

6. Simulation of Rayleigh Distillation

liquid that has been used ($1-L/L_o$). Equation (6) relates the vapor- and liquid-phase concentrations of the light component, but can be rewritten to relate the concentrations of the heavy component:

$$y_B = x_B/[\alpha + (1-\alpha)x_B]. \tag{8}$$

Noting that we are in a regime in which $x_B \ll 1$, and hence $(1-\alpha)x_B \ll \alpha$, equation (8) can be approximated as

$$y_B = x_B/\alpha. \tag{9}$$

The enrichment multiple therefore applies to both the vapor and liquid phases.

The pure-component vapor pressures needed to determine α can be calculated from tabulated data [10]. The predicted relative volatility of DME/Freon 11 near room temperature is shown in Table 2.

In the regime of relative volatility ($5.5<\alpha<5.8$) and initial Freon concentration ($x_{Bo}<10^{-4}$) in which we are interested, the solution of equation (7) is not sensitive to variations in either of these parameters: the Freon 11 concentration doubles each time 57% of the liquid remaining in the bottle is used. The prediction for $\alpha=5.63$ and $x_{Bo}=10^{-7}$ is shown in Table 3.

Evaporation Tests with Freon 11 in Dimethyl Ether

To investigate the effect of a constant level of Freon 11 in DME, a Kin-Tek SRT-type source was used with the gas permeation system mentioned above to add ~5 ppm of Freon 11 to otherwise pure DME (Dymel A, DuPont, Wilmington, DE). (We measured the Freon 11 concentration in this DME to be ~5 ppb.) The SRT source is a ~10-cm length of Teflon tube that contains liquid Freon 11. Although Teflon has been reported to cause signal loss [7], we believe that it did not affect this test. Indeed, low aging rates have been achieved using DME in systems with certain plastics, including Teflon [11]. To ensure that the Freon 11 concentration in the DME supply would not change appreciably due to a Rayleigh distillation, less than 30% of the liquid in the DME supply bottle was used over the course of the test. The test was started without any added Freon 11; as shown in Fig. 2, the current dropped to ~25% of its initial value upon addition of the Freon. The permeation source was bypassed several times during the test, and the current returned to its initial level each time. A total of 0.45 C/cm of charge was collected during the exposure to Freon 11, and the measured aging rate during this period was consistent with a value of zero. ^{55}Fe pulse-height spectra taken at the end of the test were somewhat degraded, however

degradation pattern [12]. These data indicate that the presence of Freon 11 in DME does not result in measurable gain loss, but does cause some degradation of energy resolution.

To investigate the possibility of Freon 11 being concentrated by a Rayleigh distillation, two aging tests were performed in which all of the liquid DME (Semiconductor grade, Matheson Gas Products, Newark, CA) in the bottle was used. It was necessary to use all of the liquid because large changes in the enrichment multiple are predicted (Table 3) to occur as 80-100% of the liquid is used. The initial gas-phase Freon 11 concentration was approximately 0.2 ppm in the first test and approximately 0.04 ppm in the second test.

In each of these tests, one of which is shown in Fig. 5, the current was initially stable, but dropped rapidly toward the end of the test when most of the DME had been used. The point at which no liquid DME remained is indicated in the figure. Although no liquid DME remained, the bottle still contained gaseous DME at its room-temperature vapor pressure, ~62 psig. Subsequent to this point, the distillation process ceased, and the gas composition and wire current were nearly stable. The gas

initial level. This was because the Freon 11 concentration in the new bottle was lower than what it had been in the previous bottle at the beginning of the test.

Both of these aging tests were performed using the same proportional tube and the same wire as the first test, and a total of 1.4 C/cm of charge was collected. ^{55}Fe pulse-height spectra taken at the end of the second test were severely degraded, however (Fig. 6), indicating the presence of some deposit on the wire. (See discussion in section 8.2.)

To evaluate the effect of this deposit on the gain, a bottle of DME that had been used previously and was known not to cause aging was connected to the tube. The ^{55}Fe source that was used for the aging tests was moved along the wire and the variation in current drawn was observed to be only 1.5% between the coated and an uncoated region, corresponding to an overall aging rate of R~1 %/C/cm. During this test, however, an aging rate of R~400 %/C/cm was observed. A new proportional tube with a new wire was installed: the rapid aging continued. When all gas plumbing between the DME bottle and the proportional tube were replaced with new components, however, the aging rate returned to a value consistent with zero. These data suggest that some compound remained in the plumbing, but

of the fraction of the liquid DME used. The enrichment multiple was determined by measuring the concentration of the Freon 11 in the gas throughout the tests. A Varian 3400 gas chromatograph equipped with a Varian model 02-001972-00 electron capture detector (Varian Instrument Group, Walnut Creek, CA) was used for this purpose. The fraction of the liquid used was taken to be equivalent to the fractional elapsed time of the test because fluctuations in the gas flow rate, which was monitored, were determined to be insignificantly small.

The GC analysis was performed with a DB-5 capillary column of 30 m length, 0.25 mm inside diameter, and 0.25 μm phase thickness (J&W Scientific, Folsom, CA). To effect the desired separation, the GC temperature program consisted of a ramp to 50°C at 10°C/min after an initial three-minute hold at -30°C. A helium carrier gas pressure of 15 psig was used. The injector and detector were kept isothermal at 100°C and 200°C, respectively. Under these conditions, Freon 11 eluted in 4.7±0.02 min. The analyzed DME samples (10 μl each) were withdrawn from the downstream side of the proportional tube.

Some deviation from the Rayleigh prediction can occur as consequence of the nonzero mass of vapor in the DME bottle, which is not accounted for in the model. Only a

produced earlier, from liquid that was less enriched in Freon 11. Therefore, the concentration of Freon 11 in the vapor leaving the bottle, which is what we measured, is always lower than the prediction, and the Rayleigh prediction consequently represents an upper limit on the Freon concentration.

A lower limit on the Freon 11 concentration can be estimated from the time required for vapor-phase concentration changes to propagate from the liquid surface to the point at which samples are withdrawn for analysis. This time is given by the ratio of the corresponding vapor volume to the volumetric gas flow rate. The propagation delay is most conveniently expressed as an offset in the fraction of the liquid used. This limiting offset is numerically equal to the ratio of the propagation time to the total elasped time of the test, and a line representing the lower limit on the Freon concentration can therefore be plotted by offsetting the Rayleigh prediction by this ratio (Fig. 7). This represents a lower limit because any diffusion in or mixing of the vapor will reduce the effective propagation time. Further, when all of the liquid is used, mixing of the vapor in the bottle dilutes more-

uncertainty, the data lie between the limiting cases, indicating that the Rayleigh distillation model accurately describes the vaporization of DME in a gas bottle.

While analyzing the DME for its Freon 11 content during these tests, it was observed in the chromatograms that several species were present in addition to Freon 11, and that the concentrations of all species increased as the liquid DME was used. Further, as the liquid DME was used, progressively larger numbers of distinct species were observed in the chromatograms. These species have not been identified.

8. Discussion

8.1 Aging Results

We noted that increases in the concentration of Freon 11 can give the appearance of aging due to electron attachment. Because the concentration of Freon 11 in DME can increase as a result of Rayleigh distillation, it is important to know the initial Freon 11 concentration: the effect of electron attachment may be evident very early (if the initial Freon 11 concentration is large) or it may not be evident until nearly all of the liquid has been used (if the initial Freon 11 concentration is small). By using an

We also noted that rapid aging was observed in DME after using all of the liquid in two bottles. It has not yet been possible to identify the compound (or compounds) responsible for this aging, but we believe it to be less volatile than Freon 11, as (1) it did not appear until most, if not all, of the liquid DME had been used, and (2) it appeared to remain in the plumbing, unlike Freon 11, which is quite volatile at room temperature. It is worth noting that both DME bottles used in these tests had been used in previous aging tests in which little aging was observed [3]. Assuming that the compound inducing the aging originated in the DME bottle, which we believe to be the case, it must have been present in the earlier tests, but at too low a concentration to have had an effect. This would be further reason to use only a fraction of the DME in a given supply bottle.

8.2 Degradation of Energy Resolution

We noted that some degradation of the ^{55}Fe pulse-height spectrum was observed in the DME aging tests in which Freon 11 was added. Although this degradation indicates the presence of deposits on the wire, we believe it to be of relatively minor significance because the pulse-height

to only a 1.5% change in gain after 1.4 C/cm of charge was collected.

We expect that the degree to which the pulse-height spectrum is degraded may depend on both the concentration of the species inducing the aging and the amount of charge collected. If we take the product of these quantities as a measure of the amount of degradation expected, we find that much more degradation is expected for the wire exposed to the 5 ppm of Freon 11 (Fig. 3) than for the wire from the tests in which all of the liquid in two DME bottles of DME was used (Fig. 6):

Tests with direct addition of Freon 11 using the permeation device:

(0.45 C/cm)*(5 ppm Freon 11 concentration) = 2.25.

Tests in which all liquid DME was used:

(1.4 C/cm)*(0.3 ppm average Freon 11 concentration) = 0.42.

That the observed degradation of the spectra is actually much less in the case of the direct Freon 11 addition, rather than much more, as the above estimate predicts, can be taken as an indication that some species other than Freon 11 induces aging in DME. As previously noted, many

We note, however, that energy resolution is of major importance only when using energy-loss (dE/dx) measurements for particle identification, and it is expected that this technique will not be very useful at SSC because the particles of interest will generally have very high energies, outside the range of this technique. For particle tracking only, degradation of energy resolution, as distinct from loss of gain, is not a significant issue or limitation.

8.3 Rayleigh Distillation

As a result of Rayleigh distillation, concentration changes of trace species will occur whenever there is a liquid phase in the gas bottle. Indeed, it was noted in aging tests with propane, which has a liquid phase in the gas bottle, that the gas purity varied not only from bottle to bottle, but also within a bottle as it was used [13]. The concentrations of species less volatile than the main gas will increase while those of species more volatile than the main gas will decrease. This being so, the potential effects of changes in gas purity on wire chamber operation must be considered.

The degree to which the heavier component in a binary

severe in propane ($\alpha_{propane-Freon\ 11} \approx 9.4$ [10]) and less severe in isobutane ($\alpha_{isobutane-Freon\ 11} \approx 3.8$ [10]) than in DME ($\alpha_{DME-Freon\ 11} \approx 5.6$).

As we have shown, increases in the concentration of highly electronegative species can give the appearance of aging. This work investigated only the effects of Freon 11, but the possibility exists that other electronegative species are of the correct volatility to give the same effect. As suggested above, it is also possible that species that induce wire degradation (as contrasted with effects of electronegativity) may be concentrated so that their effect is noticeable. An alternative, less-plausible, explanation is that certain species that inhibit aging are depleted because they are more volatile than the main gas. In any case, concentration changes caused by Rayleigh distillation complicate the interpretation of aging results. The concentration changes and their consequences can be minimized, however, by using a suitably small fraction of the liquid initially in the gas bottle.

9. Conclusions

We have found no evidence that Freons in general, and

by the ^{55}Fe pulse-height spectrum, seems to be accelerated by the presence of Freon 11, however.

The large electronegativity of Freon 11 causes signal loss by attachment of primary electrons and so can give the appearance of gain loss if its concentration increases. We showed by experiment and simulation that apparent aging observed while using dimethyl ether can be explained by the natural increase in the concentration of Freon 11 that occurs in a Rayleigh distillation process. Large changes in the concentration of Freon 11 in DME and the consequent changes in wire currents can be avoided by not using all of the liquid DME in a given supply bottle.

Concentration changes of trace species are expected to occur whenever there is a liquid phase in a gas bottle. It is therefore prudent not to use all of the liquid in such cases regardless of the type of gas.

Acknowledgements

We acknowledge Stan Majewski, University of Florida (now at CEBAF), and Mohammed Jibaly, University of Florida, for discussions regarding the effects of Freon 11 and thank them for supplying us with much of the DME used in these tests.

References

[1] H. Kobayashi, M. Shen, and A.T. Bell, *J. Macromol. Sci., Chem.*, A8 (1974) 1345.

[2] D.W. Hess in Proceedings of the Workshop on Radiation Damage to Wire Chambers, J. Kadyk, ed., LBL-21170 (1986), pp. 15-23.

[3] J. Kadyk, J. Wise, D. Hess, and M. Williams, *IEEE Trans. Nucl. Sci.*, NS-37 (1990) 478.

[4] (a) A.E. O'Keeffe and G.C. Ortman, *Anal. Chem.*, 38 (1966) 760, (b) Correction, *Anal. Chem.*, 41 (1969) 1598.

[5] F. Villa, *Nucl. Instr. and Meth.*, 217 (1983) 273.

[6] I. Juricic and J. Kadyk, *IEEE Trans. Nucl. Sci.*, NS-34 (1987) 481.

[7] (a) M. Jibaly, P. Chrusch, G. Hilgenberg, S. Majewski, R. Wojcik, R. Weintraub, and F. Sauli, *Nucl. Instr. and Meth.*, A273 (1988) 161, (b) M. Jibaly, P. Chrusch, G. Hilgenberg, S. Majewski, R. Wojcik, F. Sauli, and J. Gaudean, *IEEE Trans. Nucl. Sci.*, NS-36 (1989) 552.

[8] C.J. King, Separation Processes (McGraw-Hill, New York, 1980), pp. 115-123.

[9] C.J. King, Reference 8, pp. 30,31.

[10] R.C. Reid, J.M. Prausnitz, and B.E. Poling, The Properties of Gases and Liquids, 4th ed. (McGraw-Hill, New York, 1987).

[11] G. Bari, M. Basile, G. Bonvinci *et al.*, *Nucl. Instr. and Meth.*, A251 (1986) 292.

[12] A.J.F. den Boggende, A.C. Brinkman, and W. de Graaff, *J. Sci. Instr. (J. Phys. E)*, 2 (1969) 701.

[13] M. Danilov, V. Nagovitsin, V. Shibaev, I. Tichomirov, E. Michel, and W. Schmidt-Parzefall, *Nucl. Instr. and Meth.*, A274 (1989) 189.

Table 2
Predicted relative volatility (α) of DME/Freon 11 near room temperature [10].

T, °C	α
18	5.78
19	5.74
20	5.70
21	5.66
22	5.62
23	5.59

Table 3
Numerical solution to equation 7 for α=5.63 and x_{Bo}=10^{-7}.

enrichment multiple	fraction of liquid used	enrichment multiple	fraction of liquid used
1.0	0.000	2.8	0.714
1.1	0.109	3.0	0.737
1.2	0.199	3.5	0.782
1.3	0.273	4.0	0.815
1.4	0.336	4.5	0.839
1.5	0.389	5.0	0.859
1.6	0.435	6.0	0.887
1.7	0.475	7.0	0.906
1.8	0.511	8.0	0.920
1.9	0.542	10.0	0.939
2.0	0.570	12.0	0.951
2.2	0.617	14.0	0.960
2.4	0.655	16.0	0.966
2.6	0.687	32.0	0.985

Fig. 1. Aging test in which Freon 11 at varying levels was added to 50% argon + 50% ethane. The irradiated region of the wire was 0.3 cm. Freon concentrations (ppm) were: A, 0; B, 100; C, 70; D, 45; E, 45; F, 34; G, 0.

Fig. 2. Aging test in which ~5 ppm Freon 11 was added to DME. The current dropped ~75% from its initial value (indicated by the arrow) upon addition of the Freon, but no aging was observed. The irradiated region of the wire was 0.3 cm.

Fig. 3. ^{55}Fe pulse-height spectra taken after DME aging test with ~5 ppm Freon 11. The ^{55}Fe line source was perpendicular to the wire. The classic pattern of degradation of the spectrum is seen [12]. The positions of the ^{55}Fe line source with respect to the approximate center of the irradiated region were: a, -3; b, -2; c, -1; d, 0; e, +2; f, +3; g, +4, where distances are in millimeters, and negative positions are upstream and positive positions are downstream with respect to the direction of gas flow.

Fig. 4. ^{55}Fe pulse-height spectrum taken at the center of the irradiated region of the wire after DME aging test with no added Freon 11. The ^{55}Fe line source was perpendicular to the wire. No significant degradation of the spectrum is observed.

Fig. 5. Aging test in which all of the liquid DME was used. No liquid DME remained at point A. The liquid-depleted bottle was replaced with a full bottle at point B. The enrichment multiple of the Freon 11 in this test is shown in

Fig. 7a. Predicted and experimental (▪) enrichment multiples of Freon 11 in DME. The solid line represents the Rayleigh prediction; the dashed line represents an offset of 0.058 (= 5 hrs propagation time/86.6 hrs total time). The initial amount of DME in this test was 255 g; 60 g of gas remained after all of the liquid had vaporized. The initial gas-phase Freon 11 concentration was ~0.2 ppm.

Fig. 7b. Predicted and experimental (▪) enrichment multiples of Freon 11 in DME. The solid line represents the Rayleigh prediction; the dashed line represents an offset of 0.018 (= 2.9 hrs propagation time/159.6 hrs total time). The initial amount of DME in this test was 670 g; 60 g of gas remained after all of the liquid had vaporized. The initial gas-phase Freon 11 concentration was ~0.04 ppm. The wire current as a function of the fraction of liquid used is also shown.

Table 1
Summary of aging results in which halogenated contaminants were deliberately added to 50% argon + 50% ethane. These tests and their respective control tests were run simultaneously and under otherwise identical conditions, except that no contaminants were added to the controls. No significant differences in the aging rates were observed.

additive	additive name	additive concentration, ppm	accumulated charge, mC/cm	*R*, %/C/cm	control test *R*, %/C/cm
CHF_2Cl	Freon 22	8	150	5	3
CF_2Cl_2	Freon 12	680	180	-1	5
CH_3Cl	methyl chloride	680	380	3	4
CH_3Cl	methyl chloride	550	360	3	no test

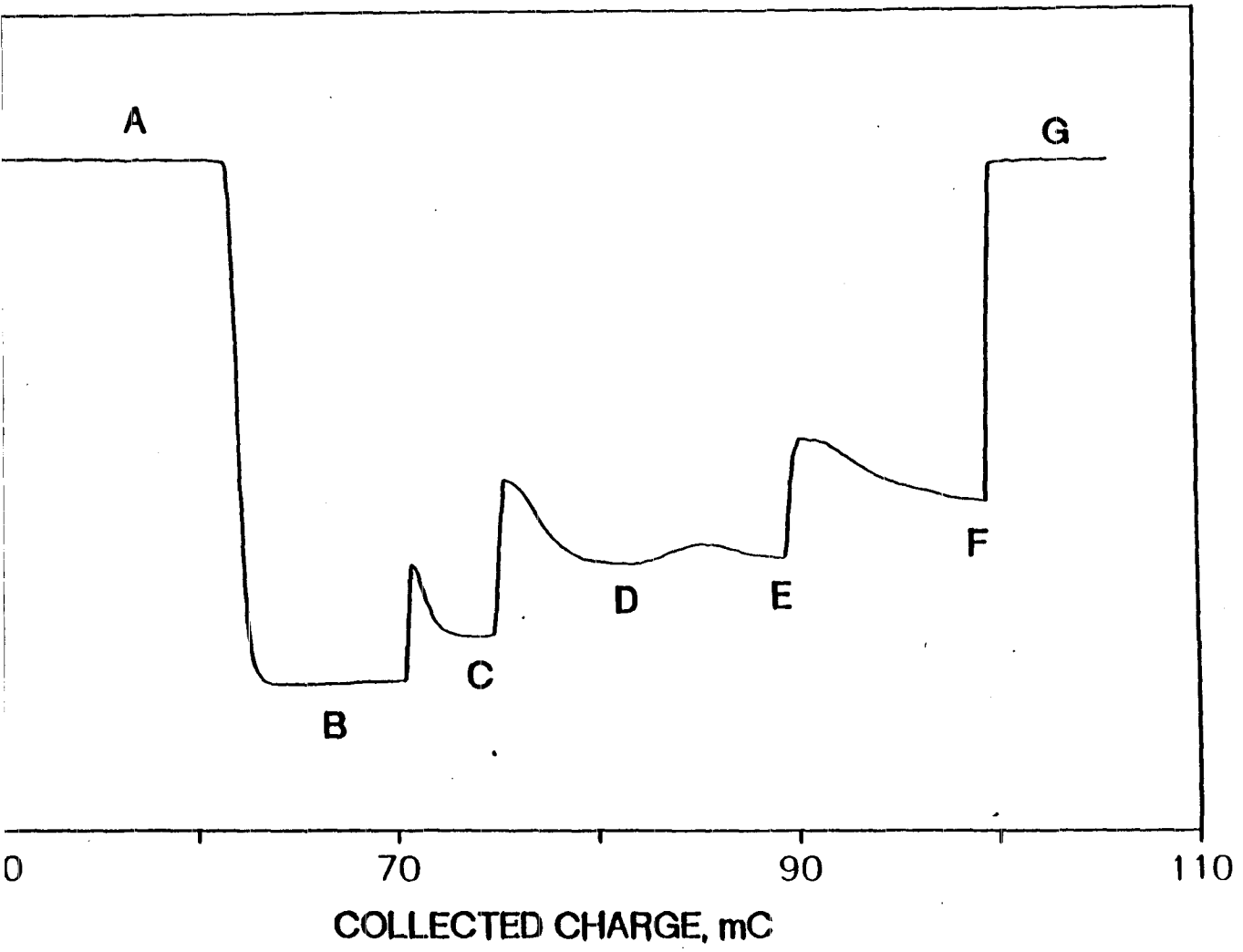
A
B
C
D
E
F
G
0
70
90
110
COLLECTED CHARGE, mC

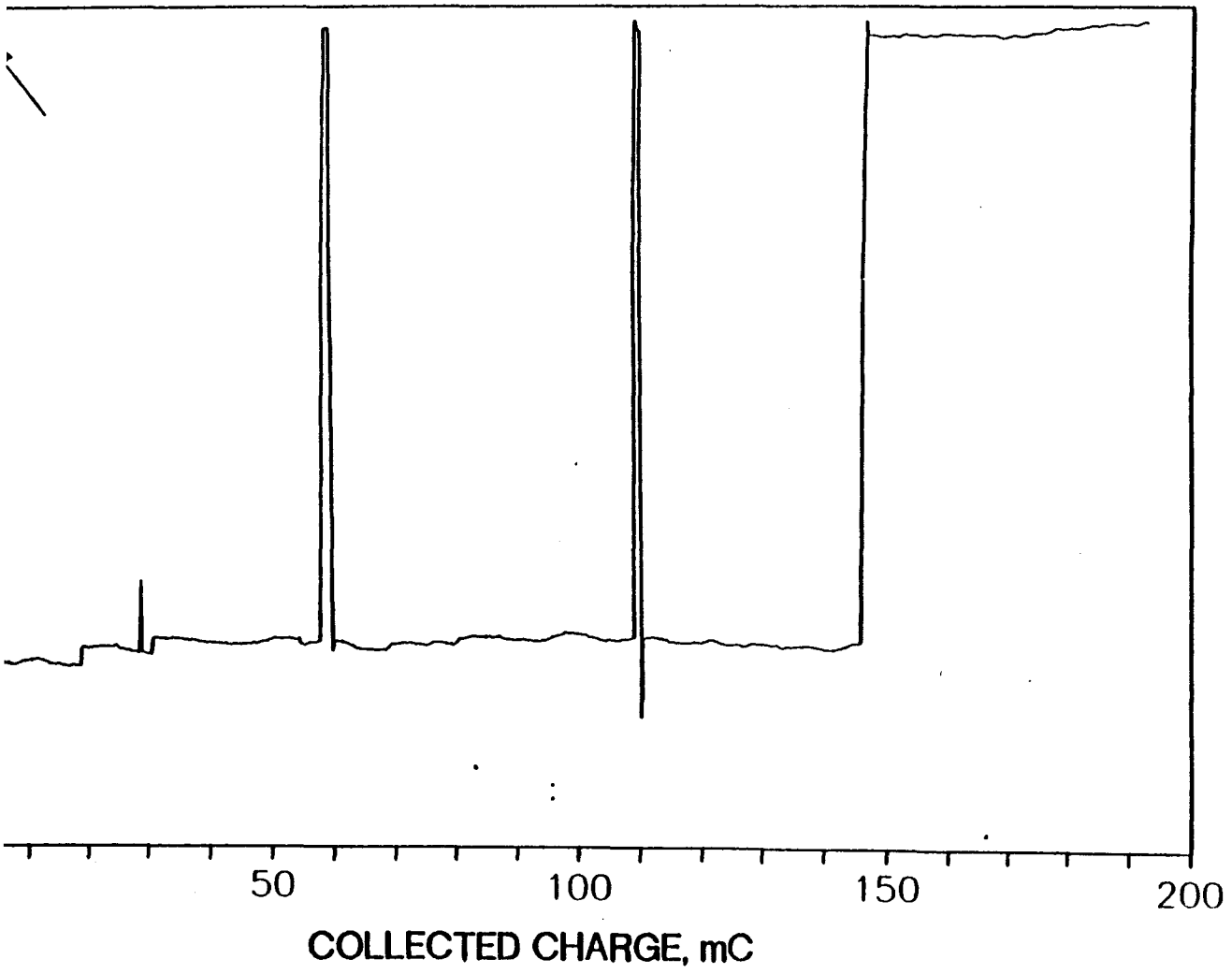
50
100
150
200
COLLECTED CHARGE, mC

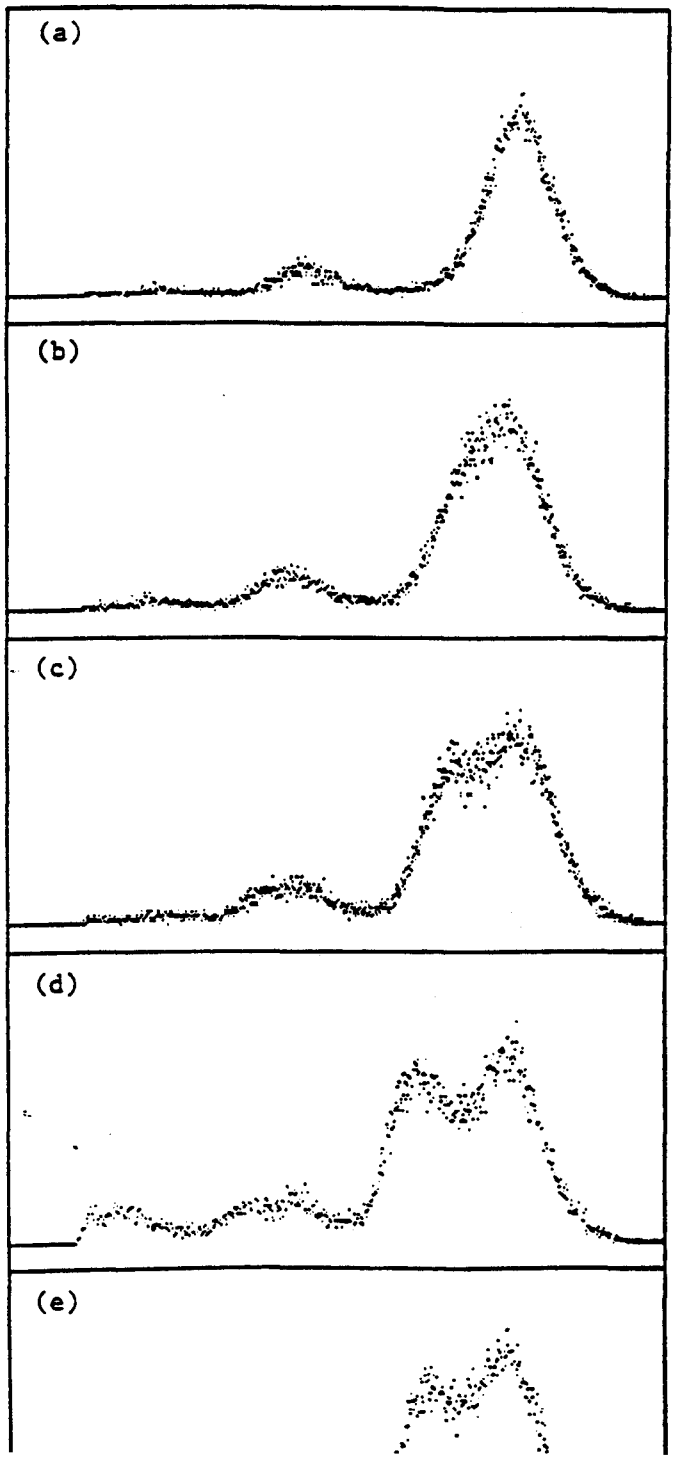
(a)
(b)
(c)
(d)
(e)

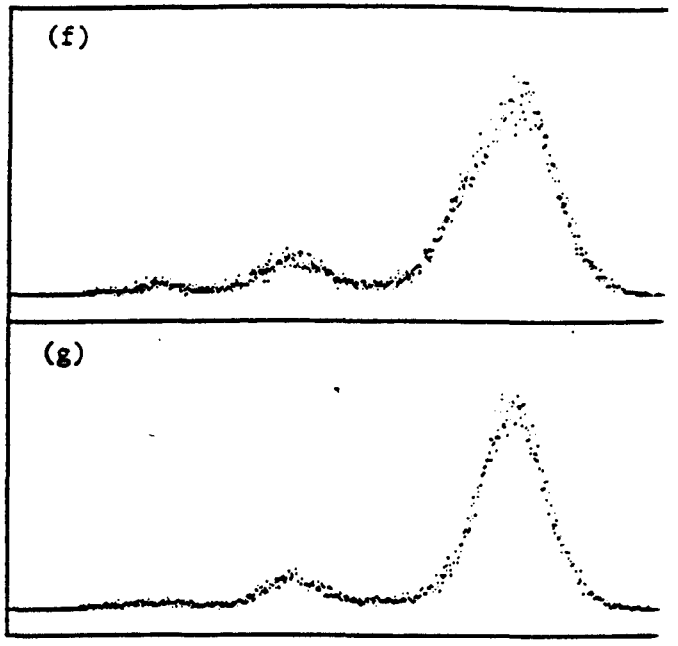
(f)
(g)

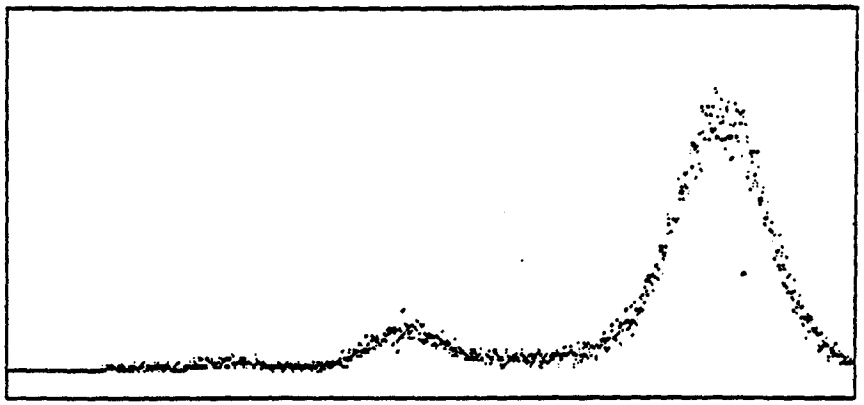

Fig 4

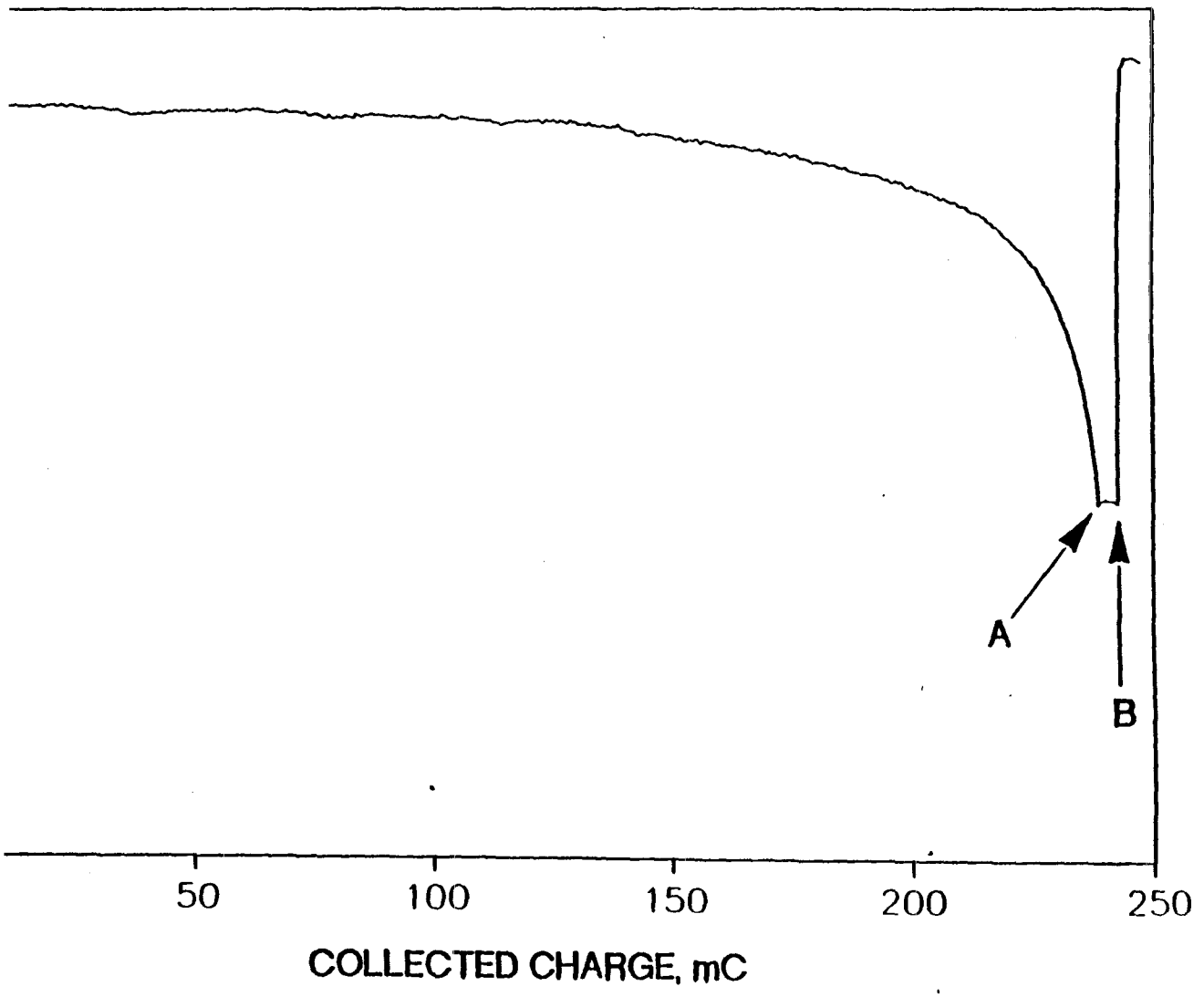
A
B
50
100
150
200
250
COLLECTED CHARGE, mC

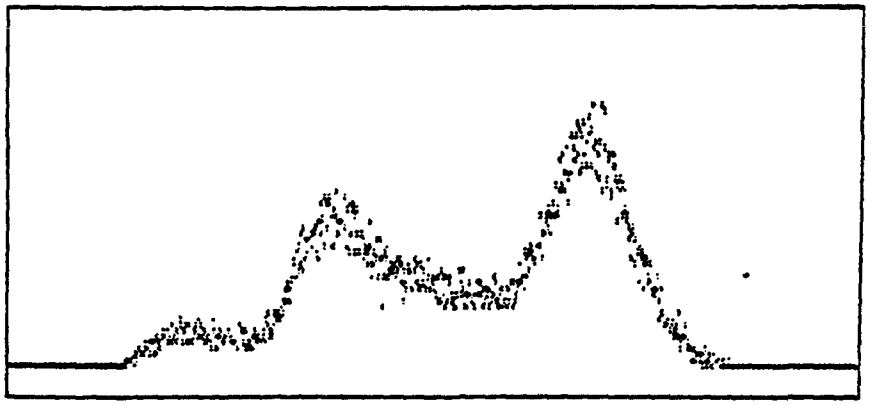

Fig 6

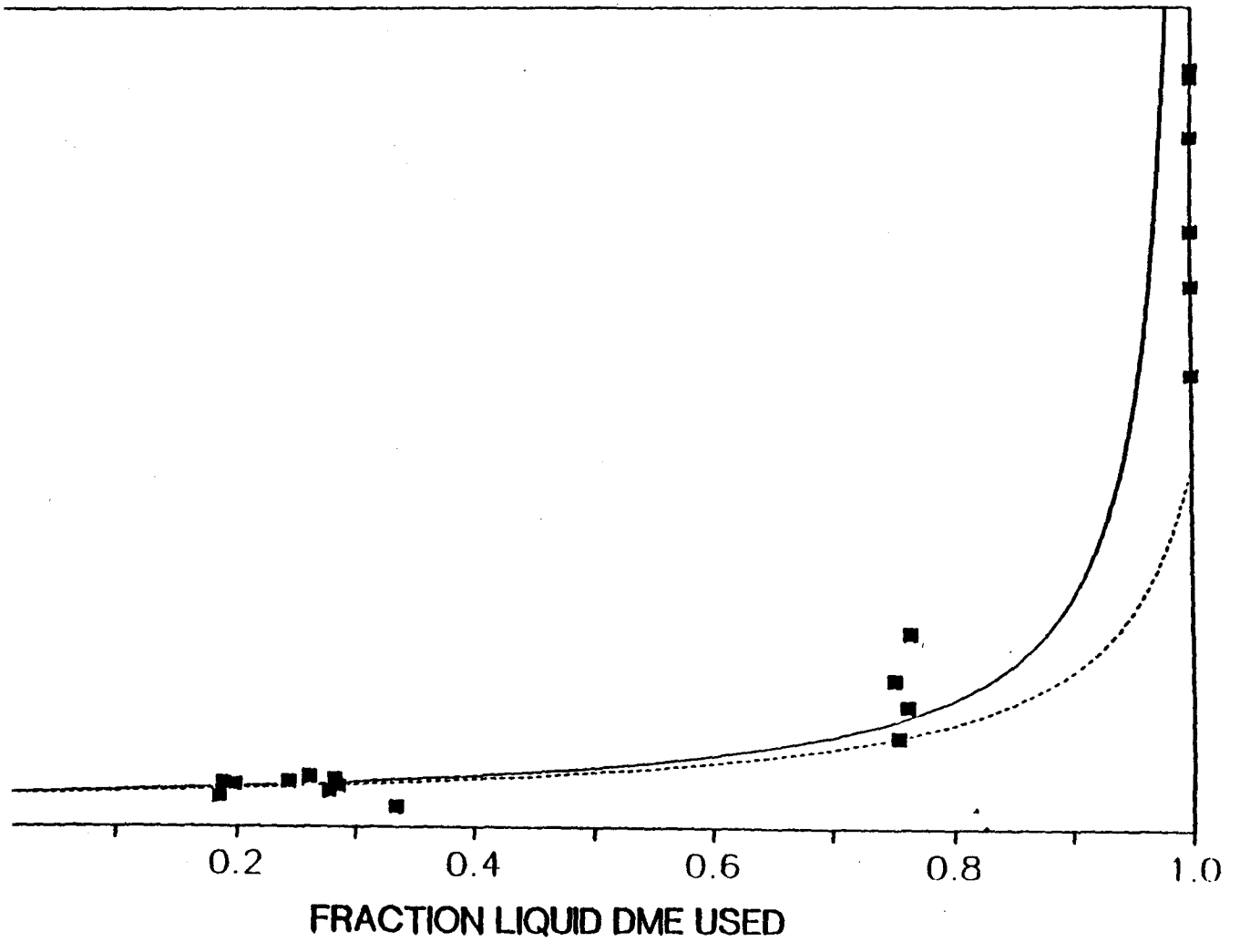
0.2
0.4
0.6
0.8
1.0
FRACTION LIQUID DME USED

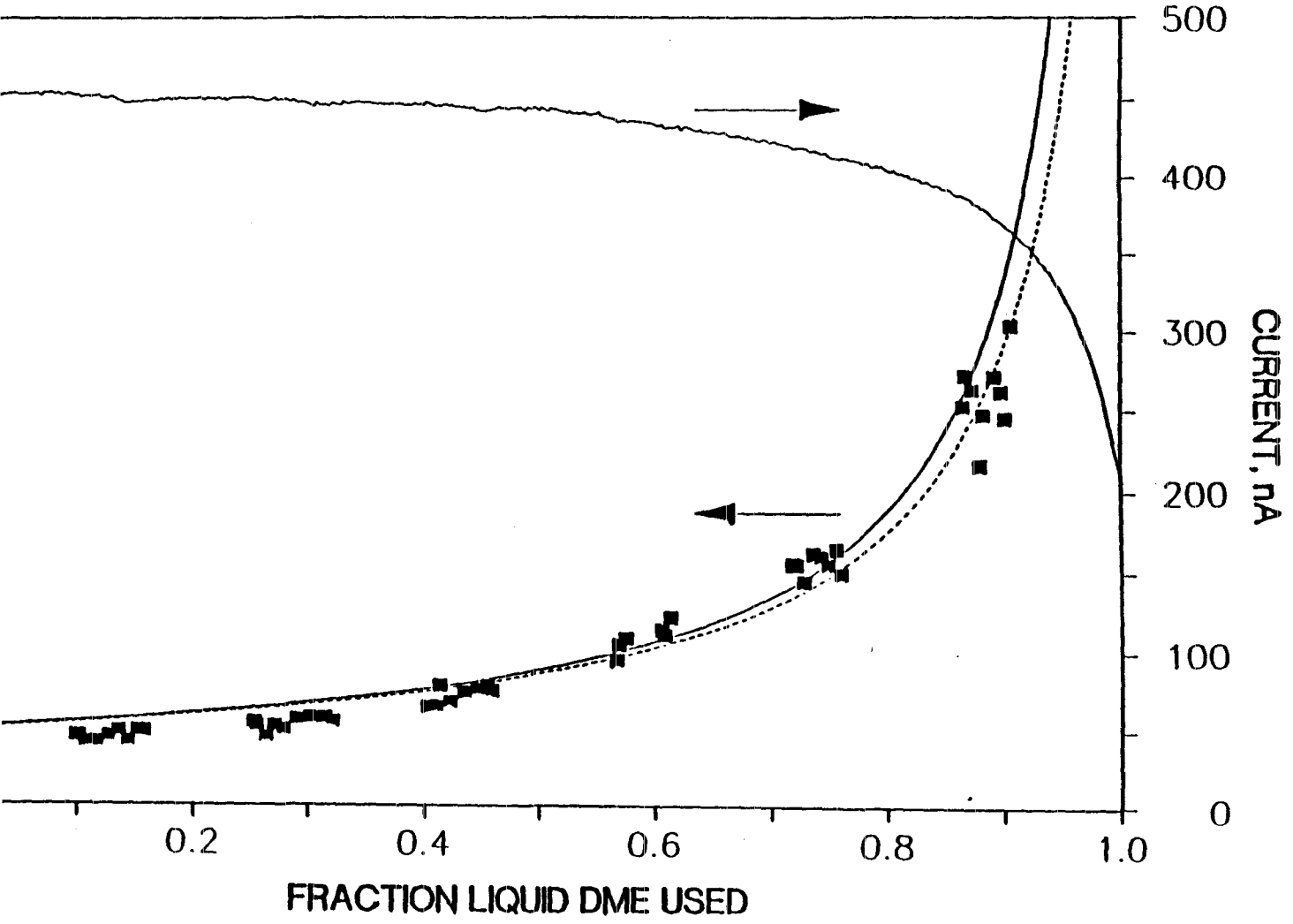
500
400
300
200
100
0
CURRENT, nA
0.2
0.4
0.6
0.8
1.0
FRACTION LIQUID DME USED

A Fast Monolithic Preamp and Shaper for High Rate Gas Tracking Detectors

F. M. Newcomer, S.Tedja, R. Van Berg, J. Van der Spiegel and H. H. Williams
University of Pennsylvania, Philadelphia, PA 19104
I. A. Koullias
AT&T Bell Labs, Reading, PA

Abstract

A fast monolithic preamplifier and shaper optimized for readout of high rate gas proportional tracking chambers at SSC has been designed and prototyped using an AT&T semi-custom bipolar array. The basis of design goals, choice of technology, circuit design and optimization of noise performance for a fixed power ($\approx 15mW$), shaping time(5ns) and dynamic range(50:1) are presented. Simulation results and measurements are compared and discussed.

1 Introduction

At SSC energies a typical interaction will produce at least 100 tracks. The mean number of interactions at each beam crossing will be 1.5 and the crossing rate will approach $60MHz$. Thus the expected number of beam associated tracks will be 10^{10} per second. In detector systems that utilize strong magnetic fields to identify charge and momentum, the density of tracks may double due to the increased path length. Ideally, the tracking volume (about $50m^3$) will be be filled with low mass sensors to catch spontaneous decays and accurately identify the track vectors. If the rate in each sensor is held to a few megahertz and 80 samples of each track are required, at least 10^5 sensors will be needed. Since the tracking system will exist within a tightly closed calorimeter and magnet structure, power dissipation, cabling, packing density and system noise will be critical system design issues.

Small diameter, proportional drift tubes, *straws*, offer excellent potential for high precision, multiple sample measurements. Straw tubes with gas gain of 10 and cathode materials are the focus of several investigations that are attempting to address questions of manufacturability, multiple scattering, electrical conductivity, and mechanical integrity.

Using the known properties of the avalanche signal and the electrical properties of the straw tube geometry, we have designed a preamp and shaper optimized for the requirements of a densely packed straw tracking system at the SSC. The availability of a well developed set of modeling tools has made it possible to accurately predict the performance of these circuits. In this paper we present important aspects of the design cycle from the definition of design goals to the fabrication and measurement of the preamp and shaper in the following sections:

Section 2 - Straw Tube Signal Characteristics
Section 3 - Noise
Section 4 - Pulse Shaping
Section 5 - Available Technology
Section 6 - Circuit Design
Section 7 - Prototype Fabrication
Section 8 - Measured Results

The signal processing electronics discussed in this paper has been designed to to fit within a highly multiplexed power efficient readout architecture proposed by us to allow a nearly deadtimeless operation of the tracking detector [2].

2 Straw tube Signal Characteristics

The measured quantity in a straw tube is the time of

Low ionization statistics (about five clusters/mm, [4]), variations in pathlength for the track through the gas and for the primary ionization clusters to the wire render pulse-height corrections of timing useless. The best timing information is therefore contained in the early part of the signal from the first arriving cluster. This implies that the shaper rise time should be fast and that the mean avalanche gain for a single cluster should produce a signal several times larger than the inherent noise of the front end electronics. The maximum gain is limited, however, to somewhere between 10^4 and 10^5 due to heat dissipation and radiation damage considerations in the high rate environment [7].

To understand the amount of available signal, we examine the time development of the straw pulse. The reader is referred to reference [11] for more detail. The ionization avalanche takes place in the high field gradient region near the wire. Freed electrons produce only a small part of the actual signal since they are at nearly the same potential as the wire. Most of the signal is produced by positive ions as they travel toward the cathode. The time development of this signal depends on positive ion mobility, μ_+, wire potential, V_0, and the geometry of tube with inner radius, b, and wire diameter, a, as given by:

$$\frac{Q}{Q_m} = \frac{\ln(1 + t/t_0)}{2ln(b/a)}, \tag{1}$$

where

$$t_0 = a^2 ln(b/a)/2\mu_+ V_0. \tag{2}$$

For a typical straw tube t_0 is slightly less than 2ns and $2ln(b/a)$ is about 10. After three t_0 (about 5ns), only 14% of the induced charge has been collected. Adding 2% for the electron contribution, only about 16% of the total charge has been collected for a single avalanche cluster. If the wire gain is 10^5, this gives a maximum available signal of 16,000 electrons. For straw tubes with impedance matching termination only half of this charge is available.

We estimated the time resolution using a Monte Carlo technique summing the input signal with random noise and recording the time to cross a selected voltage at the shaper output. Figure 1 shows a simulation result of the effect of intrinsic noise from the straw and preamplifier with multipole shaping on the timing resolution. The signal

Figure 1: The Histogram below is a simulation result sho ing of the effects of intrinsic noise from the straw, amplifier and shaper on timing resolution. The straw t_0 is 2ns, and electronic t_m, 5ns, S/N is 6:1 and the effective threshold is 3 times the RMS noise.

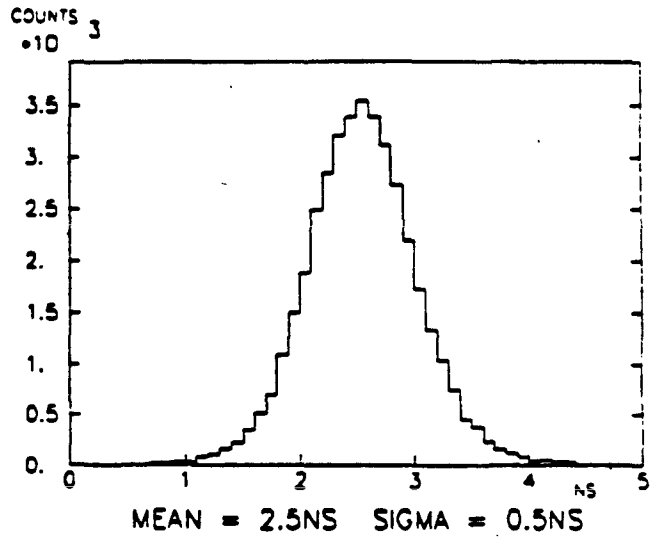

signal to remain over threshold will increase the dead time and therefore the effective occupancy. It is critical for the signal into the discriminator to return to baseline as soon as possible after the arrival of the last avalanche cluster.

With a charge collection time of 5ns, 84% of the signal from each avalanche cluster remains to contribute an unwanted *detector tail*. This may be nearly eliminated by using compensation networks [1, 4]. One concern of these cancellation networks is the saturation characteristic of the electronics. Passive cancellation depends on linear amplification of the input signal. The cancellation should therefore occur as early as possible in the signal processing chain and sufficient dynamic range should be available to handle the largest expected signals from the sensor at that point.

Table 1: Design Goals for Preamp/Shaper.

Total Noise	<2500 R.M.S. electrons E.N.C.
Power	5-20mW per channel
Dynamic Range	5 bits, good saturation recovery
Input Impedance	100-200Ω, $\leq$ straw impedance
Rise Time	5-7ns to minimize time jitter
Double Pulse Res.	<20ns
Packing Density	4 - 16 channels/cm^3

and shaper to limit the effects of process variations and to provides common mode rejection of power supply noise. In the shaper, sensitivity to common mode gain is reduced by the use of current sources in each of the differential stages.

Intrinsic noise sources are generally categorized as *thermal, shot*, and *1/f* noise. With present silicon technologies, only thermal and shot noise contribute significantly to the noise power spectrum for fast shaping times. While a thorough treatment is available in ref [10], it is useful to discuss the calculation of the RMS equivalent input noise charge, ENC_t^2.

Charge collected from the sensor during the measurement time in conjunction with ENC_t^2 can be used to define a signal to noise ratio, S/N, in charge sensitive detectors.

To evaluate intrinsic noise in the signal processing system, sources are assumed to be non-correlated. They are identified and modeled as independent voltage or current sources in *series* or *parallel* with an ideal noiseless amplifier.

Series noise sources such as connection and wire resistance inject voltage noise, e_n, between the sensor and the amplifier. *Parallel* noise sources such as termination resistance add current noise, i_n, between the input and ground.

RMS contributions from each source are summed according to category to produce the total equivalent RMS voltage, ${e_n}^2$, and current, ${i_n}^2$. These are used in conjunction with the desired shaping function to predict the equivalent noise charge, ENC_t^2, and determine the intrinsic S/N for charge sensitive amplifiers. When the shaping function is known, contributions from parallel and series noise sources can be properly weighted and the ENC_t^2 can be calculated using the expression below [9].

parallel noise that dominates ENC_t as is shown in Section 6.2 .

4 Pulse Shaping

As mentioned above, the requirements on shaping are to provide sufficient rise time for leading edge detection of avalanche clusters with sub-nanosecond accuracy, to be capable of retriggering as soon as possible after the passage of a track and to provide sufficient noise filtering to allow operation of the straw tubes at a gain of 10^5 or less. Signals into the discriminator should therefore have both a fast rise and fall time moderated only by noise and power constraints.

Detailed discussion of pulse shaping techniques can be found in references [9, 10]. For this design we have implemented a near Gaussian shaping by adding several equivalent integrations (or poles) in a shaping amplifier following the preamplifier. The preamplifier has one lower frequency pole that is cancelled by the addition of a matching *zero* prior to the shaping stage and one higher frequency pole that can be tuned to match the poles in the shaper or set to a higher frequency. The impulse response for ideal equivalent multipole shaping is given by:

$$V = (\frac{t}{nt_i})^n e^{n-t/t_i} \tag{4}$$

where there are $n+1$ poles or shaping stages with integration time t_i.

This equation is normalized to unity at its peak when $t = nt_i$ and is suitable for use as the weighting function, $h(t)$, encountered in the calculation of the factors α_s and ${\alpha_p}^1$ in the expression for ENC_t^2, (3). The value nt_i is the measurement time, t_m . A graph of this function for several values of n is shown by the solid lines in figure 2. The $n = 1$ curve corresponds to simple *RC-CR* shaping where the differentiation and integration time constants of the preamplifier are equivalent and no additional shaping poles are used. After three measurement times 40% of the pulse remains. In contrast, less than 3% remains for the $n = 4$ curve.

In our amplifier this shaping is realized using three differential stages following the preamp, each with a simple *RC* integration, t_i. The points in the figure show the SPICE simulation result for the fabricated version of the amplifier

Figure 2: Equivalent multiple pole shaping function with simulation data from the prototype shaper.

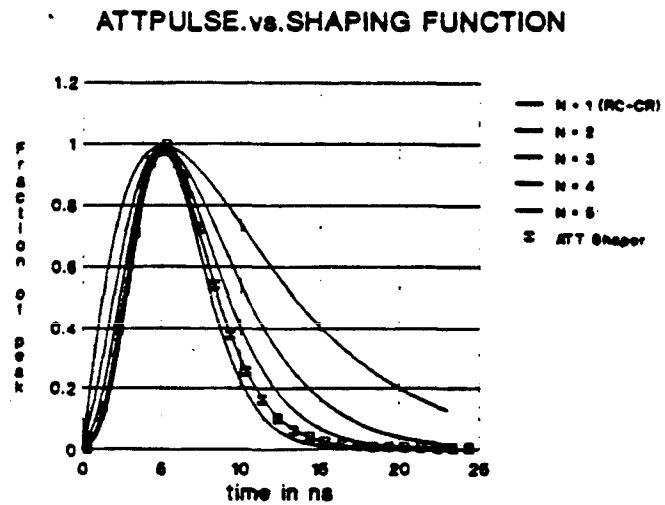

Table 2: Tabulated values are based on equivalent total drain or collector current of 1mA. Note that the large value of input capacitance for the transistor in weak inversion is a result of the low current densities required.

Technology		BIPOLAR	CMOS Strong Inv.	CMOS Weak Inv.
g_m	mS	38	11	25
f_t	GHz	1.6	1.1	0.077
R_{ns}	Ω	26	100	20-50
R_{np}	$k\Omega$	4.5	none	none
C_{in}	pF	3.2	2.0	52

lar are most common. For fast shaping, silicon bipolar offers the best noise and power performance of any available silicon transistor process. Its high intrinsic gain and low value of terminal capacitance make it competitive in power and superior in noise performance when compared with FET and MOS technologies.

Table 2 compares the intrinsic noise of the AT&T CBIC-U bipolar process with a current 1.6μm Leff CMOS technology first optimized for speed and then for noise performance. It should be noted that the base current in bipolar

Table 3: Typical matching and tolerance specifications for semi-custom bipolar integrated circuits.

Transistors		
Param.	Tolerance	
	Absolute	Matching
V_{be}	± 50mV	± 2mV
β	±50%	±5%
$C_{cs}, C_{jc}, C_{je}, C_{pi}$	± 20%	complicated
Resistors		
Type	Tolerance	
	Absolute %	Matching %
P_+	25	1
ab	25	1
NiCr	10	1-5
Capacitors		
Type	Tolerance	
	Absolute %	Matching %
MIM	±30 stray ~ 40	~ 1
MOS Gate	±15 stray~ 30	~ 1

A semi-custom array consists of a mixture of passive and active devices already fixed in position. A design is completed by specifying the choice and connection of components using one or two metalization layers. A third step that allows the deposition of custom thin film resistors is available from some manufacturers.

More expensive semi-custom options include the placement and sizing components allowing the efficient use of chip area and access to a larger range of values for design components. Since a full set of about 20 masks for the silicon processing is required, the cost is usually five to ten times greater than the semi-custom array.

Basic transistor characteristics are specified in terms of gain (β), base emitter voltage drop (V_{be}), base resistance and parasitic capacitance.

Table 3 gives typical tolerance and matching specifica-

Table 4: The Values below were compiled using data from measurements of test resistors on the AT&T ALA201 semi-custom array. Twelve sample chips were selected randomly.

Specified	Resistor type	Average Measured Value	RMS Variation
4kΩ	ab	4.39kΩ	5%
200Ω	P_+	213Ω	1%

the specification and do not tend to be gaussian.

Matching of component values on the same wafer depends primarily on mask geometry. When the components are much larger than the lithographic resolution limits, matching (or ratioing) errors are less than a few percent.

Capacitors may be fabricated simply by overlaping metal from the upper two metalization layers making a metal insulator metal, MIM, structure. This is usually not very accurate in absolute value since the insulation layer is not held to a close tolerance. A more accurate and less flexible capacitance is formed by the fabrication of an MOS transistor with a large area gate. The gate to source capacitance is defined by a thin layer of well controlled oxidation and has a much higher capacitance per unit area than the MIM capacitance.

Resistors are fabricated using P_+ or active base, ab, semi-conductor material and from thin film materials such as nickel chromium. Our measurements of resistance on twelve randomly selected AT&T ALA201 prototype chips from the same wafer are shown in Table 4. We were also able to test on-chip matching of the ab type resistance using a probe station and two 4kΩ resistors in different sub-sections of the array. The worst case on-chip variation measured was 1.25%.

6 Circuit Design

6.1 Preamplifier

Circuit Configuration

Figure 3: Simple Common Base Amplifier.

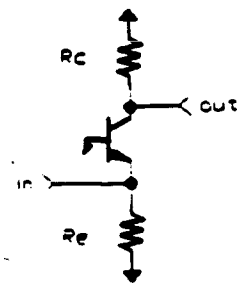

controlled by feedback and is generally higher than the common base configuration at the same collector current. For similar noise performance, at the same collector current, the common base configuration requires about four times as much resistance and dissipates much more power than the common emitter configuration [5]. For this reason, we have chosen the common emitter configuration.

The first three transistors in Figure 4 form a common emitter configuration (A simpler version would omit Q12). Expressions for the significant sources of series and parallel noise are given below:

Parallel noise

$$i_n^2 = 4KT(1/R_{ib} + 1/R_f) \tag{5}$$

where $4KT$ is the thermal noise constant and $R_{ib} = 4KT(\beta/2qI_c)$. In this form, base current contributions to parallel noise can be directly related to the noise in the feedback resistor, R_f.

Series noise

$$e_n^2 = 4KT(r_b + 1/2g_m) \tag{6}$$

where r_b is the base resistance and g_m is the transconductance. ($g_m = i_c/v_t$ where i_c is collector current, and $v_t = 26mV$ at room temperature) Since r_b is geometry dependent, the equation above is useful in optimizing the size of the input transistor.

Figure 4: Common Emitter Preamplifier with dominant pole, $1/R_fC_f$, Zero at $1/2C_sR_e$ and single stage integration, R_tC_o .

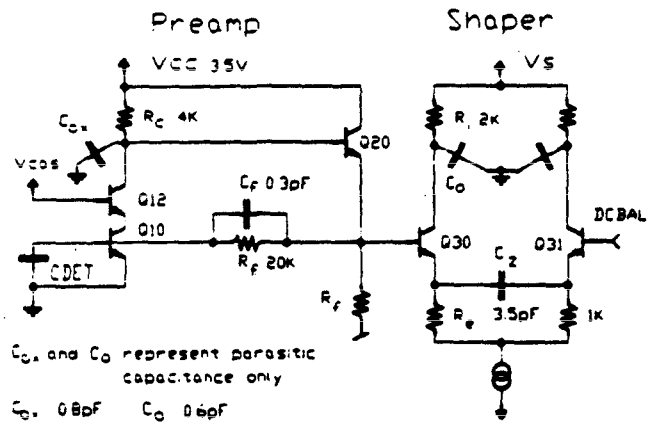

bandwidth. SPICE models for the CBIC-U process indicate that the unity gain bandwidth, f_t, of this transistor is about $1GHz$ at $500\mu A$ of collector current. The cascode transistor, Q12, serves to separate the functions of current and voltage gain. It eliminates Miller effect amplification of Q10's collector to base capacitance, Ccb, by offering a low impedance input for the collector of Q10. Q12 is effectivly a common base amplifier with a capacitance of about $2pF$ at its input (emitter) node. This transistor translates the amplified current signal into a voltage across R_c. By choosing Q12 to be a minimum sized device, the collector current density is increased. This allows operation closer to the peak f_t and minimizes the collector capacitance. The collector node is isolated from the output and the principal feedback by Q20, a voltage follower.

Feedback is applied from the emitter of Q20 to the base of Q10 by a $20k\Omega$ resistor and $0.3pF$ capacitor, completing the transimpedance amplifier. This *Shunt-Shunt* feedback serves to reduce the input impedance and stabilize the gain [6].

The current density in Q10 and Q20 is similar and therefore the base emitter voltage drop, v_{be}, is nearly the same.

The lowest frequency pole of the amplifier is given

$$P_1 = 1/R_f(C_f + \frac{C_{ds}}{g_m R_c}) \tag{8}$$

where $C_{ds} = C_{dst} + C_\pi + 2Ccb + C_f$. $C\pi$ and Ccb refer to intrinsic and parasitic capacitance of Q10.

It can be seen that the open loop gain, $g_m R_c$, is a critical parameter in determining the effect of detector and other stray capacitance on this pole. The open loop gain can be quickly estimated with a knowledege of only the power supply voltage. Ignoring the voltage drop in the feedback resistor and rearranging (7) with $g_m = I_c/v_t$, $g_m R_c \approx (V_{cc} - 2v_{be})/.026$ or about 70. Large detector capacitance is accomodated by raising the power supply voltage, V_{cc}, which increases g_m.

By keeping the term $C_{ds}/g_m R_c$ much smaller than R_fC_f, P_1 is reduced to $1/R_fC_f$. This allows excellent matching for the pole-zero cancellation.

The next higher frequency pole is approximately given by:

$$P_2 = \frac{g_m(\frac{C_{ds}}{g_m R_c} + C_f)}{C_{ds}C_{os}} \tag{9}$$

where C_{os} is the total stray capacitance at the collector of Q12. Increasing the open loop gain pushes the pole to higher frequencies. This pole determines the preamp time.

With the open loop gain much greater than one, the input impedance at frequencies below $1/R_fC_f$ is approximately given by:

$$Rin_L \approx \frac{1}{g_m}\frac{R_f}{R_c} \tag{10}$$

and at high frequencies by:

$$Rin_H \approx \frac{1}{g_m}\frac{C_{os}}{C_{fe}} \tag{11}$$

where $C_{fe} = C_f + C_{ds}/g_m R_c$.

It is useful to note the matching condition for low and high frequency for applications where the preamplifier input impedance must be controlled,

$$\frac{R_f}{\ } \quad \frac{C_{os}}{\ }$$

Figure 5: The plots below show calculated ENC_t for our prototype preamplifier as a function of detector capacitance for different numbers of shaping stages. The noise contribution due to a 300Ω termination resistor in has been included in the lower plot.

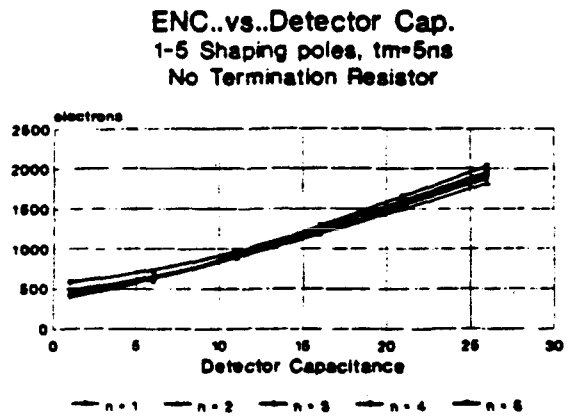

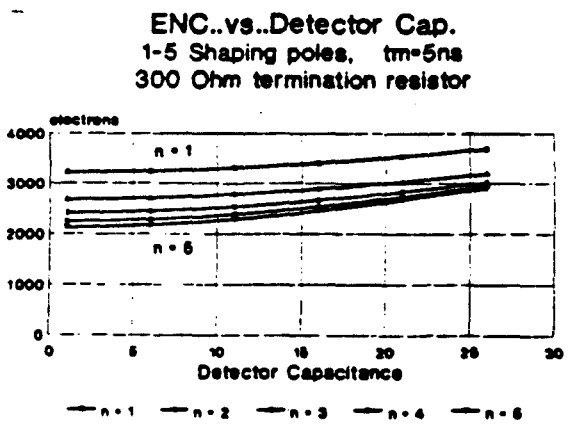

6.2 Shaping Amplifier

Referring to the schematic for the prototype preamplifier, Figure 6, transistors Q11, Q13, and Q21, form a duplicate circuit which has been bandwidth limited to provide a DC balance for input to the differential shaping amplifier.

The shaping amplifier consists of three balanced differential stages. It should be recalled that each stage acts as an independent, matched integration, or pole, to produce

Q31 contains a *zero* intended to cancel the tail due to P_1, (8), in the preamplifier. The value of this zero is given by:

$$Z = 1/2R_eC_z \tag{13}$$

where R_e is the resistance connected to one of the emitters and C_z is the capacitance that is shunt connected between them.

If P_1 is dominated by the feedback elements, the cancellation condition is:

$$R_fC_f = 2R_eC_z. \tag{14}$$

This implies that the accuracy of this cancellation is determined only by the matching of these components. It should be recalled that in integrated circuits, matching of passive components is geometry dependent and usually accurate to within a few percent. In reality, C_f above must be replaced by C_{fs} as defined in (11) if an accuracy of this precision is required.

The ratio C_z/C_f approximately sets the signal gain in the the first stage. To minimize the effects of intrinsic noise from this and following stages, it is necessary to make this ratio much larger than unity. Detailed calculations for the prototype amplifier predict a factor of two difference in ENC_t^2 for ratio values of 2.5 and 5.0 and diminishing gains afterwards as the noise in Q10 begins to dominate.

Shaping Stages

The integration time constant, t_i, in the equivalent multipole shaping equation, (4), is set by the collector resistance and total parasitic capacitance at the collector of each differential pair.

With the collector base capacitance, Ccb, the collector substrate capacitance, Ccs , the interconnect capacitance, C_i, and the collector resistor R_i, the integration time constant is given by:

$$t_i = \frac{1}{R_i(Ccs + 2Ccb + C_i)}. \tag{15}$$

For the last stage, the value of t_i will be about 10% longer due to the size of the output transistor. It is tempting to look into the design for other poles to match $1/t_i$ so that some or all of the shaping stages might be elim-

Figure 8: Input impedance measurement with simulation data superimposed.

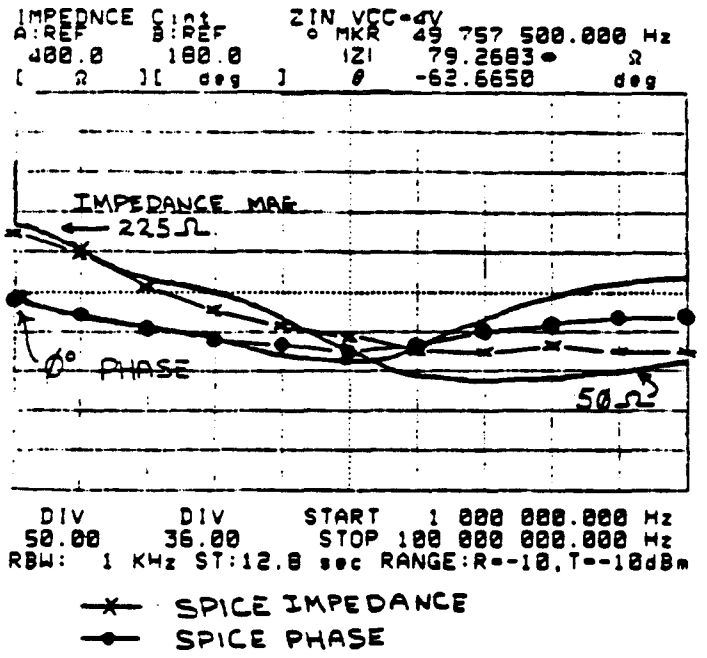

Figure 9: Shaper response for a 1fC input taken by HP54111D digitizing oscilliscope, set to average over 4u pulses.

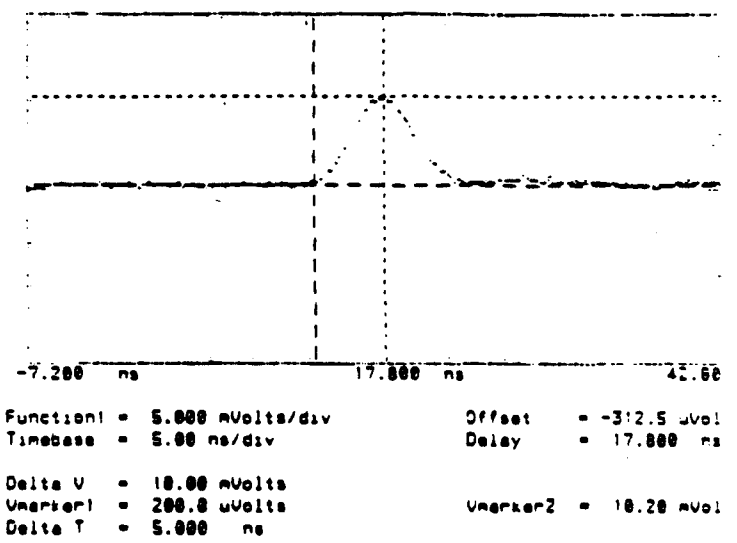

sured using an HP4195A spectrum analyzer with simulation data superimposed.

Figure 9 shows the shaper response for a 1fC input pulse formed by injecting a $1mV$ signal into a 1pF capacitor. The amplitude of this pulse is within 15% of the value predicted by SPICE simulation and is well within range of uncertainty in the measurement.

Noise has been measured using the discriminator efficiency technique described in Reference [8]. In this method a calibrated pulse is input to the preamplifier. The shaper output is connected to a discriminator and the threshold required for 12%, 50%, and 88% efficiency is recorded. The 50% point is used to calibrate the threshold [2] and the values at 12% and 88% are subtracted to find the FWHM of the noise distribution.

In Figure 10, this measurement is compared with the

supply setting was not optimized for the simulations or the measurement, the shaping time is increasing as the detector capacitance goes above $10pF$. The calculation does not account for this and eventually intersects the measured and simulated data.

Measurements with Straw tubes

Figure 11 shows signals at the shaper output with the prototype connected to a 7mm diameter stainless steel straw tube. The straw was filled with P-10 gas and operated at 1600V with a 37.5 μm sense wire. A cosmic ray coincidence was used to trigger the scope. Only about 10% of the triggers were accompanied by signals in the chamber due to the differences in sensitive area. Detected clusters

6.3 Gain

The gain in the preamplifier is largely determined by the size of the feedback capacitor, C_f, when it dominates P_1 and when P_2 is much larger than P_1. The preamplifier responds to an impulse input by placing a nearly matching charge on the feedback capacitor, effectively canceling the signal at the input. The resultant voltage across this capacitor determines the gain. In the fabricated version of the preamp the gain is approximately $2mV$ per femtocoulomb or about 70% percent of what is expected using the simplified explanation above. This allows a comfortable margin in signal to noise, since the equivalent RMS noise voltage at the input to the shaper is less than $100\mu V$.

The gain in the shaper was held to 10 to limit the power. Only the first and third stage have greater than unity gain. The second stage performs level shifting. This allows the differential pair in the output stage to have a high standing current and full dynamic range without saturation. The total gain for the preamp and shaper is then $20mV$ per femtocoulomb.

6.4 Power

The power dissipation in the preamp and balance section is about $6mW$ ($3mW$ per side) and $5mW$ in the shaper, adjusted for detector capacitance of $5pF$. When adjusted for a $10pF$ detector capacitance, simulation shows that V_{cc} must be set to about 4.2V to maintain the $n = 4$ shaping shown in Figure 2. The total power requirement is then about $16mW$.

7 Prototype Fabrication

The prototype amplifier and shaper shown in Figure 6 was fabricated using the AT&T ALA201 semi-custom array. Minimum sized NPN transistors in this array have $15\mu m$ of effective emitter length. The base resistance is typically 75Ω and current gain is 150. The maximum f_t is about $4GHz$ at about $3mA$ of collector current.

The array consists of six tile areas: five are general purpose and one contains power transistors. In each general purpose tile there are seven PNP and twelve NPN transistors. In addition, there are forty-two center tapped resistors ranging in size from 50Ω to $4k\Omega$ and three picofarads of programmable capacitance.

A simple independent driver circuit (see Figure 7) taking

Figure 6: Schematic for prototype preamp and shaper.

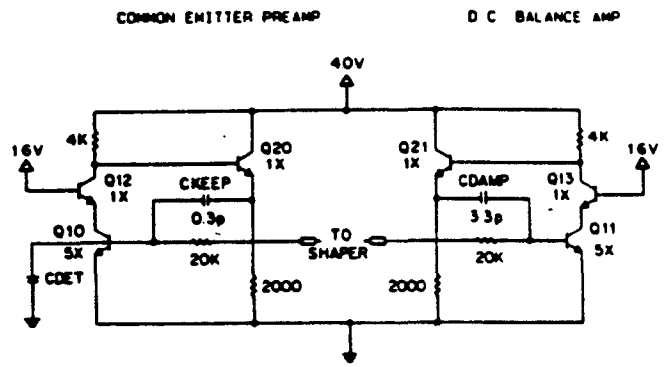

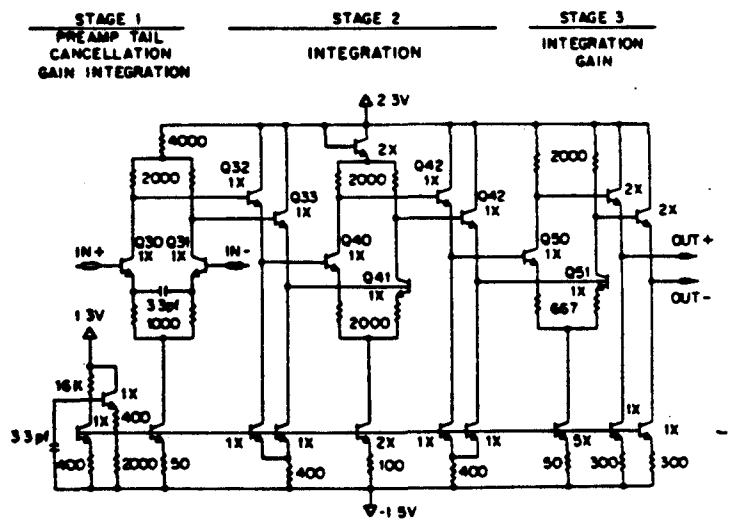

Figure 7: Schematic for line driver circuit.

Figure 10: Comparison of calculated, simulated and measured noise.

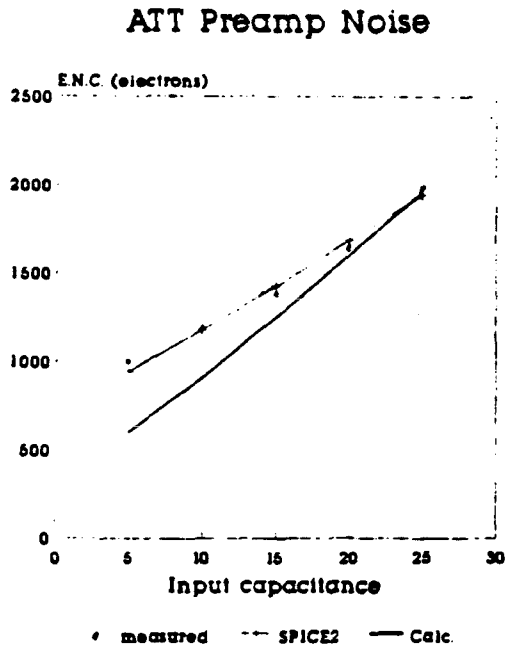

9 Conclusion

The accuracy of SPICE based simulation has been confirmed in the successful design of a fast, low power and low noise preamplifier fabricated using the AT&T ALA201 semi-custom array. Preliminary tests of the prototype amplifier and shaper indicate that the design goals have been met. Our first measurements of the prototype preamp and shaper when attached to a straw sensor suggest that it can detect single ionization clusters with good signal to noise and fast rise times. More detailed measurements must be completed to understand if the signal processing objectives of low gain operation and good position resolution for the instrumented straw sensor can be achieved using this design.

References

[1] R. A. Boie, A.T. Hrisoho and P. Rehak, *Signal Shaping and Tail Cancellation For Gas Proportional Detectors* NIM, A192 (1982) 365 - 374.

[2] L. Callewaert et al., *Front End and Signal Processing Electronics for Detectors at High Luminosity Colliders*, IEEE Transactions on Nuclear Science, Vol. 36 No. 1 (1989) 446 - 457.

[3] D. Christian et al., *The Development of Two ASIC's for a Fast Silicon Strip Detector Readout System*, IEEE Transactions on Nuclear Science, Vol. 36 No. 1 (1989) 507 - 511.

[4] J. Fischer, A. Hrisoho, V. Radeka and P. Rehak, *Proportional Chambers for Very High Counting Rates Based on Gas Mixtures of* CF_4 , NIM, A238 (1985) 249-264.

[5] E. Gatti, P.F. Manfredi, *Analysis of Low Noise, Bipolar Transistor Head Amplifiers*, NIM, A226 (1984) 142 - 155.

[6] P.R. Grey and R.G. Meyer. *Analysis and Design o, Analog Integrated Circuits* John Wiley & Sons, New York, second edition 1984.

[7] G.Hanson et.al., *Wire Chamber Requirements amd Tracking Simulation Studies for Tracking Systems at the SSC*, NIM, Vol. A283(1989) 735-743.

[8] P. Jarron M. Goyot, NIM, A226 (1984) 156 - 162.

[9] V. Radeka, *Signal, Noise and Resolution in Position-Sensitive Detectors*, IEEE Transactions Nuclear Science, Vol. 21 No.1 Feb. (1974) 51 - 64.

[10] V. Radeka, *Low Noise Techniques in Detectors*, Annual Reviews of Nuclear and Particle Science, Vol. 38

Figure 11: The plots below are selected output waveforms captured using the HP5111D digitising oscilliscope connected to the prototype shaper output. The preamplifier is connected to a 7mm straw tube with a 37.5μm berrillium copper wire at 1600V. A scintillator coincidence was used to trigger the scope. All but one of the plots below were selected due to the presence of signal. The arrival of seperate clusters is clearly indicated.

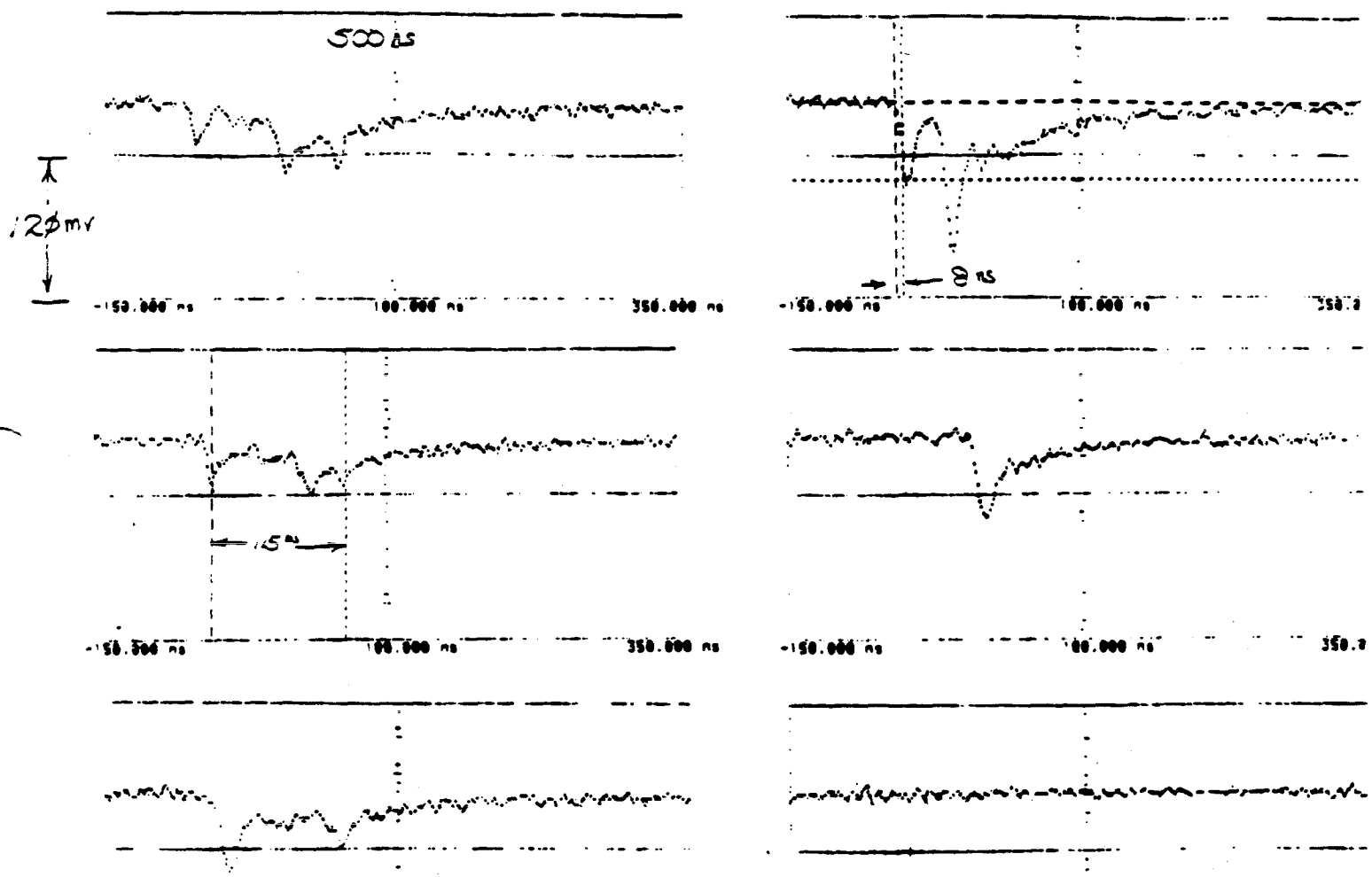

Modeling Small Diameter Straw Tubes in Terms of their High Frequency Electrical Characteristics

Tor Ekenberg and Mitch Newcomer
University of Pennsylvania
Philadelphia, PA 19104

29 January 1990

Abstract

As a part of the effort to design a prototype of a low mass tracking detector, we have developed an empirical model of the high frequency behavior of small diameter proportional *straw* tubes. The equivalent circuit is a distributed network of RLC-clusters, where the value of the discrete components is directly related to measurable characteristics of the em straws.

The model is an approximation of the *straw* as a low loss transmission line, and yields very good agreement with measurements of transmission and reflection coefficents. Measurements and simulations of input impedance in frequency domain also agree well at frequencies below 120 MHz, when termination is close to Z_0, the characteristic impedance.

Introduction

Recent emphasis on the need for low mass tracking detectors at high luminosity particle accelerators has led to an interest in the development of thin walled, small diameter gas proportional *straw* detectors.

Advanced modeling tools for electronic circuits allow us to very accurately simulate the behavior of amplifiers interfacing the drift tubes. In order to optimise the performance for low noise, low power, and fast response it is necessary to incorporate the tube as a circuit element in the design process.

It is attractive to be able to model a *straw* tube as a

impedance,

$$Z_o = R_o = \sqrt{\frac{L}{C}}.$$

L and C are the inductance and the capacitance per unit length. A complete discussion of transmission line theory is given in ref. 1. The delay time, t_d, is defined as $t_d = l\sqrt{LC}$, where l is the length of the transmission line and L and C are defined as above. If the termination is different from Z_0, part of the wave will be reflected. The reflection coefficent ρ, defined as $V_{out} = \rho V_{in}$, is given by

$$\rho = \frac{R/Z_0 - 1}{R/Z_0 + 1}.$$

A lossy transmission line is characterized by two additional terms: R, anode resistance per unit length, and G, related to the leakage current through the dielectric [2]. In this case the termination is

$$Z_o = R_o + \frac{1}{j\omega C_o},$$

with C_o given by

$$C_o = \frac{2\sqrt{LC}}{R - G(L/C)}.$$

A lossy transmission line also has an attenuation associated with it,

$$V = V_{in} \exp^{-As}$$

where

$$A = \frac{1}{2}\left(\frac{R}{\ }+G\sqrt{L/C}\right)$$

and

$$C_o = \frac{2\sqrt{LC}}{R}.$$

For high frequencies ϕ_e tends towards zero as can be seen in the equation below

$$\phi_e = \tanh\left[\frac{1}{2}\sinh^{-1}\left(\left|\frac{R}{\omega L}\right|\right)\right].$$

Our investigation shows to what extent this model is valid for small diameter *straws*.

Procedure

To perform this test we constructed a three-dimensional measurement matrix where the dimensions represented cathode resistance, anode diameter, and length of *straws*.

Two values of cathode resistance were used: commercially avaliable stainless steel tubes with a resistance of $0.02\ \Omega/m$, and $50\ \mu m$ aluminized mylar *straws* [3] with resistance of $120\ \Omega/m$. Both mylar *straws* and stainless steel tubes had an inner diameter of $6.9\ mm$.

The anode wire was gold-plated tungsten at three different diameters: $25\ \mu m$, $50\ \mu m$, and $62.5\ \mu m$. See Table 1 for wire diameters and associated resistance, capacitance, and inductance.

Measurements were made for *straws* of length $429\ mm$, $861\ mm$, and $1291\ mm$.

Transmission and reflection measurements were made with an HP 54111D oscilloscope. Input impedance as a function of frequency was measured with an HP 4195A Network/Spectrum Analyzer.

Analog modeling was performed with SPICE on an IBM 3090 by fitting output from the circuit simulator to the measurement data.

The model suggested by transmission line theory is a network of linked RLC-clusters (see Fig. 1), each representing a differential length element of the line. The value of each element in the individual cluster is simply the value for the whole *straw* divided by the number of clusters. When calculating attenuation and termination capacitance, the ground path resistance and anode resistance was combined.

Results

Equivalent circuits with 20 clusters per meter provide a good compromise between accuracy and computing cost.

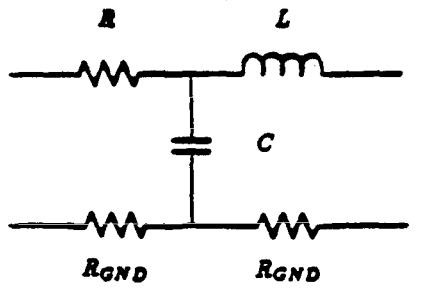

Figure 1: Individual RLC-cluster for transmission line model of *straw* tube. Values for a simulation of a 429 *mm straw* with anode diameter of $50\ \mu m$ and cathode resistance of $120\ \Omega/m$: $R = 0.69\Omega$, $C = 0.24pF$, $L = 21nH$, and $R_{GND} = 1.29\Omega$.

Models with fewer elements gave a poor fit to the data, while expanding the number of sub-circuits up to 1000 per meter increased the computer time by several orders of magnitude and provided only a few percent better agreement.

Simulations in SPICE of this model in the time domain show good agreement with data (compare Fig. 2 and Fig. 3). In frequency domain there is very good agree-

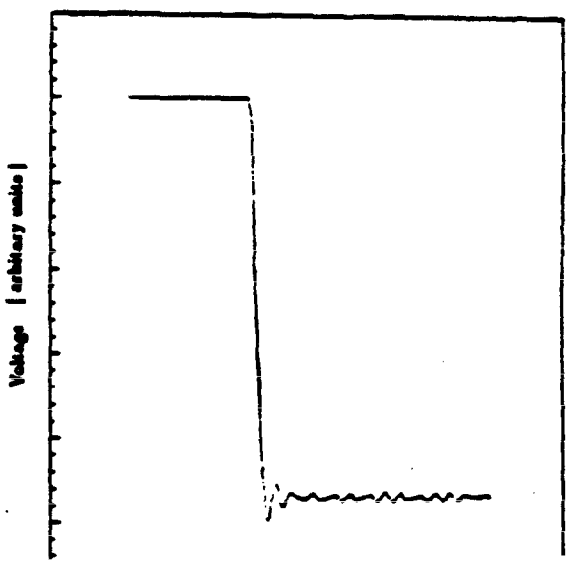

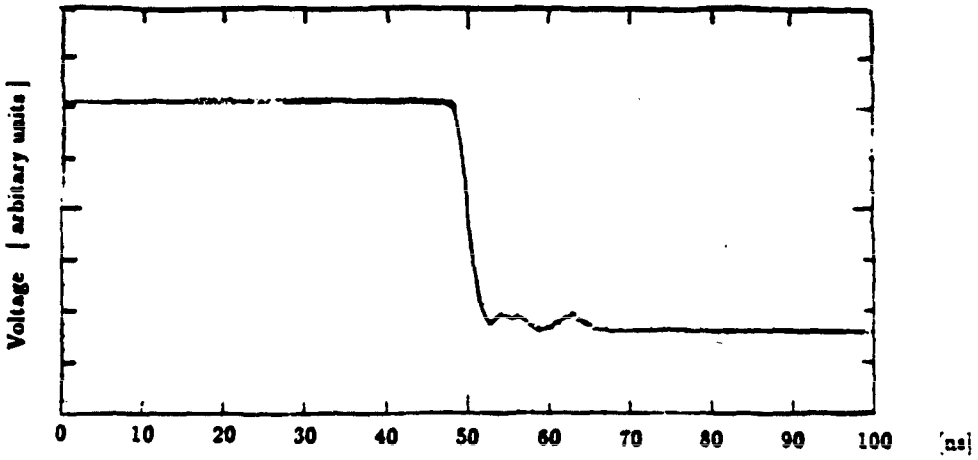

Figure 3: Measurement of step response at output of 1291 *mm straw*.

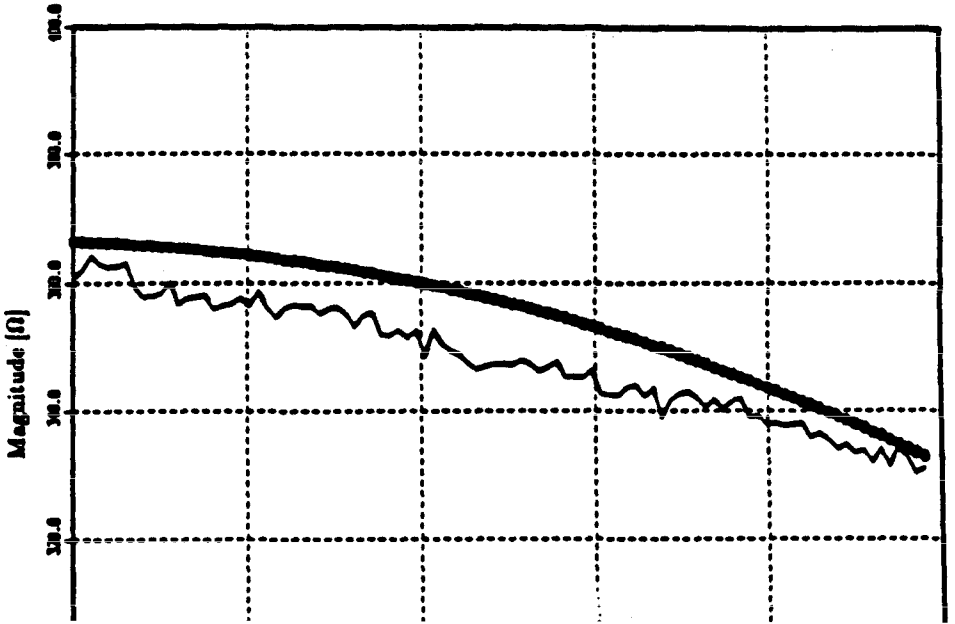

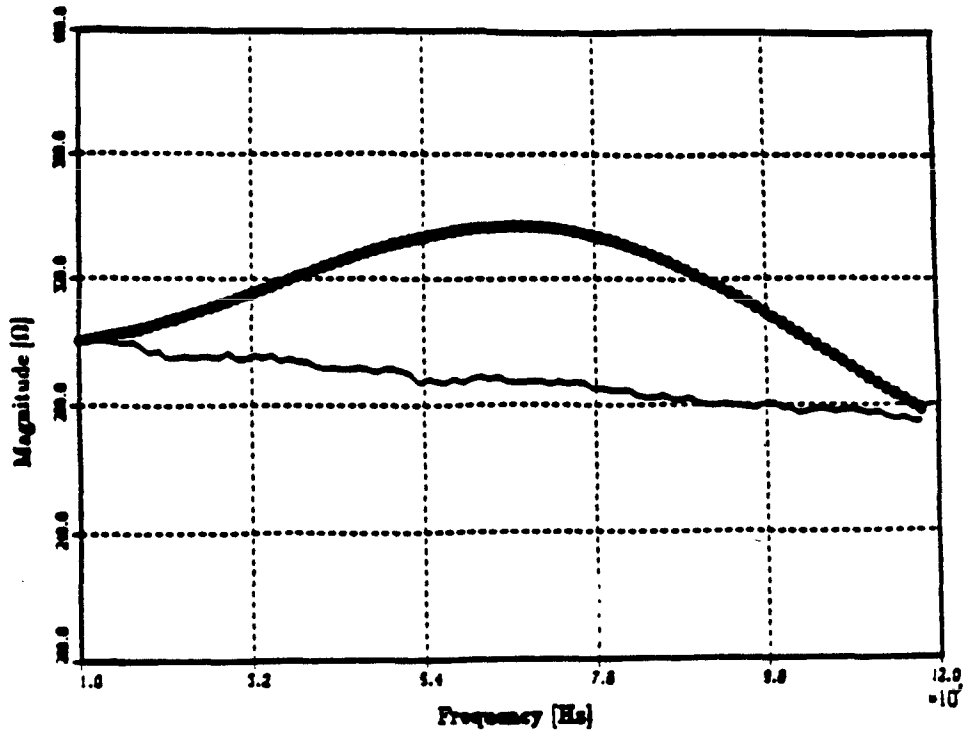

Figure 5: Comparison between measured and simulated (heavy line) input impedance (magnitude) for 861 *mm straw* with low cathode resistance and 50 μm anode diameter when terminated 10 percent away from correct termination.

ments were made with both $Z_o = R_o$ and with a complex termination, $Z_o = R_o + 1/(j\omega C_o)$. The complex termination is better, i.e. Z_{in} is closer to constant over frequency, but both cases give very good agreement between measurements and our model.

Conclusion

The empirical model we have developed is valid up to 120 MHz, if termination is close to Z_o. The results of the simulations with 20 RLC-clusters per meter agree within 5 percent of the measured characteristics.

At frequencies above 120 MHz and when termination is different from Z_o, simulations deviate strongly from measured data. Since our range of interest is only up to 100 MHz (signals with rise times of ~5 *ns*), we have not investigated the discrepancies above 120 MHz. The probable cause for the disagreement is parasitic capacitance and unaccounted for inductance.

The good agreement between our equivalent circuit and measurements makes this model a useful tool for design-

This work was funded in part by The Nassau Undergraduate Research Fund, University of Pennsylvania.

References

[1] R. W. P. King, *Transmission-line Theory*, McGraw-Hill (1955)

[2] D. H. Swant, *A Transmission Line Model for Use with Transient Analysis Computer Codes*, MSEE thesis, University of Pennsylvania, May 1973

[3] W. W. Ash, et al., *Design, Construction, Prototype Tests and Performance of a Vertex Chamber for the MAC Detector*, Nucl. Instr. and Meth. A261(1987) 399

KEK Preprint 90- 54
June 1990
H/D

Development of TMC Chip and On-Chip Processing

Yasuo ARAI
KEK, National Laboratory for High Energy Physics
1-1 Oho, Tsukuba-shi, Ibaraki-ken, 305, Japan

National Laboratory for High Energy Physics, 1990

KEK Reports are available from:

Technical Information & Library
National Laboratory for High Energy Physics
1-1 Oho, Tsukuba-shi
Ibaraki-ken, 305
JAPAN

Phone: 0298-64-1171
Telex: 3652-534 (Domestic)
(0)3652-534 (International)
Fax: 0298-64-4604

Development of TMC Chip and On-Chip Processing

Y. Arai
KEK, National Laboratory for High Energy Physics
1-1 Oho, Tsukuba-shi, Ibaraki-ken, 305, Japan

Introduction

In the time measurement system of drift chambers at SSC, low-power and high-density TDC chip is required for frontend electronics. If the circuit is composed of mostly digital circuit, further processing within the chip will be possible. Particularly in large scale electronics system, digital circuit is preferable compared with small voltage analogue electronics. Furthermore, it will be easier to buffer and move the data in multi-level trigger scheme.

To realize the above functions, idea of the TMC was born in 1986 [1] and a test chip was produced in 1988[2,3]. Encouraged at the success of the test chip, a first useful chip (TMC1004) was designed and will be available soon. The TMC1004 includes 4 channels of circuits and each channel has 1024 bits time memories. Timing resolution of the chip is 1 ns and stores 1 μs data inside the chip. Technology used for TMC is 0.8 μm Bi-CMOS process, and about 100,000 transistors are implemented in 5.0 mm by 5.6 mm chip area. Total power consumption for a channel is estimated at about 7 mW for 100 kHz trigger rate.

There are many directions to extend the ability of the TMC chip. One direction is to include data processing capability such as track finding and T0 finding. Another direction is to improve performance; increase the number of channels in a chip, improve timing resolution, extend capacity of the memory. In addition to these possibility, it may be possible to include preamp / shaper / discriminator circuits in the same chip as the TMC, because the present process already has excellent bipolar transistors.

In this paper, I will describe about the design and expected performance of the TMC1004 chip. I will also discuss about future possibility of the trigger and data processing within TMC chip.

Design of TMC

Detailed descriptions of the TMC circuit are presented in several places[1,2,3,4], so only a brief description is given here. Main components of the TMC are memories and controlled delay elements as shown in Fig.1. Write signal for the memories are delayed 1 ns for each memory, so the input signal transition is recorded in the memory. Block diagram of the TMC 1004 is shown in Fig.2. The chip has 4 channel of circuit and each channel has 32 rows times 32 columns time memory cells. To point write row and read row, there are two counters which are counted up with external clock. Initial offset of these counter , which is set through CSR registers, is corresponds to trigger decision time.

Each delay element is controlled by referencing external clock of 32 ns period. Fig.3 shows the characteristics of the delay element. If the delay time is not controlled, the delay value will change more than 20% with variation of power supply voltage, temperature and transistor threshold. By controlling a gate voltage (Vg) of the delay element by the feedback circuit, the delay time will be kept within 3%.

Data are readout in 32 bit parallel and encoded to 6 bit in 32 ns pipeline cycle. This enables us

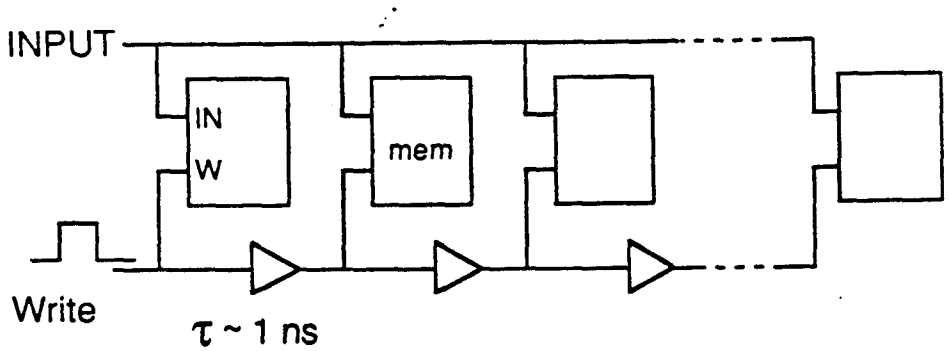

Fig.1 Basic configuration of the TMC

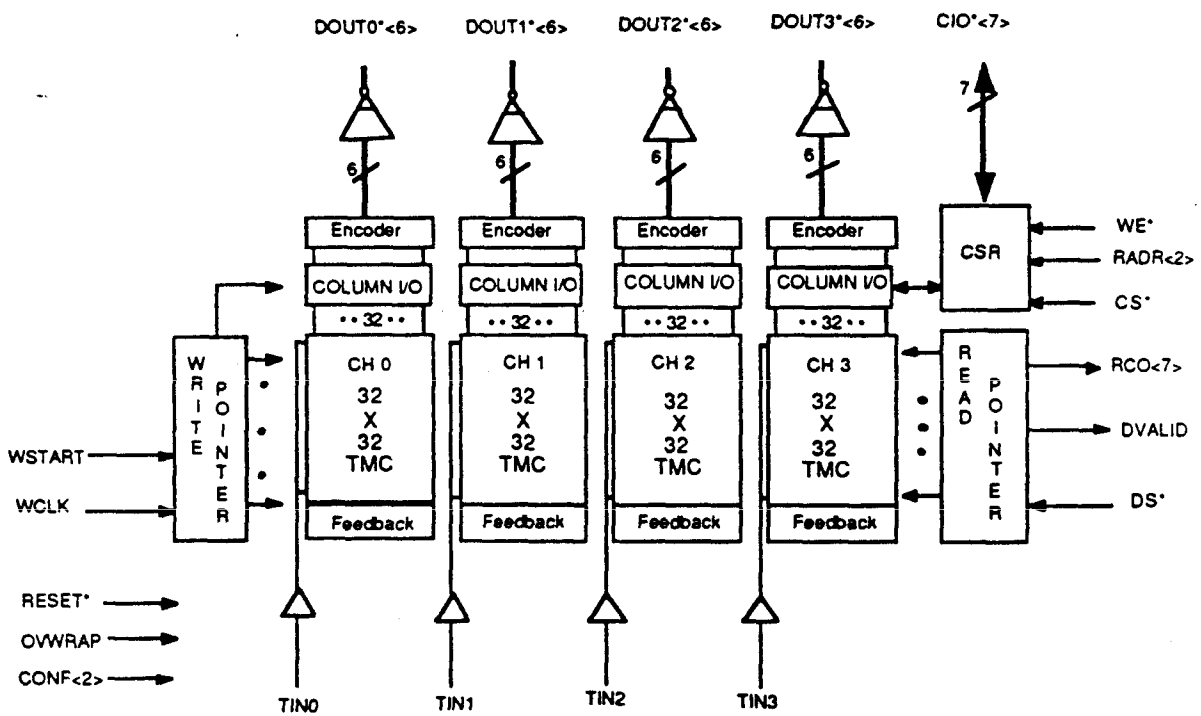

Fig.2 Block Diagram of the TMC1004

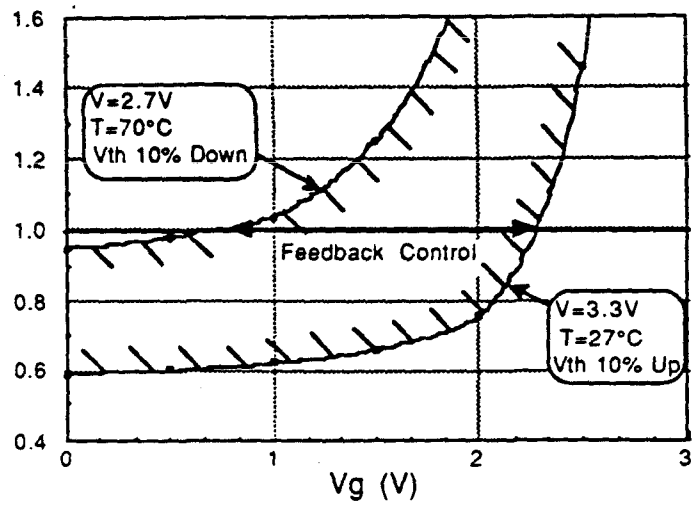

Fig.3 Delay characteristics of the delay element.

Table 1 Data Encoding Logic. Detect 0 to 1 position, and encode the position. Bit 5 of the encoded data represents the contents of the bit 0 data.

Bit Pattern	Encoded Data
3322222222221111111111 1098765432109876543210987654321 0	5 4 3 2 1 0
0000000000000000000000000000000000	0 0 0 0 0 0
xxxxxxxxxxxxxxxxxxxxxxxxxxxxxxxx10	0 0 0 0 0 1
xxxxxxxxxxxxxxxxxxxxxxxxxxxxxxx100	0 0 0 0 1 0
xxxxxxxxxxxxxxxxxxxxxxxxxxxxxx1000	0 0 0 0 1 1
:	:
1000000000000000000000000000000000	0 1 1 1 1 1
1111111111111111111111111111111111	1 0 0 0 0 0
xxxxxxxxxxxxxxxxxxxxxxxxxxxxxxx101	1 0 0 0 1 0
1xxxxxxxxxxxxxxxxxxxxxxxxxxxxx10x1	1 0 0 0 1 1
:	:
10xxxxxxxxxxxxxxxxxxxxxxxxxxxxxxx1	1 1 1 1 1 1

(x..xx..x = 1..10..0)

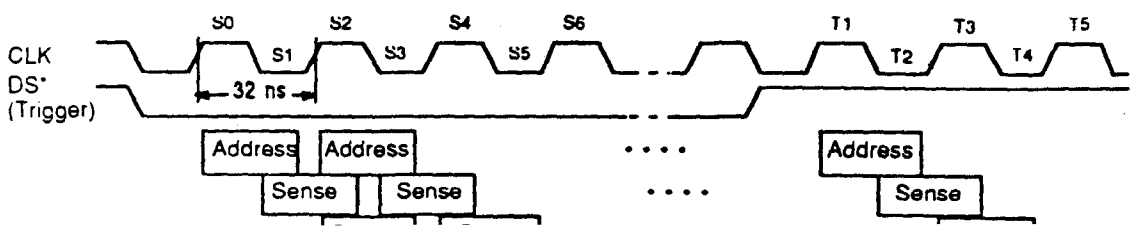

Most power consuming part of the TMC is sense amp circuit. Because each channel has 32 sense amps, there are 128 sense amps in a chip. Sense amp has DC current path, and consumes about 2 mW, so in total it consumes about 256 mW. As the readout operation is required only when trigger comes, the DC current path is cut while not reading. Power consumption was estimated and plotted as shown in Fig.5. The power consumption is depend on trigger (read out) rate. For 100 kHz trigger rate and read out data in 4 rows (128 bit), power consumption of a channel is estimated at about 7 mW. This is order 2 less than the ordinary shift register circuit.

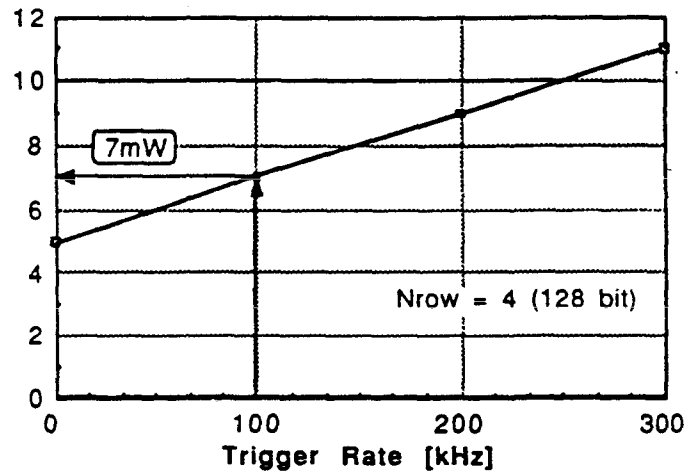

Fig.5 Estimated power consumption vs Trigger rate

Although the TMC1004 is designed to have 1 ns time resolution, it will be possible to improve time resolution. Direct way is to use more fine lithography such as 0.5 μm technology. Another method is to construct the TMC cell using bipolar and CMOS transistor, or use two delay lines and take the difference of these lines. These technique will enable us to get 0.5 ns time resolution.

The area of the present chip is only 5 mm by 5.6 mm. Even if we double the number of channels (8 channel), and expand the memory capacity to 4 times larger (4 k bit), the circuit can be contained in a 10 mm by 12 mm chip.

Trigger / Readout Processing

One attractive feature of using the VLSI chip in frontend is the possibility to include trigger logic in the chip. Here I will show some examples for stiff track finding and T0 (track passing time) finding inside the TMC chip combined with the straw tube central tracker.

Track trigger in central tracker and muon chamber has been extensively studied by J. Chapman[5] by using track synchronizer method. He used analog method in which current source/sink and capacitor are used to calculate T0 timing. This T0 finding method can be implemented more easily in digital way by using controlled delay element of the TMC. Fig. 6 and 7 shows the simplified scheme of Stiff track and T0 finding method.

Stiff track can be found by taking coincidence in a superlayer of straw tubes. If we take 3 out

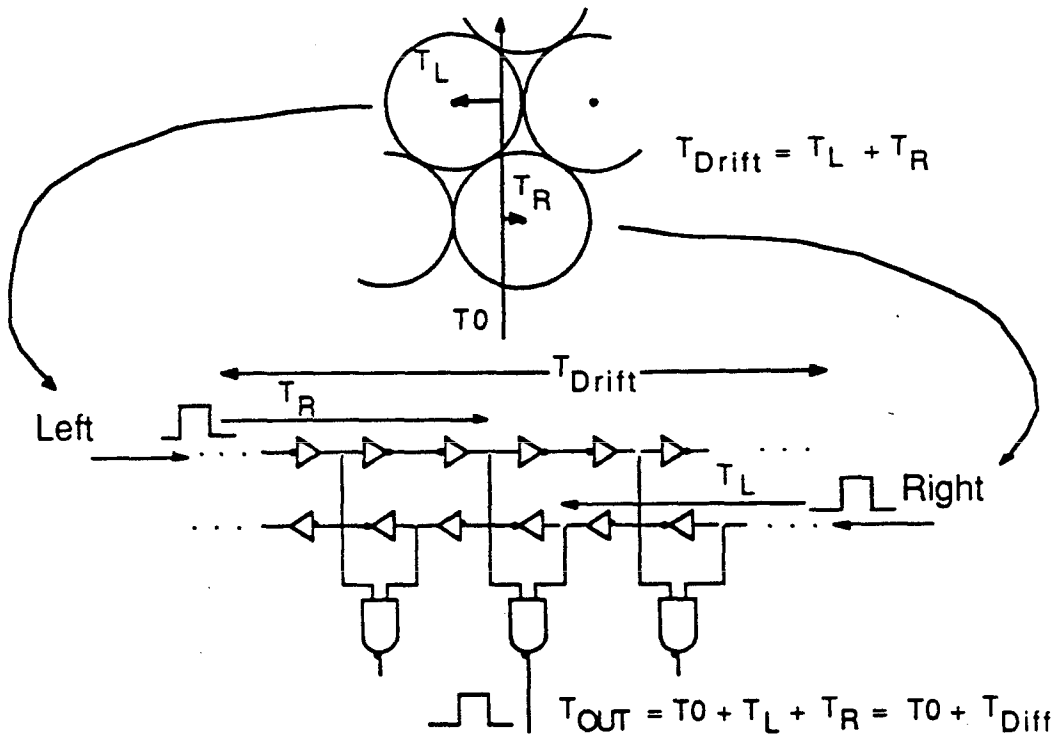

Fig.7 T0 Finding scheme

In table 2, characteristic figures of straw tube central tracker is shown. Hit rate was taken from the simulation of M. Asai[7]. Rapidity coverage of the chamber is assumed to be η=1.65 and maximum length of tube is 3 m. Each tube is divided in 2 at z=0. Time jitter and walk are calculated from naive approximation of initial signal. Jitter and walk seems to be manageable value due to the dividing of tube and using of low noise preamplifier[8]. However, the hit rate seems still to be high.

Summary

A new TDC chip which can be used in SSC environment was developed and available soon. The chip was designed to work in deadtimeless readout scheme and multiple trigger in a detector response time. The chip also has many possible features to include local trigger / data processing.

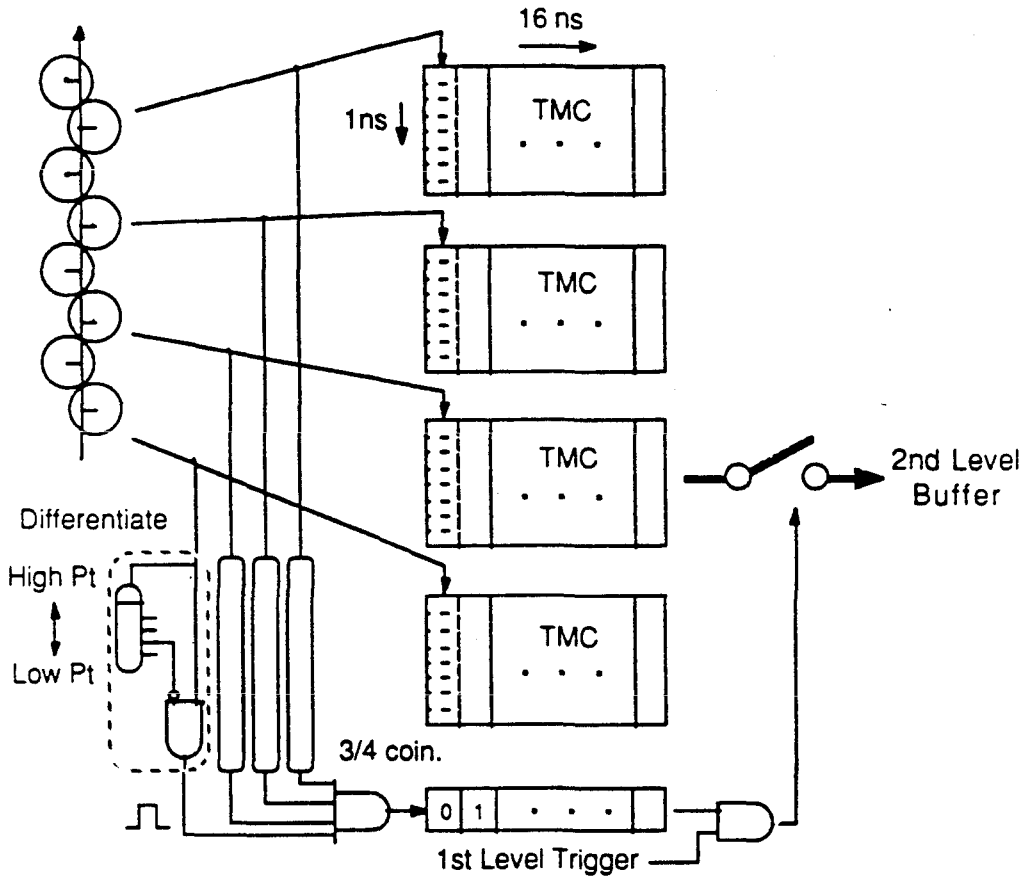

Fig.6 Stiff Track Readout Scheme

To get T0 information in the first level trigger, we can use the fact that sum of the drift time for left and right side (T_L and T_R) is almost constant for high momentum track (Fig.7). By implementing two delay line of which length is same as the maximum drift time of the tube, left and right signal coincidence at $T_{OUT} = T0 + T_L + T_R$. Because the sum of the T_L and T_R is equals to maximum drift time (T_{Drift}), T0 value is available as position of coincidence bit. T0 finding may be combined with stiff track finding, and one T0 value can be get for a track in a superlayer.

This method is also applicable for Z position finding by measuring the timing at the both ends of the tube. Z coordinate measurement by time difference has several advantage from stereo wire method. At first, the number of layers can be reduced to half. This also reduce the material in the central tracker. The number of total electronics channel is almost same. As the same readout electronics will be implemented at both sides, the electronics has redundancy. So even if one side of electronics has broken, we still be able to get r-phi information from the tube. Timing accuracy can be improved, because the pulse height variation is compensated for both ends signal. To get

Table 2. 4 mmϕ Straw characteristic figures. (xd : track distance from anode wire)

r [cm]	60	80	100	120	140	160
Hit Rate [MHz]	4.5	3.9	2.7	1.5	0.84	0.27
Length [m]	1.77	2.35	2.94	3.0	3.0	3.0
I/wire [mA]	1.38	1.20	0.83	0.46	0.26	0.08
Charge [C/cm/5year]	0.39	0.26	0.14	0.08	0.04	0.01
Capacitance [pF]	19.4	25.8	32.2	32.9	32.9	32.9
ENC [e]	1530	1800	2100	2100	2100	2100
xd=0mm Jitter [ns]	0.26	0.31	0.35	0.36	0.36	0.36
Walk [ns]	0.47	0.55	0.63	0.64	0.64	0.64
xd=1mm Jitter [ns]	0.12	0.14	0.16	0.17	0.17	0.17
Walk [ns]	0.21	0.25	0.29	0.30	0.30	0.30

(Gain=4×10^4, measuring time=5ns, Qs(xd=0mm)=30000e, Qs(xd=1mm)=67000e, Fast Gas (100μm/ns), 25μϕ wire, ATT Preamp, No magnetic Field)

References

[1] Y. Arai and T. Ohsugi; "An Idea of Deadtimeless Readout System by Using Time Memory Cell", Proceedings of the Summer Study on the Physics of the Superconducting Supercollider, Snowmass, (1986)455.

[2] Y. Arai and T. Baba, "A CMOS Time to Digital Converter VLSI for High-Energy Physics", 1988 Symposium on VLSI Circuits, Aug. 1988/Tokyo, IEEE CAT.No. 88, TH 0227-9, p121.

[3] Y. Arai and T. Ohsugi, "TMC - A CMOS Time to Digital Converter VLSI", IEEE Trans. on Nucl. Sci. Vol.36, No.1 (1989)528

[4] Y. Arai, "Time Measurement System at the SSC", Workshop on Triggering and Data Acquisition for Experiments at the Supercollider", Toronto, (1989)125. SSC-SR-1039.

[5] J. Chapman, in this workshop.

[6] T. Ohsugi, M. Asai and Y. Arai, "On-chip Filtering of Low Pt Track with Straw-Tube Chamber", HUPD-9003, JSD-NOTE-1990-3.

[7] M. Asai, in this workshop.

[8] F. M. Newcomer, private communication.

Synchronizer Development Update

J. Chapman
University of Michigan
Ann Arbor, MI 48109 USA

Introduction

As an outgrowth of work on the question of tracking and triggering options for drift tube devices in the SSC environments[1] , I discovered that very simple circuits could be implemented that held promise for first level triggering at the SSC[2] . These circuits were named "Synchronizers"[3] since they output a signal that is synchronized with the particle passage after a delay time equal to the maximum drift time of the cells used. This synchronized signal makes fast coincidence possible between axial and stereo layers for z determination and collision tagging for crossing determination. This presentation us an update of the program to explore the usefulness of these circuits and to construct versions of the circuit in Application Specific Integrated Circuits, ASICs. We have fabricated and tested at the most preliminary level, the first version of the circuit.

Circuit Concept

I will first review the features of the synchronizer circuit and then summarize the work of the past 8 months. The circuit accepts input from three 1/2 cell staggered layers of drift tubes. See figure 1 for two patterns of such tubes, the first (a) show the pattern as constructed from closely packed straw tubes and (b) shows the pattern manifest from rectangular tubes. The extreme pair of the three tubes are assumed to be radially aligned. In both cases the drift times that result from the passage of a straight track can be mathematically related. In the case of a linear drift-time distance relationship, the equation takes on the simple form:

of the last wire signal so that the total time from particle passage to the end of the wait period is always equal to a fixed time. This is electronically possible since the wait time can be calculated from the equation above using only drift time differences. When rewritten by adding and subtracting terms, the time equation takes on a form that exhibits a one to one relation to components of the synchronizer. This difference equation is of the form;

$$\frac{|t_3 - t_1|}{2} + |t_2 - \text{largest of}(t_3, t_1)| + 2t_{wait} = T$$

where t_{wait} is the time to wait from the last wire signal until the maximum drift time has been reached. The circuit to accomplish the synchronizer is shown in figure 2. The inputs labeled 1, 2, and 3 are assumed to be digital signals from the individual wire amplifier-discriminator circuits. They each set a flip-flop that retains the hit condition until reset. A discussion of the reset conditions appears later.

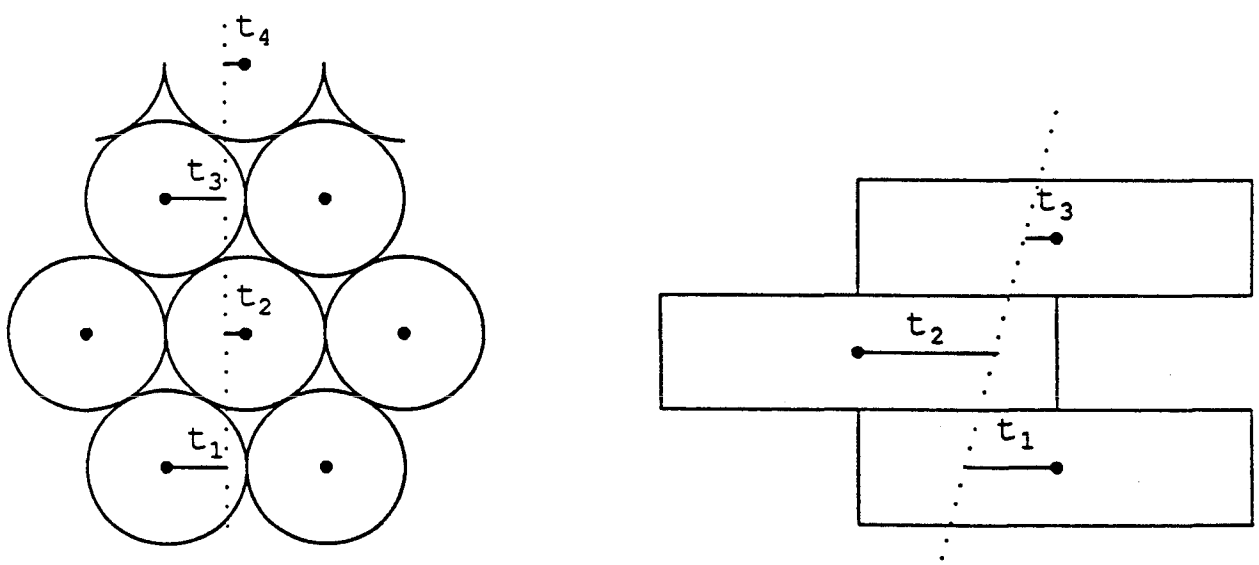

Synchronizer

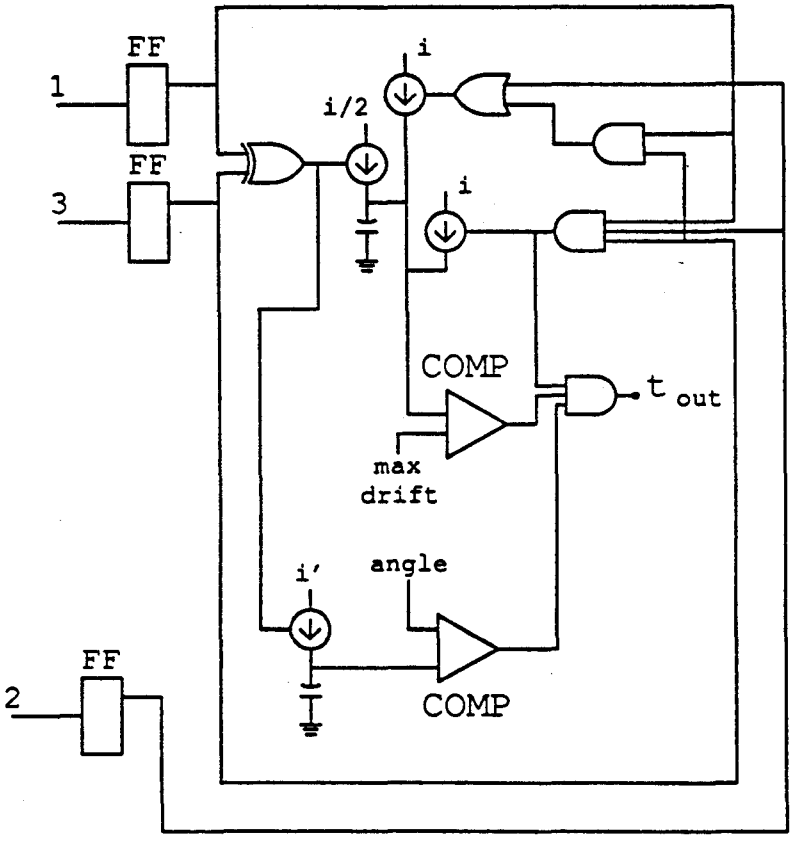

Figure2. The schematic of a synchronizer with circuitry for momentum selection. The auto-reset and auto-calibration are not shown.

The three terms on the left of the difference equation are computed separately by integrating current sources onto a common capacitor. The testing that the equation is satisfied is performed by the comparator that reaches its trigger threshold when the left terms equal the constant represented on the right of the equation. The three terms on the

i/2 on a capacitor for the time between the arrival of the first of the pair and the second as given by the exclusive-or circuit. (Note also that this difference signal is used to gate the current i' onto a separate capacitor.) This part of the synchronizer computes the first term in the difference equations. The solution of the drift time equation is further pursued by the accumulation of the current i on the same capacitor beginning at the first of a) the middle wire signal or b) the last of the radially aligned wires. This corresponds to the second term in the difference equation. Logically this current should cease when the second of a) and b) arrives. However, for electronic convenience the current is left on so that the third term in the difference equation can be accomplished by the addition of a second current i rather than by the introduction of a current 2i accompanyed by the cessation of the current i. The calculation of the third term begins when all three signals have arrived. The comparator sampling the voltage on the capacitor reaches its threshold when the equation is solved. This occurs when the circuit has waited the appropriate time to extend the arrivals one maximum drift time from the particle passage.

Momentum Restriction and Auto-Reset

The second capacitor and its current i' provide for a programmable momentum restriction. The timing difference of signals on the radially aligned wires measures the track angle with respect to the chamber normal. This angle is linearly related to the track momentum for constant solenoidal fields. If the time difference between these aligned wires exceeds the threshold represented by the label "angle", then the output from the equation solution is blocked and no external signal is generated. The synchronizer will therefore output only when "stiff" tracks pass trough the tubes. The circuit resets , *i.e.*, the flip-flops are reset whenever the currently developing conditions are such that no output pulse will be generated. This occurs when the computation of the left terms reaches the threshold of the comparator without having all the tube signal flip-flops set and when the angle (momentum) inhibit has reached the blocking condition. Immediate activation of the reset

accuracy required. Another potential problem is the variability of the synchronized timing. Variations in gas pressure and temperature will change the drift time slightly. Circuit variations will also lead to output signal variations. The presence of non-linearity in the drift-time to distance relationship of gas tube detectors will also induce variations in the timing output of the synchronizers since the circuit is based on a linear relationship. To minimize the effect of these variations, a scheme of auto calibration has been proposed for the synchronizer and studied in simulation. In this scheme the two currents, i, are permitted to vary in a closed loop convergence cycle. Each current is modified until a specific condition is met.

A simultaneous pulse on the radially aligned pair of wires followed by a pulse on the 1/2 cell staggered wire at the maximum drift time later corresponds to a radially aligned track passing through the radially aligned pair. Such a pattern activates only the first current i. Adjustment of this first current to give the output at the maximum drift time (delay slightly through the circuit) represents the first step of the auto-calibration cycle. The simultaneous arrival of all three tube signals corresponds to a radial track positioned halfway between the wires. The timing of this track is representative of the half-cell drift time. In the circuit the two currents, i, are both active for the time from the half-cell time to the full-cell drift time. Adjustment of the second of the currents, i, to establish the output at the desired maximum drift time is the second step in the auto-calibration cycle. Adjustment of the currents for precise timing at the half-cell and full-cell drift time effectively removes all circuit non-uniformities and detector non-linearities as concerns. Figure 3 shows the effect of this current optimization. With the nominal currents the output timing variation rises with the fractional non-linearity in the drift-time distance relationship. With the optimized currents, it remains small up to non-linearity of 40%. The fractional non-linearity shown in figure 3 is parameterized as the magnitude of a quadratic term at the largest drift distance. The figure is for round tubes with 50ns maximum drift time.

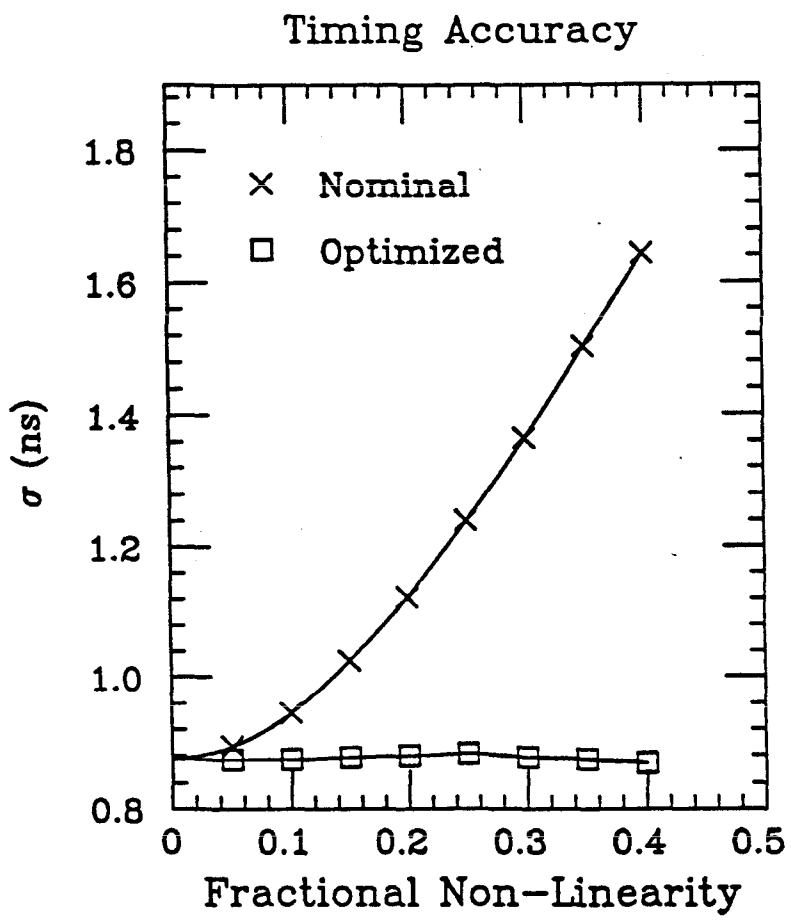

Figure3. The effect of drift-time distance non-linearities is shown for nominal currents and for auto-calibration adjusted currents. While the timing jitter shows a growth of σ with non-linearity in the case of nominal currents, no such growth is seen for the circuit where the currents are adjusted to minimize the timing variation for non-linear terms up to 40%.

Circuit Fabrication

The first fabrication of the synchronizer circuit includes auto-reset but does not include auto-calibration electronics. The currents are derived from external supplied voltages so that auto-calibration can be investigated through the use of external electronics. The

on the oscilloscope. Figure 5 exhibits the scope traces for this condition. The results track with amazing precision the simulation.

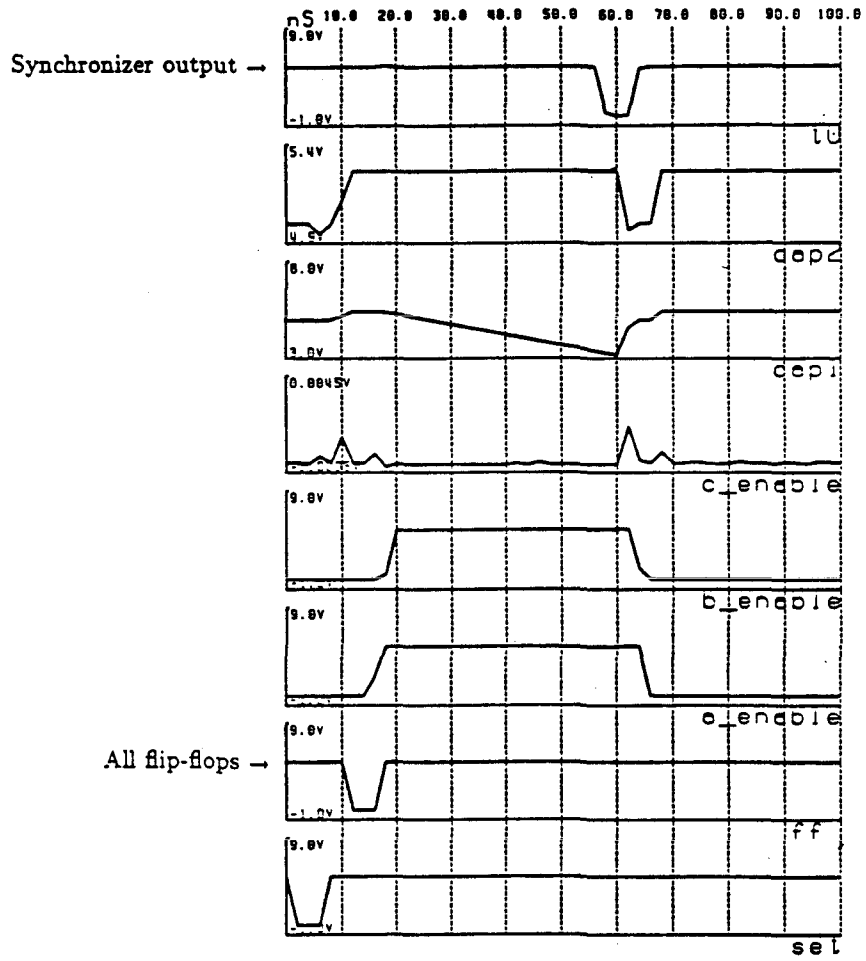

Figure4. An MSpice simulation of the synchronizer on the Mentor Graphics CAD station.

Future Plans

We will test the first versions of the synchronizers over a wide range of track positions

of the kind used in μ detector systems. We plan to operate both long and short drift time synchronizers with real chambers in a cosmic ray stand.

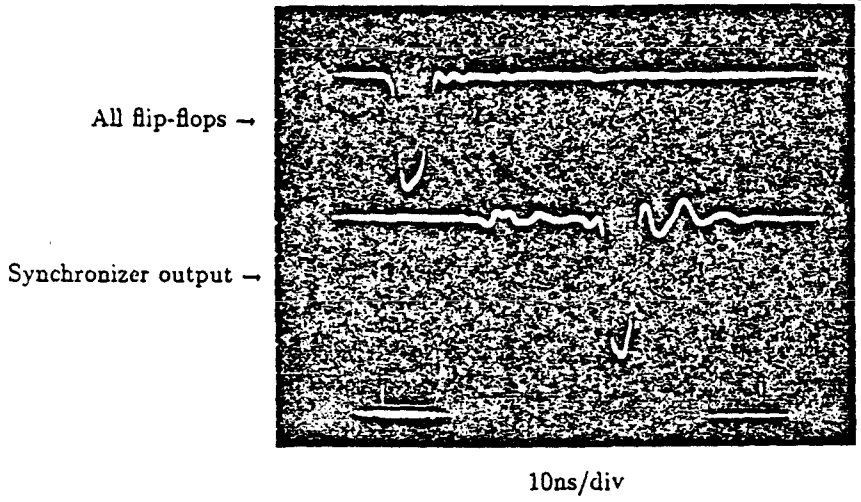

Figure5. A comparative measurement of the chip performance under the same conditions as in figure 4. The actual timing is essentially identical to that of the simulation.

REFERENCES

1. J. Chapman, Measurement of the Third Coordinate, Berkeley Workshop on Front-End Electronics for the SSC, March 6-8, 1989

2. J. Chapman, Drift Tube Synchronizers, Berkeley Workshop on Triggering for the SSC, June 13-16, 1989

3. Drift Tube Synchronizers, J. Chapman, University of Michigan Preprint, UM-HE-89-10, June, 1989